SECOND LIGHT-SCATTERING AND KERR-EFFECT VIRIAL COEFFICIENTS OF MOLECULES WITH LINEAR AND LOWER SYMMETRY

by

VINCENT WILLIAM COULING
M Sc (Natal)

A thesis submitted in partial fulfilment
of the requirements for the degree of
Doctor of Philosophy
in the Department of Physics
University of Natal

PIETERMARITZBURG
JANUARY 1995

Acknowledgements

I wish to express my sincerest gratitude to all those people who assisted and encouraged me throughout this work. In particular:

my supervisor, Prof. C. Graham, for his guidance during the past two years. The personal kindness he has shown me is greatly appreciated;

Mr. A. Hill and Mr. J. Wilsenach of the Physics Department Workshop, and Mr. G. Dewar of the Electronics Workshop, for the skilful manner in which they assisted with the experimental aspects of this project;

Mr. K. Penzhorn of the Physics Department technical staff for his tireless assistance in getting the Fortran programs used in this work to run on the Physics Department's new IBM RISC/6000 workstation;

the Foundation for Research Development for a Doctoral Bursary, and Prof. R. E. Raab for generous financial assistance; and finally

my mother, Carol, for her unconditional support and encouragement.

Declaration

This thesis is the result of my own original work, unless specifically indicated to the contrary in the text.

Vincent Carling

Abstract

Theoretical descriptions of the effects of molecular pair interactions on the bulk optical properties of gases often lead to prohibitively large volumes of algebraic manipulation, even for molecules of high symmetry. For this reason, manual derivations of these molecular tensor theories have generally been subject to sweeping approximations, with only the simplest of the large series of molecular-interaction terms being treated. Under such circumstances it is impossible to know whether any discrepancies between experiment and theory should be attributed to deficiencies in the theoretical model, to uncertainties in the molecular parameters used in the calculations, or to perhaps substantial contributions arising from the neglected higher-order interaction terms. The advent of powerful new symbolic manipulation packages for personal computers means that *complete* molecular tensor theories of the effects of pair interactions on the various molecular-optic phenomena can now be undertaken. By systematically evaluating successively higher-order terms in the molecular interactions, convergence of the series of contributing terms can now be definitively established. The particular effects considered in this thesis are depolarized Rayleigh light scattering and electro-optic birefringence, and the order of investigation is as follows:

The molecular theory of the second light-scattering virial coefficient B_ρ describing the effects of interacting pairs of molecules on the depolarization ratio ρ of Rayleigh-scattered light is reviewed, and our extended theory, yielding tensor expressions for contributions to B_ρ applicable to axially-symmetric molecules, is presented. These expressions include dipole-dipole interactions up to the fifth power in the molecular polarizability α, as well as additional contributions arising from field gradient effects and induced quadrupole moments in the molecular interactions. At these levels of approximation it is shown that convergence of the expressions is assured. The expressions for B_ρ have been evaluated numerically by computer for ten gases: carbon dioxide (CO_2), nitrogen (N_2), ethane (CH_3CH_3), ethene (CH_2CH_2), carbonyl sulphide (OCS), carbon monoxide (CO), fluoromethane (CH_3F), trifluoromethane (CHF_3) and hydrogen chloride (HCl). The results enabled judicious selection of those molecules for which experimental investigation would be most fruitful. A light scattering apparatus was

developed, and measurements of B_ρ for the five linear molecules CO_2, N_2, CH_3CH_3, CH_3Cl and CO were undertaken at room temperature with incident light of λ = 514.5 nm. These are presented together with tabulations of earlier measurements, and are compared with the calculated values. For CO_2, N_2 and CH_3Cl the calculated values agree with our measured values to within 10%; while for CO and CH_3CH_3, theory and experiment agree to within 20%.

It is then shown how application of the above molecular tensor theory for axially-symmetric molecules to molecules of lower symmetry leads to calculated values of B_ρ which are grossly discrepant with measured values. Subsequently, a complete molecular tensor theory of B_ρ for non-linear molecules is presented, and the resulting expressions are evaluated numerically for ethene (CH_2CH_2), sulphur dioxide (SO_2) and dimethyl ether ($(CH_3)_2O$). This theory is more complete in the sense that it can be used for molecules of higher symmetry, and checks confirm that it yields the same values for the B_ρ of linear molecules as the simpler theory to within seven significant figures.

Our experimental investigations of linear and quasi-linear molecules were extended to include ethene and sulphur dioxide. The apparatus used in the investigations of the pressure-dependence of the depolarization ratio ρ is discussed. Substantial improvements to the apparatus since the measurements on linear molecules now allow for experiments on corrosive gases and vapours at elevated temperatures. Measured values of B_ρ for ethene and sulphur dioxide are presented and critically compared with the calculated values. It is shown that acceptable agreement between measured and calculated B_ρ values of about 10% to 20% is only achieved after a molecule's symmetry has been fully taken into consideration.

The levels of success achieved for B_ρ of linear and non-linear molecules prompted application of the new techniques to a different second virial coefficient, namely that of the Kerr effect. A full review of all theoretical and experimental work undertaken on the second Kerr-effect virial coefficient B_K is given. A theory of B_K for molecules with non-linear symmetry is then presented. Again, the theory is general, and includes molecules of higher symmetry as a special case. Calculated values for the polar axially-symmetric molecules fluoromethane (CH_3F)

and trifluoromethane (CHF_3) revealed good agreement with experiment, although the large uncertainties of ±50% in the measured data do not provide a stringent assessment of the success of the theory. Values of B_K calculated for the non-linear polar molecules sulphur dioxide and dimethyl ether are generally within the uncertainty limits of the rather precise experimental values quoted in the literature. B_K values for non-polar molecules are often two orders of magnitude smaller than those for polar species, making precise experimental measurements difficult to undertake. Calculations for the linear molecules carbon dioxide, nitrogen and ethane, and for the non-linear molecule ethene are presented, and comparisons made with available experimental data.

Contents

CHAPTER 1

A REVIEW

1.1 Introduction

One of the primary tasks of the molecular physicist is the elucidation of the electromagnetic properties of individual molecules. This is often achieved by experimental investigation of the interaction of light with macroscopic samples of matter, coupled with theories which relate the macroscopic observables of such experiments to the molecular property tensors of the molecules in the specimen. A typical example of this technique is the measurement of the depolarization ratio ρ_o of light scattered by linear and quasi-linear molecules *at low gas pressures*, which by suitable theoretical interpretation has long provided a means for the accurate determination of the magnitude of the difference in principal molecular polarizabilities, $|\alpha_{\parallel} - \alpha_{\perp}|$ [1,2]. Often implicit in such theories is the assumption that each molecule in the gas sample can be treated as an independent system. This approximation is only applicable to a perfect gas, the typical gas sample in the laboratory having bulk properties which differ from the ideal due to the presence of molecular interactions.

Theoretical studies of the effects of these molecular interactions on the optical properties of gases have, up until now, been limited to the very restricted classes of spherical, quasi-spherical, linear and quasi-linear molecules. The reasons for this are twofold. Firstly, there is the almost prohibitively large volume of algebraic manipulation which is required for the derivation of *complete* molecular tensor theories describing the contributions even of pair interactions to the various molecular-optic phenomena such as electric birefringence, molar refraction and depolarized light-scattering. Secondly, the dipole-induced-dipole (DID) model of Silberstein [3], where the dipoles induced in molecules by an incident light wave $\mathcal{E}_o(t)$ interact with one another leading to DID coupling, appears to break down in calculations of the various second virial coefficients of large quasi-spherical molecules

(see, for example, [4] and [5]). This may have led to a degree of scepticism in the application of DID theory to molecules of lower symmetry.

It has recently been shown how the problem of lengthy and tedious hand-worked tensor manipulation can be managed by invoking the use of the powerful algebraic manipulation packages now available for personal computers. In undertaking a molecular tensor theory of the second light-scattering virial coefficient B_ρ for linear and quasi-linear molecules, Graham [6] made use of the Derive algebraic package. Later, Couling and Graham [7] used the more powerful Macsyma symbolic manipulation package, which unlike Derive has built-in tensor manipulation facilities, to extend the series of tensor expressions contributing to B_ρ to include field-gradient effects and induced quadrupole moments in the molecular interactions. This allowed a definitive assessment of where the series of interaction terms had converged to a meaningful numerical value for B_ρ.

Once such theories for the second virial coefficients have been developed for axially-symmetric molecules, there is a strong temptation to approximate non-linear molecules to be of axial symmetry, and hence calculate their virial coefficients. This thesis serves to show that such approximations are grossly unsatisfactory. It will be shown, for example, that if the ethene molecule, which belongs to the D_{2h} symmetry point group, is approximated to be of axial symmetry, the calculated B_ρ value differs from the experimental value by 40%. A similar discrepancy has already been observed for sulphur dioxide, which is of C_{2v} symmetry: when measured values of the second Kerr-effect virial coefficient, B_κ, for sulphur dioxide [8] were compared with values calculated using a recent statistical-mechanical theory of B_κ for axially-symmetric polar molecules [9], the predicted values were generally found to be more than twice as large as the experimental ones.

In this work we illustrate how the Macsyma package, which we ran on a 486 DX-2 66 MHz PC with 32 Mb of RAM, can be used to facilitate the development of complete molecular tensor theories of second light-scattering and Kerr-effect virial coefficients for *non-linear* molecules. It will become apparent that only when full account of a non-linear molecule's symmetry is taken into consideration do we find acceptable agreement between measured and calculated second virial

coefficients.

Treatment of the various other second virial coefficients is not considered here, although the same general methods are applicable to them, opening up new experimental possibilities in many molecular-optic phenomena.

1.2 A general expression for second virial coefficients

In 1956, Buckingham and Pople demonstrated how the effects of molecular interactions can be systematically accounted for by means of a virial-type expansion [10]. If Q represents a suitably chosen measurable molecular-optic property, then its observed value can be expanded in inverse powers of the molar volume V_m.

$$Q = A_Q + \frac{B_Q}{V_m} + \frac{C_Q}{V_m^2} + \ldots \qquad (1.1)$$

where the virial coefficients A_Q, B_Q, C_Q, ..., are functions of temperature alone. As expected, the ideal gas value for an assembly of non-interacting molecules is recovered in the limit of infinite dilution $(V_m \to \infty)$, when Q becomes A_Q. The higher-order virial coefficients B_Q, C_Q, ... represent the deviations due to pair, triplet, ... interactions respectively.

If we consider one mole of non-interacting gas molecules, the macroscopic property Q is simply the sum of N_A mean contributions $\bar{q}$ of the individual molecules. We have

$$Q = A_Q = N_A \bar{q} \; . \qquad (1.2)$$

At higher densities, however, the contribution of molecule 1 to Q is not always $\bar{q}$ since there are times when molecule 1 must be treated as half of an interacting pair. If molecule 1 has a neighbouring molecule 2, the relative configuration of which is given by the collective symbol τ, then the contribution of molecule 1 to Q at that instant is given by $\frac{1}{2}q_{12}(\tau)$, where $q_{12}(\tau)$ is the corresponding contribution of the pair. If we neglect triplet and higher-order interactions we obtain

$$Q = N_A\left\{\bar{q} + \int\left[\frac{1}{2}q_{12}(\tau) - \bar{q}\right] P(\tau)d\tau\right\} \qquad (1.3)$$

where $P(\tau)d\tau$ is the probability of molecule 1 having a neighbour in the range $(\tau, \tau + d\tau)$. $P(\tau)$ is related to the intermolecular potential energy $U_{12}(\tau)$ by

$$P(\tau) = \frac{N_A}{\Omega V_m} \exp\left[-U_{12}(\tau)/kT\right] , \qquad (1.4)$$

where $\Omega = V_m^{-1} \int d\tau$ is the integral over the orientational co-ordinates of the neighbouring molecule. Now we have from equation (1.1)

$$B_Q = \lim_{V_m \to \infty} \left[Q - A_Q\right]V_m , \qquad (1.5)$$

which coupled with equations (1.2), (1.3) and (1.4) yields a general expression for B_Q:

$$B_Q = \frac{N_A^2}{\Omega} \int\left[\frac{1}{2}q_{12}(\tau) - \bar{q}\right] \exp\left[-U_{12}(\tau)/kT\right] d\tau . \qquad (1.6)$$

This basic formula can then be applied to the various molecular-optic properties Q.

The main thrust of this thesis is the extension of our previous theoretical [6,7] and experimental [11] work on the second light-scattering virial coefficient B_ρ for axially-symmetric molecules into the regime of non-linear molecules. Hence, we proceed by reviewing all previous work on B_ρ for molecules with spherical and linear symmetry. Our theoretical work on the second Kerr-effect virial coefficient B_K for non-linear molecules grew out of the apparent success of the dipole-induced-dipole model in describing B_ρ for molecules of low symmetry (as will be seen in Chapters 2 and 3), and so is presented as a separate, self-contained piece of work in Chapter 4.

1.3 Light-scattering phenomena

1.3.1 Historical background

Historically, the study of light scattering began in 1869 when Tyndall conducted a series of experiments on aerosols [12]. A strong beam of white light was passed through a colloidal suspension of particles, and when viewed at right angles to the incident beam the scattered light was seen to be blue in colour and linearly polarized. This provided some justification for the already suggested idea that the blue colour of skylight and its observed polarization was due to the scattering of sunlight by small particles suspended in the atmosphere. Nevertheless, the mechanisms involved in the scattering process remained unexplained, with Tyndall saying (see Kerker [13]) "The blue colour of the sky, and the polarization of skylight ... constitute, in the opinion of our most eminent authorities, the two great standing enigmas of meteorology."

This enigma was resolved in 1871 by the third Baron Rayleigh, J. W. Strutt, who in his theoretical discussion of the light-scattering phenomenon [14] treated the incident light as vibrations in the ether which, when encountering the suspended particles, set up forced vibrations in them. These particles then in turn acted as secondary sources of vibrations in all directions, hence scattering the incident light. Rayleigh went on to show that the intensity of the light scattered by a particle, assumed to be an *isotropic* sphere of diameter much smaller than the wavelength λ of the incident light vibration, was proportional to $1/\lambda^4$, and that the component scattered at right angles was completely linearly polarized perpendicular to the scattering plane. This explained why blue light, which has a shorter wavelength than red light, is more strongly scattered than red, leading to the blue colour of the sky and of Tyndall's aerosols.

Lord Rayleigh refined his theory in 1899 by suggesting, as originally postulated by Maxwell, that the blue skylight was not due to scattering of sunlight by particles suspended in the air, but rather due to scattering by the *individual air molecules* themselves [15]. It was only some seventeen years later, in 1916, that this theoretical prediction was experimentally confirmed, with Cabannes [16] passing an incident beam of white light through a pure, dust-free gas sample and observing

the 90° scattered light to be blue in colour and linearly polarized, but much weaker in intensity than the light scattered by the relatively larger particles in Tyndall's colloidal suspensions.

Imperfections in Lord Rayleigh's theory became apparent when his son R. J. Strutt, the fourth Baron Rayleigh, conducted his own experiments [17]. He found that the light scattered at right angles to the incident beam was in fact *not* completely linearly polarized, and that the exact extent to which depolarization occurred was a characteristic constant of a particular gas. R. J. Strutt then extended his father's theory, which assumed *isotropic* spherical scattering centres, by relating the depolarization ratio to *departures* from spherical symmetry of the optical properties of the gas molecules [18].

The following decade saw a prolific number of measurements being made on a variety of gases and vapours, despite the almost insurmountable experimental difficulties encountered. During this activity, the Raman effect was discovered, in which the scattered light has well defined frequency shifts. Most of the subsequent work was diverted into this new field, and the conventional Rayleigh scattering was only seriously revisited in 1961 when J. Powers [19] published new values for the depolarization ratio of several gases. Powers, like the earlier workers in this field, used a white light source; but rather than using the less than adequate visual or photographic detection techniques of the earlier workers, he employed a photomultiplier as the detector of scattered light. His results indicated that the depolarization ratios measured in the 1920-30 era were too high often by as much as 10%. The advent of the laser had a revolutionizing impact on work in this field, its highly intense and parallel beam of monochromatic light first being exploited by Bridge and Buckingham [20] and then by various other workers [2,21-25] who made detailed and accurate measurements of the depolarization ratios of many gases and vapours. Their values were even lower than those of Powers, further confirming the inadequacy of the experimental techniques used by workers in the 1920-30 era.

1.3.2 Interacting spherical molecules

Although isolated spherical molecules cannot depolarize the light which they scatter, in gases of spherical molecules at elevated pressures a small depolarization ratio is observed. This has been attributed to the modification of the effective molecular polarizability α of a molecule as a result of the molecular interactions which occur during collisions or close encounters between neighbouring molecules, and has been the subject of intensive theoretical and experimental investigation [4,26,27].

This pressure-dependent depolarization ratio is best interpreted by means of the virial expansion [28]

$$\rho = \frac{B_\rho}{V_m} + \frac{C_\rho}{V_m^2} + \ldots \quad , \tag{1.7}$$

where the second light-scattering virial coefficient B_ρ describes the contribution to ρ arising from interactions between pairs of molecules, and where C_ρ describes contributions due to triplet interactions, etc. V_m is the molar volume of the gas. Using dipole-induced-dipole theory [26], B_ρ can be written

$$B_\rho = \frac{4\pi N_A}{(4\pi\varepsilon_o)^2} \frac{6\alpha^2}{5} \int_o^\infty R^{-4} \exp\left[-U_{pq}(R)/kT\right] dR \ , \tag{1.8}$$

where N_A is Avogadro's number, α is the molecular polarizability, and $U_{pq}(R)$ is the intermolecular potential energy between interacting molecules p and q which are separated by a distance R. Retaining only the leading term in equation (1.7), the depolarization ratio can now be written

$$\rho = V_m^{-1} \times \frac{4\pi N_A}{(4\pi\varepsilon_o)^2} \frac{6\alpha^2}{5} \int_o^\infty R^{-4} \exp\left[-U_{pq}(R)/kT\right] dR \ . \tag{1.9}$$

In early calculations, this integral was evaluated using the H_k functions of Buckingham and Pople [28]:

$$\int_o^\infty R^{-k} \exp\left[-U_{pq}^{LJ}(R)/kT\right] R^2 \, dR = \frac{1}{12} R_o^{3-k} \, y^{-4} \, H_k(y) \ , \tag{1.10}$$

where $U_{pq}^{LJ}(R)$ is the Lennard-Jones 6:12 potential [29]. Values of $H_k(y)$ have been tabulated [28] for k ranging from 6 to 17 in integral steps.

Watson and Rowell's calculated values of B_ρ [4] obtained from equation (1.8) are presented in table 1.1, together with their experimentally measured values of B_ρ. Subsequent workers have further confirmed the $B_\rho^{expt}/B_\rho^{theory}$ ratios given in table 1.1 for both argon [33,34,36] and methane [33,35,36]. An important feature of these results is the apparent breakdown of the DID theory of molecular interactions for the larger spherical and quasi-spherical molecules. Note, for example, the stark disagreement between the theoretically predicted and experimentally measured depolarization ratios of sulphur hexafluoride and neopentane as listed in table 1.1. Watson and Rowell argued that this discrepancy between theory and experiment for the large molecules provides evidence of the inadequacy of the point-dipole approximation used in the DID theory, but this has not been established and the problem remains unresolved.

Table 1.1. Theoretical and experimental second light-scattering virial coefficients B_ρ for several isotropic gases at T = 298 K, as reported by Watson and Rowell [4] and Thibeau and Oksengorn [30].

Molecule	$10^5 B_\rho$/amagat			$\frac{B_\rho^{expt\,[4]}}{B_\rho^{theory}}$
	Theoretical	Experimental [4]	Experimental [30]	
argon	1.313[a]	<2	0.88 ± 0.04	
	1.206[b]			
krypton	2.72[a]	2.3 ± 0.3		0.85
	2.205[b]			1.04
methane	2.41[a]	2.9 ± 0.4	1.80 ± 0.06	1.20
	2.39[b]			1.21
sulphur hexafluoride	2.43[a]	6.1 ± 0.2		2.51
	1.93[b]			3.16
neopentane	4.7[b]	32 ± 4		6.8

[a] Using Lennard-Jones constants reported in [31]

[b] Using Lennard-Jones constants reported in [32]

1.3.3 Interacting linear and quasi-linear molecules

Non-interacting anisotropic molecules (i.e. molecules which have a departure from spherical symmetry of their optical properties) inherently produce a scattered *depolarized* intensity which has been found to be proportional to the square of the polarizability anisotropy (to be defined in due course). At elevated pressures, molecular interactions modify this inherent depolarization ratio ρ_o of anisotropic molecules. The density dependence of the depolarization ratio ρ is described by means of the virial expansion

$$\rho = \rho_o + \frac{B_\rho}{V_m} + \frac{C_\rho}{V_m^2} + \ldots , \qquad (1.11)$$

where the second light-scattering virial coefficient B_ρ describes the deviations from ρ_o due to pair interactions, C_ρ the deviations from ρ_o due to triplet interactions, etc. The first detailed theories of pressure-dependent light scattering by anisotropic molecules [37,38] showed that the leading interaction term in equation (1.11), that in B_ρ, has the general form

$$B_\rho = \left(\rho_o - \tfrac{4}{3}\rho_o^2\right)\left(2B + \mathcal{G}_\rho\right) \qquad (1.12)$$

where B is the normal pressure virial coefficient, and where $\mathcal{G}_\rho$ arises from angular correlation [37] and collision-induced polarizability anisotropy [38]. Dayan, Dunmur and Manterfield [39] have emphasized that the presence of B in equation (1.12) may lead to a serious degradation of the precision of $\mathcal{G}_\rho$ values deduced from experimental observations of B_ρ, especially when accurate values of B are not available. These problems are further compounded by the fact that developing a complete molecular tensor theory of B_ρ for anisotropic molecules involves extremely lengthy and tedious tensor manipulation coupled with very time-consuming numerical integration of the resulting averaging integrals even when using fast computers. A combination of these difficulties, coupled with the lack of success in explanations of the light-scattering virial coefficients of spherical molecules, probably accounts for the dearth of experimental and theoretical work that has been undertaken in this field.

By 1980, Dayan, Dunmur and Manterfield [39] had measured B_ρ for carbon dioxide, carbonyl sulphide and nitrogen; while Berrue, Chave, Dumon and Thibeau [40] had measured B_ρ for nitrogen and ethane. By 1992, B_ρ had not been measured for any other non-spherical gases, while the *only* linear molecule to have been investigated theoretically [41,42] was nitrogen. This gas probably received theoretical treatment because of its particularly small B value at around room temperature, with a very favourable $\mathcal{G}_\rho$ value of nearly five times as large. The expressions for the $\mathcal{G}_\rho$ contribution to B_ρ for nitrogen presented by Berrue, Chave, Dumon and Thibeau [41,42] included angular correlation and collision-induced polarizability, but *neglected* the polarizability anisotropy in the successive dipole-induced-dipole interactions which occur during collisions. Their result for nitrogen agreed remarkably well with experiment, although they argued that this may have been fortuitous in view of the cancellation of large terms of opposite sign.

It is quite likely that expressions with the above approximations would prove inadequate in describing the $\mathcal{G}_\rho$ contribution to B_ρ for linear molecules in general. Fortunately, the advent of powerful computer algebraic manipulation packages such as Derive and Macsyma, coupled with high speed Fortran compilers, has made possible the development of a *complete* molecular tensor theory of B_ρ. Graham [6] has presented a comprehensive set of calculations of B_ρ for molecules with threefold or higher rotation axes performed using the Derive algebraic manipulation package coupled with the fast Salford FTN77/386 Fortran compiler. However, due to the limitation of computer memory when using the Derive package on an 80386 personal computer, the calculations were limited to scattered intensities proportional to α^4 at most. A new personal-computer version of the symbolic manipulation package Macsyma, which provides access to much larger amounts of computer memory, and also to powerful tensor manipulation facilities not available on the Derive package, was acquired by our research group in 1992. Couling and Graham [7] subsequently used the Macsyma package to extend the series of tensor expressions contributing to B_ρ to include dipole-dipole scattered intensities of the fifth power in the molecular polarizability α, as well as a range of additional terms arising from field-gradient effects and induced quadrupole moments in the molecular interactions. This allowed a definitive assessment of where the series of interaction terms had converged to a meaningful numerical value for B_ρ. The higher-order terms were found in some instances to make significant contributions to

B_ρ, as shall be seen in due course, and these calculations served to establish orders of precision to which one has to work to ensure convergence.

1.4 Calculations of second light-scattering virial coefficients of linear and quasi-linear molecules

1.4.1 Expressions for molecules with threefold or higher rotation axes

Buckingham and Stephen [38] have derived an expression for the depolarization ratio ρ of Rayleigh-scattered light which includes the effects of interacting pairs of molecules, obtaining

$$\rho = \frac{N\left\langle \pi_{zx}^{(1)} \pi_{zx}^{(1)} \right\rangle + N\left\langle \pi_{zx}^{(1)} \pi_{zx}^{(2)} \right\rangle}{N\left\langle \pi_{xx}^{(1)} \pi_{xx}^{(1)} \right\rangle + N\left\langle \pi_{xx}^{(1)} \pi_{xx}^{(2)} \cos \chi_{12} \right\rangle} . \qquad (1.13)$$

Here, $\pi_{\alpha\sigma}^{(p)}$ is the differential polarizability of molecule p in space-fixed axes (x,y,z) located in the gas sample, and the angular brackets indicate an average over pair encounters. The probability that molecule 1 has a neighbour in $d\tau$ at τ has been related to the intermolecular potential energy $U_{12}(\tau)$ by Buckingham and Pople [4], yielding the expression already quoted in equation (1.4).

We follow Buckingham [43] in writing the dipole moment μ_α and quadrupole moment $\theta_{\alpha\beta}$ induced in a non-magnetic molecule by an electrostatic field E_α and its gradient $E_{\alpha\beta}$ as

$$\mu_\alpha = \alpha_{\alpha\beta} E_\beta + \frac{1}{3} A_{\alpha\beta\gamma} E_{\beta\gamma} + \ldots , \qquad (1.14)$$

and

$$\theta_{\alpha\beta} = A_{\gamma\alpha\beta} E_\gamma + C_{\alpha\beta\gamma\delta} E_{\gamma\delta} + \ldots . \qquad (1.15)$$

Using the above two equations, which allow inclusion of dipole-dipole terms as well as the leading terms arising from field gradient effects and induced quadrupole moments in the molecular interactions, the

differential polarizability may be written [6,7]

$$\pi^{(p)}_{\alpha\sigma} = \alpha^{(p)}_{\alpha\sigma} + \alpha^{(p)}_{\alpha\beta}T_{\beta\gamma}\alpha^{(q)}_{\gamma\sigma} + \alpha^{(p)}_{\alpha\beta}T_{\beta\gamma}\alpha^{(q)}_{\gamma\delta}T_{\delta\varepsilon}\alpha^{(p)}_{\varepsilon\sigma}$$

$$+ \alpha^{(p)}_{\alpha\beta}T_{\beta\gamma}\alpha^{(q)}_{\gamma\delta}T_{\delta\varepsilon}\alpha^{(p)}_{\varepsilon\phi}T_{\phi\eta}\alpha^{(q)}_{\eta\sigma} - \tfrac{1}{3}\alpha^{(p)}_{\alpha\beta}T^{(p)}_{\beta\gamma\delta}A^{(q)}_{\sigma\gamma\delta}$$

$$- \tfrac{1}{3}\alpha^{(p)}_{\alpha\beta}T_{\beta\gamma}A^{(q)}_{\gamma\delta\varepsilon}T^{(p)}_{\delta\varepsilon\phi}\alpha^{(p)}_{\phi\sigma} - \tfrac{1}{3}\alpha^{(p)}_{\alpha\beta}T^{(p)}_{\beta\gamma\delta}A^{(q)}_{\varepsilon\gamma\delta}T_{\varepsilon\phi}\alpha^{(p)}_{\phi\sigma}$$

$$+ \tfrac{1}{3}\alpha^{(p)}_{\alpha\beta}T^{(p)}_{\beta\gamma\delta}C^{(q)}_{\gamma\delta\varepsilon\phi}T^{(p)}_{\varepsilon\phi\eta}\alpha^{(p)}_{\eta\sigma} + \tfrac{1}{3}A^{(p)}_{\alpha\beta\gamma}T^{(p)}_{\beta\gamma\delta}\alpha^{(q)}_{\delta\sigma}$$

$$+ \tfrac{1}{3}A^{(p)}_{\alpha\beta\gamma}T^{(p)}_{\beta\gamma\delta}\alpha^{(q)}_{\delta\varepsilon}T_{\varepsilon\phi}\alpha^{(p)}_{\phi\sigma} + \ldots \quad . \tag{1.16}$$

Here, the superscripts p and q indicate molecule p and q respectively, while [43]

$$T^{(1)}_{\alpha\beta} = \frac{1}{4\pi\varepsilon_o}\nabla_\alpha\nabla_\beta R^{-1} = \frac{1}{4\pi\varepsilon_o}\left(3R_\alpha R_\beta - R^2\delta_{\alpha\beta}\right)R^{-5} \tag{1.17}$$

and

$$T^{(1)}_{\alpha\beta\gamma} = -\frac{1}{4\pi\varepsilon_o}\nabla_\alpha\nabla_\beta\nabla_\gamma R^{-1}$$

$$= \frac{3}{4\pi\varepsilon_o}\left[5R_\alpha R_\beta R_\gamma - R^2\left(R_\alpha\delta_{\beta\gamma} + R_\beta\delta_{\gamma\alpha} + R_\gamma\delta_{\alpha\beta}\right)\right]R^{-7} \tag{1.18}$$

are the second and third rank T-tensors used to express the electric field $E^{(1)}_\alpha$ and the electric field gradient $E^{(1)}_{\alpha\beta}$ at the origin of molecule 1 arising from the point dipole and quadrupole moments of molecule 2, which is at a position R_α from the centre of molecule 1, in the form

$$E^{(1)}_\alpha = T^{(1)}_{\alpha\beta}\mu^{(2)}_\beta - \tfrac{1}{3}T^{(1)}_{\alpha\beta\gamma}\theta^{(2)}_{\beta\gamma} + \ldots \quad , \tag{1.19}$$

and

$$E^{(1)}_{\alpha\beta} = T^{(1)}_{\alpha\beta\gamma}\mu^{(2)}_\gamma + \ldots \quad . \tag{1.20}$$

We have from [43] that

$$T^{(1)} = (-1)^n T^{(2)} \tag{1.21}$$

where n is the order of the T-tensor. It follows from equation (1.21) that the superscript may be omitted for T-tensors of second rank while it has to be retained for T-tensors of third rank.

Use of equation (1.16) in (1.13) yields

$$\rho = \frac{a_2 + a_3 + a_4 + a_5 + a_2A_1 + a_3A_1 + a_3C_1 + \ldots}{b_2 + b_3} , \tag{1.22}$$

where

$$a_2 = \left\langle \alpha^{(1)}_{zx} \alpha^{(1)}_{zx} \right\rangle + \left\langle \alpha^{(1)}_{zx} \alpha^{(2)}_{zx} \right\rangle , \tag{1.23}$$

$$a_3 = \left\langle \alpha^{(1)}_{zx} \alpha^{(1)}_{z\beta} T_{\beta\gamma} \alpha^{(2)}_{\gamma x} \right\rangle + \left\langle \alpha^{(1)}_{zx} \alpha^{(2)}_{z\beta} T_{\beta\gamma} \alpha^{(1)}_{\gamma x} \right\rangle$$

$$\left\langle \alpha^{(1)}_{z\beta} T_{\beta\gamma} \alpha^{(2)}_{\gamma x} \alpha^{(2)}_{zx} \right\rangle + \left\langle \alpha^{(1)}_{z\beta} T_{\beta\gamma} \alpha^{(2)}_{\gamma x} \alpha^{(1)}_{zx} \right\rangle , \tag{1.24}$$

$$a_4 = \left\langle \alpha^{(1)}_{z\beta} T_{\beta\gamma} \alpha^{(2)}_{\gamma x} \alpha^{(2)}_{z\delta} T_{\delta\varepsilon} \alpha^{(1)}_{\varepsilon x} \right\rangle + \left\langle \alpha^{(1)}_{z\beta} T_{\beta\gamma} \alpha^{(2)}_{\gamma x} \alpha^{(1)}_{z\delta} T_{\delta\varepsilon} \alpha^{(2)}_{\varepsilon x} \right\rangle$$

$$+ \left\langle \alpha^{(1)}_{zx} \alpha^{(2)}_{z\beta} T_{\beta\gamma} \alpha^{(1)}_{\gamma\delta} T_{\delta\varepsilon} \alpha^{(2)}_{\varepsilon x} \right\rangle + \left\langle \alpha^{(1)}_{zx} \alpha^{(1)}_{z\beta} T_{\beta\gamma} \alpha^{(2)}_{\gamma\delta} T_{\delta\varepsilon} \alpha^{(1)}_{\varepsilon x} \right\rangle$$

$$+ \left\langle \alpha^{(1)}_{z\beta} T_{\beta\gamma} \alpha^{(2)}_{\gamma\delta} T_{\delta\varepsilon} \alpha^{(1)}_{\varepsilon x} \alpha^{(2)}_{zx} \right\rangle + \left\langle \alpha^{(1)}_{z\beta} T_{\beta\gamma} \alpha^{(2)}_{\gamma\delta} T_{\delta\varepsilon} \alpha^{(1)}_{\varepsilon x} \alpha^{(1)}_{zx} \right\rangle , \tag{1.25}$$

$$a_5 = \left\langle \alpha^{(1)}_{zx} \alpha^{(1)}_{z\delta} T_{\delta\gamma} \alpha^{(2)}_{\gamma\mu} T_{\mu\nu} \alpha^{(1)}_{\nu\beta} T_{\beta\varepsilon} \alpha^{(2)}_{\varepsilon x} \right\rangle + \left\langle \alpha^{(1)}_{zx} \alpha^{(2)}_{z\delta} T_{\delta\gamma} \alpha^{(1)}_{\gamma\mu} T_{\mu\nu} \alpha^{(2)}_{\nu\beta} T_{\beta\varepsilon} \alpha^{(1)}_{\varepsilon x} \right\rangle$$

$$+ \left\langle \alpha^{(1)}_{z\delta} T_{\delta\varepsilon} \alpha^{(2)}_{\varepsilon x} \alpha^{(1)}_{z\phi} T_{\phi\gamma} \alpha^{(2)}_{\gamma\beta} T_{\beta\eta} \alpha^{(1)}_{\eta x} \right\rangle + \left\langle \alpha^{(1)}_{z\delta} T_{\delta\varepsilon} \alpha^{(2)}_{\varepsilon x} \alpha^{(2)}_{z\phi} T_{\phi\gamma} \alpha^{(1)}_{\gamma\beta} T_{\beta\eta} \alpha^{(2)}_{\eta x} \right\rangle$$

$$+ \left\langle \alpha^{(1)}_{z\delta} T_{\delta\gamma} \alpha^{(2)}_{\gamma\beta} T_{\beta\varepsilon} \alpha^{(1)}_{\varepsilon x} \alpha^{(1)}_{z\phi} T_{\phi\eta} \alpha^{(2)}_{\eta x} \right\rangle + \left\langle \alpha^{(1)}_{z\delta} T_{\delta\gamma} \alpha^{(2)}_{\gamma\beta} T_{\beta\varepsilon} \alpha^{(1)}_{\varepsilon x} \alpha^{(2)}_{z\phi} T_{\phi\eta} \alpha^{(1)}_{\eta x} \right\rangle$$

$$+ \left\langle \alpha^{(1)}_{z\delta} T_{\delta\gamma} \alpha^{(2)}_{\gamma\mu} T_{\mu\nu} \alpha^{(1)}_{\nu\beta} T_{\beta\varepsilon} \alpha^{(2)}_{\varepsilon x} \alpha^{(1)}_{zx} \right\rangle + \left\langle \alpha^{(1)}_{z\delta} T_{\delta\gamma} \alpha^{(2)}_{\gamma\mu} T_{\mu\nu} \alpha^{(1)}_{\nu\beta} T_{\beta\varepsilon} \alpha^{(2)}_{\varepsilon x} \alpha^{(2)}_{zx} \right\rangle , \tag{1.26}$$

$$a_2A_1 = -\frac{1}{3}\left\langle \alpha^{(1)}_{z\beta} T^{(1)}_{\beta\gamma\delta} A^{(2)}_{x\gamma\delta} \alpha^{(1)}_{zx} \right\rangle - \frac{1}{3}\left\langle \alpha^{(1)}_{zx} \alpha^{(1)}_{z\beta} T^{(1)}_{\beta\gamma\delta} A^{(2)}_{x\gamma\delta} \right\rangle$$

$$- \frac{1}{3}\left\langle \alpha^{(1)}_{z\beta} T^{(1)}_{\beta\gamma\delta} A^{(2)}_{x\gamma\delta} \alpha^{(2)}_{zx} \right\rangle + \frac{1}{3}\left\langle \alpha^{(1)}_{zx} \alpha^{(2)}_{z\beta} T^{(1)}_{\beta\gamma\delta} A^{(1)}_{x\gamma\delta} \right\rangle$$

$$+ \frac{1}{3}\left\langle \alpha^{(1)}_{zx} A^{(1)}_{z\beta\gamma} T_{\beta\gamma\delta} \alpha^{(2)}_{\delta x} \right\rangle + \frac{1}{3}\left\langle A^{(1)}_{z\beta\gamma} T_{\beta\gamma\delta} \alpha^{(2)}_{\delta x} \alpha^{(1)}_{zx} \right\rangle$$

$$- \frac{1}{3}\left\langle \alpha^{(1)}_{zx} A^{(2)}_{z\beta\gamma} T_{\beta\gamma\delta} \alpha^{(1)}_{\delta x} \right\rangle + \frac{1}{3}\left\langle A^{(1)}_{z\beta\gamma} T_{\beta\gamma\delta} \alpha^{(2)}_{\delta x} \alpha^{(2)}_{zx} \right\rangle , \qquad (1.27)$$

$$a_3A_1 = -\frac{1}{3}\left\langle \alpha^{(1)}_{zx} \alpha^{(1)}_{z\beta} T_{\beta\gamma} A^{(2)}_{\gamma\delta\lambda} T^{(1)}_{\delta\lambda\phi} \alpha^{(1)}_{\phi x} \right\rangle - \frac{1}{3}\left\langle \alpha^{(1)}_{z\beta} T_{\beta\gamma} A^{(2)}_{\gamma\delta\lambda} T^{(1)}_{\delta\lambda\phi} \alpha^{(1)}_{\phi x} \alpha^{(1)}_{zx} \right\rangle$$

$$+ \frac{1}{3}\left\langle \alpha^{(1)}_{zx} \alpha^{(2)}_{z\beta} T_{\beta\gamma} A^{(1)}_{\gamma\delta\lambda} T^{(1)}_{\delta\lambda\phi} \alpha^{(2)}_{\phi x} \right\rangle - \frac{1}{3}\left\langle \alpha^{(1)}_{z\beta} T_{\beta\gamma} A^{(2)}_{\gamma\delta\lambda} T^{(1)}_{\delta\lambda\phi} \alpha^{(1)}_{\phi x} \alpha^{(2)}_{zx} \right\rangle$$

$$- \frac{1}{3}\left\langle \alpha^{(1)}_{zx} \alpha^{(1)}_{z\beta} T^{(1)}_{\beta\gamma\delta} A^{(2)}_{\lambda\gamma\delta} T_{\lambda\phi} \alpha^{(1)}_{\phi x} \right\rangle - \frac{1}{3}\left\langle \alpha^{(1)}_{z\beta} T^{(1)}_{\beta\gamma\delta} A^{(2)}_{\lambda\gamma\delta} T_{\lambda\phi} \alpha^{(1)}_{\phi x} \alpha^{(1)}_{zx} \right\rangle$$

$$+ \frac{1}{3}\left\langle \alpha^{(1)}_{zx} \alpha^{(2)}_{z\beta} T^{(1)}_{\beta\gamma\delta} A^{(1)}_{\lambda\gamma\delta} T^{(1}_{\lambda\phi} \alpha^{(2)}_{\phi x} \right\rangle - \frac{1}{3}\left\langle \alpha^{(1)}_{z\beta} T^{(1)}_{\beta\gamma\delta} A^{(2)}_{\lambda\gamma\delta} T_{\lambda\phi} \alpha^{(1)}_{\phi x} \alpha^{(2)}_{zx} \right\rangle$$

$$+ \frac{1}{3}\left\langle \alpha^{(1)}_{zx} A^{(1)}_{z\beta\gamma} T^{(1)}_{\beta\gamma\delta} \alpha^{(2)}_{\delta\lambda} T_{\lambda\phi} \alpha^{(1)}_{\phi x} \right\rangle + \frac{1}{3}\left\langle A^{(1)}_{z\beta\gamma} T^{(1)}_{\beta\gamma\delta} \alpha^{(2)}_{\delta\lambda} T_{\lambda\phi} \alpha^{(1)}_{\phi x} \alpha^{(1)}_{zx} \right\rangle$$

$$- \frac{1}{3}\left\langle \alpha^{(1)}_{zx} A^{(2)}_{z\beta\gamma} T^{(1)}_{\beta\gamma\delta} \alpha^{(1)}_{\delta\lambda} T_{\lambda\phi} \alpha^{(2)}_{\phi x} \right\rangle + \frac{1}{3}\left\langle A^{(1)}_{z\beta\gamma} T^{(1)}_{\beta\gamma\delta} \alpha^{(2)}_{\delta\lambda} T_{\lambda\phi} \alpha^{(1)}_{\phi x} \alpha^{(2)}_{zx} \right\rangle , \qquad (1.28)$$

$$a_3C_1 = \frac{1}{3}\left\langle \alpha^{(1)}_{zx} \alpha^{(1)}_{z\delta} T^{(1)}_{\delta\rho\gamma} C^{(2)}_{\rho\gamma\beta\phi} T^{(1)}_{\beta\phi\varepsilon} \alpha^{(1)}_{\varepsilon x} \right\rangle + \frac{1}{3}\left\langle \alpha^{(1)}_{z\delta} T^{(1)}_{\delta\rho\gamma} C^{(2)}_{\rho\gamma\beta\phi} T^{(1)}_{\beta\phi\varepsilon} \alpha^{(1)}_{\varepsilon x} \alpha^{(1)}_{zx} \right\rangle$$

$$+ \frac{1}{3}\left\langle \alpha^{(1)}_{zx} \alpha^{(2)}_{z\delta} T^{(1)}_{\delta\rho\gamma} C^{(1)}_{\rho\gamma\beta\phi} T^{(1)}_{\beta\phi\varepsilon} \alpha^{(2)}_{\varepsilon x} \right\rangle + \frac{1}{3}\left\langle \alpha^{(1)}_{z\delta} T^{(1)}_{\delta\rho\gamma} C^{(2)}_{\rho\gamma\beta\phi} T^{(1)}_{\beta\phi\varepsilon} \alpha^{(1)}_{\varepsilon x} \alpha^{(2)}_{zx} \right\rangle , \qquad (1.29)$$

$$b_2 = \left\langle \alpha^{(1)}_{xx} \alpha^{(1)}_{xx} \right\rangle + \left\langle \alpha^{(1)}_{xx} \alpha^{(2)}_{xx} \cos X_{12} \right\rangle , \qquad (1.30)$$

$$b_3 = \left\langle \alpha^{(1)}_{xx} \alpha^{(1)}_{x\beta} T_{\beta\gamma} \alpha^{(2)}_{\gamma x} \right\rangle + \left\langle \alpha^{(1)}_{xx} \alpha^{(2)}_{x\beta} T_{\beta\gamma} \alpha^{(1)}_{\gamma x} \right\rangle . \qquad (1.31)$$

To proceed, the explicit forms of $T_{\alpha\beta}$, $T_{\alpha\beta\gamma}$, $\alpha_{\alpha\beta}$, $A_{\alpha\beta\gamma}$, and $C_{\alpha\beta\gamma\delta}$ are required. The molecular property tensors $\alpha_{\alpha\beta}$, $A_{\alpha\beta\gamma}$, and $C_{\alpha\beta\gamma\delta}$ simplify considerably for molecules of high symmetry, with far fewer tensor components being required to describe the molecular properties of, say, a linear molecule than a molecule of lower symmetry.

The ensuing analysis is restricted to linear and quasi-linear molecules, and if the rotation axis of such a molecule co-incides with the 3-axis of a molecule-fixed system (1,2,3) then α_{ij} is diagonal with $\alpha_{11} = \alpha_{22} = \alpha_{\perp}$ and $\alpha_{33} = \alpha_{\parallel}$.

The term $\left\langle \alpha^{(1)}_{zx} \alpha^{(1)}_{zx} \right\rangle$ in equation (1.23) refers to space-fixed axes, and may be referred to molecule-fixed axes by the normal tensor-projection procedure to yield

$$\left\langle \alpha^{(1)}_{zx} \alpha^{(1)}_{zx} \right\rangle = \left\langle \alpha^{(1)}_{ij} \alpha^{(1)}_{kl} \right\rangle \left\langle a^{z}_{i} a^{z}_{k} a^{x}_{j} a^{x}_{l} \right\rangle \qquad (1.32)$$

where a^{α}_{i} is the direction cosine between the α space-fixed and i molecule-fixed axes, and where the average is over all isotropic orientations of molecule 1 in the space-fixed axes. Use of the standard isotropic average [44]

$$\left\langle a^{z}_{i} a^{z}_{k} a^{x}_{j} a^{x}_{l} \right\rangle = \frac{1}{30} \left(4\delta_{ik}\delta_{jl} - \delta_{ij}\delta_{kl} - \delta_{il}\delta_{kj} \right) \qquad (1.33)$$

leads to the familiar expression

$$\left\langle \alpha^{(1)}_{zx} \alpha^{(1)}_{zx} \right\rangle = \frac{1}{15} \left(\alpha_{\parallel} - \alpha_{\perp} \right)^2 . \qquad (1.34)$$

Similar arguments, together with the result [44,1]

$$\left\langle a^{x}_{i} a^{x}_{j} a^{x}_{k} a^{x}_{l} \right\rangle = \frac{1}{15} \left(\delta_{ij}\delta_{kl} + \delta_{ik}\delta_{jl} + \delta_{il}\delta_{jk} \right) , \qquad (1.35)$$

allows $\left\langle \alpha^{(1)}_{xx} \alpha^{(1)}_{xx} \right\rangle$ in equation (1.30) to be simplified to

$$\left\langle \alpha^{(1)}_{xx} \alpha^{(1)}_{xx} \right\rangle = \alpha^2 + \frac{4}{45} \left(\alpha_{\parallel} - \alpha_{\perp} \right)^2 \qquad (1.36)$$

where

$$\alpha = \frac{1}{3}\left(2\alpha_{\perp} + \alpha_{\parallel}\right) . \qquad (1.37)$$

Now, *in their own molecular axes*, $\alpha^{(1)}_{ij}$ and $\alpha^{(2)}_{i'j'}$, are diagonal, and the remaining averages in equations (1.23) to (1.26), and (1.30) and (1.31), must be expressed in terms of these diagonal elements and a set of interaction parameters. Equations (1.27) to (1.29) with their added complications of third and fourth rank tensors, shall be dealt with in due course. Meanwhile, the more manageable averages shall be considered.

Figure 1.1 shows pictorially how the relative configuration τ of two axially-symmetric molecules may be specified by the four parameters θ_1, θ_2, ϕ and R [43]. Here, R is the distance between the centres; θ_1 and θ_2 are the angles between the line of centres and the dipole axes of molecules 1 and 2; and ϕ is the angle between the planes formed by the molecular axes and the line of centres. The unit vectors $\underset{\sim}{\ell}^{(1)}$ and $\underset{\sim}{\ell}^{(2)}$ along the dipole axes, and $\underset{\sim}{\lambda}$ along $\underset{\sim}{R}$, will be required later.

Now, the molecular property tensors of a molecule are generally specified relative to a co-ordinate system of mutually perpendicular axes that is fixed in the molecule such that one of the axes co-incides with a symmetry axis of the molecule. This is seen in figure 1.1 where the co-ordinate systems of molecules 1 and 2 are O(1,2,3) (referred to by tensor indices i, j, k, ...) and O'(1'2'3') (referred to by tensor indices i', j', k', ...) with axes 3 and 3' chosen as the symmetry-axes for molecules 1 and 2 respectively. The space-fixed system O(x,y,z) (referred to by tensor indices α, β, γ, ...) has its origin at molecule 1, which does not shift with the changing orientation of either molecule.

Initially, all tensors are referred to (1,2,3), including $\alpha^{(2)}_{ij}$ which is in general *not* diagonal in (1,2,3). A projection from (1,2,3) into (1',2',3'), where $\alpha^{(2)}_{i'j'}$, *is* diagonal, will be carried out later. The reason for initially referring all tensors to (1,2,3) lies in the fact that for a given relative configuration of the pair of molecules, the tensor product in (1,2,3) is fixed. If the pair of molecules is then allowed to rotate isotropically *as a rigid whole* in (x,y,z), then the projection into (x,y,z) of this pair property (referred to (1,2,3)) can be averaged over all orientations. Averaging over the interaction parameters may subsequently be carried out. Simplification during the

above procedure is facilitated by the following well-established relationships, which allow the expressions to be cast in terms of the four interaction parameters:

$$a_i^{3'} = \ell_i^{(2)} \quad , \tag{1.38}$$

$$\ell_i^{(1)}\ell_i^{(2)} = \ell_3^{(2)} = \cos\theta_{12} = -\cos\theta_1\cos\theta_2 + \sin\theta_1\sin\theta_2\cos\phi \quad , \tag{1.39}$$

$$\ell_i^{(1)}\lambda_i = \lambda_3 = \cos\theta_1 \quad , \tag{1.40}$$

$$\ell_2^{(2)}\lambda_i = -\cos\theta_2 \quad . \tag{1.41}$$

Buckingham [43] has also shown that for axially-symmetric molecules, the molecular property tensors themselves may be expressed in terms of $\ell_i^{(2)}$. For example

$$\alpha_{ij}^{(2)} = \alpha_\perp\delta_{ij} + \left[\alpha_\parallel - \alpha_\perp\right]\ell_i^{(2)}\ell_j^{(2)} \quad . \tag{1.42}$$

Use of the anisotropy κ in the molecular polarizability tensor $\alpha_{\alpha\beta}$, defined by

$$\kappa = \frac{\alpha_\parallel - \alpha_\perp}{3\alpha} \quad , \tag{1.43}$$

together with equation (1.37) allows equation (1.42) to be recast as

$$\alpha_{ij}^{(2)} = \alpha(1 - \kappa)\delta_{ij} + 3\kappa\alpha\ell_i^{(2)}\ell_j^{(2)} \quad . \tag{1.44}$$

Benoît and Stockmayer [37] were the first to establish the now familiar results

$$\left\langle \alpha_{zx}^{(1)}\alpha_{zx}^{(2)} \right\rangle = \frac{1}{30}\left[\alpha_\parallel - \alpha_\perp\right]^2 \left\langle 3\cos^2\theta_{12} - 1 \right\rangle \quad , \tag{1.45}$$

which is a contribution known as the angular correlation term; and

$$\left\langle \alpha_{xx}^{(1)}\alpha_{xx}^{(2)}\cos\chi_{12} \right\rangle = \frac{1}{15}\frac{2}{3}\left[\alpha_\parallel - \alpha_\perp\right]^2 \left\langle 3\cos^2\theta_{12} - 1 \right\rangle + \alpha^2\left[\frac{-2B}{V_m}\right] \quad , \tag{1.46}$$

where B is the second pressure virial coefficient.

The new higher-order terms are evaluated using a procedure which will be illustrated by considering a specific example, i.e. the term $\left\langle \alpha^{(1)}_{zx}\alpha^{(1)}_{z\delta}T_{\delta\gamma}\alpha^{(2)}_{\gamma\mu}T_{\mu\nu}\alpha^{(1)}_{\nu\beta}T_{\beta\varepsilon}\alpha^{(2)}_{\varepsilon x}\right\rangle$, which is the first term in a_5 given by equation (1.26). The first step is to project the term from space-fixed axes (x,y,z) into the molecule-fixed axes (1,2,3) of molecule 1:

$$\left\langle \alpha^{(1)}_{zx}\alpha^{(1)}_{z\delta}T_{\delta\gamma}\alpha^{(2)}_{\gamma\mu}T_{\mu\nu}\alpha^{(1)}_{\nu\beta}T_{\beta\varepsilon}\alpha^{(2)}_{\varepsilon x}\right\rangle$$

$$= \left\langle \alpha^{(1)}_{ij}a^{z}_{i}a^{x}_{j}\,\alpha^{(1)}_{kl}a^{z}_{k}a^{\delta}_{l}\,T_{mn}a^{\delta}_{m}a^{\gamma}_{n}\,\alpha^{(2)}_{pq}a^{\gamma}_{p}a^{\mu}_{q}\,T_{rs}a^{\mu}_{r}a^{\nu}_{s}\,\alpha^{(1)}_{tu}a^{\nu}_{t}a^{\beta}_{u}T_{vw}a^{\beta}_{v}a^{\varepsilon}_{w}\alpha^{(2)}_{gh}a^{\varepsilon}_{g}a^{x}_{h}\right\rangle$$

$$= \left\langle \alpha^{(1)}_{ij}\alpha^{(1)}_{km}T_{mn}\alpha^{(2)}_{nr}T_{rs}\alpha^{(1)}_{sv}T_{vw}\alpha^{(2)}_{wh}\right\rangle \left\langle a^{z}_{i}a^{z}_{k}a^{x}_{j}a^{x}_{h}\right\rangle . \qquad (1.47)$$

If the interaction configuration is fixed, then the term $\left\langle \alpha^{(1)}_{ij}\alpha^{(1)}_{km}T_{mn}\alpha^{(2)}_{nr}T_{rs}\alpha^{(1)}_{sv}T_{vw}\alpha^{(2)}_{wh}\right\rangle$ is a constant; and if the rigid pair of molecules is allowed to rotate isotropically, then equation (1.33) may be invoked to yield the average projection

$$\left\langle \alpha^{(1)}_{zx}\alpha^{(1)}_{z\delta}T_{\delta\gamma}\alpha^{(2)}_{\gamma\mu}T_{\mu\nu}\alpha^{(1)}_{\nu\beta}T_{\beta\varepsilon}\alpha^{(2)}_{\varepsilon x}\right\rangle$$

$$= \frac{1}{30}\left(4\delta_{ik}\delta_{jh} - \delta_{ij}\delta_{kh} - \delta_{ih}\delta_{kj}\right)\left\langle \alpha^{(1)}_{ij}\alpha^{(1)}_{km}T_{mn}\alpha^{(2)}_{nr}T_{rs}\alpha^{(1)}_{sv}T_{vw}\alpha^{(2)}_{wh}\right\rangle$$

$$= \frac{1}{30}\left\langle 4\alpha^{(1)}_{kh}\alpha^{(1)}_{km}T_{mn}\alpha^{(2)}_{nr}T_{rs}\alpha^{(1)}_{sv}T_{vw}\alpha^{(2)}_{wh} - \alpha^{(1)}_{ii}\alpha^{(1)}_{km}T_{mn}\alpha^{(2)}_{nr}T_{rs}\alpha^{(1)}_{sv}T_{vw}\alpha^{(2)}_{wk}\right.$$

$$\left. - \alpha^{(1)}_{hk}\alpha^{(1)}_{km}T_{mn}\alpha^{(2)}_{nr}T_{rs}\alpha^{(1)}_{sv}T_{vw}\alpha^{(2)}_{wh}\right\rangle$$

$$= \frac{1}{30}\left\langle 3\alpha^{(1)}_{hk}\alpha^{(1)}_{km}T_{mn}\alpha^{(2)}_{nr}T_{rs}\alpha^{(1)}_{sv}T_{vw}\alpha^{(2)}_{wh} - \alpha^{(1)}_{ii}\alpha^{(1)}_{km}T_{mn}\alpha^{(2)}_{nr}T_{rs}\alpha^{(1)}_{sv}T_{vw}\alpha^{(2)}_{wk}\right\rangle , \qquad (1.48)$$

in which the angular brackets now indicate an average over the pair interaction co-ordinates R, θ_1, θ_2, and ϕ according to the general relationship

$$\langle X\rangle = \int_{\tau} X\, P(\tau)\, d\tau \quad , \qquad (1.49)$$

where $P(\tau)$ is the probability that molecule 1 has a neighbour in

$d\tau$ at τ. This probability has been related to the intermolecular potential energy $U_{12}(\tau)$ in equation (1.4), which when substituted into (1.49) yields

$$\langle X \rangle = \frac{N_A}{2V_m} \int_{R=0}^{\infty} \int_{\theta_1=0}^{\pi} \int_{\theta_2=0}^{\pi} \int_{\phi=0}^{2\pi} X \exp\left[-U_{12}/kT\right] R^2 dR \sin\theta_1 \sin\theta_2 d\theta_1 d\theta_2 d\phi. \tag{1.50}$$

When the appropriate values for $\alpha_{ij}^{(1)}$, $\alpha_{ij}^{(2)}$, and T_{ij} are substituted into (1.48) there results a lengthy expression containing redundant interaction parameters $\ell_1^{(2)}$, $\ell_2^{(2)}$, λ_1, and λ_2. Averaging according to equation (1.50) can only be performed after these redundant interaction parameters have been eliminated from the right hand side of equation (1.48), and this is achieved by making use of equations (1.38) to (1.44). When performed manually, this manipulation is extremely tedious and time-consuming: one of the reasons why higher-order terms were neglected from earlier calculations of B_ρ for linear molecules. Graham [6] initially carried out all of the work up to a_4 manually, and then verified the results with the assistance of Derive, which is a computer algebraic manipulation package from Soft Warehouse Inc. However, the derivation of the a_4 expression in equation (1.25) was found to be only just within the 640 kb computer memory limitations of the Derive package even when evaluating each of the terms in a_4 individually. Subsequently, Couling and Graham [7] evaluated the a_5 term, as well as the a_2A_1, a_3A_1, and a_3C_1 terms which required tensor manipulation techniques not available in the Derive package, using the algebraic manipulation package Macsyma. A new version of Macsyma, compatible with the 80386 series of personal computers, was obtained, providing access to much greater amounts of computer memory as well as to powerful tensor manipulation facilities. Adequate speed and capacity were only obtained after installation of 8 Mb of memory, the standard 4 Mb being totally inadequate.

Elimination of $\ell_1^{(2)}$, $\ell_2^{(2)}$, λ_1, and λ_2 from the expanded expressions may be achieved on computer by the piecemeal substitution of powers and multiples of the parameters

$$d = \lambda_1^2 + \lambda_2^2 = \left(1 - \cos^2\theta_1\right) , \tag{1.51}$$

$$e = \left[\ell_1^{(2)}\right]^2 + \left[\ell_2^{(2)}\right]^2 = \left(1 - \cos^2\theta_{12}\right) , \tag{1.52}$$

and

$$f = \ell_1^{(2)}\lambda_1 + \ell_2^{(2)}\lambda_2 = -\cos\theta_2 - \cos\theta_1\cos\theta_{12}\ , \qquad (1.53)$$

into the expanded forms, until they contain d, e, and f only, and *no* terms in the redundant parameters. This elimination procedure is by no means automatic, with considerable human intervention being required. Such intervention carries with it the possibility of errors, but the *back-substitution* of the explicit forms of d, e, and f (in terms of $\ell_i^{(2)}$ and λ_i) into the simplified expressions followed by comparison with the original expanded expression provides a quick and absolute means of guaranteeing the correctness of the simplified expressions. This is followed by final substitution according to the second parts of equations (1.51) to (1.53), and compression of terms of similar order into a single term. It was found that

$$\begin{aligned} a_3 = \frac{(4\pi\varepsilon_o)^{-1}}{30}\,\alpha^3 \Big\langle R^{-3}\big[&-27\kappa(\kappa-1)(2\kappa+3)\cos^2\theta_1 \\ &- 324\kappa^2(\kappa+1)\cos\theta_{12}\cos\theta_2\cos\theta_1 + 27\kappa(\kappa-1)(2\kappa-1)\cos^2\theta_2 \\ &- 108\kappa^2(\kappa+1)\cos^2\theta_{12} + 36\kappa(\kappa-1)\big]\Big\rangle\ , \end{aligned} \qquad (1.54)$$

$$\begin{aligned} a_4 = \frac{(4\pi\varepsilon_o)^{-2}}{30}\,\alpha^4 \Big\langle R^{-6}\big[&324\kappa^2(\kappa^2-2\kappa+1)\cos^4\theta_1 \\ &+ 1944\kappa^3(\kappa-1)\cos\theta_{12}\cos\theta_2\cos^3\theta_1 + ((5103\kappa^4\cos^2\theta_{12} \\ &+ 81\kappa^2(17\kappa^2+8\kappa+20))\cos^2\theta_2 + 405\kappa^3(\kappa-1)\cos^2\theta_{12} \\ &- 27\kappa(12\kappa^3-22\kappa^2+17\kappa-7))\cos^2\theta_1 \\ &+ (1944\kappa^3(\kappa-1)\cos\theta_{12}\cos^3\theta_2 + (3402\kappa^4\cos^3\theta_{12} - 162\kappa^2(4\kappa^2 \\ &- 14\kappa-5)\cos\theta_{12})\cos\theta_2)\cos\theta_1 + 324\kappa^2(\kappa^2-2\kappa+1)\cos^4\theta_2 \\ &+ (405\kappa^3(\kappa-1)\cos^2\theta_{12} - 27\kappa(8\kappa^3-24\kappa^2+21\kappa-5))\cos^2\theta_2 \\ &+ 567\kappa^4\cos^4\theta_{12} - 27\kappa^2(9\kappa^2-10\kappa-14)\cos^2\theta_{12} \\ &+ 18(2\kappa^4-9\kappa^3+11\kappa^2-6\kappa+2)\big]\Big\rangle\ , \end{aligned} \qquad (1.55)$$

$$b_3 = \frac{(4\pi\varepsilon_o)^{-1}}{30}\alpha^3\left\langle R^{-3}\left[-36\kappa(\kappa-1)(2\kappa+7)\cos^2\theta_1 - 108\kappa^2(2\kappa+7)\cos\theta_2\cos\theta_{12}\cos\theta_1 - 36\kappa^2(2\kappa+7)\cos^2\theta_{12} + 36\kappa(\kappa-1)(2\kappa-5)\cos^2\theta_2 + 144\kappa(\kappa-1)\right]\right\rangle , \quad (1.56)$$

$$a_5 = \frac{(4\pi\varepsilon_o)^{-3}}{30}\alpha^5\left\langle 9R^{-9}\left[243\kappa^3(\kappa^2-2\kappa+1)\cos^6\theta_1 + 1458\kappa^4(\kappa-1)\cos\theta_2\cos\theta_{12}\cos^5\theta_1 + 9\kappa^2(27\kappa^2(9\kappa\cos^2\theta_2+2\kappa-2)\cos^2\theta_{12} - 9\kappa(7\kappa^2+25\kappa-23)\cos^2\theta_2 - 23\kappa^3+75\kappa^2-81\kappa+29)\cos^4\theta_1 + 27\kappa^3\cos\theta_2\cos\theta_{12}(54\kappa^2\cos^2\theta_{12} - (54\kappa(2\kappa+5)\cos^2\theta_2+52\kappa^2-23k-11))\cos^3\theta_1 + 3\kappa(81\kappa^4\cos^4\theta_{12} - 3\kappa^2(243\kappa(2\kappa+3)\cos^2\theta_2+32\kappa^2-22\kappa-1)\cos^2\theta_{12} + 81\kappa^2(\kappa^2-7\kappa+6)\cos^4\theta_2 - 3\kappa(\kappa^3-228\kappa^2+225\kappa-55)\cos^2\theta_2 + 36\kappa^4-115\kappa^3+159\kappa^2-117\kappa+37)\cos^2\theta_1 - 9\kappa^2\cos\theta_2\cos\theta_{12}(27\kappa^2(7\kappa+9)\cos^2\theta_{12} + 9\kappa(\kappa^2+3\kappa-4)\cos^2\theta_2 - (55\kappa^3+70\kappa^2-86\kappa-21))\cos\theta_1 - 27\kappa^4(7\kappa+10)\cos^4\theta_{12} + 3\kappa^2(35\kappa^3+50\kappa^2-52\kappa-24)\cos^2\theta_{12} - 27\kappa^2(5\kappa^3-14\kappa^2+13\kappa-4)\cos^4\theta_2 + 3\kappa(29\kappa^4-118\kappa^3+168\kappa^2-98\kappa+19)\cos^2\theta_2 + 8(-2\kappa^5+7\kappa^4-13\kappa^3+14\kappa^2-7\kappa+1)\right]\right\rangle . \quad (1.57)$$

The presence of the third and fourth rank tensors A_{ijk}, T_{ijk}, and C_{ijkl} in the terms (1.27) to (1.29) necessitated the use of the tensor manipulation facilities of Macsyma. Buckingham [43] has shown that for axially-symmetric molecules, the molecular property tensors A_{ijk} and C_{ijkl} may be expressed in terms of the $\ell_i^{(2)}$ as follows:

$$A_{ijk}^{(2)} = \frac{1}{2}A_{\parallel}^{(2)}\ell_i^{(2)}\left[3\ell_j^{(2)}\ell_k^{(2)} - \delta_{ij}\right] + A_{\perp}^{(2)}\left[\ell_j^{(2)}\delta_{ik} + \ell_k^{(2)}\delta_{ij} - 2\ell_i^{(2)}\ell_j^{(2)}\ell_k^{(2)}\right] , \quad (1.58)$$

$$C^{(2)}_{ijkl} = \frac{1}{10}\left(C_{3333} + 8C_{1313} + 8C_{1111}\right)\left[\frac{1}{2}\left(\delta_{ik}\delta_{jl} + \delta_{il}\delta_{jk}\right) - \frac{1}{3}\delta_{ij}\delta_{kl}\right]$$

$$+ \frac{1}{28}\left(5C_{3333} + 4C_{1313} - 8C_{1111}\right)\left[\left(3\ell^{(2)}_i\ell^{(2)}_k - \delta_{ik}\right)\delta_{jl}\right.$$

$$+ \left(3\ell^{(2)}_i\ell^{(2)}_l - \delta_{il}\right)\delta_{jk} + \left(3\ell^{(2)}_j\ell^{(2)}_k - \delta_{jk}\right)\delta_{il}$$

$$+ \left(3\ell^{(2)}_j\ell^{(2)}_l - \delta_{jl}\right)\delta_{ik} - \frac{4}{3}\left(3\ell^{(2)}_i\ell^{(2)}_j - \delta_{ij}\right)\delta_{kl}$$

$$\left. - \frac{4}{3}\left(3\ell^{(2)}_k\ell^{(2)}_l - \delta_{kl}\right)\delta_{ij}\right]$$

$$+ \frac{1}{35}\left(2C_{3333} - 4C_{1313} + C_{1111}\right)\left[35\ell^{(2)}_i\ell^{(2)}_j\ell^{(2)}_k\ell^{(2)}_l\right.$$

$$- 5\left(\ell^{(2)}_i\ell^{(2)}_j\delta_{kl} + \ell^{(2)}_i\ell^{(2)}_k\delta_{jl} + \ell^{(2)}_i\ell^{(2)}_l\delta_{jk} + \ell^{(2)}_j\ell^{(2)}_k\delta_{il}\right.$$

$$\left.\left. + \ell^{(2)}_j\ell^{(2)}_l\delta_{ik} + \ell^{(2)}_k\ell^{(2)}_l\delta_{ij}\right) + \delta_{ij}\delta_{kl} + \delta_{ik}\delta_{jl} + \delta_{il}\delta_{jk}\right] . \quad (1.59)$$

These tensors, with their superscript (2), refer to molecule 2 as seen from the molecule-fixed axes of molecule 1. Now, since $\underset{\sim}{\ell}^{(1)}$ and $\underset{\sim}{\ell}^{(2)}$ are unit vectors along the dipole axes of molecules 1 and 2 respectively, in the axes (1,2,3) the vector $\underset{\sim}{\ell}^{(1)}$ must have components $\ell^{(1)}_1 = \ell^{(1)}_2 = 0$ and $\ell^{(1)}_3 = 1$. Hence, to obtain an expression for $A^{(1)}_{ijk}$ from (1.58), $\ell^{(2)}_i$ must be replaced by $\ell^{(1)}_i = \delta_{i3}$; while $\ell^{(2)}_i\ell^{(2)}_j\ell^{(2)}_k$ must be replaced by $\ell^{(1)}_i\ell^{(1)}_j\ell^{(1)}_k = \delta_{i3}\delta_{j3}\delta_{k3}$ etc. Similarly, to obtain an expression for $C^{(1)}_{ijkl}$ from (1.59), $\ell^{(2)}_i \ldots \ell^{(2)}_j$ must be replaced by $\delta_{i3}\ldots\delta_{j3}$ etc.

Finally the tensor expressions for each term in a_2A_1, a_3A_1, and a_3C_1 are explicitly expressed in terms of $\alpha^{(1)}_{ij}$, $\alpha^{(2)}_{ij}$, T_{ij}, $T^{(1)}_{ijk}$, $A^{(1)}_{ijk}$, $A^{(2)}_{ijk}$, $C^{(1)}_{ijkl}$, and $C^{(2)}_{ijkl}$; after which Macsyma is used to eliminate redundant interaction parameters and to compress the results as before, yielding the final expressions

$$a_2A_1 = \frac{(4\pi\varepsilon_o)^{-1}}{30}\,\alpha^2\left\langle -\tfrac{1}{2}R^{-4}\{A_\perp[180\kappa(\kappa-1)\cos^3\theta_2 + \cos\theta_1((-540\kappa(\kappa+1)\cos\theta_{12}+540\kappa^2)\cos^2\theta_2+216\kappa^2\cos^2\theta_{12} - 108\kappa(\kappa+1)\cos\theta_{12}-216\kappa^2+108\kappa)+(-216\kappa(\kappa+1)\cos^2\theta_{12} + 108\kappa^2\cos\theta_{12}+216\kappa)\cos\theta_2 + 540\kappa\cos^2\theta_1(\kappa\cos\theta_{12}-\kappa-1)\cos\theta_2+180\kappa(\kappa-1)\cos^3\theta_1] + A_\parallel[-135\kappa(\kappa-1)\cos^3\theta_2+\cos\theta_1(405\kappa(\kappa+1)\cos\theta_{12}\cos^2\theta_2 + 324\kappa^2\cos^2\theta_{12}-81\kappa(\kappa+1)\cos\theta_{12}-162\kappa^2+162\kappa) + (162\kappa(\kappa+1)\cos^2\theta_{12}-162\kappa^2\cos\theta_{12}+81\kappa^2-81\kappa)\cos\theta_2 + 810\kappa^2\cos^2\theta_1\cos\theta_{12}\cos\theta_2+270\kappa(\kappa-1)\cos^3\theta_1]\}\right\rangle, \quad (1.60)$$

$$a_3A_1 = \frac{(4\pi\varepsilon_o)^{-2}}{30}\,\alpha^3\left\langle -\tfrac{1}{2}R^{-7}\{A_\perp[12\kappa(135(\kappa^2-2\kappa+1)\cos^5\theta_1 + 810\kappa(\kappa-1)\cos\theta_2\cos\theta_{12}\cos^4\theta_1+(27\kappa(45\kappa\cos^2\theta_2+11\kappa - 11)\cos^2\theta_{12}-45\kappa(\kappa+8)\cos^2\theta_2-182\kappa^2+364\kappa-182)\cos^3\theta_1 + 3\cos\theta_2(297\kappa^2\cos^3\theta_{12}+27\kappa^2(15\cos^2\theta_2-7)\cos^2\theta_{12}-\kappa(236\kappa - 137)\cos\theta_{12}+15(9\kappa^2+2\kappa+4)\cos^2\theta_2-7(9\kappa^2+2\kappa+4))\cos^2\theta_1 + 3(54\kappa^2\cos^4\theta_{12}+27\kappa^2(11\cos^2\theta_2-2)\cos^3\theta_{12}-\kappa(189\kappa\cos^2\theta_2 + 5(13\kappa-4))\cos^2\theta_{12}+(270\kappa(\kappa-1)\cos^4\theta_2-(126\kappa^2-247\kappa - 44)\cos^2\theta_2-22\kappa-8)\cos\theta_{12}+7\kappa(\kappa+8)\cos^2\theta_2+20\kappa^2 - 30\kappa+19)\cos\theta_1+162\kappa^2\cos\theta_2\cos^4\theta_{12}-162\kappa^2\cos\theta_2\cos^3\theta_{12}) + 3\cos\theta_2(99\kappa(\kappa-1)\cos^2\theta_2-(45\kappa^2-40\kappa-8))\cos^2\theta_{12}$$

(continued...)

$$+ 6\kappa(10\kappa - 1)\cos\theta_2\cos\theta_{12} + 135(\kappa^2 - 2\kappa + 1)\cos^5\theta_2$$

$$- 190(\kappa^2 - 2\kappa + 1)\cos^3\theta_2 + 3(14\kappa^2 - 48\kappa + 19)\cos\theta_2)]$$

$$+ A_{\|}[-9\kappa(135(\kappa^2 - 2\kappa + 1)\cos^5\theta_1$$

$$+ 810\kappa(\kappa - 1)\cos\theta_2\cos\theta_{12}\cos^4\theta_1 + (27\kappa(45\kappa\cos^2\theta_2$$

$$+ 11\kappa(\kappa - 1))\cos^2\theta_{12} + 45\kappa(5\kappa - 2)\cos^2\theta_2 - 2(85\kappa^2 - 146\kappa$$

$$+ 61))\cos^3\theta_1 + 3\cos\theta_2(297\kappa^2\cos^3\theta_{12} + 81\kappa^2(5\cos^2\theta_2$$

$$- 1)\cos^2\theta_{12} - \kappa(98\kappa - 131)\cos\theta_{12} + 3(9\kappa^2 + 2\kappa + 4)(5\cos^2\theta_2$$

$$- 1))\cos^2\theta_1 + 3(54\kappa^2\cos^4\theta_{12} + 27\kappa^2(11\cos^2\theta_2 - 1)\cos^3\theta_{12}$$

$$- \kappa(81\kappa\cos^2\theta_2 + 35\kappa - 41)\cos^2\theta_{12} + (270\kappa(\kappa - 1)\cos^4\theta_2$$

$$- (54\kappa^2 - 175\kappa - 44)\cos^2\theta_2 - (11\kappa + 4))\cos\theta_{12} - 3(\kappa(5\kappa$$

$$- 2)\cos^2\theta_2 - 3\kappa^2 + 6\kappa - 3))\cos\theta_1 + \cos\theta_2(162\kappa^2\cos^4\theta_{12}$$

$$- 81\kappa^2\cos^3\theta_{12} + 3(99\kappa(\kappa - 1)\cos^2 - (27\kappa^2 - 49\kappa$$

$$- 8))\cos^2\theta_{12} + 3\kappa(4\kappa - 7)\cos\theta_{12} + (\kappa^2 - 2\kappa + 1)(135\cos^4\theta_2$$

$$- 154\cos^2\theta_2 + 27)))]\Big)\Big\rangle , \qquad (1.61)$$

$$A_3C_1 = \frac{(4\pi\varepsilon_o)^{-2}}{10}\,\alpha^3\left\langle R^{-8}\Big(6C_{3333}\kappa[150(\kappa^2 - 2\kappa + 1)\cos^6\theta_1\right.$$

$$+ 900\kappa(\kappa - 1)\cos\theta_{12}\cos\theta_2\cos^5\theta_1 + 5(30\kappa(9\kappa\cos^2\theta_{12} - (\kappa + 2))\cos^2\theta_2$$

$$+ 72\kappa(\kappa - 1)\cos^2\theta_{12} - 35(\kappa^2 - 2\kappa + 1))\cos^4\theta_1 + 30\kappa\cos\theta_{12}(36\kappa\cos^2\theta_{12}$$

$$+ 13 - 25\kappa)\cos\theta_2\cos^3\theta_1 + 3(50(3\kappa^2 + 2\kappa + 1)\cos^4\theta_2 - 15(9\kappa^2\cos^2\theta_{12}$$

$$+ 2\kappa^2 + 1)\cos^2\theta_2 + 72\kappa^2\cos^4\theta_{12} - 5\kappa(13\kappa - 10)\cos^2\theta_{12} + 16\kappa^2 - 28\kappa$$

$$+ 15)\cos^2\theta_1 + 6\cos\theta_{12}\cos\theta_2(20(3\kappa^2 + 2\kappa + 1)\cos^2\theta_2 + (5\kappa^2 - 9\kappa - 2)$$

(continued...)

$$- 18\kappa^2\cos^2\theta_{12})\cos\theta_1 - 10(\kappa^2 - 2\kappa + 1)\cos^4\theta_2 + 3((33\kappa^2 + 16\kappa + 8)\cos^2\theta_{12}$$

$$+ 2\kappa^2 + 1)\cos^2\theta_2 + 27\kappa^2\cos^4\theta_{12} - 3(7\kappa^2 - 1)\cos^2\theta_{12} - (4\kappa^2 + 4\kappa + 1)]$$

$$- 24C_{1313}\kappa[75(\kappa^2 - 2\kappa + 1)\cos^6\theta_1 + 450\kappa(\kappa - 1)\cos\theta_{12}\cos\theta_2\cos^5\theta_1$$

$$+ 5(15\kappa(9\kappa\cos^2\theta_{12} - (\kappa + 2))\cos^2\theta_2 + 2(18\kappa(\kappa - 1)\cos^2\theta_{12} - 11(\kappa^2 - 2\kappa$$

$$+ 1)))\cos^4\theta_1 + 30\kappa\cos\theta_{12}(18\kappa\cos^2\theta_{12} + 11 - 17\kappa)\cos\theta_2\cos^3\theta_1 + 3(25(3\kappa^2$$

$$+ 2\kappa + 1)\cos^4\theta_2 - 15(9\kappa^2(\cos^2\theta_{12} + 2\kappa^2 + 1)\cos^2\theta_2 + 36\kappa^2\cos^4\theta_{12} - \kappa(55\kappa$$

$$- 34)\cos^2\theta_{12} + 14\kappa^2 - 24\kappa + 13)\cos^2\theta_1 + 12\cos\theta_{12}\cos\theta_2(5(3\kappa^2 + 2\kappa$$

$$+ 1)\cos^2\theta_2 - 2(9\kappa^2\cos^2\theta_{12} - (\kappa^2 - 3\kappa - 1)))\cos\theta_1 - (5(\kappa^2 - 2\kappa + 1)\cos^4\theta_2$$

$$- 3(4(3\kappa^2 + 2\kappa + 1)\cos^2\theta_{12} - (\kappa^2 + 6\kappa - 1))\cos^2\theta_2 + 27\kappa^2\cos^4\theta_{12} - 3(4\kappa^2$$

$$- 6\kappa - 1)\cos^2\theta_{12} + \kappa^2 - 2\kappa + 1)]$$

$$+ 6C_{1111}\kappa[75(\kappa^2 - 2\kappa + 1)\cos^6\theta_1 + 450\kappa(\kappa - 1)\cos\theta_{12}\cos\theta_2\cos^5\theta_1$$

$$+ 5(15\kappa(9\kappa\cos^2\theta_{12} - (\kappa + 2))\cos^2\theta_2 + 36\kappa(\kappa - 1)\cos^2\theta_{12} - 31(\kappa^2 - 2\kappa$$

$$+ 1))\cos^4\theta_1 + 60\kappa\cos\theta_{12}(9\kappa\cos^2\theta_{12} + 10 - 13\kappa)\cos\theta_2\cos^3\theta_1 + 3(25(3\kappa^2$$

$$+ 2\kappa + 1)\cos^4\theta_2 - 30(9\kappa^2\cos^2\theta_{12} + 2\kappa^2 + 1)\cos^2\theta_2 + 36\kappa^2\cos^4\theta_{12} - 4\kappa(25\kappa$$

$$- 13)\cos^2\theta_{12} + 2(25\kappa^2 - 22\kappa + 18))\cos^2\theta_1 + 30\cos\theta_{12}\cos\theta_2(2(3\kappa^2 + 2\kappa$$

$$+ 1)\cos^2\theta_2 + (5\kappa^2 - 9\kappa - 2) - 18\kappa^2\cos^2\theta_{12})\cos\theta_1 - 5(\kappa^2 - 2\kappa + 1)\cos^4\theta_2$$

$$+ 3((57\kappa^2 + 8\kappa + 4)\cos^2\theta_{12} - (11\kappa^2 + 30\kappa - 2))\cos^2\theta_2 - 108\kappa^2\cos^4\theta_{12}$$

$$+ 12(7\kappa^2 - 1)\cos^2\theta - 2(\kappa^2 - 26\kappa + 7)]]\Big\rangle . \qquad (1.62)$$

Upon gathering the results in equations (1.34), (1.36), (1.45), (1.46), (1.54) to (1.57), and (1.60) to (1.62), equation (1.22) for ρ takes the form

$$\rho = \left[\frac{1}{15}(\alpha_{\parallel} - \alpha_{\perp})^2 + \frac{1}{30}(\alpha_{\parallel} - \alpha_{\perp})^2 \left\langle 3\cos^2\theta_{12} - 1 \right\rangle + \frac{1}{30}(4\pi\varepsilon_o)^{-1}\alpha^3 a'_3 \right.$$

$$+ \frac{1}{30}(4\pi\varepsilon_o)^{-2}\alpha^4 a'_4 + \frac{1}{30}(4\pi\varepsilon_o)^{-3}\alpha^5 a'_5 + \frac{3}{90}(4\pi\varepsilon_o)^{-1}\alpha^2 a_2 A'_1$$

$$+ \frac{3}{90}(4\pi\varepsilon_o)^{-2}\alpha^3 a_3 A'_1 + \frac{3^2}{90}(4\pi\varepsilon_o)^{-2}\alpha^3 a_3 C'_1 + \ldots \Big] \Big/ \left[\frac{1}{15}\left[15\alpha^2\right.\right.$$

$$\left.\left. + \frac{4}{3}(\alpha_{\parallel} - \alpha_{\perp})^2\right] + \frac{1}{15} \times \frac{2}{3}(\alpha_{\parallel} - \alpha_{\perp})^2 \left\langle 3\cos^2\theta_{12} - 1 \right\rangle + \alpha^2\left[\frac{-2B}{V_m}\right]\right.$$

$$\left. + \frac{1}{30}(4\pi\varepsilon_o)^{-1}\alpha^3 b'_3\right] , \qquad (1.63)$$

in which a'_3 represents that part of a_3 in equation (1.54) which is contained within the angular brackets, with similar definitions for a'_4, a'_5, $a_2A'_1$, $a_3A'_1$, and $a_3C'_1$ which occur in equations (1.55), (1.57), (1.60), (1.61), and (1.62) respectively.

Equation (1.63) must now be cast in the virial form of equation (1.11). We require the following expression for ρ_o for linear molecules, which was first derived by Bridge and Buckingham [21]:

$$\rho_o = \frac{3(\Delta\alpha)^2}{45\alpha^2 + 4(\Delta\alpha)^2} , \qquad (1.64)$$

where

$$\Delta\alpha = \alpha_{\parallel} - \alpha_{\perp} . \qquad (1.65)$$

This allows equation (1.63) to be written in the form

$$\rho = \rho_o\left[1 + \frac{1}{2}\left\langle 3\cos^2\theta_{12} - 1 \right\rangle + \frac{1}{2}(4\pi\varepsilon_o)^{-1}\frac{\alpha^3}{(\Delta\alpha)^2} a'_3 + \frac{1}{2}(4\pi\varepsilon_o)^{-2}\frac{\alpha^4}{(\Delta\alpha)^2} a'_4\right.$$

$$+ \frac{1}{2}(4\pi\varepsilon_o)^{-3}\frac{\alpha^5}{(\Delta\alpha)^2} a'_5 + \frac{1}{2}(4\pi\varepsilon_o)^{-1}\frac{\alpha^2}{(\Delta\alpha)^2} a_2 A'_1$$

$$\left. + \frac{1}{2}(4\pi\varepsilon_o)^{-2}\frac{\alpha^3}{(\Delta\alpha)^2} a_3 A'_1 + \frac{3}{2}(4\pi\varepsilon_o)^{-2}\frac{\alpha^3}{(\Delta\alpha)^2} a_3 C'_1 + O\left[\frac{1}{V_m^2}\right]\right] \Big/ \left\{1\right.$$

$$\left. + \frac{4}{3}\rho_o\left[\frac{1}{2}\left\langle 3\cos^2\theta_{12} - 1 \right\rangle + \frac{3}{8}(4\pi\varepsilon_o)^{-1}\frac{\alpha^3}{(\Delta\alpha)^2} b'_3 + \frac{2B}{V_m} + O\left[\frac{1}{V_m^2}\right]\right]\right\} ,$$

(1.66)

which reduces to

$$\rho = \rho_o + \rho_o\left(1 - \tfrac{4}{3}\rho_o\right)\left[\frac{2B}{V_m} + \tfrac{1}{2}\left\langle 3\cos^2\theta_{12} - 1\right\rangle + \frac{\alpha}{18\kappa^2}\left\{1 + \tfrac{4}{5}\kappa^2\right\}(4\pi\varepsilon_o)^{-1}a_3' \right.$$
$$+ \frac{\alpha^2}{18\kappa^2}\left\{1 + \tfrac{4}{5}\kappa^2\right\}(4\pi\varepsilon_o)^{-2}\,a_4' + \frac{\alpha^3}{18\kappa^2}\left\{1 + \tfrac{4}{5}\kappa^2\right\}(4\pi\varepsilon_o)^{-3}\,a_5'$$
$$+ \frac{1}{18\kappa^2}\left\{1 + \tfrac{4}{5}\kappa^2\right\}(4\pi\varepsilon_o)^{-1}\,a_2A_1' + \frac{\alpha}{18\kappa^2}\left\{1 + \tfrac{4}{5}\kappa^2\right\}(4\pi\varepsilon_o)^{-2}\,a_3A_1'$$
$$\left. + \frac{\alpha}{6\kappa^2}\left\{1 + \tfrac{4}{5}\kappa^2\right\}(4\pi\varepsilon_o)^{-2}\,a_3C_1' - \frac{\alpha}{30}(4\pi\varepsilon_o)^{-1}\,b_3' + O\left[\frac{1}{V_m^2}\right]\right] . \qquad (1.67)$$

It follows that

$$B_\rho = \rho_o\left(1 - \tfrac{4}{3}\rho_o\right)\left(2B + G + a_3 + a_4 + a_5 + a_2\mathcal{A}_1 + a_3\mathcal{A}_1 + a_3\mathcal{C}_1 + \mathcal{b}_3 + \ldots\right) \qquad (1.68)$$

where

$$G = \tfrac{1}{2}\left\langle 3\cos^2\theta_{12} - 1\right\rangle V_m , \qquad (1.69)$$

$$a_3 = \frac{\alpha}{18\kappa^2}\left\{1 + \tfrac{4}{5}\kappa^2\right\}(4\pi\varepsilon_o)^{-1}V_m\,a_3' , \qquad (1.70)$$

$$a_4 = \frac{\alpha^2}{18\kappa^2}\left\{1 + \tfrac{4}{5}\kappa^2\right\}(4\pi\varepsilon_o)^{-2}V_m\,a_4' , \qquad (1.71)$$

$$a_5 = \frac{\alpha^3}{18\kappa^2}\left\{1 + \tfrac{4}{5}\kappa^2\right\}(4\pi\varepsilon_o)^{-3}V_m\,a_5' , \qquad (1.72)$$

$$a_2\mathcal{A}_1 = \frac{1}{18\kappa^2}\left\{1 + \tfrac{4}{5}\kappa^2\right\}(4\pi\varepsilon_o)^{-1}V_m\,a_2A_1' , \qquad (1.73)$$

$$a_3\mathcal{A}_1 = \frac{\alpha}{18\kappa^2}\left\{1 + \tfrac{4}{5}\kappa^2\right\}(4\pi\varepsilon_o)^{-2}V_m\,a_3A_1' , \qquad (1.74)$$

$$a_3\mathcal{C}_1 = \frac{\alpha}{6\kappa^2}\left\{1 + \tfrac{4}{5}\kappa^2\right\}(4\pi\varepsilon_o)^{-2}V_m\,a_3C_1' , \qquad (1.75)$$

and

$$\mathcal{b}_3 = -\frac{\alpha}{30}(4\pi\varepsilon_o)^{-1}V_m\,b_3' . \qquad (1.76)$$

As with the normal second pressure virial coefficient B, the above eight coefficients are independent of the molar volume but dependent on temperature. It is the parameter B_ρ which is directly accessible from a plot of experimentally measured ρ versus V_m^{-1} values, and knowledge of ρ_o allows calculation of

$$B'_\rho = \left[2B + G + a_3 + a_4 + a_5 + a_2\mathcal{A}_1 + a_3\mathcal{A}_1 + a_3\mathcal{C}_1 + \mathcal{B}_3 + \ldots\right] \quad . \tag{1.77}$$

The appearance of 2B in this expression for B'_ρ can mask the more interesting contributions from the remaining terms, which are summed to allow comparison with 2B, giving

$$B'_\rho = \left[2B + \mathcal{S}_\rho\right] \tag{1.78}$$

where the sum $\mathcal{S}_\rho$ arises purely from angular correlation and dipole-dipole, field gradient, and induced quadrupole moment effects in the molecular interaction. Numerical evaluation of $\mathcal{S}_\rho$ would allow calculation of the ratio $\left[\mathcal{S}_\rho/2B\right]$ which would prove particularly useful for the theoretical selection of molecules which could be fruitfully studied experimentally.

1.4.2 Classical expressions for the intermolecular potential $U_{12}(\tau)$

a'_3 is that part of equation (1.54) contained within the angular brackets, indicating an average over the pair interaction co-ordinates according to equation (1.50); with a similar understanding for the terms a'_4 to $a_3C'_1$. Now, evaluation of the average $\langle X \rangle$ of a quantity X over the pair interaction co-ordinates according to equation (1.50) requires the classical intermolecular potential energy U_{12}. The general form of $U_{12}(\tau)$ used in our calculations is [1,45,46]

$$U_{12}(\tau) = U_{LJ} + U_{\mu,\mu} + U_{\mu,\theta} + U_{\theta,\theta} + U_{\mu,\,\mathrm{ind}\,\mu} + U_{\theta,\,\mathrm{ind}\,\mu} + U_{\mathrm{shape}} \tag{1.79}$$

in which U_{LJ} is the familiar Lennard-Jones 6:12 potential

$$U_{LJ} = 4\varepsilon\left[\left[\frac{R_o}{R}\right]^{12} - \left[\frac{R_o}{R}\right]^{6}\right] \quad . \tag{1.80}$$

$U_{\mu,\mu}$, $U_{\mu,\theta}$ and $U_{\theta,\theta}$ are the electrostatic dipole-dipole, dipole-quadrupole and quadrupole-quadrupole interaction energies of the permanent moments of the two molecules; while $U_{\mu,\text{ind}\,\mu}$ and $U_{\theta,\text{ind}\,\mu}$ are dipole–induced-dipole and quadrupole–induced-dipole interaction energies. The anisotropy of repulsive forces is represented by U_{shape}. For interacting linear molecules in the co-ordinate system shown in figure 1.1

$$U_{\mu,\mu} = \frac{1}{4\pi\varepsilon_o}\left\{\mu^2 R^{-3}\left(2\cos\theta_1\cos\theta_2 + \sin\theta_1\sin\theta_2\cos\phi\right)\right\}, \tag{1.81}$$

$$U_{\mu,\theta} = \frac{1}{4\pi\varepsilon_o}\left\{\frac{3}{2}\,\mu\theta R^{-4}\left[\cos\theta_1\left(3\cos^2\theta_2 - 1\right) + \cos\theta_2\left(3\cos^2\theta_1 - 1\right) + 2\sin\theta_1\sin\theta_2\cos\theta_2\cos\phi + 2\sin\theta_1\cos\theta_1\sin\theta_2\cos\phi\right]\right\}, \tag{1.82}$$

$$U_{\theta,\theta} = \frac{1}{4\pi\varepsilon_o}\left\{\frac{3}{4}\,\theta^2 R^{-5}\left(1 - 5\cos^2\theta_1 - 5\cos^2\theta_2 + 17\cos^2\theta_1\cos^2\theta_2 + 2\sin^2\theta_1\sin^2\theta_2\cos^2\phi + 16\sin\theta_1\cos\theta_1\sin\theta_2\cos\theta_2\cos\phi\right)\right\}, \tag{1.83}$$

$$U_{\mu,\text{ind}\,\mu} = \frac{1}{\left(4\pi\varepsilon_o\right)^2}\left\{-\frac{1}{2}\,\alpha_s\mu^2 R^{-6}\left[\left(3\cos^2\theta_1 - 1\right) + \left(3\cos^2\theta_2 - 1\right)\right]\right\}, \tag{1.84}$$

and

$$U_{\theta,\text{ind}\,\mu} = \frac{1}{\left(4\pi\varepsilon_o\right)^2}\left\{-\frac{9}{8}\,\alpha_s\theta^2 R^{-8}\left(4\cos^4\theta_1 + 4\cos^4\theta_2 + \sin^4\theta_1 + \sin^4\theta_2\right)\right\}. \tag{1.85}$$

Here, $U_{\mu,\text{ind}\,\mu}$ has been written so that its unweighted orientational average is zero and the orientational-independent part is assumed to be incorporated in the R^{-6} term of U_{LJ} [28]. In the two induction terms, the mean static polarizability α_s is used to describe the quasi-static interaction.

The shape potential is [28]

$$U_{\text{shape}} = 4D\varepsilon\left[\frac{R_o}{R}\right]^{12}\left(3\cos^2\theta_1 + 3\cos^2\theta_2 - 2\right), \tag{1.86}$$

where D is a dimensionless parameter called the shape factor, and which

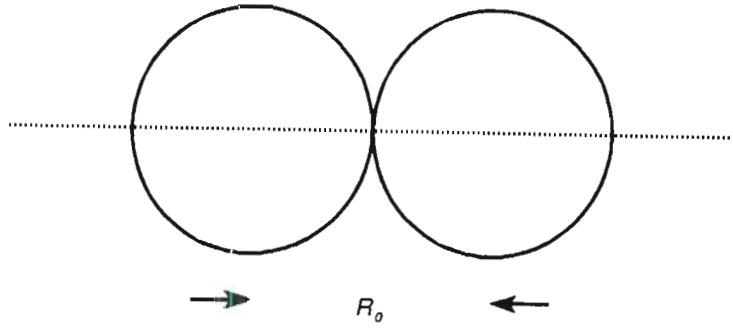

Figure 1.2 (a). Colliding spheres.

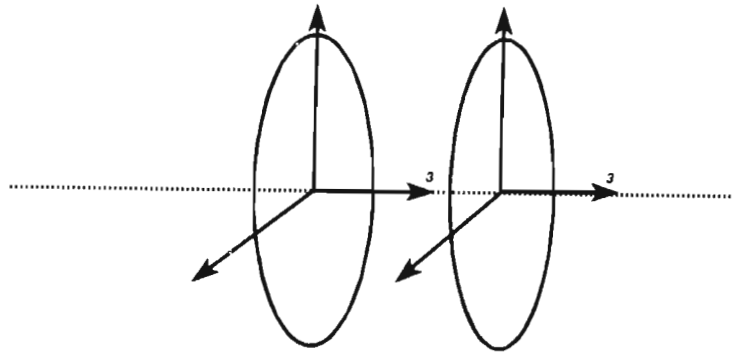

Figure 1.2 (b). Colliding plates where θ_1 and θ_2 are 0 or π.

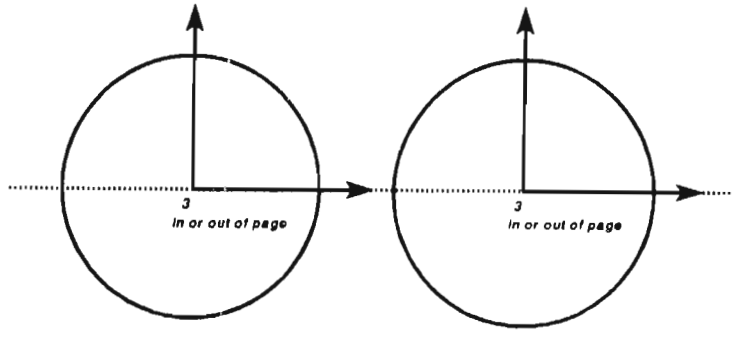

Figure 1.2 (c). Colliding plates where θ_1 and θ_2 are $\pm(\pi/2)$.

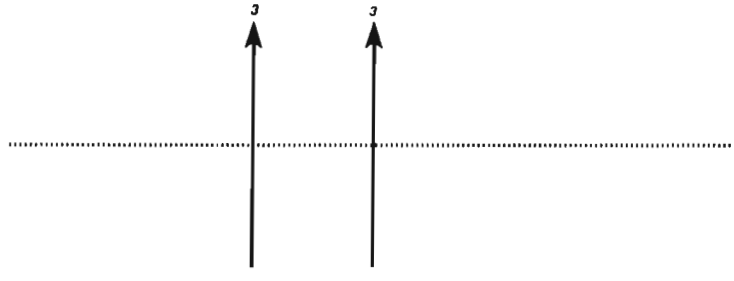

Figure 1.2 (d). Colliding infinitely thin rods where θ_1 and θ_2 are $\pm(\pi/2)$.

lies in the range -0.25 to +0.50 to ensure that the R^{-12} term is always repulsive at short range. D is zero for spherical molecules, positive for rod-like molecules (i.e. molecules which are elongated in the direction of the axis of the dipole moment [47], such as fluoromethane), and negative for plate-like molecules (i.e. molecules which are fore-shortened along the axis of the dipole moment [47], such as trifluoromethane). This can be seen more clearly by the following analysis.

For colliding spheres of diameter R_o, as depicted in figure 1.2 (a), the Lennard-Jones potential is zero at an approach distance $R = R_o$; while for approach distances $R < R_o$, the potential is positive and repulsive. In the case of colliding plate-like molecules in the configuration depicted in figure 1.2 (b), where θ_1 and θ_2 are 0 or π, the approach distance can be less than R_o before the onset of contact forces. The repulsive R^{-12} term of U_{LJ} must be *reduced*, and we require a *negative* U_{shape} and hence a negative shape factor D. The very closest possible approach of two infinitely thin planes in the configuration of figure 1.2 (b) is for R = 0: there is *no* repulsive or contact potential, and $D = -\frac{1}{4}$. Of course, for plate-like molecules of finite thickness, D will not reach this extreme value. When the colliding molecules approach as in figure 1.2 (c), where θ_1 and θ_2 are $\pm\frac{\pi}{2}$, a negative D yields a *positive* U_{shape} which enhances the repulsive potential, so that contact forces first occur for $R > R_o$. A similar analysis can be applied to rod-like molecules, where the closest possible approach of two infinitely thin rods in the configuration of figure 1.2 (d), where θ_1 and θ_2 are $\pm\frac{\pi}{2}$, occurs for R = 0. For this extreme case, $D = +\frac{1}{2}$, and any finite thickness in the molecules will reduce this number.

The energy expressions in equations (1.80) to (1.86) are directly applicable to pair interactions of linear dipolar molecules, but are easily adjusted to accommodate for interactions between non-polar linear molecules or between spherical molecules simply by setting the relevant multipole moments to zero. Earlier workers [45-48] have considered CH_3F, CHF_3, CH_3Cl, and CH_3CH_3 to be linear molecules with their dipoles lying along their threefold rotation axes; and the calculations of B_ρ undertaken in [6,7] were based upon this treatment.

1.4.3 Evaluation of B_ρ by numerical integration

The calculation of second virial coefficients of various molecular properties such as the second refractivity virial coefficient B_R [49,28,46,50] and the second Kerr virial coefficient B_K [80,52] requires integration of the relevant functions over the molecular interaction co-ordinates τ. Early calculations were performed using the H_K functions tabulated by Buckingham and Pople [28]; and subsequently, the advent of the computer either simplified, or in some cases *made possible*, the theoretical evaluation of virial coefficients. Initially the numerical integrations were computed using Simpson's rule for integration, primarily because of the ease with which this method is programmed into the computer [53]. Weller [53] undertook an extensive comparison of this integration method with that of Gaussian quadrature, showing that for a given precision only half the number of intervals per integration variable are required for the Gaussian method. This was found to yield a saving in computer time by a factor of at least sixteen for the integration of interaction effects for linear molecules over the four co-ordinates θ_1, θ_2, R, and ϕ. Consequently, all the calculations of B_ρ in [6,7] (requiring the calculation of the averages $\langle X \rangle$ in equations (1.69) to (1.76) by numerical integration of the appropriate form of equation (1.50)) were performed using Gaussian quadrature. A very useful feature of the Macsyma symbolic manipulation package is its ability to translate the final expressions for a_3' to $a_3 C_1'$ directly into Fortran code, thus preventing the introduction of errors into the integration arguments.

In the integration procedure, the ranges of θ_1, θ_2, and ϕ were divided into sixteen intervals while R was given a range of 0.1 to 3.0 nm divided into sixty four intervals. Since ϕ always enters through the cosine function, the ϕ integral from 0 to 2π was replaced by twice the integral from 0 to π to further reduce the time taken for computer calculation. The Fortran programs were run in double precision on an AST 25 MHz 80386 personal computer (with an Intel 80387 maths coprocessor) using the fast University of Salford FTN77/386 compiler. Typical running times of the programs ranged from 4 minutes to 15 minutes, depending on the complexity of the integration argument. Doubling the number of intervals for θ_1, θ_2, and ϕ to 32 led to numerical results which, on

Table 1.2. Wavelength-independent molecular parameters used in the calculations.

Molecule	$\frac{10^{40}\alpha_s}{C^2m^2J^{-1}}$	$\frac{10^{30}\mu}{Cm}$	$\frac{10^{40}\theta}{Cm^2}$	$\frac{R_o}{nm}$	$\frac{\varepsilon/k}{K}$	D
N_2	1.936 [60]	0	-4.72 [69]	0.368 [54]	91.50 [54]	0.112 * [(76)]
CO_2	3.245 [51]	0	-15.0 [70]	0.400 [74]	190.0 [74]	0.250 * [(59,76)]
CH_3CH_3	4.940 [61]	0	-3.34 [71]	0.4418 [54]	230 [54]	0.200 * [(59)]
CH_2CH_2	4.69 [62]	0	6.60 [58]	0.4232 [63]	205 [54]	0.240 * [(76,77)]
OCS	6.353 [63]	2.365 [66]	-2.635 [72]	0.413 [54]	335 [54]	0.200 †
CO	2.17 [54]	0.3740 [67]	-8.58 [69]	0.3765 *	92 *	0.050 * [(59,77)]
CH_3F	3.305 [48]	6.170 [45]	7.70 [45]	0.377 *	200 *	0.256 * [(59)]
CHF_3	3.970 [48]	5.50 [45]	15.0 [45]	0.440 *	178.5 *	-0.050 * [(59)]
CH_3Cl	5.25 [64]	6.32 [64]	4.00 [73]	0.395 [60]	350 [64]	0.210 * [(59)]
HCl	2.867 [65]	3.646 [68]	12.4 [68]	0.3641 [75]	191.4 [75]	0.010 †

* Obtained by fitting to the pressure virial coefficients quoted in the references denoted [( )].

† Assigned on the basis of shape.

comparison with those obtained when using 16 intervals, were found to agree to at least seven significant figures. Hence, the division into 16 intervals was retained for all calculations in order to save on computer time. A useful double check on the calculations was the evaluation of, for example, the integral of each of the six components of a_4 in equation (1.25); the sum of these component parts then being compared with the integral of the compact form of a_4 in equation (1.55). Repeating this procedure for a_5, etc., the values obtained from the two methods were always found to agree at least to within the sixth significant figure for all the gases investigated.

1.4.4 Molecular properties used in the calculations

The data used in the calculations of B_ρ are summarized in table 1.2, table 1.3, and table 1.4. Table 1.2 lists the wavelength-independent molecular parameters, while table 1.3 gives values of ρ_o, α_ν, and κ at 632.8 nm, 514.5 nm, and 488.0 nm respectively, with table 1.4 giving the only available A-tensor and C-tensor components for the molecules studied in [6,7], many of which are estimated trial values. Wherever possible, published experimental values were used.

Few, if any, definitive values of the shape factor D are available in the literature, and those listed here were obtained by fitting calculated values of the second pressure virial coefficient B(T) to reported experimental values over a wide range of temperatures. B(T) was calculated according to the well-known expression for axially-symmetric molecules [54-56]

$$B(T) = \frac{N_A}{2}\int_{R=0}^{\infty}\int_{\theta_1=0}^{\pi}\int_{\theta_2=0}^{\pi}\int_{\phi=0}^{2\pi}\left[1-\exp\left(-U_{12}/kT\right)\right]R^2 dR\,\sin\theta_1\sin\theta_2 d\theta_1 d\theta_2 d\phi. \tag{1.87}$$

The values thus obtained for D were all physically reasonable in terms of the criteria stated in section *1.4.2*.

It should be noted that calculations of the terms arising from field-gradient effects and induced quadrupole moments in the molecular

able 1.3. Values of ρ_o, α_ν and κ at 632.8 nm, 514.5 nm and 488.0 nm used in the calculations. Unless otherwise stated, all data re drawn from Bogaard, Buckingham, Pierens and White [2].

olecule	$100\rho_o$ at λ/nm			$10^{40}\alpha_\nu/C^2m^2J^{-1}$ at λ/nm			κ at λ/nm		
	632.8	514.5	488.0	632.8	514.5	488.0	632.8	514.5	488.0
N_2	1.042	1.059 [11]	1.05 [39]	1.961 [46, 78]	1.979	1.984	0.1327	0.1338 [11]	0.1332 [39]
CO_2	4.049	4.085	4.12	2.907 [46, 78]	2.957	2.965	0.2671	0.2683	0.2696
CH_3CH_3	0.166	0.188	0.190	5.01	5.06	5.07	0.0526	0.0560	0.0563
CH_2CH_2	1.207	1.247	1.266	4.70	4.76	4.78	0.1428*	0.1454*	0.1466*
OCS	3.88	3.95	4.00	5.79	5.85	5.86	0.261	0.264	0.2654
CO	0.480	0.519	0.521	2.200	2.223	2.231	0.0897	0.0933	0.0935
CH_3F	0.094	-	-	2.916 [46, 78]	-	-	0.0396	-	-
CHF_3	0.0504	0.07	0.07	3.097 [46, 78]	3.139	3.145	-0.029	-0.034	-0.034
CH_3Cl	0.755	0.779	0.787	5.04	5.10	5.12	0.133	0.115	0.115
HCl	0.079 [21]	-	-	2.893 [46, 78]	-	-	0.0365	-	-

*Effective $|\kappa|$ treating CH_2CH_2 as a quasi-linear molecule.

interactions are severely hampered by a dearth of numerical values for the A- and C-tensor components. It is, of course, highly desirable to know the relative magnitudes of these terms to gain insight into how significant their contributions to B_ρ are. Fortunately, the molecule HCl has an almost comprehensive range of calculated and observed molecular parameters at the wavelength 632.8 nm. Even so, values for the C-tensor for HCl were *not* available, and so these were estimated by scaling the values quoted by Rivail and Cartier [57] for HF in proportion to the relative values of the α- and A-tensor components for HCl and HF at λ = 632.8 nm. The scaled C-tensor components for HCl were in turn scaled in proportion to the α-tensor to obtain estimated trial values for the molecules CHF_3 and CH_3F at λ = 632.8 nm. A-tensor components at this wavelength are available for CH_3F and CO, but not for CHF_3.

Table 1.4. Estimated A-tensor and C-tensor components at λ = 632.8 nm. (Unless otherwise indicated, all data are drawn from Burns, Graham and Weller [46].)

	HCl	CO	$CHF_3^{(a)}$	$CHF_3^{(b)}$	CH_3F^*
$10^{50}A_{\parallel}/C^2m^3J^{-1}$	1.16	-0.981 [58]	-	-	1.72 [58]
$10^{50}A_{\perp}/C^2m^3J^{-1}$	0.133	-1.181 [58]	-	-	2.77 [58]
$10^{60}C_{1111}/C^2m^4J^{-1}$	0.8144†	-	1.10	0.90	0.85
$10^{60}C_{1313}/C^2m^4J^{-1}$	0.6588†	-	0.75	0.75	0.67
$10^{60}C_{3333}/C^2m^4J^{-1}$	1.0504†	-	0.90	1.10	1.06

† Estimated values by scaling of values quoted for HF by Rivail and Cartier [57].

(a), (b), and * are trial values of the relevant C-tensor components estimated by scaling the corresponding components of HCl in proportion to the polarizability tensors α [46].

Published experimental pressure virial coefficients for HCl and OCS were not found in the literature, and so the fitting procedure to find D was not possible. A D value of 0.20 was assigned to OCS, while a value of 0.01 was assigned to HCl; these values being considered physically

Table 1.5. Summary of calculations for T = 298.2 K and λ = 632.8 nm, with relative magnitudes of the a_5 dipole-dipole contribution to B_ρ.

Molecule	$10^6 G$ / $m^3 mole^{-1}$	$10^6 \mathfrak{G}_3$ / $m^3 mole^{-1}$	$10^6 a_3$ / $m^3 mole^{-1}$	$10^6 a_4$ / $m^3 mole^{-1}$	$10^6 a_5$ / $m^3 mole^{-1}$	$10^6 \varphi'_\rho$ ** / $m^3 mole^{-1}$	$10^6 B$ / $m^3 mole^{-1}$	$10^6 B_\rho^{\dagger}(a_5)$ / $m^3 mole^{-1}$	$10^6 B_\rho^{\ddagger}(a_4)$ / $m^3 mole^{-1}$	$B_\rho(a_5)/B_\rho(a_4)$
N_2	0.250	0.174	-4.701	27.571	0.733	24.027	-4.6	0.152	0.145	1.05
CO_2	4.151	1.500	-11.800	19.010	0.138	12.999	-122	-8.848	-8.854	1.00
CH_3CH_3	4.786	0.846	-133.352	768.633	41.454	682.367	-185	0.517	0.449	1.15
CH_2CH_2 *	4.709	2.298	-54.161	110.455	3.970	62.562	-136	-2.487	-2.534	0.98
OCS	8.785	8.797	-73.259	88.947	0.614	33.884	-304 ††	-21.123	-21.125	1.00
CH_3Cl	24.647	3.271	-121.445	421.765	25.671	353.909	-406	-3.424	-3.616	0.95

* This calculation is for positive κ (A negative κ is not physically reasonable [6]).

** φ'_ρ includes the a_5 contribution.

† $B_\rho(a_5)$ includes the a_5 contribution.

‡ $B_\rho(a_4)$ does not include the a_5 term.

†† Calculated.

reasonable bearing in mind the constraints on D for rod-like molecules discussed in section *1.4.2*. The B(T) values required in the evaluation of B_ρ for HCl and for OCS were calculated according to equation (1.87). For all the other molecules studied, *experimental* values of B(T) were used in the evaluation of B_ρ, as given in equation (1.68).

1.4.5 Results and discussion

The results of the calculations for T = 298.2 K are presented as follows:

(i) Table 1.5 contains a summary of the calculations at λ = 632.8 nm for those molecules which have no available A- and C-tensor components. A comparison is made of B_ρ containing terms up to α^4 in the scattered intensity (i.e. the series of terms in the scattered intensity is truncated after the a_4 term) with B_ρ containing terms up to α^5 (i.e. now including the a_5 contributions). It is apparent that the a_5 term *does* make a significant contribution of between -5% and 15% to B_ρ; however, it can be seen that the series is now rapidly converging so that the a_6 and higher-order terms in the dipole-dipole interaction should contribute negligibly to B_ρ.

(ii) Table 1.6 contains a summary of the calculations at λ = 632.8 nm for those molecules which have known A-tensor and/or C-tensor components. It is evident that while the a_5 contribution is significant (from about 5% to 10%), the field gradient and induced quadrupole terms for HCl and CO are much smaller and hence negligible. For CH_3F, the $a_2\mathcal{A}_1$ term makes quite a significant contribution to B_ρ of -9%, whilst the $a_3\mathcal{A}_1$ and $a_3\mathcal{C}_1$ terms make negligible contributions.

(iii) Table 1.7 and table 1.8 contain a summary of the calculations at λ = 514.5 nm and λ = 488.0 nm respectively; once again a comparison being made of B_ρ correct to a_4 with B_ρ correct to a_5. Unfortunately, at both wavelengths there are *no available* A- and C-tensor components for any of the gases investigated here.

Table 1.6. Relative magnitudes of the various contributions to B_ρ for T = 298.2 K and λ = 632.8 nm where A- and C-tensors are available.

Term	HCl		CO		CHF_3 (a)		CHF_3 (b)		CH_3F	
	10^6 numerical value $m^3 mole^{-1}$	% of B_ρ	10^6 numerical value $m^3 mole^{-1}$	% of B_ρ	10^6 numerical value $m^3 mole^{-1}$	% of B_ρ	10^6 numerical value $m^3 mole^{-1}$	% of B_ρ	10^6 numerical value $m^3 mole^{-1}$	% of B_ρ
G	4.707	0.56	0.474	0.87	5.410	0.83	5.410	0.83	19.302	2.93
$\mathfrak{b}_3$	-0.221	-0.03	0.014	0.03	0.196	0.03	0.196	0.03	0.344	0.05
a_3	60.023	7.14	-0.767	-1.41	-95.601	-14.72	-95.601	-14.72	-97.054	-14.76
a_4	973.693	115.81	69.156	127.45	1046.500	161.15	1046.500	161.12	1083.593	164.83
a_5	63.926	7.60	2.438	4.49	47.004	7.24	47.004	7.24	66.920	10.18
$a_2\mathcal{A}_1$	-8.410	-1.00	-0.444	-0.82	-	-	-	-	-58.704	-8.93
$a_3\mathcal{A}_1$	-0.661	-0.08	-0.009	-0.02	-	-	-	-	-3.296	-0.49
$a_3\mathcal{C}_1$	1.157	0.14	-	-	0.126	0.02	0.025	0.00_4	0.305	-0.05
2B	-254.2	-30.23	-16.6	-30.57	-354	-54.51	-354	-54.51	-418	-53.85
B'_ρ	840.7		593.4		649.4		593.4		649.4	
B_ρ	0.663		0.557		0.327		0.557		0.327	

Table 1.7. Summary of calculations for T = 298.2 K and λ = 514.5 nm, showing relative magnitudes of the a_5 dipole-dipole contribution to B_ρ.

Molecule	$10^6 G$ / $m^3 mole^{-1}$	$10^6 \ell_3$ / $m^3 mole^{-1}$	$10^6 a_3$ / $m^3 mole^{-1}$	$10^6 a_4$ / $m^3 mole^{-1}$	$10^6 a_5$ / $m^3 mole^{-1}$	$10^6 \varphi'_\rho$ ** / $m^3 mole^{-1}$	$10^6 B$ / $m^3 mole^{-1}$	$\frac{\varphi'_\rho}{2B}$	$10^6 B_\rho^{\dagger}(a_5)$ / $m^3 mole^{-1}$	$10^6 B_\rho^{\ddagger}(a_4)$ / $m^3 mole^{-1}$	$\frac{B_\rho(a_5)}{B_\rho(a_4)}$
N_2	0.250	0.177	-4.646	27.276	0.738	23.795	-4.6	-2.59	0.152	0.145	1.05
CO_2	4.151	1.533	-11.321	18.485	0.140	12.988	-122	-0.05	-8.923	-8.928	1.00
CH_3CH_3	4.786	0.910	-126.652	690.688	37.206	606.938	-185	-1.64	0.444	0.375	1.18
CH_2CH_2 *	4.709	2.371	-53.164	107.860	3.918	65.694	-136	-0.24	-2.530	-2.578	0.98
OCS	8.785	8.996	-69.673	84.739	0.540	33.387	-304 ††	-0.05	-21.501	-21.522	1.00
CO	0.474	0.015	-0.745	65.064	2.301	67.109	-8.3	-4.04	0.260	0.248	1.05
CHF_3	5.410	0.233	-82.595	781.840	35.943	740.831	-177	-2.09	0.271	0.245	1.11
CH_3Cl	24.647	3.371	-119.902	413.607	25.431	347.154	-406	-0.43	-3.584	-3.780	0.95

* This calculation is for positive κ (A negative κ is not physically reasonable [6]).

** φ'_ρ includes the a_5 contribution.

† $B_\rho(a_5)$ includes the a_5 contribution.

‡ $B_\rho(a_4)$ does not include the a_5 term.

†† Calculated.

Table 1.8. Summary of calculations for T = 298.2 K and λ = 488.0 nm, showing relative magnitudes of the a_5 dipole-dipole contribution to B_ρ.

Molecule	$10^6 G$ / $m^3 mole^{-1}$	$10^6 \mathfrak{a}_3$ / $m^3 mole^{-1}$	$10^6 a_3$ / $m^3 mole^{-1}$	$10^6 a_4$ / $m^3 mole^{-1}$	$10^6 a_5$ / $m^3 mole^{-1}$	$10^6 \varphi'_\rho$ ** / $m^3 mole^{-1}$	$10^6 B$ / $m^3 mole^{-1}$	$\frac{\varphi'_\rho}{2B}$	$10^6 B^{\dagger}_\rho(a_5)$ / $m^3 mole^{-1}$	$10^6 B^{\ddagger}_\rho(a_4)$ / $m^3 mole^{-1}$	$\frac{B_\rho(a_5)}{B_\rho(a_4)}$
N_2	0.250	0.176	-4.742	28.032	0.752	24.468	-4.6	-2.66	0.158	0.150	1.05
CO_2	4.151	1.545	-11.973	19.527	0.142	13.392	-122	-0.05	-8.979	-8.985	1.00
CH_3CH_3	4.786	0.917	-126.584	687.837	36.987	603.942	-185	-1.63	0.443	0.373	1.19
CH_2CH_2 *	4.709	2.401	-53.934	108.994	3.875	66.044	-136	-0.24	-2.563	-2.612	0.98
OCS	8.785	9.062	-73.461	89.146	0.512	34.045	-304 ††	-0.06	-21.734	-21.753	1.00
CO	0.474	0.015	-0.752	65.721	2.315	67.773	-8.3	-4.08	0.265	0.253	1.05
CHF_3	5.410	0.233	-82.830	785.558	36.149	744.520	-177	-2.10	0.273	0.248	1.10
CH_3Cl	24.647	3.384	-121.646	421.268	25.731	353.384	-406	-0.44	-3.571	-3.772	0.95

* This calculation is for positive κ (A negative κ is not physically reasonable [6]).

** φ'_ρ includes the a_5 contribution.

† $B_\rho(a_5)$ includes the a_5 contribution.

‡ $B_\rho(a_4)$ does not include the a_5 term.

†† Calculated.

In deciding on whether a term's percentage contribution to B_ρ was significant or not, consideration was made of the fact that typical uncertainties in careful experimental observations of B_ρ lie between 1% and 10%. Dymond and Smith [59] in their compilation of pressure virial coefficients classify the values as Class I if the precision is better than 2%, Class II if it lies between 2% and 10%, and Class III if worse than 10%. Class I or at least Class II data are available for most gases. Therefore, in theoretical investigations of the scattering contribution $\mathcal{Y}_\rho$ to B_ρ through equation (1.68) it is not realistic to attach significance to contributions less than 1%. On the other hand, contributions of the order of 10% are significant, and the work carried out in [7] serves to establish that the dipole-dipole terms up to the fifth order in the scattered intensities *must* be retained, while the $a_2 A_1$ term also needs attention. Disagreements between experiment and theory are unlikely to be due to convergence problems beyond these limits; and would then most probably be due to uncertainties in molecular data, the intermolecular potential expression, or other deficiencies in the model. It is worth noting that the numerical integration procedures used in [6,7] have a precision of much better than 1%, and are not a factor in comparisons between experiment and theory.

Now, in selecting gases which could be profitably investigated experimentally, it is useful to combine equations (1.68) and (1.78); yielding

$$B_\rho = \rho_o \left(1 - \tfrac{4}{3}\rho_o\right)\left(2B + \mathcal{Y}_\rho\right) . \qquad (1.88)$$

As has already been mentioned, the appearance of 2B in the expressions for B_ρ can mask the more interesting $\mathcal{Y}_\rho$ contributions; the ratio $\left(\mathcal{Y}_\rho/2B\right)$ thus providing a means of selecting those gases where the $\mathcal{Y}_\rho$ terms contribute more substantially to B_ρ. Table 1.7 and table 1.8 contain the ratio $\left(\mathcal{Y}_\rho/2B\right)$ for several gases at λ = 514.5 nm and λ = 488.0 nm respectively, the ratio being most favourable for HCl, CO, N_2, CH_3F, CHF_3, and CH_3CH_3. For CO_2 and OCS, the ratio is particularly *unfavourable*.

Table 1.9 Suppliers and minimum stated purity of the gases used.

Gas	Supplier	Grade	Stated minimum purity %
N_2	Fedgas	High purity	99.98
CO_2	Matheson	Coleman instrument	99.99
CH_3Cl	Matheson	Standard	99.5
CH_3CH_3	Matheson	C.P.	99.0
CO	Matheson	C.P.	99.5

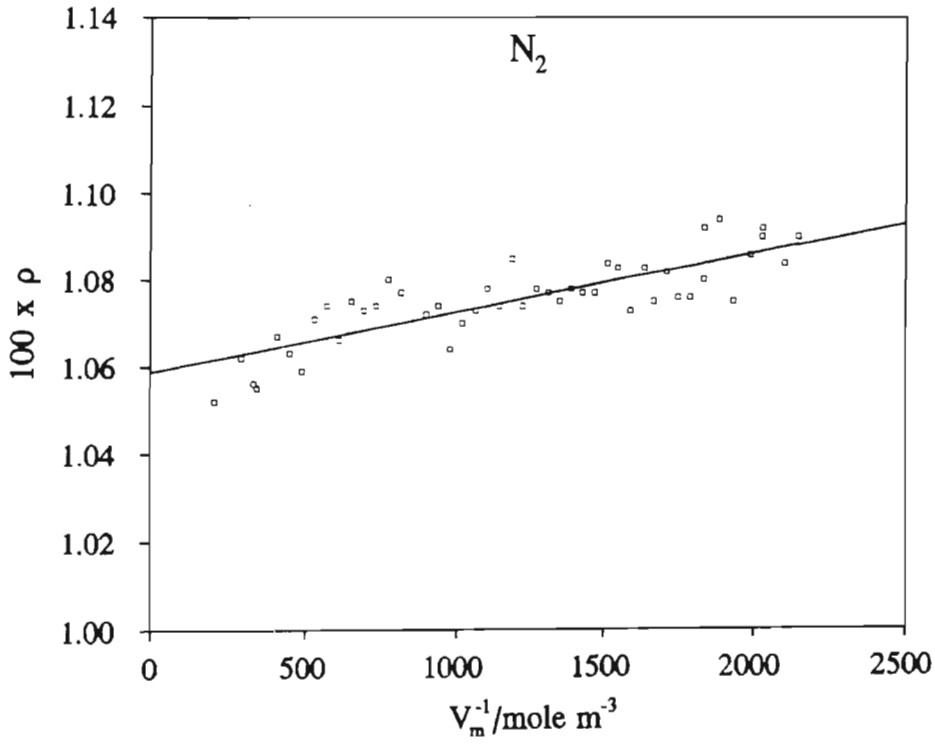

Figure 1.3. Experimental depolarization ratio as a function of gas density for N_2.

Measurements of the second light-scattering virial coefficient B_ρ for five different gases were undertaken by Couling and Graham [11], and the results are now presented and compared with the above calculated values. Where possible, comparisons are also made with experimental values in the literature.

1.5 Comparison of measured and calculated second light-scattering virial coefficients of linear and quasi-linear molecules

The light-scattering apparatus used in the measurements reported in [11] is described in detail in Chapter 3. Depolarization ratios ρ were measured at λ = 514.5 nm over a range of gas densities for N_2, CO_2, CH_3CH_3, CH_3Cl and CO at room temperature; and a value of B_ρ for each gas was obtained as the slope of the linear region of a ρ versus V_m^{-1} plot. The molar volumes V_m were determined using the appropriate second and third pressure virial coefficients deduced from tabulations by Dymond and Smith [59].

The results for N_2, CO_2, CH_3CH_3, CH_3Cl and CO are plotted in figures 1.3 to 1.7, each of which shows the depolarization as a function of inverse molar volume. Gas purities are specified in table 1.9, while deduced values of ρ_o are summarized in table 1.10 together with values measured by other workers. Deduced values of B_ρ and $\mathcal{G}_\rho$, together with any comparable literature values, are summarized in table 1.11; which also includes a comparison with calculated theoretical values.

For the five gases investigated experimentally in [11], the observed B_ρ values are between 3% and 18% lower than the corresponding calculated values. As expected, the experimental $\mathcal{G}_\rho$ for CO_2, which accounts for only 5% of the observed second light-scattering virial coefficient, is considerably in error, and is not a fair test of the theory. Also shown in table 1.11 are calculated values of B_ρ at the conditions of reported literature experimental values of other workers. The molecular data used in the calculations are as reported in tables 1.2 to 1.4. There is a large scatter of between 3% and 22% in the levels of agreement, but here the sources of error are unknown.

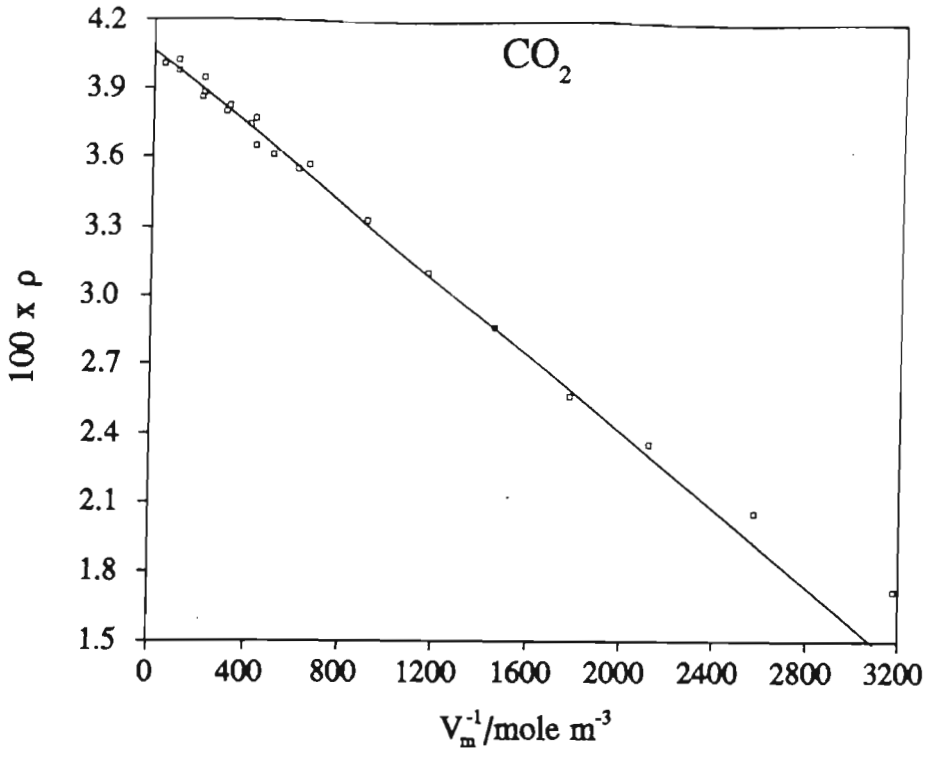

Figure 1.4. Experimental depolarization ratio as a function of gas density for CO_2.

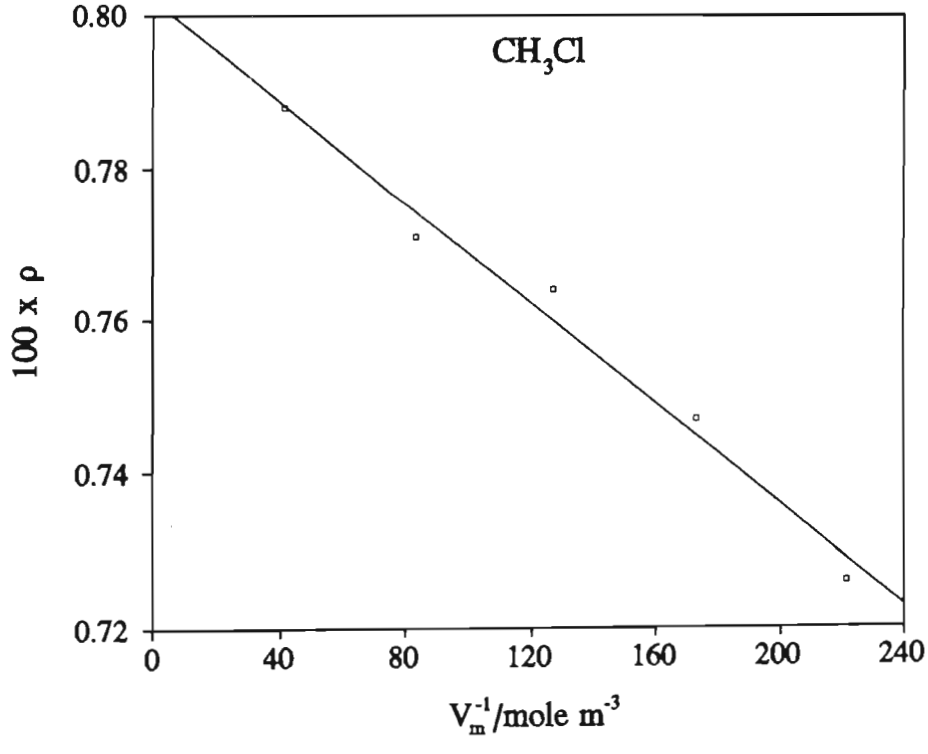

Figure 1.5. Experimental depolarization ratio as a function of gas density for CH_3Cl.

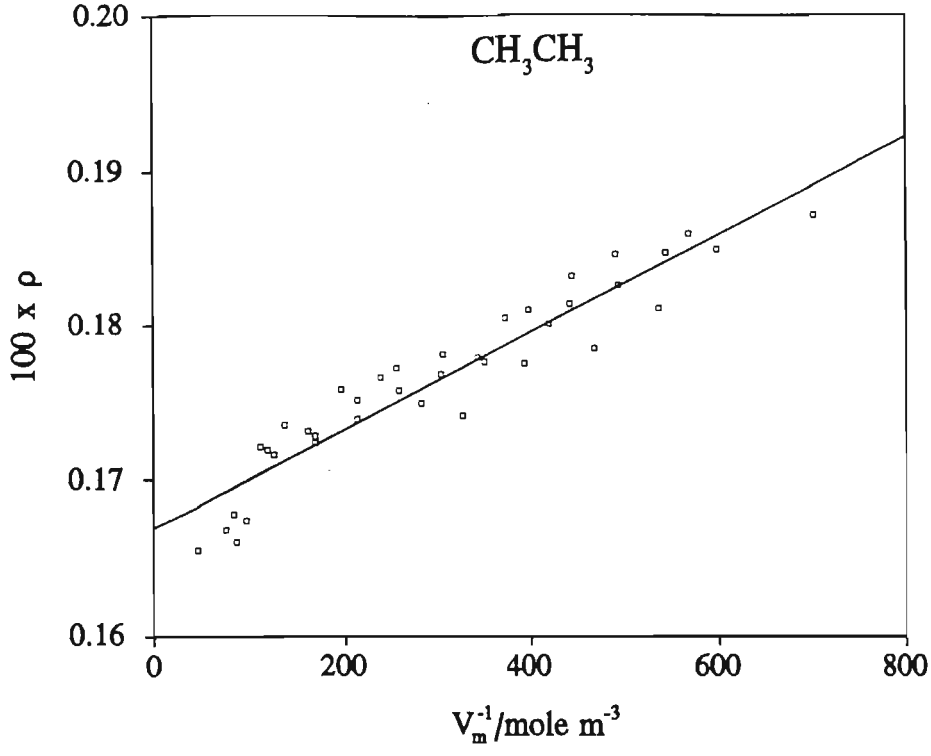

Figure 1.6. Experimental depolarization ratio as a function of gas density for CH_3CH_3.

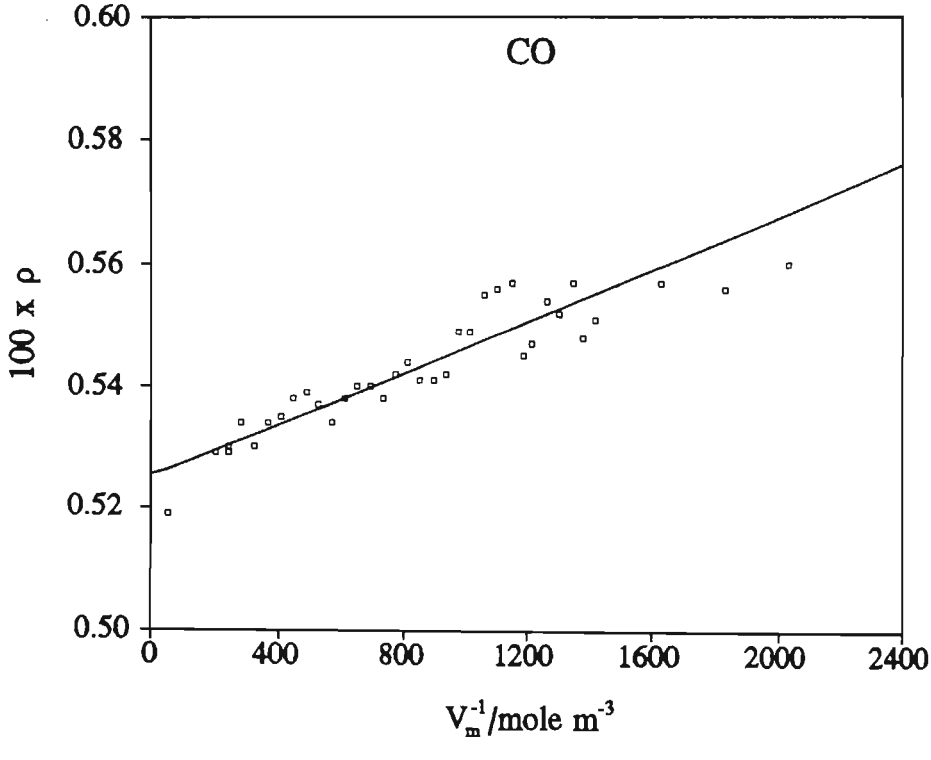

Figure 1.7. Experimental depolarization ratio as a function of gas density for CO.

Table 1.10. A collective summary of measured depolarization ratios ρ_o at a wavelength of 514.5 nm for the five gases investigated [11].

Molecule	$100 \times \rho_o$			
	Couling and Graham [11]	Bogaard *et al.* [2]	Baas *et al.* [25]	Alms *et al.* [23]
N_2	1.0587 ± 0.0019	-	1.01 ± 0.03	1.06 ± 0.02
CO_2	4.072 ± 0.011	4.085 ± 0.02	4.0 ± 0.1	4.15 ± 0.05
CH_3Cl	0.802 ± 0.004	0.779 ± 0.008	0.75 ± 0.02	0.78 ± 0.01
CH_3CH_3	0.1669 ± 0.006	0.188 ± 0.004	0.168 ± 0.006	-
CO	0.5251 ± 0.0014	0.519 ± 0.007	0.49 ± 0.02	-

Table 1.11. Summary of our measured B_ρ values for linear and quasi-linear molecules [11], together with all literature values. Comparison is made with values calculated at the experimental temperatures and wavelengths. $\mathcal{G}_\rho$ values deduced from our measured B_ρ values are also compared with calculated $\mathcal{G}_\rho$ values.

Molecule	Reference	λ/nm	T/K	$10^6 B_\rho^{(expt)}$ / $m^3 mole^{-1}$	$10^6 B_\rho^{(theory)}$ / $m^3 mole^{-1}$	$B_\rho^{(expt)} / B_\rho^{(theory)}$	$10^6 \mathcal{G}_\rho^{(expt)}$ / $m^3 mole^{-1}$	$\mathcal{G}_\rho^{(expt)} / \mathcal{G}_\rho^{(theory)}$
N_2	[39]	488.0	290	0.14	0.115	1.22		
	[41]	514.5	310	0.16	0.199	0.80		
	[11]	514.5	295.5	0.138 ± 0.014	0.142	0.97	23.4	0.98
CO_2	[39]	488.0	300	-10	-9	1.11		
	[11]	514.5	298.2	-8.29 ± 0.16	-8.89	0.93	28.7	2.21
CH_3Cl	[11]	514.5	299.6	-3.30 ± 0.26	-3.68	0.90	386	1.14
CH_3CH_3	[11]	514.5	295.9	0.315 ± 0.018	0.381	0.83	565	0.93
CO	[11]	514.5	298.2	0.213 ± 0.016	0.259	0.82	57.4	0.87
CH_2CH_2 †	[40]	514.5	328	-1.78	-1.94	0.92		
OCS †	[39]	488.0	291	-21	-21.7	0.97		

† measurements of these gases were not undertaken in [11] because of unfavourable $\mathcal{G}/2B$ ratios.

1.6 The aim of this work

Studies undertaken by several workers on the various virial coefficients, such as the second refractivity virial coefficient B_R [46,79], the second dielectric virial coefficient [48,51], and the second Kerr-effect virial coefficient [80,52,9], have revealed good agreement between theory and experiment for some spherical and linear molecules, and very poor agreement for others.

The inclusion of the second light-scattering virial coefficient in the range of studied second virial coefficients makes possible a critical overview of the full range of coefficients. Certainly, for the five linear and quasi-linear gases investigated in [6,7,11], the agreement between experiment and theory for B_ρ is much better than might have been expected, especially in view of the apparent breakdown in the long-range dipole-induced-dipole theory in calculations of B_ρ for the larger quasi-spherical molecules [4]. It is this success that has prompted us to extend the theory of second virial coefficients to describe the effects which interactions between pairs of non-linear molecules have on molecular-optic phenomena.

This thesis is concerned in part with extending the molecular tensor theory of the second light-scattering virial coefficient B_ρ into the regime of molecules with non-linear symmetry. Chapter 2 contains this new theory, together with the results of calculations for ethene, sulphur dioxide and dimethyl ether. In Chapter 3, the development of the light-scattering apparatus is discussed. The apparatus has been substantially improved since the paper by Couling and Graham [11] to allow for experiments at elevated temperatures. This feature allows pressure-dependence measurements of vapours with low saturation vapour pressures to be undertaken. The experimental results for ethene and sulphur dioxide are presented, together with a comprehensive comparison with the values predicted theoretically. The levels of success achieved prompted application of the new techniques to a different second virial coefficient, namely that of the Kerr effect.

In Chapter 4, all theoretical and experimental work undertaken on the second Kerr-effect virial coefficient B_K to date is reviewed. A theory of B_K for molecules with non-linear symmetry is then developed. Values of B_K for several linear and non-linear molecules are calculated and compared with measured data in the literature.

1.7 References

[1] Andrews, A. L., and Buckingham, A. D., 1960, *Molec. Phys.*, **3,** 183.

[2] Bogaard, M. P., Buckingham, A. D., Pierens, R. K., and White, A. H., 1978, *J. chem. Soc. Faraday Trans.* I, **74,** 3008.

[3] Silberstein, L., 1917, *Phil. Mag.*, **33,** 92, 521.

[4] Watson, R. C., and Rowell, R. L., 1974, *J. chem. Phys.*, **52,** 132.

[5] Dunmur, D. A., Hunt, D. C., and Jessup, N. E., 1979, *Molec. Phys.*, **37,** 713.

[6] Graham, C., 1992, *Molec. Phys.*, **77,** 291.

[7] Couling, V. W., and Graham, C., 1993, *Molec. Phys.*, **79,** 859.

[8] Gentle, I. R., Laver, D. R., and Ritchie, G. L. D., 1990, *J. phys. Chem.*, **94,** 3434.

[9] Buckingham, A. D., Galwas, P. A., and Liu Fan-Chen, 1983, *J. Mol. Struct.*, **100,** 3.

[10] Buckingham, A. D., and Pople, J. A., 1956, *Disc. Faraday Soc.*, **22,** 17.

[11] Couling, V. W., and Graham, C., 1994, *Molec. Phys.*, **82,** 235.

[12] Tyndall, J., 1869, *Phil. Mag.*, **37,** 384.

[13] Kerker, M., 1969, *The Scattering of Light* (New York: Academic).

[14] Strutt, J. W., (Third Baron Rayleigh), 1871, *Phil. Mag.*, **44,** 28.

[15] Strutt, J. W., (Third Baron Rayleigh), 1899, Scientific Papers IV, 397.

[16] Cabannes, J., 1915, *Comptes Rendus*, **160,** 62.

[17] Strutt, R. J., (Fourth Baron Rayleigh), 1918, *Proc. Roy. Soc. Lond.* A, **94,** 453.

[18] Strutt, R. J., (Fourth Baron Rayleigh), 1920, *Proc. Roy. Soc. Lond.* A, **97,** 435.

[19] Powers, J., 1961, *J. chem. Phys.*, **35,** 376.

[20] Bridge, N. J., and Buckingham, A. D., 1964, *J. chem. Phys.*, **40,** 2733.

[21] Bridge, N. J., and Buckingham, A. D., 1966, *Proc. Roy. Soc. Lond.* A, **295,** 334.

[22] Rowell, R. L., Aval, G. M., and Barrett, J. J., 1971, *J. chem. Phys.*, **54,** 1960.

[23] Alms, G. R., Burnham, A. K., and Flygare, W. H., 1975, *J. chem. Phys.*, **63,** 3321.

[24] Burnham, A. K., Buxton, L. W., and Flygare, W. H., 1977, *J. chem. Phys.*, **67,** 4990.

[25] Baas, F., and Van Den Hout, K. D., 1979, *Physica* A, **95,** 597.

[26] McTague, J. P., and Birnbaum, G., 1968, *Phys. Rev. Lett.*, **21,** 661.

[27] Gelbart, W. M., 1974, *Adv. chem. Phys.*, **26,** 1.

[28] Buckingham, A. D., and Pople, J. A., 1955, *Trans. Faraday Soc.*, **51,** 1173.

[29] Lennard-Jones, J. E., 1924, *Proc. Roy. Soc. Lond.* A, **106,** 441.

[30] Thibeau, M., and Oksengorn, B., 1972, *J. Phys. (Paris)*, **33,** C1-247.

[31] Hirschfelder, J. O., Curtiss, C. F., and Bird, R. B., 1954, *Molecular Theory of Gases and Liquids* (Chichester: Wiley).

[32] Tee, L. S., Gotoh, S., and Stewart, W., 1966, *Ind. Eng. Chem. Fundam.*, **5,** 356.

[33] Lallemand, P., 1971, *J. Phys. Paris*, **32,** 119.

[34] McTague, J. P., Elleson, W. D., and Hall, L. H., 1972, *J. Phys. Paris*, **33,** C1-241.

[35] Barocchi, F., and McTague, J. P., 1975, *Phys. Lett.* A, **53,** 488.

[36] Berrue, J., Chave, A., Dumon, B., and Thibeau, M., 1979, *Opt. Comm.*, **31,** 317.

[37] Benoît, H., and Stockmayer, W. H., 1956, *J. Phys. Radium*, **17,** 21.

[38] Buckingham, A. D., and Stephen, M. J., 1957, *Trans. Faraday Soc.*, **53,** 884.

[39] Dayan, E., Dunmur, D. A., and Manterfield, M. R., 1980, *J. chem. Soc. Faraday Trans.* II, **76,** 309.

[40] Berrue, J., Chave, A, Dumon, B., and Thibeau, M., 1977, *Rev. Phys. appl.*, **12,** 1743.

[41] Berrue, J., Chave, A, Dumon, B., and Thibeau, M., 1978, *J. Phys.*, **39,** 815.

[42] Berrue, J., Chave, A, Dumon, B., and Thibeau, M., 1981, *Can. J. Phys.*, **59,** 1510.

[43] Buckingham, A. D., 1967, *Adv. chem. Phys.*, **12,** 107.

[44] Buckingham, A. D., and Pople, J. A., 1955, *Proc. Phys. Soc.* A, **68,** 905.

[45] Copeland, T. G., and Cole, R. H., 1976, *J. chem. Phys.*, **64**, 1741.

[46] Burns, R. C., Graham, C., and Weller, A. R. M., 1986, *Molec. Phys.*, **59**, 41.

[47] Brookmeyer, B., 1973, M. Sc. Thesis, Brown University.

[48] Sutter, H., and Cole, R. H., 1970, *J. chem. Phys.*, **52**, 132.

[49] Graham, C., 1971, Ph. D. Thesis, University of Cambridge.

[50] Kielich, S., 1962, *Acta Phys. Polon.*, **22**, 477.

[51] Bose, T. K., and Cole, R. H., 1970, *J. chem. Phys.*, **52**, 140.

[52] Dunmur, D. A., and Jessup, N. E., 1979, *Molec. Phys.*, **37**, 697.

[53] Weller, A. R. M., 1985, M. Sc. Thesis, University of Natal.

[54] Hirschfelder, J. O., Curtiss, C. F., and Bird, R. B., 1954, *Molecular Theory of Gases and Liquids* (Chichester: Wiley).

[55] Maitland, G. C., Rigby, M., Smith, E. B., and Wakeham, W. A., 1981, *Intermolecular Forces, their Origin and Determination* (Oxford: Clarendon).

[56] Dymond, J. H., and Smith, E. B., 1964, *Trans. Faraday Soc.*, **60**, 1378.

[57] Rivail, J. L., and Cartier, A., 1978, *Molec. Phys.*, **36**, 1085.

[58] Amos, R. D., 1982, *Chem. Phys. Lett.*, **85**, 123.

[59] Dymond, J. H., and Smith, E. B., 1980, *The Virial Coefficients of Gases* (Oxford: Clarendon).

[60] Orcutt, R. H., and Cole, R. H., 1967, *J. chem. Phys.*, **46**, 697.

[61] Battaglia, M. R., 1978, *Non-linear Behaviour of Molecules, Atoms and Ions in Electric, Magnetic or Electromagnetic Fields* (Amsterdam: Elsevier).

[62] Amos, R. D., 1979, *Chem. Phys. Lett.*, **66**, 471.

[63] Maryott, A. A., and Buckley, F., 1953, US National Bureau of Standards Circular No. 537; see also WEAST, J., 1989, *Handbook of Chemistry and Physics*, 70th Edn (CRC Press).

[64] Sutter, H., 1969, Ph. D. Thesis, Brown University.

[65] Williams, J. H., and Amos, R. D., 1980, *Chem. Phys. Lett.*, **70**, 162.

[66] Stogryn, D. E.,and Stogryn, A. P., 1966, *Molec. Phys.*, **11**, 371.

[67] Buckingham, A. D., 1970, *Physical Chemistry: An Advanced Treatise*, edited by W. Jost, H. Eyring, and D. Henderson (London: Academic).

[68] De Leeuw, F., and Dynamus, A., 1973, *J. Molec. Spectrosc.*, **48**, 427.

[69] Graham, C., Pierrus, J., and Raab, R. E., 1989, *Molec. Phys.*, **67,** 939.

[70] Battaglia, M. R., Buckingham, A. D., Neumark, D., Pierens, R. K., and Williams, J. H., 1981, *Molec. Phys.*, **43,** 1015.

[71] Buckingham, A. D., Graham, C., and Williams, J. H., 1983, *Molec. Phys.*, **49,** 703.

[72] Amos, R. D., and Battaglia, M. R., 1978, *Molec. Phys.*, **36,** 1517.

[73] Nanderhart, D., and Flygare, W. H., 1969, *Molec. Phys.*, **18,** 77.

[74] Mason, E. A., and Spurling, T. H., *The Virial Equation of State* (Oxford: Pergamon).

[75] Caldo, J. C. G. *et al.*, 1978, *J. chem. Soc. Faraday Trans.* I, **74,** 893.

[76] Butcher, E. G., and Dadson, R. S., 1964, *Proc. Roy. Soc. Lond.* A, **277,** 448.

[77] Michels, A., Lupton, J. M., Wassenaar, T. and de Graaf, W., 1952, *Physica, 's Grav.*, **18,** 121.

[78] Burns, R. C., 1978, Ph. D. Thesis, University of Natal.

[79] Buckingham, A. D., and Graham, C., 1974, *Proc. R. Soc. Lond.* A, **336,** 275.

[80] Buckingham, A. D., 1955, *Proc. Phys. Soc.* A, **68,** 910.

CHAPTER 2

CALCULATION OF THE SECOND LIGHT-SCATTERING VIRIAL COEFFICIENTS OF NON-LINEAR MOLECULES

2.1 A general theory of light scattering

The scattering of light by a single molecule can be considered to arise when the incident light wave induces oscillating multipole moments in the molecule, which then give rise to retarded scalar and vector potentials and therefore to electric and magnetic fields at all points. Landau and Lifshitz [1] and Buckingham and Raab [2] have related these fields to the electric and magnetic multipole moments of the system. At a point a distance R from an origin O fixed within the molecule's system of oscillating charges, where R is very much larger than both the dimensions of the system of charges and the wavelength of the radiated light, the scattered electric field $E_\alpha^{(s)}$ can be considered to be a plane wave, and is then given by [2]

$$E_\alpha^{(s)} = -\frac{1}{4\pi\varepsilon_o}\frac{1}{Rc^2}\left[\left(\ddot{\mu}_\alpha - n_\alpha n_\beta \ddot{\mu}_\beta\right) - \frac{1}{c}\varepsilon_{\alpha\beta\gamma} n_\beta \ddot{m}_\gamma + \frac{1}{3c}\left(n_\beta \dddot{\theta}_{\alpha\beta} - n_\alpha n_\beta n_\gamma \dddot{\theta}_{\beta\gamma}\right) + \ldots\right] . \quad (2.1)$$

Here, n_α is a unit vector in the direction in which the wave is scattered, while μ_α is the α-component of the electric dipole moment of the system of charges, with each dot above it representing a partial derivative with respect to time taken at the retarded time $t' = t - R/c$. $\theta_{\alpha\beta}$ is the *traceless* electric quadrupole moment, and m_α is the magnetic dipole moment. These multipole moments are defined in Appendix 1. A cautionary comment which must be mentioned here is that several workers [3] have demonstrated the existence of electrodynamic situations where it is necessary to retain the *primitive* multipole moments (also defined in Appendix 1). However, this work is carried out with the use of the

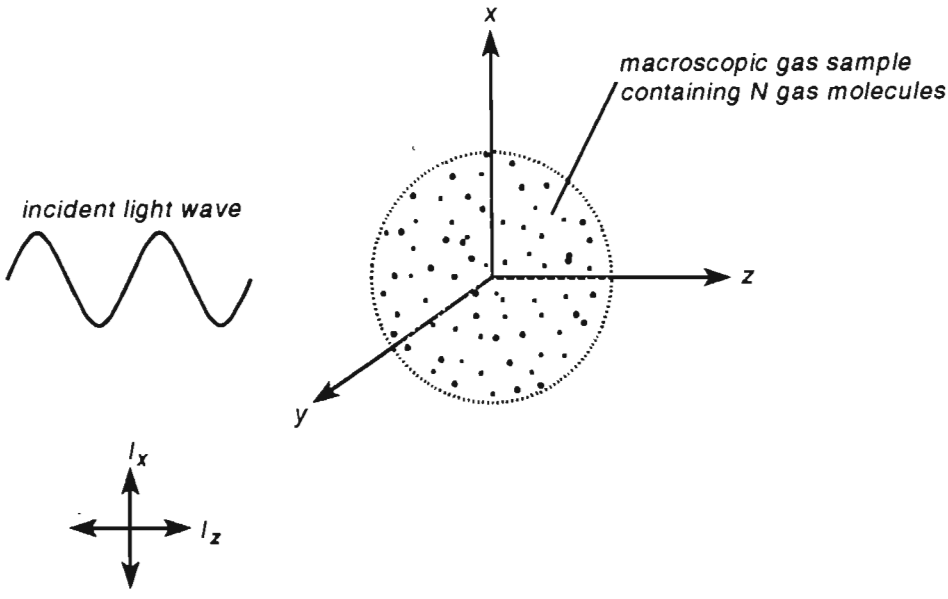

Figure 2.1. The space-fixed system of axes used to describe the scattering of light by a macroscopic gas sample containing N molecules.

traditional traceless quadrupole moment, and future work will need to consider this subtlety.

Now consider the arrangement in figure 2.1 where the origin of a space-fixed system of axes O(x,y,z) is placed within a macroscopic gas sample, the specimen containing a large number N of identical gas molecules. Consider that this system under the influence of a uniform, parallel beam of incident light which is linearly polarized in the vertical xz plane and travelling in the z direction. The wavelength of the incident light is assumed to be very large relative to the dimensions of the gas molecules, and its frequency is supposed to be well below that of any electronic absorption transition. The Rayleigh-scattered light is observed at a point on the y-axis, with the depolarization ratio being given by

$$\rho = \frac{I_z}{I_x} , \tag{2.2}$$

where I_z and I_x are the scattered light intensities with the electric vector parallel to the z and x axes respectively.

Since ρ in equation (2.2) requires scattered intensities with the electric vector parallel to the z and x axes, and since for light travelling along the y axis the unit vector n_α has components $n_x = n_z = 0$ and $n_y = 1$, the expression for the scattered electric field in equation (2.1) summed for the contributions from each molecule in the system of N molecules simplifies to

$$E_\alpha^{(s)} = - \frac{1}{4\pi\varepsilon_o} \frac{1}{Rc^2} \sum_{p=1}^{N} \ddot{\mu}_\alpha^{(p)}(t') \tag{2.3}$$

where $\ddot{\mu}_\alpha^{(p)}$ is the dipole acceleration of the p^{th} molecule, and where the electric dipole radiation alone has been considered. The electric quadrupole and magnetic dipole contributions are much smaller and are neglected.

Now, $\mu_\alpha = \mu_\alpha(E)$ so that

$$\frac{\partial \mu_\alpha}{\partial t} = \dot{\mu}_\alpha = \frac{\partial \mu_\alpha}{\partial E_\beta} \frac{\partial E_\beta}{\partial t}$$

with

$$\frac{\partial^2 \mu_\alpha}{\partial t^2} = \ddot{\mu}_\alpha = \frac{\partial E_\beta}{\partial t}\frac{\partial E_\gamma}{\partial t}\frac{\partial^2 \mu_\alpha}{\partial E_\gamma \partial E_\beta} + \frac{\partial \mu_\alpha}{\partial E_\beta}\frac{\partial^2 E_\beta}{\partial t^2} . \qquad (2.4)$$

Even when using intense laser beams, the term non-linear in the field in equation (2.4) can safely be neglected; and bearing in mind that

$$E_\alpha = E_\alpha^{(o)} e^{-i\omega(t-R/c)}$$

so that

$$\frac{\partial^2 E_\beta}{\partial t^2} = - \omega^2 E_\beta ,$$

it follows from equations (2.3) and (2.4) for a monochromatic incident light beam of wavelength λ that

$$E_\alpha^{(s)} = \frac{1}{4\pi\varepsilon_o}\left[\frac{2\pi}{\lambda}\right]^2 \frac{1}{R} \sum_{p=1}^{N} \frac{\partial \mu_\alpha^{(p)}}{\partial E_\delta^{(p)}} E_\delta^{(p)} . \qquad (2.5)$$

Here, $E_\delta^{(p)}$ implies the value of the E-field at the p^{th} molecule. It is useful to write

$$\frac{\partial \mu_\alpha^{(p)}}{\partial E_\sigma^{(p)}} = \pi_{\alpha\sigma}^{(p)} , \qquad (2.6)$$

where $\pi_{\alpha\sigma}^{(p)}$ is called the differential polarizability.

In general, the intensity I of a light wave with electric field vector $\underset{\sim}{E}$ is given by

$$I = \frac{1}{2\mu_o c} \underset{\sim}{E} . \underset{\sim}{E}^* \qquad (2.7)$$

where the asterisk denotes the complex conjugate. Equation (2.2) then yields

$$\rho = \frac{I_z}{I_x} = \frac{\left\langle E_z E_z^* \right\rangle}{\left\langle E_x E_x^* \right\rangle} = \frac{\left\langle \sum_{p=1}^{N} \sum_{q=1}^{N} \pi_{zx}^{(p)} \pi_{zx}^{(q)} \exp i\chi_{pq} \right\rangle}{\left\langle \sum_{p=1}^{N} \sum_{q=1}^{N} \pi_{xx}^{(p)} \pi_{xx}^{(q)} \exp i\chi_{pq} \right\rangle}, \qquad (2.8)$$

where χ_{pq} is the phase difference in the light scattered by molecules p and q as seen at the observation point, and where the angular brackets indicate an average over all configurations of the specimen. This equation, first obtained by Buckingham and Stephen [4], has been used as a basis for the discussion of the effects of pair interactions on the depolarization ratio ρ for linear and quasi-linear molecules by Graham [5] and Couling and Graham [6].

2.1.1 Non-interacting molecules

For a dilute gas where molecular interactions are negligible, the oscillating dipole moment $\mu_\alpha^{(p)}$ of molecule p arises solely due to the polarizing action of the applied field $\mathcal{E}_o$, there being no neighbouring molecules q which are close enough for their moments to set up significant fields and field gradients at molecule p. The differential polarizability $\pi_{\alpha\beta}$ then becomes simply the molecular polarizability tensor $\alpha_{\alpha\beta}$. Furthermore, there is no average phase relationship between the fields from any one pair of molecules, self-correlations alone contributing to the summation. The summations in equation (2.8) are thus replaced by N times the contribution of a representative molecule 1, yielding

$$\rho = \frac{N\left\langle \alpha_{zx}^{(1)} \alpha_{zx}^{(1)} \right\rangle}{N\left\langle \alpha_{xx}^{(1)} \alpha_{xx}^{(1)} \right\rangle} \qquad (2.9)$$

where the angular brackets now indicate an average over all unbiased orientations of a molecule. The molecular tensors in (2.9) are referred to the space-fixed axes (x,y,z) and must be projected into molecule-fixed axes (1,2,3). The normal tensor-projection procedure yields

$$\left\langle \alpha_{zx}^{(1)} \alpha_{zx}^{(1)} \right\rangle = \alpha_{ij}^{(1)} \alpha_{kl}^{(1)} \left\langle a_i^z a_k^z a_j^x a_l^x \right\rangle \qquad (2.10)$$

where a_i^{α} is the direction cosine between the α space-fixed and i molecule-fixed axes, and where the average is over all isotropic orientations of molecule 1 in the space-fixed axes. For molecules with C_{2v} and D_{2h} symmetry the polarizability tensor α_{ij}, when expressed in molecule-fixed axes with the 3-axis as the principal axis, is diagonal and has three independent components:

$$\alpha_{ij}^{(1)} = \begin{bmatrix} \alpha_{11} & 0 & 0 \\ 0 & \alpha_{22} & 0 \\ 0 & 0 & \alpha_{33} \end{bmatrix} . \qquad (2.11)$$

The mean polarizability α is then

$$\alpha = \frac{1}{3}\alpha_{ii} = \frac{1}{3}\left(\alpha_{11} + \alpha_{22} + \alpha_{33}\right) , \qquad (2.12)$$

while the anisotropy in the polarizability tensor is often defined in the current literature (e.g. [7,8]) as

$$\Delta\alpha = \frac{1}{\sqrt{2}}\left\{\left(\alpha_{11} - \alpha_{22}\right)^2 + \left(\alpha_{22} - \alpha_{33}\right)^2 + \left(\alpha_{33} - \alpha_{11}\right)^2\right\}^{1/2} . \qquad (2.13)$$

Use of the standard isotropic average [9]

$$\left\langle a_i^z a_k^z a_j^x a_l^x \right\rangle = \frac{1}{30}\left(4\delta_{ik}\delta_{jl} - \delta_{ij}\delta_{kl} - \delta_{il}\delta_{kj}\right) \qquad (2.14)$$

in equation (2.10) leads to

$$\begin{aligned} \left\langle \alpha_{zx}^{(1)} \alpha_{zx}^{(1)} \right\rangle &= \frac{1}{30}\left(3\alpha_{ij}^{(1)}\alpha_{ij}^{(1)} - \alpha_{ii}^{(1)}\alpha_{jj}^{(1)}\right) \\ &= \frac{1}{30} 2\left(\alpha_{11}^2 + \alpha_{22}^2 + \alpha_{33}^2 - \alpha_{11}\alpha_{22} - \alpha_{11}\alpha_{33} - \alpha_{22}\alpha_{33}\right) \\ &= \frac{1}{15}\left(\Delta\alpha\right)^2 . \end{aligned} \qquad (2.15)$$

Similarly the term $\left\langle \alpha_{xx}^{(1)} \alpha_{xx}^{(1)} \right\rangle$ in equation (2.9), together with the result [9,10]

$$\left\langle a_i^x a_k^x a_j^x a_l^x \right\rangle = \frac{1}{15}\left(\delta_{ij}\delta_{kl} + \delta_{ik}\delta_{jl} + \delta_{il}\delta_{kj}\right) , \qquad (2.16)$$

yields

$$\left\langle \alpha_{xx}^{(1)} \alpha_{xx}^{(1)} \right\rangle = \alpha^2 + \frac{4}{45} (\Delta\alpha)^2 \quad . \tag{2.17}$$

Hence, equation (2.9) may now be expressed in the form

$$\rho_o = \frac{\frac{1}{15} (\Delta\alpha)^2}{\alpha^2 + \frac{4}{45} (\Delta\alpha)^2} \quad . \tag{2.18}$$

The anisotropy in the molecular polarizability tensor $\alpha_{\alpha\beta}$ was originally defined as the *dimensionless* quantity κ [11]:

$$\kappa^2 = \frac{\left(3\alpha_{ij}\alpha_{ij} - \alpha_{ii}\alpha_{jj}\right)}{2\alpha_{ii}\alpha_{jj}}$$

$$= \frac{(\Delta\alpha)^2}{9\alpha^2} \quad , \tag{2.19}$$

where $\Delta\alpha$ is the alternative definition of the polarizability anisotropy given in equation (2.13). It is a simple matter to show from equation (2.18) that ρ_o and κ^2 are related by the expression

$$\rho_o = \frac{3\kappa^2}{5 + 4\kappa^2} \quad . \tag{2.20}$$

This equation, first derived by Bridge and Buckingham [11], allows the use of measured values of ρ_o to obtain values for κ.

For non-interacting spheres, the anisotropy κ in equation (2.19) is zero, and it follows from equation (2.20) that $\rho_o = 0$. This confirms the well-known result that scattering from non-interacting spheres produces no depolarization. Scattering from interacting spherical, quasi-spherical, linear and quasi-linear molecules has been reviewed in the previous chapter.

2.1.2 Interacting non-linear molecules

The depolarization ratio ρ_o of the light scattered by a dilute gas sample of non-interacting *anisotropic* molecules is modified if the gas pressure is elevated to such an extent that molecular interactions occur. This density dependence of ρ is described by means of the virial expansion [4]

$$\rho = \rho_o + \frac{B_\rho}{V_m} + \frac{C_\rho}{V_m^2} + \ldots \quad , \tag{2.21}$$

in which the leading term is the second light-scattering virial coefficient B_ρ, which describes deviations from ρ_o due to pair interactions.

A complete molecular tensor theory of B_ρ for interacting non-linear molecules is now presented. In a gas, these molecules are moving randomly relative to one another, and so the scattered light waves emitted by each of these molecules arrive at the distant observation point with different and randomly fluctuating phases. This allows the summation in equation (2.8) to be considerably simplified. Apart from self-correlation, there is significant correlation of phase only when pairs of molecules are in the process of a close encounter. Since the interaction mechanism for all terms (with *one* exception) is significant only at short ranges of about 0.5 nm to 2 nm which are a small fraction of typical wavelengths of around 500 nm, the phase differences χ_{12} between beams from interacting molecules p and q is effectively zero. The exception is the term $\left\langle \pi_{xx}^{(1)} \pi_{xx}^{(2)} \cos\chi_{12} \right\rangle$, as established by Benoît and Stockmayer [12]. This means that there is no need for the general retention of χ_{pq}, $\exp\left[i\chi_{pq}\right]$ being set to unity in all but the abovementioned term. Thus, allowing only for self-correlation and pairwise contributions to the coherent fields, the summations in equation (2.8) are replaced by N times the contribution of a representative molecule 1, averaged over all pair encounters, giving

$$\rho = \frac{N\left\langle \pi_{zx}^{(1)} \pi_{zx}^{(1)} \right\rangle + N\left\langle \pi_{zx}^{(1)} \pi_{zx}^{(2)} \right\rangle}{N\left\langle \pi_{xx}^{(1)} \pi_{xx}^{(1)} \right\rangle + N\left\langle \pi_{xx}^{(1)} \pi_{xx}^{(2)} \cos \chi_{12} \right\rangle} \quad , \tag{2.22}$$

where the angular brackets now indicate an average over pair encounters. Here, the probability that molecule 1 has a neighbour in $d\tau$ at τ is related to the intermolecular potential energy $U_{12}(\tau)$ by [9]

$$P(\tau) = \frac{N_A}{\Omega V_m} \exp\left[-U_{12}(\tau)/kT\right] \tag{2.23}$$

where $\Omega = V_m^{-1}\int d\tau$ is the integral over the orientational co-ordinates of the neighbouring molecule 2.

To obtain expressions for the differential polarizabilities in equation (2.22), as defined in (2.6), the treatment of Graham [13] is followed. The dipole moment μ_α and quadrupole moment $\theta_{\alpha\beta}$ induced in a molecule by an electric field E_β and an electric field gradient $E_{\beta\gamma}$ are (Buckingham [14])

$$\mu_\alpha = \alpha_{\alpha\beta}E_\beta + \tfrac{1}{3} A_{\alpha\beta\gamma}E_{\beta\gamma} + \ldots , \tag{2.24}$$

and

$$\theta_{\alpha\beta} = A_{\gamma\alpha\beta}E_\gamma + C_{\alpha\beta\gamma\delta}E_{\gamma\delta} + \ldots . \tag{2.25}$$

The T-tensors [14] are now introduced to simplify the discussion. If $E_\alpha^{(1)}$ and $E_{\alpha\beta}^{(1)}$ are the electric field and electric field gradient at the origin of molecule 1 arising from the point dipole and quadrupole moments of molecule 2, which is at a position R_α from the centre of molecule 1, then

$$E_\alpha^{(1)} = T_{\alpha\beta}^{(1)}\mu_\beta^{(2)} - \tfrac{1}{3} T_{\alpha\beta\gamma}^{(1)}\theta_{\beta\gamma}^{(2)} + \ldots , \tag{2.26}$$

and

$$E_{\alpha\beta}^{(1)} = T_{\alpha\beta\gamma}^{(1)}\mu_\gamma^{(2)} + \ldots ; \tag{2.27}$$

where

$$T_{\alpha\beta}^{(1)} = \frac{1}{4\pi\varepsilon_o}\nabla_\alpha\nabla_\beta R^{-1} = \frac{1}{4\pi\varepsilon_o}\left(3R_\alpha R_\beta - R^2\delta_{\alpha\beta}\right)R^{-5} \tag{2.28}$$

and

$$T^{(1)}_{\alpha\beta\gamma} = -\frac{1}{4\pi\varepsilon_o}\nabla_\alpha\nabla_\beta\nabla_\gamma R^{-1}$$

$$= \frac{3}{4\pi\varepsilon_o}\left[5R_\alpha R_\beta R_\gamma - R^2\left(R_\alpha\delta_{\beta\gamma} + R_\beta\delta_{\gamma\alpha} + R_\gamma\delta_{\alpha\beta}\right)\right]R^{-7} \qquad (2.29)$$

are the second and third rank T-tensors respectively. Here,

$$T^{(1)} = (-1)^n\, T^{(2)} \ , \qquad (2.30)$$

where n is the order of the T-tensor. It follows from equation (2.30) that the superscript may be omitted for T-tensors of second rank while it has to be retained for T-tensors of third rank.

Graham [13] argued that the total oscillating dipole moment of molecule 1, $\mu^{(1)}_\alpha$, arises in part from the direct polarizing action of the incident light wave field $\mathcal{E}_o$, and in part from the fields and field gradients at molecule 1 due to the oscillating moments of a neighbouring molecule 2, equation (2.24) becoming

$$\mu^{(1)}_\alpha\left(\mathcal{E}_o\right) = \alpha^{(1)}_{\alpha\beta}\left[\mathcal{E}_{o\beta} + \mathcal{F}^{(1)}_\beta\right] + \frac{1}{3}A^{(1)}_{\alpha\beta\gamma}\left[\mathcal{E}_{o\beta\gamma} + \mathcal{F}^{(1)}_{\beta\gamma}\right] . \qquad (2.31)$$

Here, $\mathcal{E}_{o\beta}$ and $\mathcal{E}_{o\beta\gamma}$ are the field and field gradient of the incident light wave experienced by molecule 1, while $\mathcal{F}^{(1)}_\beta$ and $\mathcal{F}^{(1)}_{\beta\gamma}$ are the additional field and field gradient arising at molecule 1 due to the oscillating multipole moments of the neighbouring molecule 2.

The molecular polarizability tensor of molecule 1, $\alpha^{(1)}_{\alpha\beta}$, in equation (2.31) is assumed independent of the field and field gradient at it. If, however, molecule 2 has permanent multipole moments which set up an intense electric field $F^{(1)}_\gamma$ and electric field gradient $F^{(1)}_{\gamma\delta}$ at molecule 1, then non-linear terms should be included and equation (2.31) must be modified to become

$$\mu^{(1)}_\alpha\left(\mathcal{E}_o\right) =$$

$$\left[\alpha^{(1)}_{\alpha\beta} + \beta^{(1)}_{\alpha\beta\gamma}F^{(1)}_\gamma + \frac{1}{2}\gamma^{(1)}_{\alpha\beta\gamma\delta}F^{(1)}_\gamma F^{(1)}_\delta + \phi^{(1)}_{\alpha\beta\gamma\delta}F^{(1)}_{\gamma\delta} + \ldots\right]\left[\mathcal{E}_{o\beta} + \mathcal{F}^{(1)}_\beta\right]$$

$$+ \frac{1}{3}A^{(1)}_{\alpha\beta\gamma}\left[\mathcal{E}_{o\beta\gamma} + \mathcal{F}^{(1)}_{\beta\gamma}\right] + \ldots \ . \qquad (2.32)$$

The field gradient of the applied light wave $\mathcal{E}_{o\beta\gamma}$ may be neglected since molecular dimensions are usually very small compared with the wavelength of the incident light wave. Furthermore, the non-linear effects resulting from the intermolecular fields of permanent multipole moments will be neglected. This should be borne in mind if numerical values of B_ρ *for strongly polar molecules* calculated using this approximation are found to disagree with experimentally measured B_ρ values. In such instances, the calculations might have to be re-worked with inclusion of the hyperpolarizability effects. It is possible, however, to proceed on the precedent of the refractivity virial coefficient B_R of axially-symmetric molecules for which Burns, Graham and Weller [15] showed that hyperpolarizability effects were negligible. Equation (2.32) is now written as

$$\mu_\alpha^{(1)}\left(\mathcal{E}_o\right) = \alpha_{\alpha\beta}^{(1)}\left[\mathcal{E}_{o\beta} + \mathcal{F}_\beta^{(1)}\right] + \tfrac{1}{3} A_{\alpha\beta\gamma}^{(1)} \mathcal{F}_{\beta\gamma}^{(1)} \quad . \tag{2.33}$$

If the oscillating octopoles and higher-order multipoles on molecule 2 are neglected, the field $\mathcal{F}_\beta^{(1)}$ at molecule 1 due to the oscillating dipole and quadrupole moments on molecule 2 will, from equation (2.26), have the form

$$\mathcal{F}_\beta^{(1)} = T_{\beta\gamma}^{(1)}\mu_\gamma^{(2)} - \tfrac{1}{3} T_{\beta\gamma\delta}^{(1)}\theta_{\gamma\delta}^{(2)} \quad . \tag{2.34}$$

It must be emphasized that $\mu_\gamma^{(2)}$ itself is the oscillating dipole induced on molecule 2 by the fields and field gradients arising at 2 due not only to the direct influence of $\mathcal{E}_o$, but also to the oscillating dipole and quadrupole moments of molecule 1. The oscillating quadrupole induced on molecule 2, $\theta_{\gamma\delta}^{(2)}$, arises similarly. Using equations (2.24) and (2.25) to provide expressions for $\mu_\gamma^{(2)}$ and $\theta_{\gamma\delta}^{(2)}$, and substituting these expressions into (2.34), yields

$$\mathcal{F}_\beta^{(1)} = T_{\beta\gamma}^{(1)}\left[\alpha_{\gamma\delta}^{(2)}\left[\mathcal{E}_{o\delta} + \mathcal{F}_\delta^{(2)}\right] + \tfrac{1}{3} A_{\gamma\delta\varepsilon}^{(2)} \mathcal{F}_{\delta\varepsilon}^{(2)}\right]$$

$$- \tfrac{1}{3} T_{\beta\gamma\delta}^{(1)}\left[A_{\varepsilon\gamma\delta}^{(2)}\left[\mathcal{E}_{o\varepsilon} + \mathcal{F}_\varepsilon^{(2)}\right] + C_{\gamma\delta\varepsilon\phi}^{(2)}\mathcal{F}_{\varepsilon\phi}^{(2)}\right] \quad . \tag{2.35}$$

The terms $\mathcal{F}_\delta^{(2)}$ and $\mathcal{F}_{\delta\varepsilon}^{(2)}$ refer to the field and field gradient at molecule 2 arising from the oscillating dipole and quadrupole moments of molecule 1, and have the form given by equations (2.26) and (2.27) respectively. Equation (2.35) becomes

$$\mathcal{F}_{\beta}^{(1)} = T_{\beta\gamma}^{(1)}\alpha_{\gamma\delta}^{(2)}\mathcal{E}_{\circ\delta} + T_{\beta\gamma}^{(1)}\alpha_{\gamma\delta}^{(2)}\left[T_{\delta\varepsilon}^{(2)}\mu_{\varepsilon}^{(1)} - \tfrac{1}{3}T_{\delta\varepsilon\phi}^{(2)}\theta_{\varepsilon\phi}^{(1)}\right] + \tfrac{1}{3}T_{\beta\gamma}^{(1)}A_{\gamma\delta\varepsilon}^{(2)}\left[T_{\delta\varepsilon\phi}^{(2)}\mu_{\phi}^{(1)}\right]$$

$$- \tfrac{1}{3}T_{\beta\gamma\delta}^{(1)}A_{\varepsilon\gamma\delta}^{(2)}\mathcal{E}_{\circ\varepsilon} - \tfrac{1}{3}T_{\beta\gamma\delta}^{(1)}A_{\varepsilon\gamma\delta}^{(2)}\left[T_{\varepsilon\phi}^{(2)}\mu_{\phi}^{(1)} - \tfrac{1}{3}T_{\varepsilon\phi\eta}^{(2)}\theta_{\phi\eta}^{(1)}\right]$$

$$- \tfrac{1}{3}T_{\beta\gamma\delta}^{(1)}C_{\gamma\delta\varepsilon\phi}^{(2)}\left[T_{\varepsilon\phi\eta}^{(2)}\mu_{\eta}^{(1)}\right] . \qquad (2.36)$$

Substitution of the expressions for $\mu_{\alpha}^{(1)}$ and $\theta_{\alpha\beta}^{(1)}$ given in equations (2.24) and (2.25) respectively yields

$$\mathcal{F}_{\beta}^{(1)} = T_{\beta\gamma}^{(1)}\alpha_{\gamma\delta}^{(2)}\mathcal{E}_{\circ\delta} + T_{\beta\gamma}^{(1)}\alpha_{\gamma\delta}^{(2)}\left[T_{\delta\varepsilon}^{(2)}\left\{\alpha_{\varepsilon\phi}^{(1)}\left(\mathcal{E}_{\circ\phi} + \mathcal{F}_{\phi}^{(1)}\right) + \tfrac{1}{3}A_{\varepsilon\phi\eta}^{(1)}\mathcal{F}_{\phi\eta}^{(1)}\right\}\right.$$

$$\left. - \tfrac{1}{3}T_{\delta\varepsilon\phi}^{(2)}\left\{A_{\eta\varepsilon\phi}^{(1)}\left(\mathcal{E}_{\circ\eta} + \mathcal{F}_{\eta}^{(1)}\right) + C_{\varepsilon\phi\eta\lambda}^{(1)}\mathcal{F}_{\eta\lambda}^{(1)}\right\}\right]$$

$$+ \tfrac{1}{3}T_{\beta\gamma}^{(1)}A_{\gamma\delta\varepsilon}^{(2)}T_{\delta\varepsilon\phi}^{(2)}\left[\alpha_{\phi\eta}^{(1)}\left(\mathcal{E}_{\circ\eta} + \mathcal{F}_{\eta}^{(1)}\right) + \tfrac{1}{3}A_{\phi\eta\lambda}^{(1)}\mathcal{F}_{\eta\lambda}^{(1)}\right]$$

$$- \tfrac{1}{3}T_{\beta\gamma\delta}^{(1)}A_{\varepsilon\gamma\delta}^{(2)}\mathcal{E}_{\circ\varepsilon} - \tfrac{1}{3}T_{\beta\gamma\delta}^{(1)}A_{\varepsilon\gamma\delta}^{(2)}\left[T_{\varepsilon\phi}^{(2)}\left\{\alpha_{\phi\eta}^{(1)}\left(\mathcal{E}_{\circ\eta} + \mathcal{F}_{\eta}^{(1)}\right) + \tfrac{1}{3}A_{\phi\eta\lambda}^{(1)}\mathcal{F}_{\eta\lambda}^{(1)}\right\}\right.$$

$$\left. - \tfrac{1}{3}T_{\varepsilon\phi\eta}^{(2)}\left\{A_{\lambda\phi\eta}^{(1)}\left(\mathcal{E}_{\circ\lambda} + \mathcal{F}_{\lambda}^{(1)}\right) + C_{\phi\eta\lambda\tau}^{(1)}\mathcal{F}_{\lambda\tau}^{(1)}\right\}\right]$$

$$- \tfrac{1}{3}T_{\beta\gamma\delta}^{(1)}C_{\gamma\delta\varepsilon\phi}^{(2)}T_{\varepsilon\phi\eta}^{(2)}\left\{\alpha_{\eta\lambda}^{(1)}\left(\mathcal{E}_{\circ\lambda} + \mathcal{F}_{\lambda}^{(1)}\right) + \tfrac{1}{3}A_{\eta\lambda\tau}^{(1)}\mathcal{F}_{\lambda\tau}^{(1)}\right\} . \qquad (2.37)$$

Successive substitutions of $\mathcal{F}_{\beta}^{(1)}$ and $\mathcal{F}_{\beta\gamma}^{(1)}$, and of $\mathcal{F}_{\beta}^{(2)}$ and $\mathcal{F}_{\beta\gamma}^{(2)}$, leads to a lengthy series of terms. It is difficult to know a priori after how many terms the series is to be truncated since little is known about the rate of convergence of the contributing terms. For some insight into the problem, we turn to our work on B_{ρ} for linear and quasi-linear molecules [5,6], where B_{ρ} was calculated to successively higher orders until the higher order terms were seen to make a negligible contribution. Hence, under the guidance of [5,6], the series for $\mathcal{F}_{\beta}^{(1)}$ is truncated at a point which will lead to scattered intensities in α^5, as well as all scattered intensities in $\alpha^2 A$, $\alpha^3 A$ and $\alpha^3 C$. Equation (2.37) then yields

$$\mathcal{F}^{(1)}_{\beta} = T^{(1)}_{\beta\gamma}\alpha^{(2)}_{\gamma\delta}\mathcal{E}_{o\delta} + T^{(1)}_{\beta\gamma}\alpha^{(2)}_{\gamma\delta}T^{(2)}_{\delta\varepsilon}\alpha^{(1)}_{\varepsilon\phi}\mathcal{E}_{o\phi} + \frac{1}{3}T^{(1)}_{\beta\gamma}A^{(2)}_{\gamma\delta\varepsilon}T^{(2)}_{\delta\varepsilon\phi}\alpha^{(1)}_{\phi\eta}\mathcal{E}_{o\eta}$$

$$+ T^{(1)}_{\beta\gamma}\alpha^{(2)}_{\gamma\delta}T^{(2)}_{\delta\varepsilon}\alpha^{(1)}_{\varepsilon\phi}T^{(1)}_{\phi\eta}\alpha^{(2)}_{\eta\lambda}\mathcal{E}_{o\lambda} - \frac{1}{3}T^{(1)}_{\beta\gamma\delta}A^{(2)}_{\varepsilon\gamma\delta}\mathcal{E}_{o\varepsilon}$$

$$- \frac{1}{3}T^{(1)}_{\beta\gamma\delta}A^{(2)}_{\varepsilon\gamma\delta}T^{(2)}_{\varepsilon\phi}\alpha^{(1)}_{\phi\eta}\mathcal{E}_{o\eta} - \frac{1}{3}T^{(1)}_{\beta\gamma\delta}C^{(2)}_{\gamma\delta\varepsilon\phi}T^{(2)}_{\varepsilon\phi\eta}\alpha^{(1)}_{\eta\lambda}\mathcal{E}_{o\lambda} + \ldots \quad . \qquad (2.38)$$

To understand the physical meaning of the terms in (2.38), consider as an example the term $-\frac{1}{3}T^{(1)}_{\beta\gamma\delta}C^{(2)}_{\gamma\delta\varepsilon\phi}T^{(2)}_{\varepsilon\phi\eta}\alpha^{(1)}_{\eta\lambda}\mathcal{E}_{o\lambda}$ which can be interpreted as follows: the incident light wave field $\mathcal{E}_{o\lambda}$ induces on molecule 1 an oscillating dipole moment $\alpha^{(1)}_{\eta\lambda}\mathcal{E}_{o\lambda}$, which in turn gives rise to an oscillating field gradient at molecule 2 through the third rank T-tensor $T^{(2)}_{\varepsilon\phi\eta}$. This field gradient results in an oscillating quadrupole on molecule 2 as described by $C^{(2)}_{\gamma\delta\varepsilon\phi}$, this quadrupole moment now making an additional oscillating field contribution at molecule 1.

The field gradient $\mathcal{F}^{(1)}_{\beta\gamma}$ at molecule 1 in equation (2.33), due to induced oscillating multipole moments on molecule 2, is in turn given by equation (2.27):

$$\mathcal{F}^{(1)}_{\beta\gamma} = T^{(1)}_{\beta\gamma\delta}\mu^{(2)}_{\delta} \quad . \qquad (2.39)$$

Here, oscillating quadrupoles and multipoles of higher order have been neglected, and substitution of $\mu^{(2)}_{\delta}$ yields only two terms whose contributions to B_{ρ} were found to be significant enough for retention:

$$\mathcal{F}^{(1)}_{\beta\gamma} = T^{(1)}_{\beta\gamma\delta}\alpha^{(2)}_{\delta\varepsilon}\mathcal{E}_{o\varepsilon} + T^{(1)}_{\beta\gamma\delta}\alpha^{(2)}_{\delta\varepsilon}T^{(2)}_{\varepsilon\phi}\alpha^{(1)}_{\phi\eta}\mathcal{E}_{o\eta} + \ldots \quad . \qquad (2.40)$$

It is worth sounding a cautionary note that the above field gradients between interacting molecules at short range are not to be confused with the field gradients of the light-wave fields which are negligible over the small dimensions of the molecules.

Substitution of equations (2.38) and (2.40) into (2.33) yields a final expression for the oscillating dipole induced on molecule 1 by the light wave field $\mathcal{E}_{o}$ in the presence of molecule 2. To obtain the differential polarizability $\pi_{\alpha\sigma}$ as defined in (2.6), the dummy indices of the terms in (2.33) have to be rewritten to allow for differentiation with respect to $\mathcal{E}_{o\sigma}$. For example, the term $-\frac{1}{3}T^{(1)}_{\beta\gamma\delta}C^{(2)}_{\gamma\delta\varepsilon\phi}T^{(2)}_{\varepsilon\phi\eta}\alpha^{(1)}_{\eta\lambda}\mathcal{E}_{o\lambda}$ in (2.36) must be

rewritten as $-\frac{1}{3} T^{(1)}_{\beta\gamma\delta} C^{(2)}_{\gamma\delta\varepsilon\phi} T^{(2)}_{\varepsilon\phi\eta} \alpha^{(1)}_{\eta\sigma} \mathcal{E}_{o\sigma}$. Expression (2.33) now appears as

$$\mu^{(1)}_{\alpha}\left[\mathcal{E}_{o}\right] = \alpha^{(1)}_{\alpha\sigma}\mathcal{E}_{o\sigma} + \alpha^{(1)}_{\alpha\beta} T_{\beta\gamma} \alpha^{(2)}_{\gamma\sigma} \mathcal{E}_{o\sigma} + \alpha^{(1)}_{\alpha\beta} T_{\beta\gamma} \alpha^{(2)}_{\gamma\delta} T_{\delta\varepsilon} \alpha^{(1)}_{\varepsilon\sigma} \mathcal{E}_{o\sigma}$$

$$+ \alpha^{(1)}_{\alpha\beta} T_{\beta\gamma} \alpha^{(2)}_{\gamma\delta} T_{\delta\varepsilon} \alpha^{(1)}_{\varepsilon\phi} T_{\phi\eta} \alpha^{(2)}_{\eta\sigma} \mathcal{E}_{o\sigma} - \frac{1}{3} \alpha^{(1)}_{\alpha\beta} T^{(1)}_{\beta\gamma\delta} A^{(2)}_{\sigma\gamma\delta} \mathcal{E}_{o\sigma}$$

$$- \frac{1}{3} \alpha^{(1)}_{\alpha\beta} T_{\beta\gamma} A^{(2)}_{\gamma\delta\varepsilon} T^{(1)}_{\delta\varepsilon\phi} \alpha^{(1)}_{\phi\sigma} \mathcal{E}_{o\sigma} - \frac{1}{3} \alpha^{(1)}_{\alpha\beta} T^{(1)}_{\beta\gamma\delta} A^{(2)}_{\varepsilon\gamma\delta} T_{\varepsilon\phi} \alpha^{(1)}_{\phi\sigma} \mathcal{E}_{o\sigma}$$

$$+ \frac{1}{3} \alpha^{(1)}_{\alpha\beta} T^{(1)}_{\beta\gamma\delta} C^{(2)}_{\gamma\delta\varepsilon\phi} T^{(1)}_{\varepsilon\phi\eta} \alpha^{(1)}_{\eta\sigma} \mathcal{E}_{o\sigma} + \frac{1}{3} A^{(1)}_{\alpha\beta\gamma} T^{(1)}_{\beta\gamma\delta} \alpha^{(2)}_{\delta\sigma} \mathcal{E}_{o\sigma}$$

$$+ \frac{1}{3} A^{(1)}_{\alpha\beta\gamma} T^{(1)}_{\beta\gamma\delta} \alpha^{(2)}_{\delta\varepsilon} T_{\varepsilon\phi} \alpha^{(1)}_{\phi\sigma} \mathcal{E}_{o\sigma} + \ldots \,. \qquad (2.41)$$

When the operation $\frac{\partial}{\partial \mathcal{E}_{o\sigma}}$ is performed on this expression for $\mu^{(1)}_{\alpha}$, the resulting expression for the differential polarizability is

$$\pi^{(p)}_{\alpha\sigma} = \alpha^{(p)}_{\alpha\sigma} + \alpha^{(p)}_{\alpha\beta} T_{\beta\gamma} \alpha^{(q)}_{\gamma\sigma} + \alpha^{(p)}_{\alpha\beta} T_{\beta\gamma} \alpha^{(q)}_{\gamma\delta} T_{\delta\varepsilon} \alpha^{(p)}_{\varepsilon\sigma}$$

$$+ \alpha^{(p)}_{\alpha\beta} T_{\beta\gamma} \alpha^{(q)}_{\gamma\delta} T_{\delta\varepsilon} \alpha^{(p)}_{\varepsilon\phi} T_{\phi\eta} \alpha^{(q)}_{\eta\sigma} - \frac{1}{3} \alpha^{(p)}_{\alpha\beta} T^{(p)}_{\beta\gamma\delta} A^{(q)}_{\sigma\gamma\delta}$$

$$- \frac{1}{3} \alpha^{(p)}_{\alpha\beta} T_{\beta\gamma} A^{(q)}_{\gamma\delta\varepsilon} T^{(p)}_{\delta\varepsilon\phi} \alpha^{(p)}_{\phi\sigma} - \frac{1}{3} \alpha^{(p)}_{\alpha\beta} T^{(p)}_{\beta\gamma\delta} A^{(q)}_{\varepsilon\gamma\delta} T_{\varepsilon\phi} \alpha^{(p)}_{\phi\sigma}$$

$$+ \frac{1}{3} \alpha^{(p)}_{\alpha\beta} T^{(p)}_{\beta\gamma\delta} C^{(q)}_{\gamma\delta\varepsilon\phi} T^{(p)}_{\varepsilon\phi\eta} \alpha^{(p)}_{\eta\sigma} + \frac{1}{3} A^{(p)}_{\alpha\beta\gamma} T^{(p)}_{\beta\gamma\delta} \alpha^{(q)}_{\delta\sigma}$$

$$+ \frac{1}{3} A^{(p)}_{\alpha\beta\gamma} T^{(p)}_{\beta\gamma\delta} \alpha^{(q)}_{\delta\varepsilon} T_{\varepsilon\phi} \alpha^{(p)}_{\phi\sigma} + \ldots \,, \qquad (2.42)$$

where the superscripts p and q indicate molecule p and q respectively. Use of equation (2.42) in (2.22) yields

$$\rho = \frac{a_2 + a_3 + a_4 + a_5 + a_2 A_1 + a_3 A_1 + a_3 C_1 + \ldots}{b_2 + b_3} \,, \qquad (2.43)$$

where

$$a_2 = \left\langle \alpha^{(1)}_{zx} \alpha^{(1)}_{zx} \right\rangle + \left\langle \alpha^{(1)}_{zx} \alpha^{(2)}_{zx} \right\rangle \,, \qquad (2.44)$$

$$a_3 = \left\langle \alpha^{(1)}_{zx}\alpha^{(1)}_{z\beta}T_{\beta\gamma}\alpha^{(2)}_{\gamma x}\right\rangle + \left\langle \alpha^{(1)}_{zx}\alpha^{(2)}_{z\beta}T_{\beta\gamma}\alpha^{(1)}_{\gamma x}\right\rangle$$

$$\left\langle \alpha^{(1)}_{z\beta}T_{\beta\gamma}\alpha^{(2)}_{\gamma x}\alpha^{(2)}_{zx}\right\rangle + \left\langle \alpha^{(1)}_{z\beta}T_{\beta\gamma}\alpha^{(2)}_{\gamma x}\alpha^{(1)}_{zx}\right\rangle , \qquad (2.45)$$

$$a_4 = \left\langle \alpha^{(1)}_{z\beta}T_{\beta\gamma}\alpha^{(2)}_{\gamma x}\alpha^{(2)}_{z\delta}T_{\delta\varepsilon}\alpha^{(1)}_{\varepsilon x}\right\rangle + \left\langle \alpha^{(1)}_{z\beta}T_{\beta\gamma}\alpha^{(2)}_{\gamma x}\alpha^{(1)}_{z\delta}T_{\delta\varepsilon}\alpha^{(2)}_{\varepsilon x}\right\rangle$$

$$+ \left\langle \alpha^{(1)}_{zx}\alpha^{(2)}_{z\beta}T_{\beta\gamma}\alpha^{(1)}_{\gamma\delta}T_{\delta\varepsilon}\alpha^{(2)}_{\varepsilon x}\right\rangle + \left\langle \alpha^{(1)}_{zx}\alpha^{(1)}_{z\beta}T_{\beta\gamma}\alpha^{(2)}_{\gamma\delta}T_{\delta\varepsilon}\alpha^{(1)}_{\varepsilon x}\right\rangle$$

$$+ \left\langle \alpha^{(1)}_{z\beta}T_{\beta\gamma}\alpha^{(2)}_{\gamma\delta}T_{\delta\varepsilon}\alpha^{(1)}_{\varepsilon x}\alpha^{(2)}_{zx}\right\rangle + \left\langle \alpha^{(1)}_{z\beta}T_{\beta\gamma}\alpha^{(2)}_{\gamma\delta}T_{\delta\varepsilon}\alpha^{(1)}_{\varepsilon x}\alpha^{(1)}_{zx}\right\rangle , \qquad (2.46)$$

$$a_5 = \left\langle \alpha^{(1)}_{zx}\alpha^{(1)}_{z\delta}T_{\delta\gamma}\alpha^{(2)}_{\gamma\mu}T_{\mu\nu}\alpha^{(1)}_{\nu\beta}T_{\beta\varepsilon}\alpha^{(2)}_{\varepsilon x}\right\rangle + \left\langle \alpha^{(1)}_{zx}\alpha^{(2)}_{z\delta}T_{\delta\gamma}\alpha^{(1)}_{\gamma\mu}T_{\mu\nu}\alpha^{(2)}_{\nu\beta}T_{\beta\varepsilon}\alpha^{(1)}_{\varepsilon x}\right\rangle$$

$$+ \left\langle \alpha^{(1)}_{z\delta}T_{\delta\varepsilon}\alpha^{(2)}_{\varepsilon x}\alpha^{(1)}_{z\phi}T_{\phi\gamma}\alpha^{(2)}_{\gamma\beta}T_{\beta\eta}\alpha^{(1)}_{\eta x}\right\rangle + \left\langle \alpha^{(1)}_{z\delta}T_{\delta\varepsilon}\alpha^{(2)}_{\varepsilon x}\alpha^{(2)}_{z\phi}T_{\phi\gamma}\alpha^{(1)}_{\gamma\beta}T_{\beta\eta}\alpha^{(2)}_{\eta x}\right\rangle$$

$$+ \left\langle \alpha^{(1)}_{z\delta}T_{\delta\gamma}\alpha^{(2)}_{\gamma\beta}T_{\beta\varepsilon}\alpha^{(1)}_{\varepsilon x}\alpha^{(1)}_{z\phi}T_{\phi\eta}\alpha^{(2)}_{\eta x}\right\rangle + \left\langle \alpha^{(1)}_{z\delta}T_{\delta\gamma}\alpha^{(2)}_{\gamma\beta}T_{\beta\varepsilon}\alpha^{(1)}_{\varepsilon x}\alpha^{(2)}_{z\phi}T_{\phi\eta}\alpha^{(1)}_{\eta x}\right\rangle$$

$$+ \left\langle \alpha^{(1)}_{z\delta}T_{\delta\gamma}\alpha^{(2)}_{\gamma\mu}T_{\mu\nu}\alpha^{(1)}_{\nu\beta}T_{\beta\varepsilon}\alpha^{(2)}_{\varepsilon x}\alpha^{(1)}_{zx}\right\rangle + \left\langle \alpha^{(1)}_{z\delta}T_{\delta\gamma}\alpha^{(2)}_{\gamma\mu}T_{\mu\nu}\alpha^{(1)}_{\nu\beta}T_{\beta\varepsilon}\alpha^{(2)}_{\varepsilon x}\alpha^{(2)}_{zx}\right\rangle ,$$

(2.47)

$$a_2A_1 = -\frac{1}{3}\left\langle \alpha^{(1)}_{z\beta}T^{(1)}_{\beta\gamma\delta}A^{(2)}_{x\gamma\delta}\alpha^{(1)}_{zx}\right\rangle - \frac{1}{3}\left\langle \alpha^{(1)}_{zx}\alpha^{(1)}_{z\beta}T^{(1)}_{\beta\gamma\delta}A^{(2)}_{x\gamma\delta}\right\rangle$$

$$- \frac{1}{3}\left\langle \alpha^{(1)}_{z\beta}T^{(1)}_{\beta\gamma\delta}A^{(2)}_{x\gamma\delta}\alpha^{(2)}_{zx}\right\rangle + \frac{1}{3}\left\langle \alpha^{(1)}_{zx}\alpha^{(2)}_{z\beta}T^{(1)}_{\beta\gamma\delta}A^{(1)}_{x\gamma\delta}\right\rangle$$

$$+ \frac{1}{3}\left\langle \alpha^{(1)}_{zx}A^{(1)}_{z\beta\gamma}T_{\beta\gamma\delta}\alpha^{(2)}_{\delta x}\right\rangle + \frac{1}{3}\left\langle A^{(1)}_{z\beta\gamma}T_{\beta\gamma\delta}\alpha^{(2)}_{\delta x}\alpha^{(1)}_{zx}\right\rangle$$

$$- \frac{1}{3}\left\langle \alpha^{(1)}_{zx}A^{(2)}_{z\beta\gamma}T_{\beta\gamma\delta}\alpha^{(1)}_{\delta x}\right\rangle + \frac{1}{3}\left\langle A^{(1)}_{z\beta\gamma}T_{\beta\gamma\delta}\alpha^{(2)}_{\delta x}\alpha^{(2)}_{zx}\right\rangle , \qquad (2.48)$$

$$a_3A_1 = -\frac{1}{3}\left\langle \alpha^{(1)}_{zx}\alpha^{(1)}_{z\beta}T_{\beta\gamma}A^{(2)}_{\gamma\delta\lambda}T^{(1)}_{\delta\lambda\phi}\alpha^{(1)}_{\phi x}\right\rangle - \frac{1}{3}\left\langle \alpha^{(1)}_{z\beta}T_{\beta\gamma}A^{(2)}_{\gamma\delta\lambda}T^{(1)}_{\delta\lambda\phi}\alpha^{(1)}_{\phi x}\alpha^{(1)}_{zx}\right\rangle$$

$$+\frac{1}{3}\left\langle \alpha^{(1)}_{zx}\alpha^{(2)}_{z\beta}T_{\beta\gamma}A^{(1)}_{\gamma\delta\lambda}T^{(1)}_{\delta\lambda\phi}\alpha^{(2)}_{\phi x}\right\rangle - \frac{1}{3}\left\langle \alpha^{(1)}_{z\beta}T_{\beta\gamma}A^{(2)}_{\gamma\delta\lambda}T^{(1)}_{\delta\lambda\phi}\alpha^{(1)}_{\phi x}\alpha^{(2)}_{zx}\right\rangle$$

$$-\frac{1}{3}\left\langle \alpha^{(1)}_{zx}\alpha^{(1)}_{z\beta}T^{(1)}_{\beta\gamma\delta}A^{(2)}_{\lambda\gamma\delta}T_{\lambda\phi}\alpha^{(1)}_{\phi x}\right\rangle - \frac{1}{3}\left\langle \alpha^{(1)}_{z\beta}T^{(1)}_{\beta\gamma\delta}A^{(2)}_{\lambda\gamma\delta}T_{\lambda\phi}\alpha^{(1)}_{\phi x}\alpha^{(1)}_{zx}\right\rangle$$

$$+\frac{1}{3}\left\langle \alpha^{(1)}_{zx}\alpha^{(2)}_{z\beta}T^{(1)}_{\beta\gamma\delta}A^{(1)}_{\lambda\gamma\delta}T^{(1}_{\lambda\phi}\alpha^{(2)}_{\phi x}\right\rangle - \frac{1}{3}\left\langle \alpha^{(1)}_{z\beta}T^{(1)}_{\beta\gamma\delta}A^{(2)}_{\lambda\gamma\delta}T_{\lambda\phi}\alpha^{(1)}_{\phi x}\alpha^{(2)}_{zx}\right\rangle$$

$$+\frac{1}{3}\left\langle \alpha^{(1)}_{zx}A^{(1)}_{z\beta\gamma}T^{(1)}_{\beta\gamma\delta}\alpha^{(2)}_{\delta\lambda}T_{\lambda\phi}\alpha^{(1)}_{\phi x}\right\rangle + \frac{1}{3}\left\langle A^{(1)}_{z\beta\gamma}T^{(1)}_{\beta\gamma\delta}\alpha^{(2)}_{\delta\lambda}T_{\lambda\phi}\alpha^{(1)}_{\phi x}\alpha^{(1)}_{zx}\right\rangle$$

$$-\frac{1}{3}\left\langle \alpha^{(1)}_{zx}A^{(2)}_{z\beta\gamma}T^{(1)}_{\beta\gamma\delta}\alpha^{(1)}_{\delta\lambda}T_{\lambda\phi}\alpha^{(2)}_{\phi x}\right\rangle + \frac{1}{3}\left\langle A^{(1)}_{z\beta\gamma}T^{(1)}_{\beta\gamma\delta}\alpha^{(2)}_{\delta\lambda}T_{\lambda\phi}\alpha^{(1)}_{\phi x}\alpha^{(2)}_{zx}\right\rangle , \tag{2.49}$$

$$a_3C_1 = \frac{1}{3}\left\langle \alpha^{(1)}_{zx}\alpha^{(1)}_{z\delta}T^{(1)}_{\delta\rho\gamma}C^{(2)}_{\rho\gamma\beta\phi}T^{(1)}_{\beta\phi\varepsilon}\alpha^{(1)}_{\varepsilon x}\right\rangle + \frac{1}{3}\left\langle \alpha^{(1)}_{z\delta}T^{(1)}_{\delta\rho\gamma}C^{(2)}_{\rho\gamma\beta\phi}T^{(1)}_{\beta\phi\varepsilon}\alpha^{(1)}_{\varepsilon x}\alpha^{(1)}_{zx}\right\rangle$$

$$+\frac{1}{3}\left\langle \alpha^{(1)}_{zx}\alpha^{(2)}_{z\delta}T^{(1)}_{\delta\rho\gamma}C^{(1)}_{\rho\gamma\beta\phi}T^{(1)}_{\beta\phi\varepsilon}\alpha^{(2)}_{\varepsilon x}\right\rangle + \frac{1}{3}\left\langle \alpha^{(1)}_{z\delta}T^{(1)}_{\delta\rho\gamma}C^{(2)}_{\rho\gamma\beta\phi}T^{(1)}_{\beta\phi\varepsilon}\alpha^{(1)}_{\varepsilon x}\alpha^{(2)}_{zx}\right\rangle , \tag{2.50}$$

$$b_2 = \left\langle \alpha^{(1)}_{xx}\alpha^{(1)}_{xx}\right\rangle + \left\langle \alpha^{(1)}_{xx}\alpha^{(2)}_{xx}\cos X_{12}\right\rangle , \tag{2.51}$$

$$b_3 = \left\langle \alpha^{(1)}_{xx}\alpha^{(1)}_{x\beta}T_{\beta\gamma}\alpha^{(2)}_{\gamma x}\right\rangle + \left\langle \alpha^{(1)}_{xx}\alpha^{(2)}_{x\beta}T_{\beta\gamma}\alpha^{(1)}_{\gamma x}\right\rangle . \tag{2.52}$$

There are no literature values of the A- and C-tensor components for non-linear molecules, and we therefore cannot calculate the contributions arising from the a_2A_1, a_3A_1 or a_3C_1 terms. Once again, we turn to our work on linear and quasi-linear molecules [5,6] for some insight into the problem. The a_3C_1 term is known to contribute less than 1% to B_ρ for *all* linear molecules studied thus far [6], and its omission here does not arouse concern. However, the a_2A_1 term, which exists only for polar molecules (the A-tensor vanishes for non-polar species), can make significant contributions to B_ρ of as much as 9% [6]. The higher-order a_3A_1 term contributes less than 1% to B_ρ for the linear molecules investigated in [6]. The problem remains unresolved until *ab initio* calculated estimates of the A-tensor components of non-linear polar molecules are forthcoming.

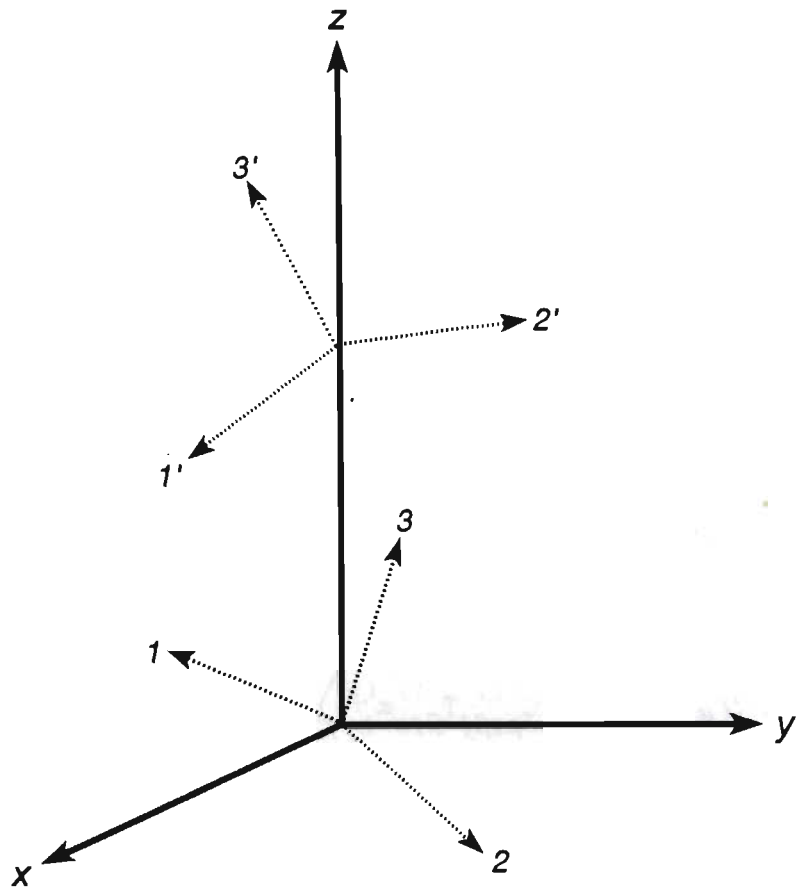

Figure 2.2. The molecule-fixed axes (1,2,3) and (1',2',3') of interacting molecules 1 and 2 respectively. The space-fixed axes are (x,y,z).

2.2 Describing the relative configuration of two non-linear molecules

To exploit the symmetry of a molecule, its physical property tensors must be referred to a system of molecule-fixed axes. However, the experimental measurement of the depolarization ratio ρ is performed in the space-fixed system of axes which is orientated with respect to the direction of propagation of the incident light beam. As a molecule in the gas sample tumbles in space, its set of molecule-fixed axes is continually changing with respect to the space-fixed axes. The average projection of the molecule's tensor properties in the space-fixed axes is obtained by (i) referring the molecular property tensors to molecule-fixed axes, (ii) projecting these tensors into the space-fixed axes, and (iii) averaging the projection over the orientational motion of the molecule.

Let (x,y,z) be the space-fixed system of axes (referred to by tensor indices α,β,γ, ...), and let (1,2,3) (referred to by i,j,k ...) and (1′,2′,3′) (referred to by i′,j′,k′ ...) be the axes fixed in molecules 1 and 2 respectively as shown in figure 2.2. Seven parameters are used to describe the relative configuration of the two molecules, and these are as follows:

(i) The displacement of the two molecular centres is described by the parameter R, *which is initially fixed along the z-axis.*

(ii) The relative orientation of the molecule-fixed axes of molecule 1 and the space-fixed system of axes is described by the nine direction cosines a_i^{α}. However, it must be recognized that the complete specification of an arbitrary rotation of a system of cartesian axes about its origin requires only three parameters. We shall describe such a rotation by the three Euler angles α_1, β_1 and γ_1. To rotate (1,2,3) into (x,y,z), three successive rotations are required [16,17]:

(a) rotation about the 3-axis through an angle α_1 $(0 \le \alpha_1 \le 2\pi)$,

(b) rotation about the new 2′-axis through an angle β_1 $(0 \le \beta_1 \le \pi)$,

(c) rotation about the new 3″-axis (co-inciding with the z-axis) through an angle γ_1 $(0 \le \gamma_1 \le 2\pi)$.

The *nine* direction cosines a_i^{α} can now in turn be expressed as functions of the *three* Euler angles α_1, β_1 and γ_1. We have [16,17]

$$a_i^{\alpha} = \begin{bmatrix} \cos\gamma_1 & \sin\gamma_1 & 0 \\ -\sin\gamma_1 & \cos\gamma_1 & 0 \\ 0 & 0 & 1 \end{bmatrix} \begin{bmatrix} \cos\beta_1 & 0 & -\sin\beta_1 \\ 0 & 1 & 0 \\ \sin\beta_1 & 0 & \cos\beta_1 \end{bmatrix} \begin{bmatrix} \cos\alpha_1 & \sin\alpha_1 & 0 \\ -\sin\alpha_1 & \cos\alpha_1 & 0 \\ 0 & 0 & 1 \end{bmatrix}$$

$$= \begin{bmatrix} \cos\alpha_1\cos\beta_1\cos\gamma_1 - \sin\alpha_1\sin\gamma_1 & \sin\alpha_1\cos\beta_1\cos\gamma_1 + \cos\alpha_1\sin\gamma_1 & -\sin\beta_1\cos\gamma_1 \\ -\cos\alpha_1\cos\beta_1\sin\gamma_1 - \sin\alpha_1\cos\gamma_1 & -\sin\alpha_1\cos\beta_1\sin\gamma_1 + \cos\alpha_1\cos\gamma_1 & \sin\beta_1\sin\gamma_1 \\ \cos\alpha_1\sin\beta_1 & \sin\alpha_1\sin\beta_1 & \cos\beta_1 \end{bmatrix}. \tag{2.53}$$

(iii) Similarly, the relative orientation of the molecule-fixed axes of molecule 2 and the space-fixed system of axes is described by the nine direction cosines $a_{i'}^{\alpha}$, which are in turn expressed as functions of the three Euler angles α_2, β_2 and γ_2. The components of $a_{i'}^{\alpha}$ are as for equation (2.53), except that the rotation angles now have the subscript 2:

$$a_{i'}^{\alpha} =$$

$$\begin{bmatrix} \cos\alpha_2\cos\beta_2\cos\gamma_2 - \sin\alpha_2\sin\gamma_2 & \sin\alpha_2\cos\beta_2\cos\gamma_2 + \cos\alpha_2\sin\gamma_2 & -\sin\beta_2\cos\gamma_2 \\ -\cos\alpha_2\cos\beta_2\sin\gamma_2 - \sin\alpha_2\cos\gamma_2 & -\sin\alpha_2\cos\beta_2\sin\gamma_2 + \cos\alpha_2\cos\gamma_2 & \sin\beta_2\sin\gamma_2 \\ \cos\alpha_2\sin\beta_2 & \sin\alpha_2\sin\beta_2 & \cos\beta_2 \end{bmatrix}. \tag{2.54}$$

Expressing the T-tensors in space-fixed axes (x,y,z) is a simple matter since R is initially fixed along the z-axis. This is illustrated with the second-rank T-tensor given in equation (2.28), which becomes

$$T_{\alpha\beta} = \left(4\pi\varepsilon_o\right)^{-1} R^{-3} \begin{bmatrix} -1 & 0 & 0 \\ 0 & -1 & 0 \\ 0 & 0 & 2 \end{bmatrix}. \tag{2.55}$$

Extension to higher-order T-tensors is obvious.

2.3 Expressions for contributions to B_ρ from non-linear molecules

The averages in equations (2.44) to (2.47), (2.51) and (2.52) must now be expressed in terms of the elements of the diagonal tensors $\alpha_{ij}^{(1)}$ and $\alpha_{i'j'}^{(2)}$, as given in (2.11) $\left[\alpha_{ij}^{(1)} = \alpha_{i'j'}^{(2)}\right]$, and the seven interaction parameters R, α_1, β_1, γ_1, α_2, β_2 and γ_2. Initially, all tensors must be

referred to (1,2,3): this ensures that for a given relative configuration of the two molecules the tensor product in (1,2,3) is fixed. If the pair of molecules is then allowed to rotate isotropically *as a rigid whole* in (x,y,z), then the projection into (x,y,z) of this pair property (referred to (1,2,3)) can be averaged over all orientations. Averaging over the interaction parameters may subsequently be carried out, the average $\langle X \rangle$ of the pair property X over the interaction co-ordinates following from the probability in equation (2.23):

$$\langle X \rangle = \frac{N_A}{16\pi^3 V_m} \int_{R=0}^{\infty} \int_{\alpha_1=0}^{2\pi} \int_{\beta_1=0}^{\pi} \int_{\gamma_1=0}^{2\pi} \int_{\alpha_2=0}^{2\pi} \int_{\beta_2=0}^{\pi} \int_{\gamma_2=0}^{2\pi} X \exp\left[-U_{12}(\tau)/kT\right]$$

$$\times \; R^2 \sin\beta_1 \sin\beta_2 \, dR \, d\alpha_1 d\beta_1 d\gamma_1 d\alpha_2 d\beta_2 d\gamma_2 \; . \quad (2.56)$$

The term $\left\langle \alpha_{zx}^{(1)} \alpha_{zx}^{(2)} \right\rangle$ from equation (2.44) is now referred to molecule-fixed axes:

$$\left\langle \alpha_{zx}^{(1)} \alpha_{zx}^{(2)} \right\rangle = \left\langle \alpha_{ij}^{(1)} \alpha_{kl}^{(2)} \right\rangle \left\langle a_i^z a_k^z a_j^x a_l^x \right\rangle$$

$$= \frac{1}{30} \left\langle 3\alpha_{ij}^{(1)} \alpha_{ij}^{(2)} - 9\alpha^2 \right\rangle , \quad (2.57)$$

where $\alpha_{ij}^{(2)}$ is the polarizability tensor of molecule 2 expressed in the molecule-fixed axes of molecule 1. To express $\alpha_{i'j'}^{(2)}$ in (1,2,3), we must first rotate (1',2',3') into (x,y,z) (bearing in mind that for the time being, R is fixed along the z-axis), and then rotate the resulting $\alpha_{\alpha\beta}^{(2)}$ from (x,y,z) into (1,2,3). We have

$$\alpha_{\alpha\beta}^{(2)} = a_i^{\alpha} , a_j^{\beta} , \alpha_{i'j'}^{(2)} , \quad (2.58)$$

where a_i^{α}, is given in equation (2.54). Then,

$$\alpha_{ij}^{(2)} = a_{\alpha}^{i} a_{\beta}^{j} \alpha_{\alpha\beta}^{(2)}$$

$$= a_{\alpha}^{i} a_{\beta}^{j} a_i^{\alpha} , a_j^{\beta} , \alpha_{i'j'}^{(2)} , \quad (2.59)$$

where a_{α}^{i} may be viewed as the transpose of equation (2.53), but this is taken care of by the summation over indices.

The tensor facilities of Macsyma were used to evaluate the term in angular brackets in equation (2.57), yielding

$$\left\langle 3\alpha_{ij}^{(1)}\alpha_{ij}^{(2)} - 9\alpha^2 \right\rangle = \left\langle \alpha_{11}\alpha_{22}\left[2A_1\left(A_7B_2B_8 + A_4B_2B_5\right) + 2A_2\left(A_8B_1B_7 + A_5B_1B_4\right)\right.\right.$$
$$+ A_1^2B_2^2 + A_2^2B_1^2 + A_4^2B_5^2 + A_5^2B_4^2 + A_7^2B_8^2 + A_8^2B_7^2 + 2A_4A_7B_5B_8 + 2A_5A_8B_4B_7\Big]$$
$$+ \alpha_{11}\alpha_{33}\left[2A_1\left(A_7B_3B_9 + A_4B_3B_6\right) + 2A_3\left(A_9B_1B_7 + A_6B_1B_4\right) + A_1^2B_3^2 + A_3^2B_1^2\right.$$
$$+ A_4^2B_6^2 + A_6^2B_4^2 + A_7^2B_9^2 + A_9^2B_7^2 + 2A_4A_7B_6B_9 + 2A_6A_9B_4B_7\Big] + \alpha_{22}\alpha_{33}\Big[2A_2$$
$$\times \left(A_8B_3B_9 + A_5B_3B_6\right) + 2A_3\left(A_9B_2B_8 + A_6B_2B_5\right) + A_2^2B_3^2 + A_3^2B_2^2 + A_5^2B_6^2$$
$$+ A_6^2B_5^2 + A_8^2B_9^2 + A_9^2B_8^2 + 2A_5A_9B_6B_9 + 2A_6A_9B_5B_8\Big] + \alpha_{11}^2\Big[2A_1\left(A_7B_1B_7\right.$$
$$+ A_4B_1B_4\Big) + 2A_4A_7B_4B_7 + A_1^2B_1^2 + A_4^2B_4^2 + A_7^2B_7^2\Big] + \alpha_{22}^2\Big[2A_2\left(A_8B_2B_8\right.$$
$$+ A_5B_2B_5\Big) + 2A_5A_8B_5B_8 + A_2^2B_2^2 + A_5^2B_5^2 + A_8^2B_8^2\Big] + \alpha_{33}^2\Big[2A_3\left(A_9B_3B_9\right.$$
$$\left.\left.\left.+ A_6B_3B_6\right) + 2A_6A_9B_6B_9 + A_3^2B_3^2 + A_6^2B_6^2 + A_9^2B_9^2\right] - 9\alpha^2\right\rangle . \qquad (2.60)$$

Here, $A_1 \ldots A_9$ are the components of equation (2.53) while $B_1 \ldots B_9$ are the components of (2.54):

$$\begin{aligned} A_1 &= \cos\alpha_1\cos\beta_1\cos\gamma_1 - \sin\alpha_1\sin\gamma_1 \\ B_1 &= \cos\alpha_2\cos\beta_2\cos\gamma_2 - \sin\alpha_2\sin\gamma_2 \end{aligned} \qquad (2.61)$$

$$\begin{aligned} A_2 &= \sin\alpha_1\cos\beta_1\cos\gamma_1 + \cos\alpha_1\sin\gamma_1 \\ B_2 &= \sin\alpha_2\cos\beta_2\cos\gamma_2 + \cos\alpha_2\sin\gamma_2 \end{aligned} \qquad (2.62)$$

$$\begin{aligned} A_3 &= -\sin\beta_1\cos\gamma_1 \\ B_3 &= -\sin\beta_2\cos\gamma_2 \end{aligned} \qquad (2.63)$$

$$\begin{aligned} A_4 &= -\cos\alpha_1\cos\beta_1\sin\gamma_1 - \sin\alpha_1\cos\gamma_1 \\ B_4 &= -\cos\alpha_2\cos\beta_2\sin\gamma_2 - \sin\alpha_2\cos\gamma_2 \end{aligned} \qquad (2.64)$$

$$\begin{aligned} A_5 &= -\sin\alpha_1\cos\beta_1\sin\gamma_1 + \cos\alpha_1\cos\gamma_1 \\ B_5 &= -\sin\alpha_2\cos\beta_2\sin\gamma_2 + \cos\alpha_2\cos\gamma_2 \end{aligned} \qquad (2.65)$$

$$A_6 = \sin\beta_1 \sin\gamma_1$$
$$B_6 = \sin\beta_2 \sin\gamma_2 \qquad (2.66)$$

$$A_7 = \cos\alpha_1 \sin\beta_1$$
$$B_7 = \sin\alpha_2 \sin\beta_2 \qquad (2.67)$$

$$A_8 = \sin\alpha_1 \sin\beta_1$$
$$B_8 = \sin\alpha_2 \sin\beta_2 \qquad (2.68)$$

$$A_9 = \cos\beta_1$$
$$B_9 = \cos\beta_2 \qquad (2.69)$$

When we refer the $\left\langle \alpha^{(1)}_{xx}\alpha^{(2)}_{xx}\cos\chi_{12}\right\rangle$ term from equation (2.51) to molecule-fixed axes using an analogous procedure to that of Benoît and Stockmayer [12], and Graham [5]; we obtain

$$\left\langle \alpha^{(1)}_{xx}\alpha^{(2)}_{xx}\cos\chi_{12}\right\rangle = \frac{1}{15}\frac{2}{3}\left\langle 3\alpha^{(1)}_{ij}\alpha^{(2)}_{ij} - 9\alpha^2\right\rangle + \alpha^2\left[\frac{-2B}{V_m}\right], \qquad (2.70)$$

where B is the second pressure virial coefficient, and where the term in angular brackets has already been evaluated in equation (2.60).

We now illustrate the procedure for evaluating the higher-order terms by considering a specific example, namely the $\left\langle \alpha^{(1)}_{zx}\alpha^{(2)}_{z\beta}T_{\beta\gamma}\alpha^{(1)}_{\gamma\delta}T_{\delta\varepsilon}\alpha^{(2)}_{\varepsilon x}\right\rangle$ term in equation (2.46). Projection from (x,y,z) into (1,2,3) yields

$$\left\langle \alpha^{(1)}_{zx}\alpha^{(2)}_{z\beta}T_{\beta\gamma}\alpha^{(1)}_{\gamma\delta}T_{\delta\varepsilon}\alpha^{(2)}_{\varepsilon x}\right\rangle$$
$$= \left\langle \alpha^{(1)}_{ij}a^z_i a^x_j \alpha^{(2)}_{kl}a^z_k a^\beta_l T_{mn}a^\beta_m a^\gamma_n \alpha^{(1)}_{pq}a^\gamma_p a^\delta_q T_{rs}a^\delta_r a^\varepsilon_s \alpha^{(2)}_{tu}a^\varepsilon_t a^x_u\right\rangle$$
$$= \left\langle \alpha^{(1)}_{ij}\alpha^{(2)}_{kl}T_{ln}\alpha^{(1)}_{nq}T_{qs}\alpha^{(2)}_{su}\right\rangle \left\langle a^z_i a^z_k a^x_j a^x_u\right\rangle . \qquad (2.71)$$

For a *fixed* interaction configuration, $\left\langle \alpha^{(1)}_{ij}\alpha^{(2)}_{kl}T_{ln}\alpha^{(1)}_{nq}T_{qs}\alpha^{(2)}_{su}\right\rangle$ is a constant, and if the pair of molecules is allowed to rotate isotropically *as a rigid whole*, then use of equation (2.14) leads to the average projection

$$\left\langle \alpha^{(1)}_{zx}\alpha^{(2)}_{z\beta}T_{\beta\gamma}\alpha^{(1)}_{\gamma\delta}T_{\delta\varepsilon}\alpha^{(2)}_{\varepsilon x}\right\rangle$$

$$= \frac{1}{3\,0}\left\langle 3\alpha^{(1)}_{ij}\alpha^{(2)}_{jl}T_{ln}\alpha^{(1)}_{nq}T_{qs}\alpha^{(2)}_{si} - (3\alpha)\alpha^{(2)}_{kl}T_{ln}\alpha^{(1)}_{nq}T_{qs}\alpha^{(2)}_{sk}\right\rangle , \qquad (2.72)$$

in which the angular brackets now indicate an average over the pair interaction co-ordinates according to equation (2.56). We introduce the following notation to simplify the symbolic form of the expressions:

$\alpha^{(1)}_{ij}$ is as in equation (2.11). $T_{ij} = a^{i}_{\alpha}a^{j}_{\beta}T_{\alpha\beta}$, where $T_{\alpha\beta}$ is given in (2.55), and where a^{i}_{α} is the *transpose* of (2.53), yielding

$$T_{ij} = (4\pi\varepsilon_o)^{-1} R^{-3} \begin{bmatrix} T_{11} & T_{12} & T_{13} \\ T_{12} & T_{22} & T_{23} \\ T_{13} & T_{23} & T_{33} \end{bmatrix} \qquad (2.73)$$

where

$$\left.\begin{aligned} T_{11} &= 2A_7^2 - A_4^2 - A_1^2 \\ T_{22} &= 2A_8^2 - A_5^2 - A_2^2 \\ T_{33} &= 2A_9^2 - A_6^2 - A_3^2 \\ T_{12} &= 2A_7A_8 - A_4A_5 - A_1A_2 \\ T_{13} &= 2A_7A_9 - A_4A_6 - A_1A_3 \\ T_{23} &= 2A_8A_9 - A_5A_6 - A_2A_3 \end{aligned}\right\} . \qquad (2.74)$$

Finally, $\alpha^{(2)}_{ij} = a^{i}_{\alpha}a^{j}_{\beta}a^{\alpha}_{l},a^{\beta}_{j},\alpha^{(2)}_{l',j'},$, yielding

$$\alpha^{(2)}_{ij} = \begin{bmatrix} Z_{11} & Z_{12} & Z_{13} \\ Z_{12} & Z_{22} & Z_{23} \\ Z_{13} & Z_{23} & Z_{33} \end{bmatrix} \qquad (2.75)$$

where

$$
\left.
\begin{aligned}
Z_{11} &= \begin{bmatrix} \alpha_{11}\left[A_1^2B_1^2 + A_4^2B_4^2 + A_7^2B_7^2 + 2A_1A_4B_1B_4 + 2B_7\left(A_4A_7B_4 + A_1A_7B_1\right)\right] + \alpha_{22}\left[A_1^2B_2^2 + A_4^2B_5^2 + A_7^2B_8^2 + 2A_1A_4B_2B_5 + 2B_8\left(A_4A_7B_5 + A_1A_7B_2\right)\right] \\ + \alpha_{33}\left[A_1^2B_3^2 + A_4^2B_6^2 + A_7^2B_9^2 + 2A_1A_4B_3B_6 + 2B_9\left(A_4A_7B_6 + A_1A_7B_3\right)\right] \end{bmatrix} \\
Z_{22} &= \begin{bmatrix} \alpha_{11}\left[A_2^2B_1^2 + A_5^2B_4^2 + A_8^2B_7^2 + 2A_2A_5B_1B_4 + 2B_7\left(A_5A_8B_4 + A_2A_8B_1\right)\right] + \alpha_{22}\left[A_2^2B_2^2 + A_5^2B_5^2 + A_8^2B_8^2 + 2A_2A_5B_2B_5 + 2B_8\left(A_5A_8B_5 + A_2A_8B_2\right)\right] \\ + \alpha_{33}\left[A_2^2B_3^2 + A_5^2B_6^2 + A_8^2B_9^2 + 2A_2A_5B_3B_6 + 2B_9\left(A_5A_8B_6 + A_2A_8B_3\right)\right] \end{bmatrix} \\
Z_{33} &= \begin{bmatrix} \alpha_{11}\left[A_3^2B_1^2 + A_6^2B_4^2 + A_9^2B_7^2 + 2A_3A_6B_1B_4 + 2B_7\left(A_6A_9B_4 + A_3A_9B_1\right)\right] + \alpha_{22}\left[A_3^2B_2^2 + A_6^2B_5^2 + A_9^2B_8^2 + 2A_3A_6B_2B_5 + 2B_8\left(A_6A_9B_5 + A_3A_9B_2\right)\right] \\ + \alpha_{33}\left[A_3^2B_3^2 + A_6^2B_6^2 + A_9^2B_9^2 + 2A_3A_6B_3B_6 + 2B_9\left(A_6A_9B_6 + A_3A_9B_3\right)\right] \end{bmatrix} \\
Z_{12} &= \begin{bmatrix} \alpha_{11}\left[A_1A_2B_1^2 + A_4A_5B_4^2 + A_7A_8B_7^2 + B_1B_4\left(A_1A_5 + A_2A_4\right) + B_7\left[B_4\left(A_4A_8 + A_5A_7\right) + B_1\left(A_1A_8 + A_2A_7\right)\right]\right] + \alpha_{22}\left[A_1A_2B_2^2 + A_4A_5B_5^2 + A_7A_8B_8^2\right. \\ \left. + B_2B_5\left(A_1A_5 + A_2A_4\right) + B_8\left[B_5\left(A_4A_8 + A_5A_7\right) + B_2\left(A_1A_8 + A_2A_7\right)\right]\right] + \alpha_{33}\left[A_1A_2B_3^2 + A_4A_5B_6^2 + A_7A_8B_9^2 + B_3B_6\left(A_1A_5 + A_2A_4\right)\right. \\ \left. + B_9\left[B_6\left(A_4A_8 + A_5A_7\right) + B_3\left(A_1A_8 + A_2A_7\right)\right]\right] \end{bmatrix} \\
Z_{13} &= \begin{bmatrix} \alpha_{11}\left[A_1A_3B_1^2 + A_4A_6B_4^2 + A_7A_9B_7^2 + B_1B_4\left(A_1A_6 + A_3A_4\right) + B_7\left[B_4\left(A_4A_9 + A_6A_7\right) + B_1\left(A_1A_9 + A_3A_7\right)\right]\right] + \alpha_{22}\left[A_1A_3B_2^2 + A_4A_6B_5^2 + A_7A_9B_8^2\right. \\ \left. + B_2B_5\left(A_1A_6 + A_3A_4\right) + B_8\left[B_5\left(A_4A_9 + A_6A_7\right) + B_2\left(A_1A_9 + A_3A_7\right)\right]\right] + \alpha_{33}\left[A_1A_3B_3^2 + A_4A_6B_6^2 + A_7A_9B_9^2 + B_3B_6\left(A_1A_6 + A_3A_4\right)\right. \\ \left. + B_9\left[B_6\left(A_4A_9 + A_6A_7\right) + B_3\left(A_1A_9 + A_3A_7\right)\right]\right] \end{bmatrix} \\
Z_{23} &= \begin{bmatrix} \alpha_{11}\left[A_2A_3B_1^2 + A_5A_6B_4^2 + A_8A_9B_7^2 + B_1B_4\left(A_2A_6 + A_3A_5\right) + B_7\left[B_4\left(A_5A_9 + A_6A_8\right) + B_1\left(A_2A_9 + A_3A_8\right)\right]\right] + \alpha_{22}\left[A_2A_3B_2^2 + A_5A_6B_5^2 + A_8A_9B_8^2\right. \\ \left. + B_2B_5\left(A_2A_6 + A_3A_5\right) + B_8\left[B_5\left(A_5A_9 + A_6A_8\right) + B_2\left(A_2A_9 + A_3A_8\right)\right]\right] + \alpha_{33}\left[A_2A_3B_3^2 + A_5A_6B_6^2 + A_8A_9B_9^2 + B_3B_6\left(A_2A_6 + A_3A_5\right)\right. \\ \left. + B_9\left[B_6\left(A_5A_9 + A_6A_8\right) + B_3\left(A_2A_9 + A_3A_8\right)\right]\right] \end{bmatrix}
\end{aligned}
\right\} \qquad (2.76)
$$

Once the Macsyma tensor manipulation facilities are invoked to evaluate the expressions for averages such as in equation (2.72), we obtain for the key parameters in equation (2.43):

$$b_3 = \frac{(4\pi\varepsilon_o)^{-1}}{15} \left\langle R^{-3}\left\{6\alpha\left[\alpha_{11}(Z_{11}T_{11}+ Z_{12}T_{12}+ Z_{13}T_{13}) + \alpha_{22}(Z_{12}T_{12}+ Z_{22}T_{22} + Z_{23}T_{23}) + \alpha_{33}(Z_{13}T_{13}+ Z_{23}T_{23}+ Z_{33}T_{33})\right] + 4\left[\alpha_{11}^2(Z_{11}T_{11}+ Z_{12}T_{12} + Z_{13}T_{13}) + \alpha_{22}^2(Z_{12}T_{12}+ Z_{22}T_{22}+ Z_{23}T_{23}) + \alpha_{33}^2(Z_{13}T_{13}+ Z_{23}T_{23} + Z_{33}T_{33})\right]\right\}\right\rangle , \tag{2.77}$$

$$a_3 = \frac{(4\pi\varepsilon_o)^{-1}}{30} \left\langle R^{-3}\left\{-4\alpha\left[\alpha_{11}(Z_{11}T_{11}+ Z_{12}T_{12}+ Z_{13}T_{13}) + \alpha_{22}(Z_{12}T_{12}+ Z_{22}T_{22} + Z_{23}T_{23}) + \alpha_{33}(Z_{13}T_{13}+ Z_{23}T_{23}+ Z_{33}T_{33})\right] + 3\left[\alpha_{11}^2(Z_{11}T_{11}+ Z_{12}T_{12} + Z_{13}T_{13}) + \alpha_{22}^2(Z_{12}T_{12}+ Z_{22}T_{22}+ Z_{23}T_{23}) + \alpha_{33}^2(Z_{13}T_{13}+ Z_{23}T_{23} + Z_{33}T_{33})\right] + \alpha_{11}\left[T_{11}(Z_{11}^2+ Z_{12}^2+ Z_{13}^2) + T_{12}(Z_{11}Z_{12}+ Z_{12}Z_{22}+ Z_{13}Z_{23}) + T_{13}(Z_{11}Z_{13}+ Z_{12}Z_{23}+ Z_{13}Z_{33})\right] + \alpha_{22}\left[T_{12}(Z_{11}Z_{12}+ Z_{12}Z_{22}+ Z_{13}Z_{23}) + T_{22}(Z_{12}^2+ Z_{22}^2+ Z_{23}^2) + T_{23}(Z_{12}Z_{13}+ Z_{22}Z_{23}+ Z_{23}Z_{33})\right] + \alpha_{33}\left[T_{13} \times (Z_{11}Z_{13}+ Z_{12}Z_{23}+ Z_{13}Z_{33}) + T_{23}(Z_{12}Z_{13}+ Z_{22}Z_{23}+ Z_{23}Z_{33}) + T_{33}(Z_{13}^2 + Z_{23}^2+ Z_{33}^2)\right]\right\}\right\rangle , \tag{2.78}$$

$$
\begin{aligned}
a_4 = \frac{(4\pi\varepsilon_o)^{-2}}{30} \Big\langle R^{-6} \Big\{ & 3\alpha_{11}\alpha_{22}\Big[Z_{13}^2T_{23}^2 + 2T_{23}\Big[Z_{12}Z_{13}T_{22} + T_{13}(Z_{12}Z_{33} + Z_{13}Z_{23}) + T_{12}(Z_{12}Z_{13} + Z_{13}Z_{22} + Z_{11}Z_{13}) + 2Z_{12}Z_{13}T_{11}\Big] + Z_{12}^2T_{22}^2 \\
& + 2T_{22}\Big[2Z_{12}Z_{23}T_{13} + T_{12}(2Z_{12}Z_{22} + Z_{11}Z_{12}) + 2Z_{12}^2T_{11}\Big] + Z_{23}^2T_{13}^2 + 2T_{13}\Big[T_{12}(Z_{22}Z_{23} + Z_{11}Z_{23} + Z_{12}Z_{13}) + Z_{12}Z_{23}T_{11}\Big] + Z_{12}^2T_{11}^2 \\
& + T_{12}^2(Z_{22}^2 + 2Z_{11}Z_{22} + 2Z_{12}^2 + Z_{11}^2) + 2T_{11}T_{12}(Z_{12}Z_{22} + 2Z_{11}Z_{12})\Big] + 3\alpha_{11}\alpha_{33}\Big[Z_{13}^2T_{33}^2 + 2T_{33}\Big[Z_{12}Z_{13}T_{23} + T_{13}(2Z_{13}Z_{33} + Z_{11}Z_{13}) \\
& + 2Z_{13}Z_{23}T_{12} + 2Z_{13}^2T_{11}\Big] + T_{13}^2(Z_{33}^2 + 2Z_{11}Z_{33} + 2Z_{13}^2 + Z_{11}^2) + Z_{12}^2T_{23}^2 + 2T_{23}^2\Big[T_{13}(Z_{12}Z_{33} + Z_{13}Z_{23} + Z_{11}Z_{12}) + T_{12}(Z_{12}Z_{23} + Z_{13}Z_{22}) \\
& + 2Z_{12}Z_{13}T_{11}\Big] + Z_{23}^2T_{12}^2 + 2Z_{13}Z_{23}T_{11}T_{12} + Z_{13}^2T_{11}^2 + 2T_{13}\Big[T_{12}(Z_{23}Z_{33} + Z_{11}Z_{23} + Z_{12}Z_{13}) + T_{11}(Z_{13}Z_{33} + 2Z_{11}Z_{13})\Big]\Big] + 3\alpha_{22}\alpha_{33}\Big[Z_{23}^2T_{33}^2 \\
& + 2T_{33}\Big[T_{23}(2Z_{23}Z_{33} + Z_{22}Z_{23}) + 2Z_{23}^2T_{22} + Z_{12}Z_{23}T_{13} + 2Z_{13}Z_{23}T_{12}\Big] + T_{23}^2(Z_{33}^2 + 2Z_{22}Z_{33} + 2Z_{23}^2 + Z_{22}^2) + Z_{23}^2T_{22}^2 + 2T_{23}\Big[T_{22}(Z_{23}Z_{33} \\
& + 2Z_{22}Z_{23}) + T_{13}(Z_{12}Z_{33} + Z_{13}Z_{23} + Z_{12}Z_{22}) + T_{12}(Z_{13}Z_{33} + Z_{12}Z_{23} + Z_{13}Z_{22})\Big] + Z_{12}^2T_{13}^2 + Z_{13}^2T_{12}^2 + 2T_{22}(2Z_{12}Z_{23}T_{13} + Z_{13}Z_{23}T_{12}) \\
& + T_{12}T_{13}(Z_{11}Z_{23} + Z_{12}Z_{13})\Big] + 3\alpha_{11}^2\Big[T_{13}^2(Z_{33}^2 + Z_{11}Z_{33} + Z_{23}^2 + 3Z_{13}^2) + 2T_{13}\Big[T_{12}(Z_{23}Z_{33} + Z_{22}Z_{23} + Z_{11}Z_{23} + 3Z_{12}Z_{13}) + T_{11}(Z_{13}Z_{33} \\
& + Z_{12}Z_{23} + 4Z_{11}Z_{13})\Big] + T_{12}^2(Z_{23}^2 + Z_{22}^2 + Z_{11}Z_{22} + 3Z_{12}^2) + 2T_{11}T_{12}(Z_{13}Z_{23} + Z_{12}Z_{22} + 4Z_{11}Z_{12}) + T_{11}^2(Z_{13}^2 + Z_{12}^2 + 4Z_{11}^2)\Big] + 3\alpha_{22}^2\Big[T_{23}^2(Z_{33}^2 \\
& + Z_{22}Z_{33} + 3Z_{23}^2 + Z_{13}^2) + 2T_{23}\Big[T_{22}(Z_{23}Z_{33} + 4Z_{22}Z_{23} + Z_{12}Z_{13}) + T_{12}(Z_{13}Z_{33} + 3Z_{12}Z_{23} + Z_{13}Z_{22} + Z_{11}Z_{13})\Big] + T_{22}^2(Z_{23}^2 + 4Z_{22}^2 + Z_{12}^2) \\
& + 2T_{12}T_{22}(Z_{13}Z_{23} + 4Z_{12}Z_{22} + Z_{11}Z_{12}) + T_{12}^2(Z_{11}Z_{22} + Z_{13}^2 + 3Z_{13}^2 + Z_{11}^2)\Big] + 3\alpha_{33}^2\Big[T_{33}^2(4Z_{33}^2 + Z_{23}^2 + Z_{13}^2) + 2T_{33}\Big[T_{23}(4Z_{23}Z_{33} + Z_{22}Z_{23} \\
& + Z_{12}Z_{13}) + T_{13}(4Z_{13}Z_{33} + Z_{12}Z_{23} + Z_{11}Z_{13})\Big] + T_{23}^2(Z_{22}Z_{33} + 3Z_{23}^2 + Z_{22}^2 + Z_{12}^2) + 2T_{13}T_{23}(Z_{12}Z_{33} + 3Z_{13}Z_{23} + Z_{12}Z_{22} + Z_{11}Z_{12}) \\
& + T_{13}^2(Z_{11}Z_{33} + 3Z_{13}^2 + Z_{12}^2 + Z_{11}^2)\Big]\Big\}\Big\rangle \quad . \qquad (2.79)
\end{aligned}
$$

Even with our compact notation, the a_5 term is extremely large, and so we introduce a new tensor to further compress the final expression: $E_{ij} = \alpha^{(1)}_{ij} T_{jk} \alpha^{(2)}_{kl}$, where

$$E_{ij} = \begin{bmatrix} E_{11} & E_{12} & E_{13} \\ E_{21} & E_{22} & E_{23} \\ E_{31} & E_{32} & E_{33} \end{bmatrix}, \tag{2.80}$$

with

$$\left.\begin{aligned}
E_{11} &= \alpha_{11}\left(Z_{11}T_{11} + Z_{12}T_{12} + Z_{13}T_{13}\right) \\
E_{12} &= \alpha_{11}\left(Z_{12}T_{11} + Z_{22}T_{12} + Z_{23}T_{13}\right) \\
E_{13} &= \alpha_{11}\left(Z_{13}T_{11} + Z_{23}T_{12} + Z_{33}T_{13}\right) \\
E_{21} &= \alpha_{22}\left(Z_{11}T_{12} + Z_{12}T_{22} + Z_{13}T_{23}\right) \\
E_{22} &= \alpha_{22}\left(Z_{12}T_{12} + Z_{22}T_{22} + Z_{23}T_{23}\right) \\
E_{23} &= \alpha_{22}\left(Z_{13}T_{12} + Z_{23}T_{22} + Z_{33}T_{23}\right) \\
E_{31} &= \alpha_{33}\left(Z_{11}T_{13} + Z_{12}T_{23} + Z_{13}T_{33}\right) \\
E_{32} &= \alpha_{33}\left(Z_{12}T_{13} + Z_{22}T_{23} + Z_{23}T_{33}\right) \\
E_{33} &= \alpha_{33}\left(Z_{13}T_{13} + Z_{23}T_{23} + Z_{33}T_{33}\right)
\end{aligned}\right\}. \tag{2.81}$$

Then,

$$a_5 = \frac{(4\pi\varepsilon_o)^{-3}}{30}\left\langle R^{-9}\left\{9\alpha_{33}\left[T_{33}(E_{13}E_{31}+E_{23}E_{32}+2E_{33}^2)+T_{23}\left(E_{33}(2E_{32}+E_{23})+E_{22}E_{32}+E_{12}E_{31}\right)+E_{23}E_{32}T_{22}+T_{13}\left(E_{33}(2E_{31}+E_{13})+E_{21}E_{32}\right.\right.\right.\right.$$
$$\left.+E_{11}E_{31}\right)+T_{12}(E_{13}E_{32}+E_{23}E_{31})+E_{13}E_{31}T_{11}\Big]+9\alpha_{22}\Big[E_{23}E_{32}T_{33}+T_{23}(E_{23}E_{33}+E_{22}E_{32}+2E_{22}E_{23}+E_{13}E_{21})+T_{22}(E_{23}E_{32}+2E_{22}^2+E_{12}E_{21})$$
$$+T_{13}(E_{21}E_{32}+E_{12}E_{23})+T_{12}\left(E_{23}E_{31}+E_{22}(2E_{21}+E_{12})+9E_{11}E_{21}\right)+E_{12}E_{21}T_{11}\Big]+9\alpha_{11}\Big[E_{13}E_{31}T_{33}+T_{23}(E_{12}E_{31}+E_{13}E_{21})+E_{12}E_{21}T_{22}$$
$$+T_{13}(E_{13}E_{33}+E_{11}E_{31}+E_{12}E_{23}+2E_{11}E_{13})+T_{12}(E_{13}E_{32}+E_{12}E_{22}+E_{11}E_{21}+2E_{11}E_{12})+T_{11}(E_{13}E_{31}+E_{12}E_{21}+2E_{11}^2)\Big]+3T_{33}\Big[Z_{33}(2E_{33}^2$$
$$+E_{23}E_{32}+E_{13}E_{31})+Z_{23}\left(E_{33}(2E_{32}+E_{23})+E_{22}E_{32}+E_{12}E_{31}\right)+E_{23}E_{32}Z_{22}+Z_{13}\left(E_{33}(2E_{31}+E_{13})+E_{21}E_{32}+E_{11}E_{31}\right)+Z_{12}(E_{13}E_{32}$$
$$+E_{23}E_{31})+E_{13}E_{31}Z_{11}\Big]+3T_{23}\Big[Z_{33}\left(E_{33}(E_{32}+2E_{23})+E_{22}E_{23}+E_{13}E_{21}\right)+Z_{23}(E_{33}^2+2E_{22}E_{33}+E_{32}^2+2E_{23}E_{32}+E_{13}E_{31}+E_{23}^2+E_{22}^2+E_{12}E_{21})$$
$$+Z_{22}(E_{32}E_{33}+2E_{22}E_{32}+E_{12}E_{31}+E_{22}E_{23})+Z_{13}\left(E_{33}(E_{21}+E_{12})+E_{31}E_{32}+E_{23}E_{31}+E_{13}E_{23}+E_{21}E_{22}+E_{11}E_{21}\right)+Z_{12}\left(E_{31}E_{33}+E_{32}(E_{21}\right.$$
$$\left.+E_{12})+E_{31}(E_{22}+E_{11})+E_{21}E_{23}+E_{13}E_{22}\right)+Z_{11}(E_{12}E_{31}+E_{13}E_{21})\Big]+3T_{22}\Big[E_{23}E_{32}Z_{33}+Z_{23}(E_{23}E_{33}+E_{22}E_{32}+2E_{22}E_{23}+E_{13}E_{21})+Z_{22}$$
$$\times(E_{23}E_{32}+2E_{22}^2+E_{12}E_{21})+Z_{13}(E_{21}E_{32}+E_{12}E_{23})+Z_{12}\left(E_{23}E_{31}+E_{22}(2E_{21}+E_{12})+E_{11}E_{21}\right)+E_{12}E_{21}Z_{11}\Big]+3T_{13}\Big[Z_{33}\left(E_{33}(E_{31}+2E_{13})\right.$$
$$+E_{12}E_{23}+E_{11}E_{13}\Big)+Z_{23}\left(E_{33}(E_{21}+E_{12})+E_{32}(E_{31}+E_{13})+E_{13}E_{23}+E_{12}E_{22}+E_{11}E_{12}\right)+Z_{22}(E_{21}E_{32}+E_{12}E_{23})+Z_{13}(E_{33}^2+2E_{11}E_{33}$$
$$+E_{23}E_{32}+E_{31}^2+2E_{13}E_{31}+E_{12}E_{21}+E_{13}^2+E_{11}^2)+Z_{12}\left(E_{32}E_{33}+E_{32}(E_{22}+E_{11})+E_{31}(E_{21}+E_{12})+E_{11}E_{23}+E_{12}E_{13}\right)+Z_{11}(E_{31}E_{33}+E_{21}E_{32}$$
$$\left.+2E_{11}E_{31}+E_{11}E_{13})\right]+3T_{12}\Big[Z_{33}(E_{13}E_{32}+E_{23}E_{31})+Z_{23}\left(E_{13}E_{33}+E_{12}E_{32}+E_{22}E_{31}+E_{23}(E_{21}+E_{12})+E_{13}E_{22}+E_{11}E_{13}\right)+Z_{22}\left(E_{13}E_{32}\right.$$
$$+E_{22}(E_{21}+2E_{12})+E_{11}E_{12}\Big)+Z_{13}\left(E_{23}E_{33}+E_{11}E_{32}+E_{21}E_{31}+E_{23}(E_{22}+E_{11})+E_{13}E_{21}+E_{12}E_{13}\right)+Z_{12}(E_{23}E_{32}+E_{13}E_{31}+E_{22}^2+2E_{11}E_{22}$$
$$+E_{21}^2+2E_{12}E_{21}+E_{12}^2+E_{11}^2)+Z_{11}(E_{23}E_{31}+E_{21}E_{22}+2E_{11}E_{21}+E_{11}E_{12})\Big]+3T_{11}\Big[E_{13}E_{31}Z_{33}+Z_{23}(E_{12}E_{31}+E_{13}E_{21})+E_{12}E_{21}Z_{22}+Z_{13}(E_{13}E_{33}$$
$$+E_{11}E_{31}+E_{12}E_{23}+2E_{11}E_{13})+Z_{12}(E_{13}E_{32}+E_{12}E_{22}+E_{11}E_{21}+2E_{11}E_{12})+Z_{11}(E_{13}E_{31}+E_{12}E_{21}+2E_{11})\Big]-12\alpha\Big[T_{33}(E_{33}^2+E_{23}E_{32}+E_{13}E_{31})$$
$$+T_{23}\left(E_{33}(E_{32}+E_{23})+E_{22}E_{32}+E_{12}E_{31}+E_{22}E_{23}+E_{13}E_{21}\right)+T_{22}(E_{23}E_{32}+E_{22}^2+E_{12}E_{21})+T_{13}\left(E_{33}(E_{31}+E_{13})+E_{21}E_{32}+E_{11}E_{31}+E_{12}E_{23}\right.$$
$$\left.+E_{11}E_{13}\right)+T_{12}\left(E_{13}E_{32}+E_{23}E_{31}+E_{22}(E_{21}+E_{12})+E_{11}E_{21}+E_{11}E_{12}\right)+T_{11}(E_{13}E_{31}+E_{12}E_{21}+E_{11}^2)\Big]-(E_{11}+E_{22}+E_{33})\Big[3\alpha_{33}(E_{33}T_{33}$$
$$+E_{32}T_{23}+E_{31}T_{13})+3\alpha_{22}(E_{23}T_{23}+E_{22}T_{22}+E_{21}T_{12})+3\alpha_{11}(E_{13}T_{13}+E_{12}T_{12}+E_{11}T_{11})+T_{33}(E_{33}Z_{33}+E_{32}Z_{23}+E_{31}Z_{13})+T_{23}\left(E_{23}Z_{33}\right.$$
$$+Z_{23}(E_{33}+E_{22})+E_{32}Z_{22}+E_{21}Z_{13}+E_{31}Z_{12}\Big)+T_{22}(E_{23}Z_{23}+E_{22}Z_{22}+E_{21}Z_{12})+T_{13}\left(E_{13}Z_{33}+E_{12}Z_{23}+Z_{13}(E_{33}+E_{11})+E_{32}Z_{12}+E_{31}Z_{11}\right)$$
$$\left.\left.\left.+T_{12}\left(E_{13}Z_{23}+E_{12}Z_{22}+E_{23}Z_{13}+Z_{12}(E_{22}+E_{11})+E_{21}Z_{11}\right)+T_{11}(E_{13}Z_{13}+E_{12}Z_{12}+E_{11}Z_{11})\Big]\right\}\right\rangle \quad . \tag{2.82}$$

Upon gathering the results in equations (2.15), (2.17), (2.57), (2.60), (2.70), (2.77), (2.78), (2.79) and (2.82), equation (2.43) for ρ takes the form

$$\rho = \left[\frac{1}{15}(\Delta\alpha)^2 + \frac{1}{30}g' + \frac{1}{30}(4\pi\varepsilon_o)^{-1}a'_3 + \frac{1}{30}(4\pi\varepsilon_o)^{-2}a'_4 + \frac{1}{30}(4\pi\varepsilon_o)^{-3}a'_5 + \ldots\right] \Big/ \left[\alpha^2 + \frac{4}{45}(\Delta\alpha)^2 + \frac{1}{15}\frac{2}{3}g' + \alpha^2\left[\frac{-2B}{V_m}\right] + \frac{1}{15}(4\pi\varepsilon_o)^{-1}b'_3\right] . \tag{2.83}$$

Here, g' is the expression for $\left\langle 3\alpha_{ij}^{(1)}\alpha_{ij}^{(2)} - 9\alpha^2\right\rangle$ given in equation (2.60), while b'_3 represents that part of b_3 in equation (2.77) contained within the angular brackets, with similar definitions for a'_3, a'_4 and a'_5 with reference to equations (2.78), (2.79) and (2.82) respectively.

Equation (2.83) must now be cast into the virial form of equation (2.21). We have from equation (2.18)

$$\rho_o = \frac{3(\Delta\alpha)^2}{45\alpha^2 + 4(\Delta\alpha)^2} ,$$

$\Delta\alpha$ having been defined in equation (2.13). Equation (2.83) can now be written as

$$\rho = \rho_o\left[1 + \frac{1}{2(\Delta\alpha)^2}g' + \frac{(4\pi\varepsilon_o)^{-1}}{2(\Delta\alpha)^2}a'_3 + \frac{(4\pi\varepsilon_o)^{-2}}{2(\Delta\alpha)^2}a'_4 + \frac{(4\pi\varepsilon_o)^{-3}}{2(\Delta\alpha)^2}a'_5 + \frac{2B}{V_m} + O\left(\frac{1}{V_m^2}\right)\right] \Big/ \left\{1 + \frac{4}{3}\rho_o\left[\frac{1}{2(\Delta\alpha)^2}g' + \frac{3(4\pi\varepsilon_o)^{-1}}{2(\Delta\alpha)^2}b'_3 + \frac{2B}{V_m}\right]\right\} , \tag{2.84}$$

which reduces to

$$\rho = \rho_o + \rho_o\left(1 - \frac{4}{3}\rho_o\right)\left[\frac{2B}{V_m} + g + a_3 + a_4 + a_5 + b_3 + \ldots\right] \tag{2.85}$$

where

$$g = \frac{1}{2(\Delta\alpha)^2} V_m \, g' \ , \tag{2.86}$$

$$a_3 = \left\{\frac{1}{2(\Delta\alpha)^2} + \frac{2}{48\alpha^2}\right\}\left(4\pi\varepsilon_o\right)^{-1} V_m \, a'_3 \ , \tag{2.87}$$

$$a_4 = \left\{\frac{1}{2(\Delta\alpha)^2} + \frac{2}{48\alpha^2}\right\}\left(4\pi\varepsilon_o\right)^{-2} V_m \, a'_4 \ , \tag{2.88}$$

$$a_5 = \left\{\frac{1}{2(\Delta\alpha)^2} + \frac{2}{48\alpha^2}\right\}\left(4\pi\varepsilon_o\right)^{-3} V_m \, a'_5 \ , \tag{2.89}$$

$$b_3 = - \frac{\left(4\pi\varepsilon_o\right)^{-1}}{15\alpha^2} V_m \, b'_3 \ . \tag{2.90}$$

It follows that

$$B_\rho = \rho_o\left(1 - \tfrac{4}{3}\rho_o\right)\left(2B + g + a_3 + a_4 + a_5 + b_3 + \ldots\right) \ . \tag{2.91}$$

As with the normal second pressure virial coefficient B, the coefficients in equations (2.86) to (2.90) are independent of the molar volume but dependent on temperature. It is the parameter B_ρ which is directly accessible from a plot of experimentally measured ρ versus V_m^{-1} values, and if coupled with a measured value of ρ_o, one can extract from equation (2.91) a value for

$$B'_\rho = \left(2B + g + a_3 + a_4 + a_5 + b_3 + \ldots\right) \ . \tag{2.92}$$

It is the sum of terms arising purely from angular correlation and collision-induced polarizability anisotropy, namely

$$\mathcal{G}_\rho = g + a_3 + a_4 + a_5 + b_3 + \ldots \ , \tag{2.93}$$

which is of interest; and to extract a precise value of this sum from the value for B'_ρ requires an $\left(\mathcal{G}_\rho/2B\right)$ ratio of the order of unity or greater.

2.4 Evaluation of B_ρ by numerical integration

Evaluation of the average $\langle X \rangle$ of a quantity X over the pair interaction co-ordinates according to equation (2.56) requires the classical intermolecular potential $U_{12}(\tau)$. General tensor expressions for $U_{12}(\tau)$ have been derived by Buckingham [14], who then evaluated them for the special case of a pair of interacting linear molecules in the configuration of figure 1.1 (opposite page 16), obtaining the expressions listed in equations (1.80) to (1.86). We must now evaluate Buckingham's general expressions for $U_{12}(\tau)$ in the case of a pair of interacting non-linear molecules in the configuration described in section 2.2.

2.4.1 Classical expressions for the intermolecular potential energy $U_{12}(\tau)$

Buckingham [14] has shown that for intermolecular separations R which are large relative to molecular dimensions, the pair interaction energy $U_{12}(\tau)$ may be considered to consist of three components:

(i) The *electrostatic energy*, U_{elec}, which arises from the interactions of the zero-field electric moments (charge, dipole, quadrupole, *etc.*) of the two molecules,

(ii) The *induction energy*, U_{ind}, which arises from the distortion of the electronic structure of a molecule due to the permanent electric moments on the neighbouring molecule, and

(iii) The London *dispersion energy*, U_{disp}, which arises from interactions of the electric moments due to fluctuations in the charge distributions of the two molecules.

These interaction energies are the result of long-range forces which are well understood [9,14,18,19], and which are evaluated on the assumption that the overlap of the molecular wave functions is small. Now, at small ranges of interaction where the electron clouds of the molecules *do* overlap significantly, the *ab initio* quantum-mechanical calculations

[20] which would be required to take into account the intermediate-range exchange forces are prohibitively complicated (especially for many-electron atoms); and so it has been customary [21-23] to assume that the interaction energy components (i), (ii) and (iii) above are applicable also to *short-range* interactions provided that an additional term, $U_{overlap}$, is added to account for the repulsive short-range interactions. It is now possible to write

$$U_{12}(\tau) = U_{elec} + U_{ind} + U_{disp} + U_{overlap} . \qquad (2.94)$$

In most of the work previously undertaken on the properties of gases [21-26], the central-field Lennard-Jones 6:12 potential U_{LJ} [27] has been used to represent $(U_{disp} + U_{overlap})$:

$$U_{LJ} = 4\varepsilon\left[\left(\frac{R_o}{R}\right)^{12} - \left(\frac{R_o}{R}\right)^{6}\right] . \qquad (2.95)$$

Here, the term $\left(\frac{R_o}{R}\right)^6$ describes the attractive part of the potential, while $\left(\frac{R_o}{R}\right)^{12}$ describes the short-range repulsive part. The symbols ε and R_o are the well-known Lennard-Jones parameters.

Since U_{LJ} is spherically symmetric, Buckingham and Pople [21] proposed the addition of a further term to $U_{overlap}$ to account for the angular dependence of short-range overlap repulsive forces for non-spherical molecules. For axially-symmetric molecules, they found U_{shape} to be given by

$$U_{shape} = 4D\varepsilon\left(\frac{R_o}{R}\right)^{12}\left[3\cos^2\theta_1 + 3\cos^2\theta_2 - 2\right] , \qquad (2.96)$$

where D is a dimensionless parameter called the shape factor, and which lies in the range -0.25 to +0.50 to ensure that the shape potential is always repulsive. D is zero for spherical molecules, positive for rod-like molecules (i.e. molecules which are elongated in the direction of the axis of the dipole moment [24], such as CH_3F), and negative for plate-like molecules (i.e. molecules which are fore-shortened along the axis of the dipole moment [24], such as CHF_3).

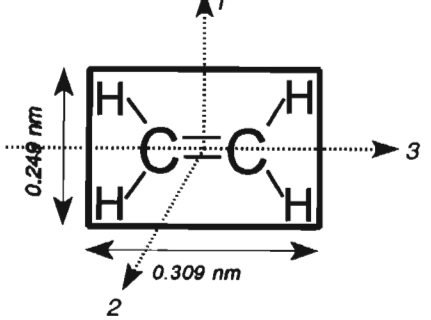

The ethene molecule. Molecular geometry is taken from [8,31].

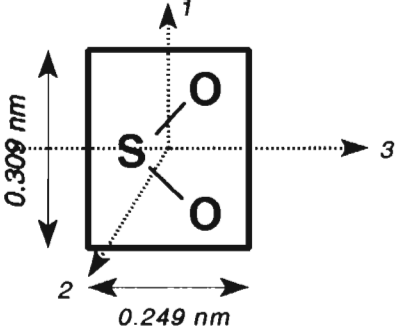

The sulphur dioxide molecule. Molecular geometry is taken from [53].

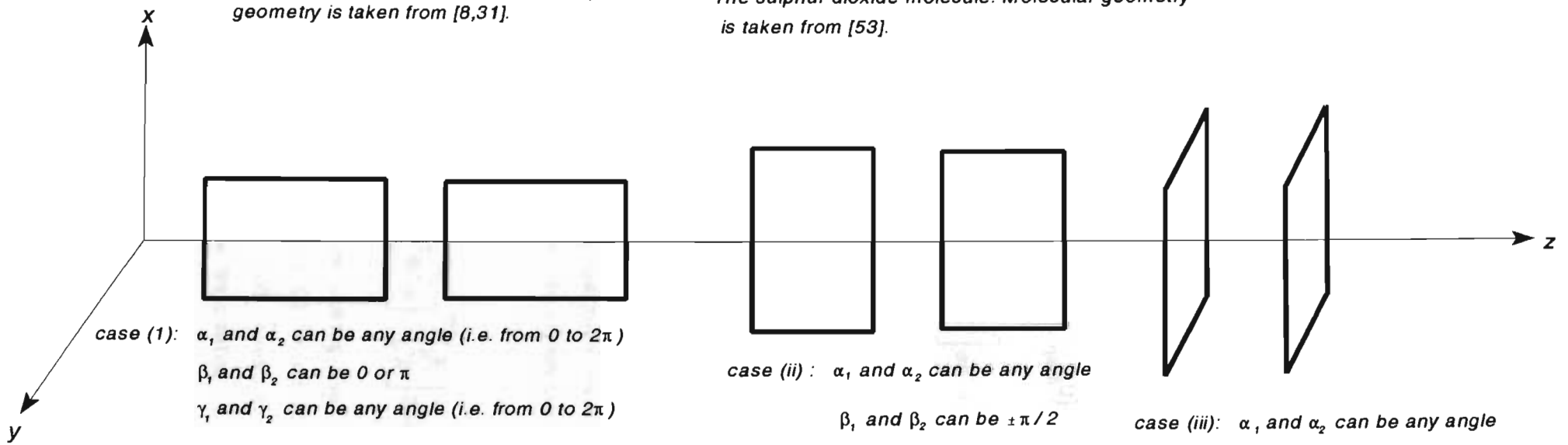

case (1): α_1 and α_2 can be any angle (i.e. from 0 to 2π)

β_1 and β_2 can be 0 or π

γ_1 and γ_2 can be any angle (i.e. from 0 to 2π)

case (ii): α_1 and α_2 can be any angle

β_1 and β_2 can be $\pm\pi/2$

γ_1 and γ_2 can be 0 or π

case (iii): α_1 and α_2 can be any angle

β_1 and β_2 can be $\pm\pi/2$

γ_1 and γ_2 can be $\pm\pi/2$

Figure 2.3. The three extreme intermolecular approaches for two colliding ethene molecules. For sulphur dioxide, replace the ethene molecules with the sulphur dioxide equivalent shown above.

We have used equation (2.96) as a basis for constructing a new shape potential which describes the orientation effects arising from short-range overlap repulsive forces for *non-linear* molecules. Since our investigations deal with molecules belonging to the D_{2h} and C_{2v} point groups, we only consider molecules with these specific symmetries. Ethene (of D_{2h} symmetry) and sulphur dioxide (of C_{2v} symmetry) are chosen as representative molecules, and we orientate the molecule-fixed axes (1,2,3) such that the 1-3 and molecular planes co-incide, with 3 along the principal molecular axis. The three extreme intermolecular approaches for both species are depicted in figure 2.3. The shape potential is seen to be independent of α_1 and α_2, and the simplest force-field which will reproduce the orientation effects of the shape of these molecules is

$$U_{shape} = 4\varepsilon\left(\frac{R_o}{R}\right)^{12}\left\{D_1\left[3\cos^2\beta_1 + 3\cos^2\beta_2 - 2\right] + D_2\left[3\sin^2\beta_1\cos^2\gamma_1 + 3\sin^2\beta_2\cos^2\gamma_2 - 2\right]\right\}, \qquad (2.97)$$

where D_1 and D_2 are dimensionless parameters called the shape factors. For axially symmetric molecules, we set $D_2 = 0$ and recover Buckingham's shape potential. To understand the physical meaning of equation (2.97), imagine two planar ethene molecules approaching as in case (iii) of figure 2.3. The approach distance R *can be less than* R_o before the onset of contact forces, and so in this orientation the repulsive part of the Lennard-Jones potential is *reduced:* a negative U_{shape} and positive $(D_1 + D_2)$ is required. The closest possible approach of two *ideal* (infinitely thin) planes before contact is R = 0. For this orientation there is no repulsive potential, and $4\varepsilon\left(\frac{R_o}{R}\right)^{12}$ from U_{LJ} must be completely offset by U_{shape}. Thus, $(D_1 + D_2) = \frac{1}{2}$. Of course, ethene has a finite thickness with π-orbitals above and below the 1-3 plane; and it is reasonable to expect $(D_1 + D_2) < \frac{1}{2}$ for this molecule. A similar analysis, based on simple molecular geometry, can be undertaken for sulphur dioxide.

Having found the two components U_{LJ} and U_{shape} of the sum $(U_{disp} + U_{overlap})$ in equation (2.94), it is now necessary to find the components of the sum $(U_{elec} + U_{ind})$. As in previous studies of this

kind [23,28-30], U_{elec} is taken to include potential energies arising from the interactions of permanent dipole and quadrupole moments, while U_{ind} comprises energies due to permanent dipole and quadrupole moments on the one molecule interacting with the *induced* dipole moment of the second molecule. The sum $\left(U_{elec} + U_{ind}\right)$ is found to then have the five components

$$U_{elec} + U_{ind} = U_{\mu,\mu} + U_{\mu,\theta} + U_{\theta,\theta} + U_{\mu,ind\ \mu} + U_{\theta,ind\ \mu} , \qquad (2.98)$$

where, $U_{\mu,\mu}$, $U_{\mu,\theta}$ and $U_{\theta,\theta}$ are the electrostatic dipole-dipole, dipole-quadrupole and quadrupole-quadrupole interaction energies of the permanent moments of the two molecules, while $U_{\mu,ind\ \mu}$ and $U_{\theta,ind\ \mu}$ are the dipole-induced-dipole and quadrupole-induced-dipole interaction energies.

We have from Buckingham [14] that the electrostatic contribution to $U_{12}(\tau)$ of two interacting molecules is

$$U_{elec} = - \mu_\alpha^{(1)} T_{\alpha\beta}^{(1)} \mu_\beta^{(2)} + \frac{1}{3} \mu_\alpha^{(1)} T_{\alpha\beta\gamma}^{(1)} \theta_{\beta\gamma}^{(2)} - \frac{1}{3} \mu_\alpha^{(2)} T_{\alpha\beta\gamma}^{(1)} \theta_{\beta\gamma}^{(1)} \qquad (2.99)$$

$$+ \frac{1}{9} \theta_{\alpha\beta}^{(1)} T_{\alpha\beta\gamma\delta}^{(1)} \theta_{\gamma\delta}^{(2)} + \ldots .$$

For interacting non-linear *polar* molecules in the co-ordinate system shown in figure 2.2, we have

$$U_{\mu,\mu} = - \mu_\alpha^{(1)} T_{\alpha\beta}^{(1)} \mu_\beta^{(2)}$$

$$= - a_i^\alpha \mu_i^{(1)} T_{\alpha\beta}^{(1)} a_j^\beta , \mu_j^{(2)} , \qquad (2.100)$$

where for molecules of C_{2v} symmetry with the 3-axis as the principal molecular axis, the dipole moment has only one independent component [14]

$$\mu_i^{(1)} = \mu_j^{(2)} = \left[0 , 0 , \mu_3 \right] . \qquad (2.101)$$

Hence,

$$U_{\mu,\mu} = \left(4\pi\varepsilon_o\right)^{-1} \left\{ \mu_3^2 R^{-3} \left(A_3 B_3 + A_6 B_6 - 2 A_9 B_9 \right) \right\} . \qquad (2.102)$$

Similarly, for C_{2v} *and* D_{2h} symmetry, the traceless quadrupole moment has two independent components [14]

$$\theta_{ij}^{(1)} = \theta_{i'j'}^{(2)} = \begin{bmatrix} \theta_1 & 0 & 0 \\ 0 & \theta_2 & 0 \\ 0 & 0 & -\theta_1 - \theta_2 \end{bmatrix}, \tag{2.103}$$

and we obtain for polar molecules

$$\begin{aligned} U_{\mu,\theta} = (4\pi\varepsilon_o)^{-1}\Big\{\mu_3 R^{-4}\Big[\theta_1\Big[A_9\big(-B_1^2 + B_3^2 - B_4^2 + B_6^2 + 2B_7^2 - 2B_9^2\big) + 2B_3\big(A_1A_7 \\ - A_3A_9\big) + 2B_6\big(A_4A_7 - A_6A_9\big) - 2B_7\big(A_3B_1 + A_6B_4\big) + B_9\big(A_1^2 - A_3^2 + A_4^2 \\ - A_6^2 - 2A_7^2 + 2A_9^2 + 2A_3B_3 + 2A_6B_6\big)\Big] + \theta_2\Big[A_9\big(-B_2^2 + B_3^2 - B_5^2 + B_6^2 \\ + 2B_8^2 - 2B_9^2\big) + 2B_3\big(A_2A_8 - A_3A_9\big) + 2B_6\big(A_5A_8 - A_6A_9\big) - 2B_8\big(A_3B_2 \\ + A_6B_5\big) + B_9\big(A_2^2 - A_3^2 + A_5^2 - A_6^2 - 2A_8^2 + 2A_9^2 + 2A_3B_3 + 2A_6B_6\big)\Big]\Big]\Big\}. \end{aligned} \tag{2.104}$$

For both polar and non-polar molecules

$$U_{\theta,\theta} = \frac{1}{3}\left(4\pi\varepsilon_o\right)^{-1}\Big\{R^{-5}\Big[\theta_1^2\Big[B_1^2\left(3A_1^2 - 3A_3^2 + A_4^2 - A_6^2 - 4A_7^2 + 4A_9^2\right) + B_3^2\left(-3A_1^2 + 3A_3^2 - A_4^2 + A_6^2 + 4A_7^2 - 4A_9^2\right) + B_4^2\left(A_1^2 - A_3^2 + 3A_4^2 - 3A_6^2 - 4A_7^2 + 4A_9^2\right) + 4\left(A_3A_6 - A_1A_4\right)\left(B_3B_6 - B_1B_4\right) + B_6^2\left(-A_1^2 + A_3^2 - 3A_4^2 + 3A_6^2 + 4A_7^2 - 4A_9^2\right) + 4\left(A_1^2 - A_3^2 + A_4^2 - A_6^2 - 2A_7^2 + 2A_9^2\right)\left(B_9 - B_7\right)\left(B_9 + B_7\right) - 16\left(A_3A_9 - A_1A_7\right)\left(B_3B_9 - B_1B_7\right) - 16\left(A_6A_9 - A_4A_7\right)\left(B_6B_9 - B_4B_7\right)\Big] + \theta_2^2\Big[B_2^2\left(3A_2^2 - 3A_3^2 + A_5^2 - A_6^2 - 4A_8^2 + 4A_9^2\right) + B_3^2\left(-3A_2^2 + 3A_3^2 - A_5^2 + A_6^2 + 4A_8^2 - 4A_9^2\right) + B_5^2\left(A_2^2 - A_3^2 + 3A_5^2 - 3A_6^2 - 4A_8^2 + 4A_9^2\right) + 4\left(A_3A_6 - A_2A_5\right)\left(B_3B_6 - B_2B_5\right) + B_6^2\left(-A_2^2 + A_3^2 - 3A_5^2 + 3A_6^2 + 4A_8^2 - 4A_9^2\right) + 4\left(A_2^2 - A_3^2 + A_5^2 - A_6^2 - 2A_8^2 + 2A_9^2\right)\left(B_9 - B_8\right)\left(B_9 + B_8\right) - 16\left(A_3A_9 - A_2A_8\right)\left(B_3B_9 - B_2B_8\right) - 16\left(A_6A_9 - A_5A_8\right)\left(B_6B_9 - B_5B_8\right)\Big] + \theta_1\theta_2\Big[B_1^2\left(3A_2^2 - 3A_3^2 + A_5^2 - A_6^2 - 4A_8^2 + 4A_9^2\right) + B_2^2\left(3A_1^2 - 3A_3^2 + A_4^2 - A_6^2 - 4A_7^2 + 4A_9^2\right) + B_3^2\left[-3\left(A_1^2 + A_2^2\right) + 6A_3^2 - A_4^2 - A_5^2 + 2A_6^2 + 4\left(A_7^2 + A_8^2\right) - 8A_9^2\right] - 4B_1B_4\left(A_3A_6 - A_2A_5\right) + B_4^2\left(A_2^2 - A_3^2 + 3A_5^2 - 3A_6^2 - 4A_8^2 + 4A_9^2\right) - 4B_2B_5\left(A_3A_6 - A_1A_4\right) + B_5^2\left(A_1^2 - A_3^2 + 3A_4^2 - 3A_6^2 - 4A_7^2 + 4A_9^2\right) + 4B_3B_6\left(2A_3A_6 - A_2A_5 - A_1A_4\right) + B_6^2\left[-A_1^2 - A_2^2 + 2A_3^2 - 3\left(A_4^2 + A_5^2\right) + 6A_6^2 + 4\left(A_7^2 + A_8^2\right) - 8A_9^2\right] + 16B_1B_7\left(A_3A_9 - A_2A_8\right) + 16B_4B_7\left(A_6A_9 - A_5A_8\right) - 4B_7^2\left(A_2^2 - A_3^2 + A_5^2 - A_6^2 - 2A_8^2 + 2A_9^2\right) + 16B_2B_8\left(A_3A_9 - A_1A_7\right) + 16B_5B_8\left(A_6A_9 - A_4A_7\right) - 4B_8^2\left(A_1^2 - A_3^2 + A_4^2 - A_6^2 - 2A_7^2 + 2A_9^2\right) - 16B_3B_9\left(2A_3A_9 - A_2A_8 - A_1A_7\right) - 16B_6B_9\left(2A_6A_9 - A_5A_8 - A_4A_7\right) + 4B_9^2\left[A_1^2 + A_2^2 + A_4^2 + A_5^2 - 2\left(A_3^2 + A_6^2 + A_7^2 + A_8^2\right) + 4A_9^2\right]\Big]\Big]\Big\}\,. \tag{2.105}$$

Buckingham [14] also gives the contribution to $U_{12}(\tau)$ arising from the induction energy:

$$U_{ind} = -\frac{1}{2}\alpha_s\left\{T^{(1)}_{\alpha\beta}\mu^{(2)}_{\beta}T^{(1)}_{\alpha\gamma}\mu^{(2)}_{\gamma} + T^{(1)}_{\alpha\beta}\mu^{(1)}_{\beta}T^{(1)}_{\alpha\gamma}\mu^{(1)}_{\gamma}\right\}$$
$$-\frac{1}{18}\alpha_s\left\{T^{(1)}_{\alpha\beta\gamma}\theta^{(1)}_{\beta\gamma}T^{(1)}_{\alpha\delta\varepsilon}\theta^{(1)}_{\delta\varepsilon} + T^{(1)}_{\alpha\beta\gamma}\theta^{(2)}_{\beta\gamma}T^{(1)}_{\alpha\delta\varepsilon}\theta^{(2)}_{\delta\varepsilon}\right\} + \ldots , \qquad (2.106)$$

where α_s is the mean static dipole polarizability. This leads to

$$U_{\mu,ind\ \mu} = (4\pi\varepsilon_o)^{-2}\left\{-\frac{1}{2}\alpha_s\mu_3^2R^{-6}(3A_9^2 + 3B_9^2 - 2)\right\} \qquad (2.107)$$

for polar molecules, and

$$\begin{aligned}U_{\theta,ind\ \mu} = (4\pi\varepsilon_o)^{-2}\Big\{&-\frac{1}{2}\alpha_s R^{-8}\Big[\theta_1^2\Big[A_1^4 - 2A_1^2A_3^2 + A_3^4 + 2A_4^2(A_1^2 - A_3^2) + A_4^4 \\ &+ 2A_6^2(-A_1^2 + A_3^2 - A_4^2) + A_6^4 + 4A_7^2(A_3^2 + A_6^2) + 4A_7^4 - 8A_7A_9(A_1A_3 \\ &+ A_4A_6) + 4A_9^2(A_1^2 + A_4^2 - 2A_7^2) + 4A_9^4\Big] + \theta_2^2\Big[A_2^4 - 2A_2^2A_3^2 + A_3^4 \\ &+ 2A_5^2(A_2^2 - A_3^2) + A_5^4 + 2A_6^2(-A_2^2 + A_3^2 - A_5^2) + A_6^4 + 4A_8^2(A_3^2 + A_6^2) \\ &+ 4A_8^4 - 8A_8A_9(A_2A_3 + A_5A_6) + 4A_9^2(A_2^2 + A_5^2 - 2A_8^2) + 4A_9^4\Big] \\ &+ 2\theta_1\theta_2\Big[A_1^2A_2^2 - A_3^2(A_1^2 + A_2^2) + A_3^4 + A_4^2(A_2^2 - A_3^2) + A_5^2(A_1^2 - A_3^2 \\ &+ A_4^2) - A_6^2(A_1^2 + A_2^2 - 2A_3^2 + A_4^2 + A_5^2) + A_6^4 + 2A_7^2(-A_2^2 + A_3^2 \\ &- A_5^2 + A_6^2) + 4A_7A_8(A_1A_2 + A_4A_5) + 2A_8^2(-A_1^2 + A_3^2 - A_4^2 + A_6^2 \\ &+ 2A_7^2) - 4A_9[A_7(A_1A_3 + A_4A_6) + A_8(A_2A_3 + A_5A_6)] + 2A_9^2(A_1^2 \\ &+ A_2^2 + A_4^2 + A_5^2 - 2A_7^2 - 2A_8^2) + 4A_9^2\Big]\Big]\Big\} \qquad (2.108)\end{aligned}$$

for both polar and non-polar molecules. Here, as in the paper by Buckingham and Pople [21], $U_{\mu,ind\ \mu}$ has been written so that its unweighted orientational average is zero: the orientation-independent part is assumed to be incorporated in the R^{-6} term of U_{LJ}.

Finally, $U_{12}(\tau)$ in equation (2.94) is written

$$U_{12}(\tau) = U_{LJ} + U_{\mu,\mu} + U_{\mu,\theta} + U_{\theta,\theta} + U_{\mu,\text{ind }\mu} + U_{\theta,\text{ind }\mu} + U_{\text{shape}} \quad (2.109)$$

with the explicit expressions of these components being given in equations (2.95), (2.97), (2.102), (2.104), (2.105), (2.107) and (2.108). These energy expressions are directly applicable to pair interactions of non-linear dipolar molecules, but are easily adjusted to accommodate for interactions between non-polar non-linear molecules, polar or non-polar axially-symmetric molecules, or even spherical molecules simply by setting the relevant multipole moments to zero.

The expressions for contributions to B_ρ given in equations (2.86) to (2.90) apply directly to non-linear molecules, and can be averaged over pair interaction co-ordinates according to equation (2.56), using the interaction energy expressions for non-linear molecules derived above. Now, these expressions for contributions to B_ρ, in conjunction with the $U_{12}(\tau)$, *must fully describe linear molecules as a special case*. Hence, an acid test of these expressions was performed by using in the calculations the molecular properties of the linear molecules studied in [6,7]. The values thus obtained *exactly* matched those calculated using the expressions for B_ρ and $U_{12}(\tau)$ derived specifically for axially-symmetric molecules [6,7], which is most reassuring.

2.4.2 The integration procedure

The averages $\langle X \rangle$ in equations (2.86) to (2.90) were calculated by numerical integration of the appropriate form of equation (2.56) using Gaussian quadrature. A very useful feature of the Macsyma package is its ability to translate the final expressions directly into Fortran code, effectively eliminating the introduction of errors into the lengthy integration arguments. The ranges of α_1, α_2, β_1, β_2, γ_1 and γ_2 were divided into sixteen intervals each, while R was given a range of 0.1 to 3.0 nm divided into sixty four intervals. The possibility of closer approaches being allowed for by our shape potential was investigated by giving R a range of 0.01 to 3.0 nm, again divided into sixty four intervals. The calculated averages were found to remain constant to

at least seven significant figures, and the range limits of 0.1 to 3.0 nm were justifiably retained.

The Fortran programs, examples of which are given in Appendix 2, were run in double precision on a 486 DX-2 66 MHz PC with 32 Mb of RAM using the fast University of Salford FTN77/486 compiler. A significant departure from the Fortran programs used in previous work on linear molecules [6,7], examples of which are given in [50], was the use of large arrays to store the numerical values of the intermolecular potential expressions for all required angular configurations. This effectively bypasses repeated calculation of these values within the Gaussian quadrature routine, yielding a speed enhancement of a staggering 50 times; but has the disadvantage of requiring large amounts of expensive memory for storing a few million double-precision numbers. When the generation of these arrays exhausted the 32 Mb of RAM, use was made of the facility to page data to hard disk, which effectively provided a further 200 Mb of memory. Running times of these programs were typically of the order of eight hours each, which is to be contrasted with around fifteen minutes for the equivalent programs for axially-symmetric molecules [6,7]. The arrival of the Physics Department's new IBM RISC system/6000 workstation in October 1994 was greeted with bated breath: the 60 MHz RISC processor yielded dedicated run-times a factor of 3.3 times faster than the DX-2 machine.

2.5 Calculations of B_ρ for ethene

2.5.1 Molecular properties of ethene

The molecular data required in the calculations of B_ρ for ethene are now presented. The molecule is taken to lie in the 1-3 plane with the C=C bond on the 3-axis, the origin of the molecule-fixed axes incident with the midpoint of the bond. For a molecule of D_{2h} symmetry, the traceless electric quadrupole moment tensor will have two independent components, while the polarizability tensor has three independent components [14].

The electric quadrupole moment of ethene has been the subject of extensive experimental and theoretical investigation. Unfortunately, the

experimental investigations are usually limited to partial determinations of the quadrupole moment, or combine various experimental data in order to determine estimates of the two independent components of the quadrupole moment tensor θ_{ij}. There are, however, the accurate theoretical estimates of Spackman [7] at the MP2 (second-order Møller-Plesset perturbation theory) level, and of Maroulis [31] at the MP4 level, which are in excellent agreement with each other. Table 2.1 summarizes the measured and calculated data.

Table 2.1. Selected experimental and theoretical values of the quadrupole moment tensor components of ethene.

Method	$\frac{10^{40}\theta_{11}}{Cm^2}$	$\frac{10^{40}\theta_{22}}{Cm^2}$	$\frac{10^{40}\theta_{33}}{Cm^2}$
Measurements of collision-induced absorption (CIA) spectra [32]	6.73	-13.33	6.60
Measurements of CIA spectra [33]	5.16	-10.41	5.52
Magnetizability anisotropy measurements [34]	4.67	-12.02	7.31
Measurements of induced birefringence + second dielectric virial coefficients + refractive index [35]	4.35	-10.99	6.68
MP2 theory [7]	5.43	-11.03	5.60
MP4 theory [31]	5.370 ± 0.22	-10.92 ± 0.45	5.549 ± 0.22

We have used Maroulis' theoretical values in our calculations, noting their good agreement with the estimates of Dagg *et al.* [33] obtained from collision-induced absorption spectra measurements in ethene rare-gas mixtures.

Whereas the two principal components of the optical frequency polarizability tensor of a linear molecule can be deduced from experimental values of ρ_o and α_ν [11,36]; in the case of a non-linear molecule, which we see from equation (2.12) has three principal polarizability tensor components, an additional physical relationship between the components is required if the three components are to be

Table 2.2. The components of the optical-frequency polarizability tensor of ethene at a wavelength of 514.5 nm obtained from independently measured sets of values for ρ_o, α_ν and R_{20}.

$100\rho_o$	$\frac{10^{40}\alpha_\nu}{C^2m^2J^{-1}}$	$\frac{10^{40}(\Delta\alpha_\nu)}{C^2m^2J^{-1}}$	R_{20}	$\frac{10^{40}\alpha_{11}}{C^2m^2J^{-1}}$	$\frac{10^{40}\alpha_{22}}{C^2m^2J^{-1}}$	$\frac{10^{40}\alpha_{33}}{C^2m^2J^{-1}}$
$1.247_5 \pm 0.005$ [36]	4.76 [36]	2.077	0.22 ± 0.03 [37]	4.34_1	3.82_6	6.11_2
1.250 ± 0.002 [This work]	4.7871 [38]	2.091	0.21 ± 0.01 [39]	4.35_3	3.85_7	6.15_1

evaluated individually. It is not surprising, then, that experimentally deduced polarizability components of non-linear molecules are extremely rare. In 1975, Hills and Jones [37] measured the pure rotational Raman spectrum of ethene, and by comparing this spectrum with that calculated using an asymmetric rotor computer simulation, they were able to deduce a value for the quantity R_{20} defined as

$$R_{20} = - \frac{\sqrt{6}}{\sqrt{2}} \frac{(\alpha_{11} - \alpha_{22})}{(\alpha_{11} + \alpha_{22} - 2\alpha_{33})} . \qquad (2.110)$$

Knowledge of ρ_o and α_ν allows extraction of the polarizability anisotropy through equation (2.18), and the polarizability anisotropy is related to the polarizability tensor components through equation (2.13). Solving equations (2.12), (2.13) and (2.110) for α_{11}, α_{22} and α_{33} leads to the values listed in table 2.2. In our calculations of $\mathcal{G}_\rho$ we have used the second set of values in table 2.2 which were obtained from our measured ρ_o for ethene (see section *3.2.1* of Chapter 3), the α_ν at 514.5 nm interpolated from Hohm's high-precision measurements of the frequency dependence of α_ν for ethene [38], and the more precise value for R_{20} recently obtained by Barbès [39]. Use of the first set of values in table 2.2, however, results in a decrease of less than 0.5% in the calculated $\mathcal{G}_\rho$.

Unlike for the optical frequency polarizability, the literature contains many *ab initio* calculations of the components of the static polarizability tensor, and table 2.3 contains a summary of selected calculations. By extrapolating Hohm's measured dynamic polarizabilities [38] to zero frequency, we have obtained an estimate for α_s of $(4.5717 \pm 0.0008) \times 10^{-40}$ $C^2m^2J^{-1}$. This value, which compares favourably with the *ab initio* estimates, has been used in all our calculations of $\mathcal{G}_\rho$. Calculations performed with the *ab initio* values yield answers different only in the sixth significant figure: this is because α_s first appears in the intermolecular potential through $U_{\theta,\mathrm{ind}\,\mu}$, which is very much smaller than $U_{\theta,\theta}$.

Table 2.4. A comparison of the most precise experimental values for the second pressure virial coefficient of ethene, together with our calculated values (see text for force-constants and shape factors).

T/K	$10^6 B(T)/m^3 mol^{-1}$					
	Douslin and Harrison [42]	McElroy and Fang [44]	Levelt Sengers and Hastings [45]	Waxman and Davis [46]	Achtermann *et al.* [47]	Calculated in this work
238.15	-220.9					-225.35
243.15	-212.0		-211.6			-215.24
248.15	-203.5					-205.87
253.15	-195.5		-194.7			-197.15
258.15	-188.1					-189.01
263.15	-180.9		-180.6			-181.39
268.15	-174.1					-174.24
273.15	-167.6		-167.5	-167.7		-167.52
278.15	-161.6					-161.18
283.15	-155.7	-155.5			-155.8	-155.18
288.15	-150.3				-150.3	-149.51
293.15	-144.9	-144.6			-145.3	-144.13
298.15	-139.8			-139.8	-140.2	-139.02
303.15	-135.0	-134.7				-134.16
323.15	-117.7	-117.9		-117.6	-118.0	-116.85
348.15	-99.7			-99.6	-100.0	-99.04
373.15	-84.8			-84.6	-85.1	-84.39
398.15	-72.3			-72.1		-72.11
423.15	-61.6			-61.3		-61.67
448.15	-52.4			-52.2		-52.67

Table 2.3. Selected values of *ab initio* calculated static polarizability tensor components of ethene.

Authors	$\frac{10^{40}\alpha_{11}}{C^2m^2J^{-1}}$	$\frac{10^{40}\alpha_{22}}{C^2m^2J^{-1}}$	$\frac{10^{40}\alpha_{33}}{C^2m^2J^{-1}}$	$\frac{10^{40}\alpha_{s}}{C^2m^2J^{-1}}$
Amos and Williams [40]	3.99	3.66	6.00	4.55
Spackman [7]	4.092	3.534	5.594	4.407
Maroulis [8]	4.157 ± 0.020	3.695 ± 0.028	5.645 ± 0.012	4.500 ± 0.020
Sekino and Bartlett [41]	4.146	3.667	5.582	4.465

Finally, we present our values for the shape factors D_1 and D_2. These were determined by fitting values of the second pressure virial coefficient B(T) calculated according to the equation

$$B(T) = \frac{N_A}{32\pi^3}\int_{R=0}^{\infty}\int_{\alpha_1=0}^{2\pi}\int_{\beta_1=0}^{\pi}\int_{\gamma_1=0}^{2\pi}\int_{\alpha_2=0}^{2\pi}\int_{\beta_2=0}^{\pi}\int_{\gamma_2=0}^{2\pi}\left[1 - \exp\left[-U_{12}(\tau)/kT\right]\right] \times R^2\sin\beta_1\sin\beta_2\, dR\, d\alpha_1 d\beta_1 d\gamma_1 d\alpha_2 d\beta_2 d\gamma_2 \qquad (2.111)$$

to the experimental values listed in table 2.4 over the temperature range 238.15 K to 448.15 K. Force constants required for the Lennard-Jones 6:12 potential are given in the appendices of the classic text of Hirschfelder *et al.* [48]. For ethene, the parameters obtained from viscosity data are ε/k = 205 K and R_o = 0.4232 nm. The more recent parameters of Das Gupta *et al.* obtained from a combination of viscosity data and second pressure virial coefficients are ε/k = 193.5 K and R_o = 0.4236 nm [49]. We optimized the force constants for best agreement between the calculated and experimental B(T) values over the full experimental temperature range, obtaining ε/k = 190.0 K and R_o = 0.4232 nm. We note that these values compare very favourably with those of Das Gupta *et al.*

In our choice of molecular shape we treat ethene as a planar molecule, the dimensions of which are taken from simple molecular geometry. This means that the approach distance R in case (iii) of figure 2.3 can be

less than R_o before the onset of contact forces, while the opposite is true for cases (i) and (ii). D_1 and D_2 must both be positive, and must satisfy the requirement that $(D_1 + D_2) \leq \frac{1}{2}$. As an initial approximation, we choose that D_1 should equal D_2 (i.e. a *square plane*), and adjust their numerical value until the calculated and experimental B(T) values agree to within 1% over the full experimental temperature range. This yields rough estimates of D_1 and D_2. The ratio of the true D_1 and D_2 values for ethene is obtained from the molecular dimensions (see figure 2.3) by taking the ratio of approaches for cases (ii) and (i) when contact forces first occur. We have

$$\frac{-2D_1 + 4D_2}{4D_1 - 2D_2} \approx \frac{0.249}{0.309} ,$$

which gives

$$\frac{D_1}{D_2} = 1.074 .$$

Using the rough $D_1 = D_2$ values obtained from the square plane treatment, in conjunction with the known ratio of D_1 and D_2, it is possible to home in on the optimum values for the shape factors by adjusting them until agreement between calculated and experimental B(T) values is reached. This procedure was repeated for various values of the force-constants ε/k and R_o until they, too, are optimized. After setting R_o to 0.4232 nm and ε/k to 190.0 K, and optimizing the shape factors $(D_1 = 0.22965$ and $D_2 = 0.21383)$, the calculated and experimental curves were found to lie within 1.0% of each other over almost the entire temperature range (see table 2.4). This excellent agreement between theory and experiment fixed our choice of force-constants and shape parameters. When the value for ε/k was adjusted a few per cent above or below 190 K, with D_1 and D_2 being re-optimized, the calculated curve was found to tilt with respect to the experimental curve, matching it *only* for the specific ε/k = 190 K. Hence, matching calculated second pressure virial coefficients to experimental data remains an excellent route to the optimization of the Lennard-Jones force constants and shape parameters even in the case of non-linear molecules with low symmetry.

2.5.2 Results of calculations for ethene

We note that calculations of B_ρ for ethene *when treated as an axially symmetric molecule* have already been performed [5,6]. Here, attempts to optimize R_o and ε/k such that the calculated B(T) values would closely fit the experimental values listed in table 2.4 were never entirely successful. Choosing the shape factor D such that agreement between theory and experiment at around 298 K was within 1% saw typical disagreements at the two extremes of the temperature range of as much as 7%. This in itself indicates just how unsatisfactory it is to assume axial symmetry for the ethene molecule. With R_o = 0.4232 nm, ε/k = 205 K and D = 0.240; the calculated $\mathcal{P}_\rho$ at 298.2 K and a wavelength of 514.5 nm is 66.04 $\times$ 10^{-6} m^3mol^{-1} [50]. Allowing for the non-linear shape of ethene changes this value to 94.36 $\times$ 10^{-6} m^3mol^{-1} (as shown below), the latter value being in much closer agreement with experiment (see Chapter 3).

Table 2.5 summarizes our calculations allowing for the non-linearity of ethene. The relative magnitudes of the various contributions to B_ρ are calculated at T = 294.92 K, which is the mean temperature of our experimental determination of B_ρ for ethene as presented in Chapter 3. Table 2.6 presents the temperature dependence of the calculated $\mathcal{P}_\rho$ and B_ρ values for ethene. The very small temperature dependence in $\mathcal{P}_\rho$ would be obscured in the experimental uncertainty of measured values over this temperature range.

We note that, as was found for most axially-symmetric molecules [5,6], the α_5 term makes a significant contribution to $\mathcal{P}_\rho$. It is obvious, however, that the series of terms is now rapidly converging so that, as was argued earlier [6], the α_6 and higher-order terms in the dipole-dipole interaction should contribute negligibly. In section *3.2.1* of Chapter 3 we report our measurement of the second light-scattering virial coefficient B_ρ for ethene, and make a detailed comparison with the value calculated here.

Table 2.5. The relative magnitudes of the various contributions to B_ρ of ethene calculated at 294.92 K and λ = 514.5 nm. The Lennard-Jones force-constants R_o = 0.4232 nm and ε/k = 190.0 K, and the shape factors D_1 = 0.22965 and D_2 = 0.21383, have been used. B_ρ is obtained from equation (2.91) using ρ_o = 0.01250. The full symmetry of the ethene molecule had been allowed for.

Contributing Term	$10^6 \times$ Value / $m^3 mol^{-1}$	% Contribution to B_ρ
g	23.42	-12.21
$\&_3$	2.94	-1.53
a_3	-68.11	35.52
a_4	128.97	-67.26
a_5	7.14	-3.72
$\mathcal{G}_\rho$	94.36	-49.21
2B	-286.12	149.21

$$B'_\rho = -191.76 \times 10^{-6}\ m^3 mol^{-1}$$

$$B_\rho = -2.357 \times 10^{-6}\ m^3 mol^{-1}$$

Table 2.6. Temperature dependence of the calculated $\mathcal{G}_\rho$ and B_ρ values of ethene at λ = 514.5 nm.

T / K	$10^6 \mathcal{G}_\rho$ / $m^3 mol^{-1}$	$10^6 B$ [42] / $m^3 mol^{-1}$	$\mathcal{G}_\rho / 2B$	$10^6 B_\rho$ / $m^3 mol^{-1}$
238.15	103.22	-220.9	-0.23	-4.162
273.15	96.80	-167.6	-0.29	-2.930
294.92	94.36	-143.1	-0.33	-2.357
328.00	91.87	-113.9	-0.40	-1.671
373.15	89.78	-84.8	-0.53	-0.981
448.15	87.97	-52.4	-0.84	-0.207

There are no other non-linear non-polar molecules for which the necessary molecular data required in a calculation of $\mathcal{S}_\rho$ have been measured or calculated. However, there are two polar molecules belonging to the C_{2v} point group for which such data are available, namely sulphur dioxide and dimethyl ether. We now focus our attention on these molecules.

2.6 Calculations of B_ρ for sulphur dioxide

2.6.1 Molecular properties of sulphur dioxide

The sulphur dioxide molecule is taken to lie in the 1-3 plane of the molecule-fixed axes (1,2,3), with 3 along the principal molecular axis. The origin of the axes is at the centre of mass of the molecule. For a molecule of C_{2v} symmetry, the electric dipole moment tensor will have one component, while the traceless electric quadrupole moment tensor will have two independent components, and the polarizability tensor three independent components [14].

The equilibrium dipole moment of sulphur dioxide has been precisely determined by molecular beam electric resonance spectroscopy [51], and this value, which is compared with theoretical estimates in table 2.7, has been used in our calculations.

Table 2.7. Selected experimental and theoretical values of the dipole moment of sulphur dioxide.

Method	$\frac{10^{30}\mu_3}{Cm}$
Value selected by the U.S. National Bureau of Standards [52]	-5.44
Molecular beam electric resonance spectroscopy [51]	-5.4262 ± 0.0010
Ab initio SCF calculations [53]	-6.6783
Ab initio SCF calculations [54] †	-6.553
Ab initio CPF(ED) calculations [54] †	-5.347

† The authors argue that the CPF(ED) values are the most accurate and reliable. Agreement between these values and experimental ones for the various molecular properties is, in general, good.

As for ethene, the electric quadrupole moment of sulphur dioxide has been the subject of extensive experimental and theoretical investigation. Table 2.8 summarizes the measured and calculated data. It is important to note that since only the leading moment of charge in the multipole expansion is origin independent [59], the quadrupole moment of a polar molecule depends on the origin to which it is referred. Buckingham and Longuet-Higgins [60] have investigated this matter in some depth, and we must specify that for the magnetizability anisotropy measurements and *ab initio* calculations in table 2.8, the origin is at the centre of mass of the molecule. We have used the values of Ellenbroek and Dymanus [57] obtained from magnetizability anisotropy measurements, this being the most accurate set of experimental values, and agreeing very well with the *ab initio* CPF(ED) calculations of Bacskay *et al.* [54].

Table 2.9. The components of the optical-frequency polarizability tensor of sulphur dioxide.

Method	λ/nm	$\frac{10^{40}\alpha_{11}}{C^2m^2J^{-1}}$	$\frac{10^{40}\alpha_{22}}{C^2m^2J^{-1}}$	$\frac{10^{40}\alpha_{33}}{C^2m^2J^{-1}}$
Experimental derivation from: R_{20} = 0.212 ± 0.035 [61] α_ν = 4.389 [36] ρ_o = 0.0185 ± 0.0001 [36]	514.5	5.92 ± 0.01	3.35 ± 0.04	3.91 ± 0.05
Experimental derivation from: R_{20} = 0.212 ± 0.035 [61] α_ν = 4.389 [36] ρ_o = 0.0188 ± 0.0001 [this work]	514.5	5.928 ± 0.01	3.336 ± 0.04	3.902 ± 0.05
Experimental derivation from: The Cotton-Mouton effect [62] α_ν = 4.326 [36] R_{20} = 0.212 ± 0.035 [61]	632.8	6.03 ± 0.29	3.16 ± 0.19	3.79 ± 0.12
Experimental derivation from: The Kerr effect [63] α_ν = 4.326 [36] ρ_o = 0.0179 ± 0.0001 [36]	632.8	5.80 ± 0.06	3.30 ± 0.04	3.88 ± 0.06
Ab initio calculation from CPF(ED) theory [54]	514.5	5.789	3.281	3.779
	632.8	5.713	3.237	3.758

Table 2.8. Selected experimental and theoretical values of the quadrupole moment tensor components of sulphur dioxide. The origin is at the centre of mass of the molecule.

Method	$\frac{10^{40}\theta_{11}}{Cm^2}$	$\frac{10^{40}\theta_{22}}{Cm^2}$	$\frac{10^{40}\theta_{33}}{Cm^2}$
Magnetizability anisotropy measurements [55]	-17.7 ± 1.3	13.3 ± 2.0	4.3 ± 1.0
Magnetizability anisotropy measurements [56]	-22.0 ± 25.4	-7.7 ± 25.4	29.7 ± 27.7
Magnetizability anisotropy measurements [57]. (This molecular beam spectrometer had 50 times better resolution than those used in [55] & [56])	-16.4 ± 0.3	12.9 ± 0.2	3.5 ± 0.1
SCF theory [58]	-22.9	17.2	5.7
SCF theory [53]	-19.64 ± 0.18	15.17 ± 0.40	4.48 ± 0.22
SCF theory [54]	-19.563	15.158	4.405
CPF(ED) theory [54]	-16.386	13.036	3.350

The optical-frequency polarizability tensor components of sulphur dioxide are particularly well-defined, having been measured by three independent experimental techniques [61-63], and having been calculated by CPF(ED) theory [54]. Table 2.9 contains a summary of these data. The values given by Murphy [61] have been deduced using the method of Hills and Jones [37] as described in section *2.5.1*. By measuring the pure rotational Raman spectrum of sulphur dioxide at 514.5 nm, and modelling the behaviour using an asymmetric rotor computer program, Murphy obtained the value of R_{20} as defined in equation (2.110). Combining this with the values of ρ_o and α_ν at 514.5 nm reported for sulphur dioxide in [36] allowed equations (2.12), (2.13) and (2.110) to be solved simultaneously for α_{11}, α_{22} and α_{33}. Of course, this yields two sets of polarizabilities, and in order to choose between them Murphy argued that the anisotropy $(\alpha_{33}-\alpha_\nu)$ should be negative since the observed Kerr constant of sulphur dioxide is negative [64,65]. This is confirmed by CPF(ED) theory [54], so that no ambiguity in the choice remains. In our calculations, we have made use of the values obtained from Murphy's R_{20}, the α_ν quoted in [36], and our ρ_o. This sees a negligible increase in $\mathcal{G}_\rho$ of less than 0.5% compared with results based on the ρ_o of Bogaard *et*

al. [36]. The two other experimental determinations of the dynamic polarizability tensor components yield values at 632.8 nm. In [62], measurements of the temperature dependence of the Cotton-Mouton effect of sulphur dioxide were combined with known values of the magnetizabilities, the mean dynamic polarizability α_ν at 632.8 nm [36], and Murphy's R_{20}; and in [63], measurements of the temperature dependence of the electro-optical Kerr effect were combined with α_ν and ρ_o [36] to yield very precise polarizability components. Notice the favourable agreement between the experimentally deduced components and those calculated using CPF(ED) theory [54].

Bacskay *et al.* have also performed *ab initio* CPF(ED) calculations of the static polarizability of sulphur dioxide, obtaining a mean static polarizability α_s of 3.974×10^{-40} $C^2m^2J^{-1}$ [54]. Extrapolation of the measured dynamic polarizabilities given in reference [36] to zero frequency yields an estimate for α_s of $(4.2072 \pm 0.0013) \times 10^{-40}$ $C^2m^2J^{-1}$, and this value, which agrees well with CPF(ED) theory, has been used in all our calculations for this molecule.

Once again, the shape factors D_1 and D_2 were determined by fitting values of the second pressure virial coefficient B(T) calculated according to equation (2.111) to experimental values. The B(T) values obtained by Kang *et al.* [66] are the most precise in the literature [43], and span the largest temperature range (from 283.15 K to 473.15 K). The Lennard-Jones force-constants given by Hirschfelder *et al.* [48], which were derived from viscosity data, are ε/k = 252 K and R_o = 0.4290 nm. Optimizing these values for best agreement between calculated and experimental B(T) values over the full experimental temperature range yielded ε/k = 220.0 K and R_o = 0.3850 nm. As in the case of ethene, we initially set $D_2 = D_1$, adjusting their numerical value for optimal agreement between the experimental and calculated B(T) values. Then, using simple molecular geometry (see figure 2.3) and the ratio of approaches for cases (ii) and (i) when contact forces first occur, we obtain

$$\frac{-2D_1 + 4D_2}{4D_1 - 2D_2} \approx \frac{0.378}{0.244}$$

and hence

Table 2.10. A comparison of the most precise experimental values for the second pressure virial coefficient of sulphur dioxide, together with our calculated values (see text for force-constants and shape factors).

T/K	$10^6 B(T)/m^3 mol^{-1}$				
	Kang *et al.* [66]	Cooper and Maass [67]	Cawood and Patterson [68]	Riedel [69] Following B values given by Balbuz [70]	Calculated in this work
283.15	-500.0 ± 20	-482*		-501	-501.32
293.15	-452.0 ± 18	-434*		-433	-450.88
303.15	-404.0 ± 16	-394*	-411.2	-395	-408.17
313.15	-367.5 ± 15	-360*		-360	-371.62
323.15	-332.8 ± 13	-332	-350.5		-340.04
348.15	-279.0 ± 11				-277.38
373.15	-232.5 ± 9				-231.04
398.15	-201.0 ± 8				-195.53
423.15	-171.1 ± 7				-167.55
448.15	-144.1 ± 7				-144.98
473.15	-125.8 ± 7				-126.43

*These values were interpolated from a least squares polynomial fit to the authors' measured values.

$$\frac{D_1}{D_2} = 0.866 \ .$$

Using this ratio in conjunction with the approximate $D_1 = D_2$, the best values for D_1 and D_2 were then obtained by performing trial and error optimization as previously described. This yielded $R_o = 0.3850$ nm, $\varepsilon/k = 220.0$ K, $D_1 = 0.0873$ and $D_2 = 0.1008$. A comparison of the experimental and calculated B(T) values is given in table 2.10. Although the calculated values always fall well within the uncertainty limits of the experimental values of Kang *et al.* [66], there are spurious discrepancies of up to nearly 3% at some of the temperatures, almost certainly due to imprecision in the measured values. Contrast this with ethene, where the second pressure virial coefficient has been determined to an extraordinarily high precision by several different workers in recent years [43-47]. The reason for this lies in economics: the growth of the petrochemical industry has seen worldwide production of ethene rise to megatons per year, and since large volume-flows of the gas have to be measured precisely, there is a demand for accurate knowledge of the compression factor. Whereas ethene's PVT properties have enjoyed experimental investigation on an almost annual basis, the PVT properties of sulphur dioxide were last measured by Kang *et al.* [66] in 1961. We know that extraction of $\mathcal{G}_\rho$ from a measured value of B_ρ requires accurate knowledge of the B(T) value at the temperature of the experimental determination, especially for a small $(\mathcal{G}_\rho/2B)$ ratio. Measurement of B(T) for sulphur dioxide ought to be revisited, especially in view of the relatively simple and yet extremely precise new method of measuring B(T) developed by Koschine and Lehmann [71].

2.6.2 Results of calculations for sulphur dioxide

Table 2.11 gives the relative magnitudes of the various contributions to B_ρ calculated at the wavelength and mean temperature of our experimental determination of B_ρ (see Chapter 3), namely $\lambda = 514.5$ nm and $T = 338.35$ K. Again we stress that contributions arising from the a_2A_1 term in equation (2.48) have been found to make, at least in the regime of linear polar molecules, a sometimes significant contribution to $\mathcal{G}_\rho$ of as much as -9% [6], although contributions to some molecules were as

small as -0.8%. We currently have no way of estimating the A-tensor components of sulphur dioxide, although calculated estimates are probably within the reach of the later versions of the CADPAC (Cambridge Analytic Derivatives Package) program of R. D. Amos and J. E. Rice, and this avenue should certainly be explored further. In Chapter 3 we report our measurement of B_ρ for sulphur dioxide, and make a comparison with the value calculated here at λ = 514.5 nm.

Table 2.11. The relative magnitudes of the various contributions to B_ρ of sulphur dioxide calculated at 338.35 K and λ = 514.5 nm. The Lennard-Jones force-constants R_o = 0.3850 nm and ε/k = 220.0 K, and the shape factors D_1 = 0.0873 and D_2 = 0.1008, have been used. B_ρ is obtained from equation (2.91) using ρ_o = 0.01879.

Contributing Term	$\frac{10^6 \times \text{Value}}{m^3 mol^{-1}}$	% Contribution to B_ρ
g	-16.89	4.89
b_3	-3.35	0.97
a_3	53.31	-15.43
a_4	194.12	-56.20
a_5	22.20	-6.43
$\mathcal{G}_\rho$	249.39	-72.20
2B	-594.82	172.20

$$B'_\rho = -345.43 \times 10^{-6}\ m^3 mol^{-1}$$

$$B_\rho = -6.328 \times 10^{-6}\ m^3 mol^{-1}$$

Table 2.12 lists the temperature dependence of the calculated $\mathcal{G}_\rho$ and B_ρ values. The rather significant temperature dependence of $\mathcal{G}_\rho$ for this molecule is surprising in as much as every other molecule investigated thus far has been found to have a relatively tiny dependence on temperature. This may be an artefact of the omission of a large and negative a_2A_1 term which would diminish with increasing temperature,

perhaps stabilizing the calculated $\mathcal{Y}_\rho(T)$. Once again, without estimates of A-tensor components, we can do no more than speculate. It would be unrealistic to turn to experiment for an answer, since the large uncertainty of about 4% in the B(T) values of Kang *et al.* [66] coupled with the low $(\mathcal{Y}_\rho/2B)$ of around -0.4 means that $\mathcal{Y}_\rho$ values extracted from a series of $B_\rho(T)$ measurements would have such large uncertainties as to obscure any temperature dependence. In any case, at T = 303.15 K the saturation vapour pressure of sulphur dioxide is only 462 kPa [66], so that the pressure range is insufficient to yield a precise experimental value for B_ρ.

Table 2.12. Temperature dependence of the calculated $\mathcal{Y}_\rho$ and B_ρ values of sulphur dioxide at λ = 514.5 nm.

$\frac{T}{K}$	$\frac{10^6\mathcal{Y}_\rho}{m^3mol^{-1}}$	$\frac{10^6B\ [66]}{m^3mol^{-1}}$	$\frac{\mathcal{Y}_\rho}{2B}$	$\frac{10^6B_\rho}{m^3mol^{-1}}$
303.15	322.99	-404.0	-0.40	-8.885
338.35	249.39	-297.4	-0.42	-6.328
473.15	146.27	-125.8	-0.58	-1.930

2.7 Calculations of B_ρ for dimethyl ether

2.7.1 Molecular properties of dimethyl ether

Dimethyl ether also belongs to the C_{2v} point group, and the molecule is taken to lie in the 1-3 plane of the molecule-fixed axes with 3 along the principal molecular axis.

The equilibrium dipole moment of dimethyl ether has been determined from the Stark effect by Blukis *et al.* [72], who found $\mu_3 = -(4.37 \pm 0.03) \times 10^{-30}$ Cm.

The electric quadrupole moment tensor components have been obtained by Benson and Flygare [73] from magnetizability anisotropy measurements. These values, which have been used in our calculations, are compared with *ab initio* calculated estimates at the MP2 level of theory in table 2.13. Once again, it is cautioned that the quadrupole moments of polar molecules are origin dependent, and the origin is placed at the centre of mass of the molecule.

Table 2.13. The experimental and theoretical values of the quadrupole moment tensor components of dimethyl ether. The origin is at the centre of mass of the molecule.

Method	$\frac{10^{40}\theta_{11}}{Cm^2}$	$\frac{10^{40}\theta_{22}}{Cm^2}$	$\frac{10^{40}\theta_{33}}{Cm^2}$
Magnetizability anisotropy measurements [73]	11.0 ± 2.0	-4.3 ± 2.0	-6.7 ± 1.7
MP2 theory [74]	11.59	-2.56	-9.04

The optical-frequency polarizability tensor components of dimethyl ether have not been measured at λ = 514.5 nm. However, *ab initio* values at the MP2 level of theory have been calculated for a range of common laser wavelengths [75], including λ = 514.5 nm. We note the excellent agreement (within 3%) between the calculated [74,75] and measured [74,76] polarizability components at λ = 632.8 nm; and so we use the calculated values at λ = 514.5 nm with confidence. These values are listed in table 2.14.

Table 2.14. The components of the optical-frequency polarizability tensor of dimethyl ether at λ = 514.5 nm, as obtained from *ab initio* calculations [75].

$\frac{10^{40}\alpha_{11}}{C^2m^2J^{-1}}$	$\frac{10^{40}\alpha_{22}}{C^2m^2J^{-1}}$	$\frac{10^{40}\alpha_{33}}{C^2m^2J^{-1}}$
6.72	5.51	5.32

Spackman and co-workers have also performed *ab initio* MP2 calculations of the static polarizability of dimethyl ether, obtaining a mean static polarizability α_s of 5.420×10^{-40} $C^2m^2J^{-1}$ [75]. Extrapolation of the measured dynamic polarizabilities for this molecule [36] to zero frequency yields an estimate for α_s of $(5.726 \pm 0.011) \times 10^{-40}$ $C^2m^2J^{-1}$. This value, which is in good agreement with the theory, has been used in all our calculations for dimethyl ether.

The shape factors D_1 and D_2 were once again determined by fitting values of the second pressure virial coefficient B(T) calculated according to equation (2.111) to the available experimental data. The only reliable set of experimental measurements of B(T) for dimethyl ether are those of Haworth and Sutton [77], which were taken at 298.2 K, 313.2 K and 328.2 K, and which have a quoted precision of less than 3%. Using the molecular geometry of dimethyl ether given by Coonan *et al.* [74], we obtain from the ratio of approaches for cases (ii) and (i) in figure 2.3 when contact forces first occur

$$\frac{-2D_1 + 4D_2}{4D_1 - 2D_2} \approx \frac{0.22}{0.16}$$

and hence

$$\frac{D_1}{D_2} = 0.90 \ .$$

As before, approximate values of D_1 and D_2 are obtained by setting $D_1 = D_2$, and optimizing their numerical value for best agreement between the calculated and measured B(T) values. Then, the ratio of D_1 and D_2 is invoked, and the process repeated. There are no Lennard-Jones force-constants for dimethyl ether in the literature, and so the values for ethanol [48], namely $R_o = 0.4455$ nm and $\varepsilon/k = 391$ K, were used as a first approximation. Optimization of the force-constants and shape factors yielded $R_o = 0.440$ nm, $\varepsilon/k = 320.0$ K, $D_1 = 0.1923$ and $D_2 = 0.2137$. Values of B(T) calculated using these parameters are compared with the experimental data in table 2.15.

Table 2.15. A comparison of the most precise experimental values for the second pressure virial coefficient of dimethyl ether, together with our calculated values (see text for force-constants and shape factors).

T/K	$10^6 B(T)/m^3 mol^{-1}$	
	Haworth and Sutton [77]	Calculated in this work
298.2	-456 ± 10	-455.7
313.2	-405 ± 10	-406.4
328.2	-368 ± 10	-366.1

2.7.2 Results of calculations for dimethyl ether

Table 2.16 gives the relative magnitudes of the various contributions to B_ρ calculated at the particular temperature of 328.2 K and wavelength of 514.5 nm. Currently, there are no available values for the A-tensor components of dimethyl ether, and so the extent to which the $a_2 A_1$ term contributes to γ_ρ cannot be estimated. Table 2.17 lists the temperature dependence of the calculated γ_ρ and B_ρ values. Dimethyl ether has a relatively high calculated $(\gamma_\rho/2B)$ ratio of -2.7, and so is an ideal candidate for experimental investigation. We are still awaiting the delivery of a cylinder of dimethyl ether, and so measurements are not reported in this work.

Table 2.16. The relative magnitudes of the various contributions to B_ρ of dimethyl ether calculated at 328.2 K and λ = 514.5 nm. The Lennard-Jones force-constants R_o = 0.3850 nm and ε/k = 220.0 K, and the shape factors D_1 = 0.0873 and D_2 = 0.1008, have been used. B_ρ is obtained from equation (2.91) using ρ_o = 0.00371 [36].

Contributing Term	$\frac{10^6 \times \text{Value}}{m^3 mol^{-1}}$	% Contribution to B_ρ
g	19.78	1.64
$\&_3$	-2.50	-0.21
a_3	201.32	16.68
a_4	1495.76	123.95
a_5	228.31	18.92
φ_ρ	1942.67	160.99
2B	-736.0	-60.99

$$B'_\rho = 1206.7 \times 10^{-6}\ m^3 mol^{-1}$$

$$B_\rho = 4.455 \times 10^{-6}\ m^3 mol^{-1}$$

Table 2.17. Temperature dependence of the calculated φ_ρ and B_ρ values of dimethyl ether at λ = 514.5 nm.

$\frac{T}{K}$	$\frac{10^6 \varphi_\rho}{m^3 mol^{-1}}$	$\frac{10^6 B\ [77]}{m^3 mol^{-1}}$	$\frac{\varphi_\rho}{2B}$	$\frac{10^6 B_\rho}{m^3 mol^{-1}}$
298.2	2545.10	-456	-2.79	6.029
313.2	2197.73	-405	-2.71	5.123
328.2	1942.67	-368	-2.64	4.455

Unfortunately, there are no other non-linear molecules for which we have all the necessary molecular data to perform calculations of φ_ρ. Molecules which could be profitably investigated include hydrogen sulphide, dichloromethane and difluoromethane; but, to the best of our knowledge, their quadrupole moments have not yet been determined.

2.8 References

[1] Landau, L. D., and Lifshitz, E. M., 1962, *The Classical Theory of Fields* (Oxford: Pergamon).

[2] Buckingham, A. D., and Raab, R. E., 1975, *Proc. Roy. Soc. Lond.* A, **345,** 365.

[3] Raab, R. E., 1975, *Molec. Phys.*, **29,** 1323; Logan, D. E., 1982, *Molec. Phys.*, **46,** 271; Imrie, D. A., and Raab, R. E., 1991, *Molec. Phys.*, **74,** 833; Graham, E. B., Pierrus, J., and Raab, R. E., 1992, *J. Phys. B: At. Mol. Opt. Phys.*, **25,** 4673.

[4] Buckingham, A. D., and Stephen, M. J., 1957, *Trans. Faraday Soc.*, **53,** 854.

[5] Graham, C., 1992, *Molec. Phys.*, **77,** 291.

[6] Couling, V. W., and Graham, C., 1993, *Molec. Phys.*, **79,** 859.

[7] Spackman, M. A., 1989, *J. phys. Chem.*, **93,** 7594.

[8] Maroulis, G, 1992, *J. chem. Phys.*, **97,** 4188.

[9] Buckingham, A. D., and Pople, J. A., 1955, *Proc. Phys. Soc.* A, **68,** 905.

[10] Andrews, A. L., and Buckingham, A. D., 1960, *Molec. Phys.*, **3,** 183.

[11] Bridge, N. J., and Buckingham, A. D., 1966, *Proc. Roy. Soc. Lond.* A, **295,** 334.

[12] Benoit, H., and Stockmayer, W. H., 1956, *J. Phys. Radium*, **17,** 21.

[13] Graham, C., 1971, Ph. D. Thesis, University of Cambridge.

[14] Buckingham, A. D., 1967, *Adv. chem. Phys.*, **12,** 107.

[15] Burns, R. C., Graham, C., and Weller, A. R. M., 1986, *Molec. Phys.*, **59,** 41.

[16] Margenau, H., and Murphy, G. M., 1956, *The Mathematics of Physics and Chemistry* (New York: Van Nostrand).

[17] Varshalovich, D. A., Moskalev, A. N., and Kharsonskii, V. K., 1988, *Quantum Theory of Angular Momentum* (Teaneck: World Scientific).

[18] Buckingham, A. D., and Utting, B. D., 1970, *Annu. Rev. Phys. Chem.*, **21,** 287.

[19] Maitland, G. C., Rigby, M., Smith, E. B., and Wakeham, W. A., 1981, *Intermolecular Forces, their Origin and Determination* (Oxford: Clarendon).

[20] Buckingham, A. D., and Watts, R. S., 1973, *Molec. Phys.*, **26,** 7.

[21] Buckingham, A. D., and Pople, J. A., 1955, *Trans. Faraday Soc.*, **51,** 1029, 1173.

[22] Buckingham, A. D., 1956, *Trans. Faraday Soc.*, **52,** 747.

[23] Copeland, T. G., and Cole, R. H., 1976, *J. chem. Phys.*, **64,** 1741.

[24] Sutter, H., and Cole, R. H., 1970, *J. chem. Phys.*, **52,** 132.

[25] Brookmeyer, B., 1973, M. Sc. Thesis, Brown University.

[26] Buckingham, A. D., and Graham, C., 1974, *Proc. Roy. Soc. Lond.* A, **336,** 275.

[27] Lennard-Jones, J. E., 1924, *Proc. Roy. Soc. Lond.* A, **106,** 441.

[28] Bose, T. K., and Cole, R. H., 1970, *J. chem. Phys.*, **52,** 140.

[29] Burns, R. C., 1978, Ph. D. Thesis, University of Natal.

[30] Weller, A. R. M., 1985, M. Sc. Thesis, University of Natal.

[31] Maroulis, G., 1993, *J. Phys. B: At. Mol. Opt. Phys.*, **26,** 775.

[32] Gray, C. G., Gubbins, K. E., Dagg, I. R., and Read, L. A. A., 1980, *Chem. Phys. Lett.*, **73,** 278.

[33] Dagg, I. R., Read, L. A. A., and Smith, W., 1982, *Can. J. Phys.*, **60,** 1431.

[34] Kukolich, S. G., Aldrich, P. D., Read, W. G., and Campbell, E. J., 1983, *J. chem. Phys.*, **79,** 1105.

[35] Bose, T. K., Boudjarane, K., Huot, J., and St Arnaud, J. M., 1988, *J. chem. Phys.*, **89,** 7435.

[36] Bogaard, M. P., Buckingham, A. D., Pierens, R. K., and White, A. H., 1978, *J. chem. Soc. Faraday Trans.* I, **74,** 3008.

[37] Hills, G. W., and Jones, W. J., 1975, *J. chem. Soc. Faraday Trans.* II, **71,** 812.

[38] Hohm, U., 1993, *Molec. Phys.*, **78,** 929.

[39] Barbès, H., 1987, *J. Raman Spectrosc.*, **18,** 507.

[40] Amos, R. D., and Williams, J. H., 1979, *Chem. Phys. Lett.*, **66,** 471.

[41] Sekino, H., and Bartlett, R. J., 1993, *J. chem. Phys.*, **98,** 3022.

[42] Douslin, D. R., and Harrison, R. H., 1976, *J. chem. Thermodyn.*, **8,** 301.

[43] Dymond, J. H., and Smith, E. B., 1980, *The Virial Coefficients of Pure Gases and Mixtures* (Oxford: Clarendon).

[44] McElroy, P. J., and Fang, J., 1993, *J. Chem. Eng. Data*, **38,** 410.

[45] Levelt Sengers, J. M. H., and Hastings, J. R., 1982, *Proceedings of the 8th Symposium on Thermophysical Properties*, **1,** 66.

[46] Waxman, M., and Davis, H. A., 1979, *Equations of State in Engineering and Research, Advances in Chemistry Series* (American Chemical Society: New York), **182,** 285.

[47] Achtermann, H. J., Bose, T. K., and Magnus, G., 1990, *Int. J. Thermophys.*, **11,** 133.

[48] Hirschfelder, J. O., Curtiss, C. F., and Bird, R. B., 1954, *Molecular Theory of Gases and Liquids* (Chichester: Wiley).

[49] Das Gupta, A., Singh, Y., and Singh, S., 1973, *J. chem. Phys.*, **59**, 1999.

[50] Couling, V. W., 1993, M. Sc. Thesis, University of Natal.

[51] Patel, D., Margolese, D., and Dyke, T. R., 1979, *J. chem. Phys.*, **70**, 2740.

[52] Nelson, R. D., Lide, D. R., and Maryott, A. A., 1967, U.S. National Bureau of Standards Standard Reference Data Series No. 10.

[53] Maroulis, G., 1992, *J. Phys. B; At. Mol. Opt. Phys.*, **25**, L77.

[54] Bacskay, G. B., Rendell, A. P. L., and Hush, N. S., 1988, *J. chem. Phys.*, **89**, 5721.

[55] Pochan, J. M., Stone, R. G., and Flygare, W. H., 1969, *J. chem. Phys.*, **51**, 4278.

[56] Bhattacharyya, P. K., and Dailey, B. P., 1969, *J. chem. Phys.*, **51**, 3051.

[57] Ellenbroek, A. W., and Dymanus, A., 1976, *Chem. Phys. Lett.*, **42**, 303.

[58] Rothenberg, S., and Schaefer III, H. F., 1970, *J. chem. Phys.*, **53**, 3014.

[59] Buckingham, A. D., 1959, *Q. Rev. Chem. Soc. Lond.*, **13**, 183.

[60] Buckingham, A. D., and Longuet-Higgins, H. C., 1968, *Molec. Phys.*, **14**, 63.

[61] Murphy, W. F., 1981, *J. Raman Spectrosc.*, **5**, 339.

[62] Lukins, P. B., and Ritchie, G. L. D., 1985, *J. phys. Chem.*, **89**, 3409.

[63] Gentle, I. R., Laver, D, R., and Ritchie, G. L. D., 1990, *J. phys. Chem.*, **94**, 3434.

[64] Szivessy, G., 1924, *Z. Phys.*, **26**, 323.

[65] Le Fèvre, R. J. W., and Ritchie, G. L. D., 1965, *J. chem. Soc.*, 3520.

[66] Kang, T. L., Hirth, L. J., Kobe, K. A., and McKetta, J. J., 1961, *J. chem. Engng. Data*, **6**, 220.

[67] Cooper, D. Le B., and Maass, O., 1931, *Can. J. Res.*, **4**, 495.

[68] Cawood, W., and Patterson, H. S., 1933, *J. chem. Soc.*, 619.

[69] Riedel, L., 1939, *Z. ges. Kalteind.*, **46**, 22.

[70] Baibuz, V. F., 1958, *Zh. fiz. Khim.*, **32**, 2644.

[71] Koschine, A, and Lehmann, J. K., 1992, *Meas. Sci. Technol.*, **3**, 411.

CHAPTER 3

EXPERIMENTAL MEASUREMENTS OF SECOND LIGHT-SCATTERING VIRIAL COEFFICIENTS OF NON-LINEAR MOLECULES

3.1 The light-scattering apparatus

Experimental determination of the second light-scattering virial coefficient B_ρ of a gas requires an apparatus which can measure the depolarization ratio ρ of the light scattered at right angles to the direction of propagation of an incident beam in the gas sample for a wide range of pressures. The initial development of the light-scattering apparatus used in this work was carried out in the period 1991-1992, and was based upon a critical choice of optical components such as the light source and the type of detection system, bearing in mind the difficulties encountered by other workers in this field. In particular, the design of the scattering cell was crucial to the success of the experiment because an extremely low level of stray light within the cell is essential if the very small horizontally polarized component of the 90° scattered light is to be accurately measured. This apparatus was limited to measurements at room temperature, and was substantially modified in the period 1993-1994 to allow vapour samples which have low saturation vapour pressures at room temperature to be heated to an upper limit of 100 $^\circ$C. The substantial increase in saturation vapour pressure at these elevated temperatures enabled a pressure-dependence study of sulphur dioxide to be performed. To place the overall design of our apparatus in its proper context, it is best to briefly review the historical evolution of light-scattering experiments.

As has already been mentioned in section **1.3**, the scattering of light by gases was first experimentally observed by Cabannes in 1915 [1], hence bringing to fruition the predictions made by Lord Rayleigh in his theoretical discussion of the phenomenon in 1899 [2]. Before the advent

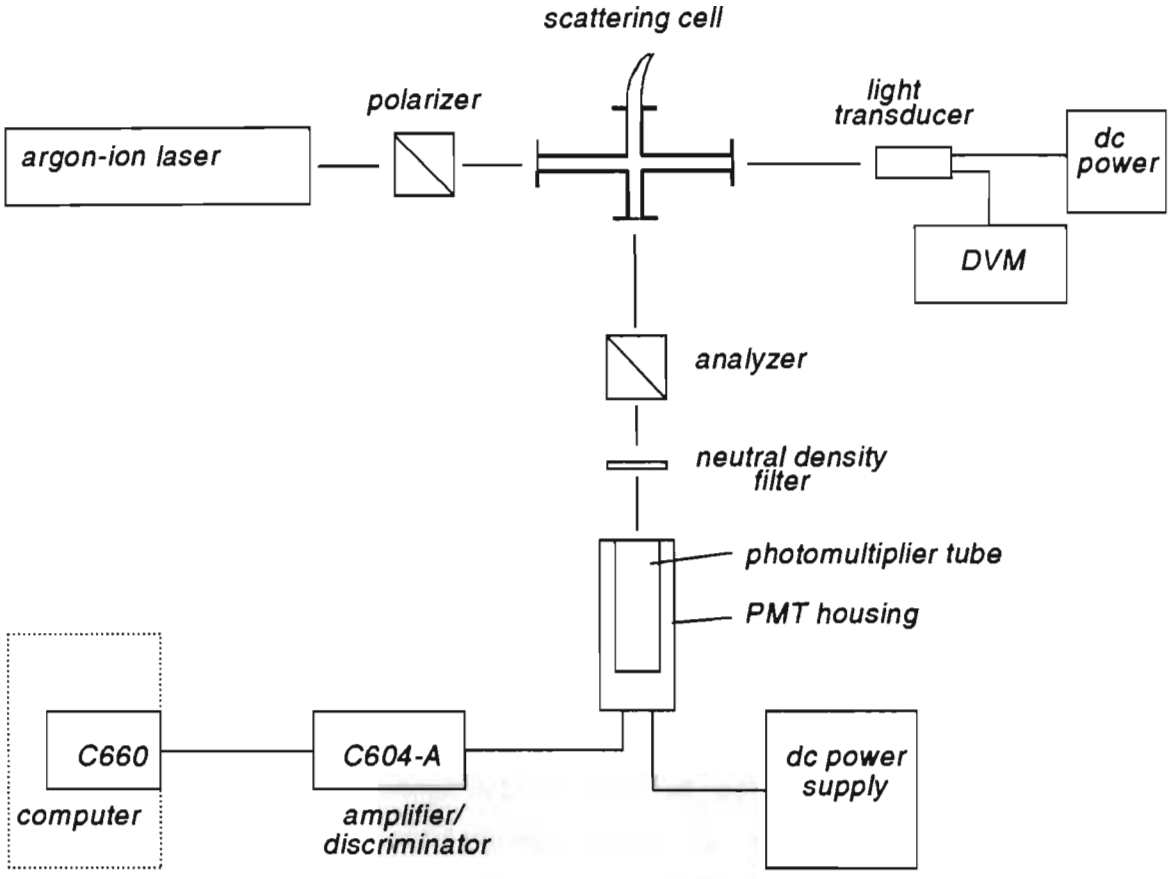

Figure 3.1. The optical system used for the measurement of the depolarization ratio of light scattered by gas samples.

of the laser, several other workers besides Cabannes made attempts to measure ρ_o, and they were all confronted by the formidable experimental difficulties of measuring an extremely low level of scattered light using photographic emulsion or visual detection techniques. Errors were compounded by the convergence of the incident light beams being used in the experiments, these being derived from the sun or from arc lamps and being converged by lenses to intensify the beams as much as possible; and it is not surprising that the results of the various workers were in poor agreement and appear to be unreliable up to about ±10%.

Accurate measurements of ρ_o became possible in part by the use of photomultipliers as scattered light detectors, but in the main due to the use of lasers as light sources. Their intense and highly parallel beams of monochromatic light are ideal for work in this field. The first workers in this field to exploit the laser were Bridge and Buckingham in 1964 [3], and they placed their scattering cell containing the gas sample *inside* the resonant cavity of the laser to obtain a very high incident beam intensity of around 100 mW. Measurement of the 90° scattered intensities polarized parallel and perpendicular to the electric vector of the incident beam are necessary for the evaluation of ρ; and these components were selected using a Glan-Thompson analyzer, and measured using a red-sensitive photomultiplier. In 1978 Bogaard, Buckingham, Pierens and White [4] reported ρ_o values for 39 gases at three different wavelengths. A 50 mW helium-neon laser was used for λ = 632.8 nm, while an argon-ion laser was used for λ = 514.5 nm and λ = 488.0 nm. The optical system was similar to that of Bridge and Buckingham's described above, but the gas sample cell was placed outside the laser cavity to enable easier alignment. The apparatus of other workers in this field is very similar in design, and so will not be discussed here. Instead, a detailed account of the apparatus used in this work is presented.

The optical system used for our experiment is shown schematically in the adjacent figure 3.1. The output beam of the argon-ion laser is nominally polarized vertical to the optical bench and pure polarized light is obtained by using a polarizing prism. The polarized beam then passes through the scattering cell and strikes a light transducer which allows the stability of the incident beam's intensity to be continuously

monitored. The 90° scattered beam passes through an analyzing prism, which allows selection of its vertically and horizontally polarized components. The neutral density filter is used to attenuate the more intense vertically polarized component, hence overcoming problems due to the slight non-linearity of the photomultiplier's response at higher count rates. The output signal from the photomultiplier is amplified and fed into an electronic photon counting system housed in an IBM compatible personal computer. Supporting software allows the computer to count discrete photons reaching the photomultiplier's photocathode, and by measuring the respective count rates of the horizontally and vertically polarized components of the scattered beam, the depolarization ratio ρ is easily calculated.

3.1.1 The optical bench

The various optical components have to be aligned as precisely as possible to reduce the presence of geometrical errors in the measurement of ρ. Bridge [5] has shown that the error in ρ will be negligible (i.e. less than 1/500) provided that the vertical of the main optical rail supporting the polarizer and scattering cell, and that of the 90° optical rail supporting the analyzer and photomultiplier, co-incide to within 1°. This necessitated a very stable, vibration free optical bench to support the optical rails, which themselves had to be easily adjustable for obtaining the vertical position.

Use was made of a very heavy L-shaped steel C-bar 2.3 m long, 25 cm wide and 9 cm high; with the small 'L-piece' side arm being 0.5 m long. This optical bench had three adjustable feet with anti-vibration pads to allow it to rest upon a granite slab (supported by brick pillars). Each of the two steel optical rails was mounted on the optical bench by resting upon the tips of three bolts screwed into the bench, hence providing a tripod support. Screwing the bolts allowed adjustment of the vertical position of the rail. The 90° optical rail was positioned on the side arm of the bench, with the main optical rail being positioned on the 2.3 m length of the bench. The rails were set to be exactly

perpendicular to each other with a T-square; a precision engineering spirit level then being used to ensure that the rails were exactly level. Finally, a plumb-bob was used to verify that the two rails were vertical. The extent to which the vertical positions of the two rails co-incided was accurately determined by aligning the transmission axis of a polarizing prism such that it was truly vertical on one rail (using the method described in section *3.1.2*), and then placing it on the other rail and re-aligning it to be vertical. The difference between the two vertical positions was found to be 45′ of arc, which satisfies the requirement that they should co-incide to within 1° to keep geometrical errors negligible.

3.1.2 The laser

The argon-ion (Ar^{+}) laser is preferable to the helium-neon (He-Ne) laser as a source of incident radiation for light-scattering experiments for three reasons. Firstly, the output power of the green line of the Ar^{+} laser is often more than ten times as great as that of the He-Ne red line. Secondly, the intensity of Rayleigh-scattered light is inversely proportional to the fourth power of the wavelength of the incident beam, and green light has a shorter wavelength than red light. Finally, most photomultipliers operate more efficiently in the blue-green spectral range than in the red.

The Spectra Physics model 165 Ar^{+} laser was used in this work, its adjustable prism allowing a selection of any one of eight different wavelengths ranging from 514.5 nm in the green part of the visible spectrum to 457.9 nm in the violet. A useful feature of the laser is the ability to vary the plasma current and hence the output power of the beam: when measuring pressure dependent effects, high density gas samples are used, and these have high intensity scattered beams which can push the response of the photomultiplier into non-linear regions. In these instances, the ability to reduce the intensity of the incident beam from the half a watt or so required for scattering samples at around atmospheric pressure to a few milliwatts proves invaluable.

The 514.5 nm line, which has a maximum output power of about 0.8 W, was used throughout this work. At this wavelength the laser beam has a diameter of 1.5 mm at its $1/e^2$ points, and a beam divergence of 0.5 milliradians. Bridge and Buckingham [6] have quantified the geometrical error that arises in measurements of ρ due to the incident beam being not exactly parallel. For a slightly divergent linearly polarized incident beam, the observed ρ deviates from the true ρ by an amount

$$\rho_{observed} = \rho_{true} + \frac{1}{4} B^2 \qquad (3.1)$$

where B is the maximum angle of divergence of the beam in radians. Hence, for the Ar^+ laser beam used in these experiments, the beam divergence of 0.5 milliradians leads to a $\frac{1}{4} B^2$ of the order of 10^{-7}, which is a completely negligible error for a ρ value of down to about 10^{-4}. The ρ values for the anisotropic molecules investigated in this study are of the order 10^{-2}, and hence remain unaffected by this geometrical error.

The laser was mounted on the optical bench by resting its four adjustable feet in holders welded onto the bench, which enabled minor adjustments of the beam's height and direction to be made with ease. The beam was carefully aligned to be exactly parallel to the main optical rail, this being verified by mounting a metal disc with a small hole on one end of the optical rail such that the beam passed exactly through the hole, and then repositioning it on the other end of the rail a distance of 1.0 m away to see if this condition was still satisfied.

The laser beam is almost completely linearly polarized in a plane approximately vertical to the optical bench. The incident beam passing through the gas sample needs to be a pure linearly polarized beam, the electric field vector of which is oscillating in an accurately defined vertical plane. This is achieved by interposing a polarizing prism between the laser and the scattering cell, with its transmission axis set exactly parallel to the vertical of the optical rail. Use was made of an air-spaced Glan-Thompson prism, suitable for use in the high-power incident beam, which was mounted in a divided circle such that its end

faces were perpendicular to the axis of rotation. The divided circle's vernier scale allowed the transmission axis of the prism to be set with a resolution of 2′ of arc, and in order to set this axis exactly vertical to the optical rail, use was made of a second reference polarizing prism in a similar mount. Both prisms were positioned on the main optical rail, the laser beam passing centrally through each of them. The transmission axis of the polarizing prism was set approximately vertical by adjusting it for extinction of the incident beam and then rotating it through 90°. The reference prism was then rotated until the transmitted reference beam was completely extinguished, the setting on the divided circle α_1 being noted. After reversing the reference prism by rotating it through 180° about a vertical axis, it was again adjusted for extinction at a setting α_2. The settings α_1 and α_2 will not be the same until the transmission axis of the polarizing prism is exactly vertical, this condition being achieved by rotating the polarizing prism through an angle $\left|\frac{1}{2}(\alpha_2 - \alpha_1)\right|$ and repeating the entire procedure until $\alpha_1 = \alpha_2$. After removing the reference prism, the beam transmitted by the polarizer was then completely linearly polarized in a plane vertical to the optical bench to within 2′ of arc.

The laser output beam was found to fluctuate in intensity from time to time, and this necessitated continuous monitoring of the intensity with adjustment of the plasma current to keep it at a fixed value. After passing through the scattering cell, the incident beam fell on the photodiode of a Photamp model A-1805 light transducer, the output voltage of which was monitored using a digital multimeter. The moment a drift in the voltage was observed, the plasma current was adjusted to maintain a constant beam intensity. Typically, the output could be kept constant to one part in a thousand throughout any one experimental determination of ρ.

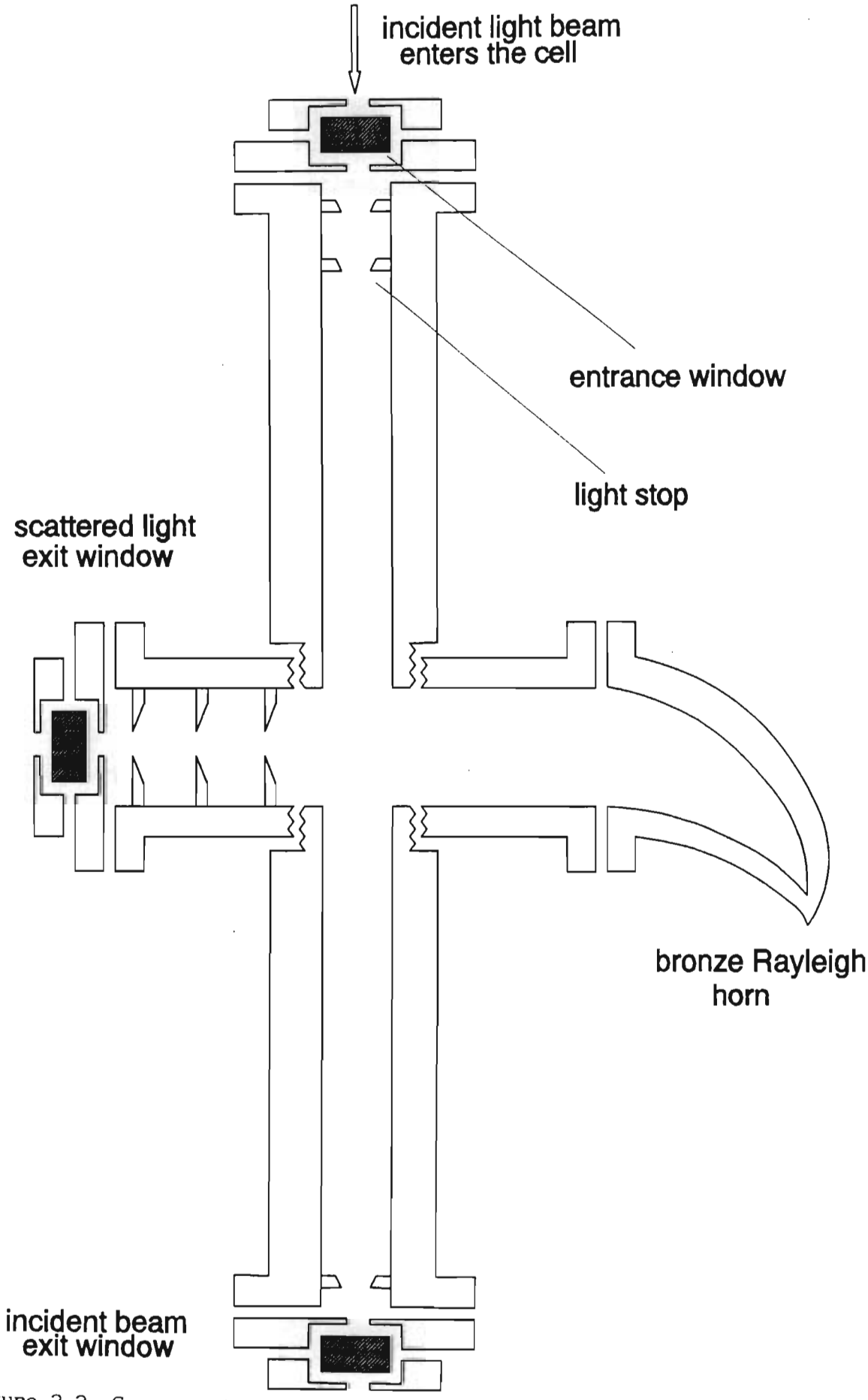

Figure 3.2 Cross-sectional view of the scattering cell.

3.1.3 The scattering cell

The essential features of the scattering cell are that it must contain the gas samples introduced into it in a pure and dust-free state, it must withstand a gas pressure of at least 4 MPa if the density dependence of ρ for a gas is to be a large enough effect so as not to be obscured by the experimental uncertainty in the ρ measurements, and it must be designed in such a manner as to keep the stray background light to a bare minimum. In addition, since non-linear polar molecules are generally vapours at room temperature, with typical saturation vapour pressures of only a few hundred kPa, provision has to be made for elevating the cell's temperature.

The cell was constructed out of stainless steel, which is inert to the two gases investigated in this work, hence eliminating the possibility of chemical reaction and subsequent contamination of the scattering medium. As can be seen from figure 3.2, the interior of the scattering cell is essentially a pair of crossed cylindrical tubes; the incident laser beam travelling along the axis of what will be called the main tube, and the 90° scattered light travelling along the axis of what will be called the perpendicular tube. The perpendicular tube was of 3.0 cm diameter, and was bored out of a solid rectangular block of stainless steel 4.9 cm by 4.9 cm by 12.4 cm, with circular end flanges 6.4 cm in diameter to allow the attachment of the exit window and the light trap. The tube was threaded throughout to allow precise positioning of light stops. The main tube, 2.0 cm in diameter and also threaded throughout, was bored out of two separate but identical cylinders of stainless steel 3.4 cm in diameter; one for the entrance of the incident beam into the cell and the other for its exit. Each cylinder had a circular flange of 6.4 cm diameter at one end to enable the attachment of a window, while the other end was threaded to allow screw-in attachment to the cell body wall, teflon O-rings providing leak-tight seals.

To ensure a dark background to the field of view of the scattered light detector, a Rayleigh horn [7] was positioned on the far end of the perpendicular tube as seen by the detector. In earlier work on axially-symmetric molecules [8] we cast a bronze horn, since stainless

steel has a much higher melting point and as a result is considerably more problematic for the foundryman to cast. Since bronze was inert to most of the gases studied in [8], this presented no serious complications. Similarly, the bronze horn sufficed for our current study of ethene. However, after attempting measurements of hot sulphur dioxide, the horn's highly polished interior surface was attacked and severely tarnished, resulting in a significant loss of performance in its ability to reflect stray light out of the detector's field of view. Attempts to flash-coat the interior of the bronze horn with both gold and hastelloy-C proved unsuccessful: the sulphur dioxide vapours penetrated the thin metallic films and attacked the bronze underneath, leaving the upper layer of inert metal in a crinkled mess. The *Metals Reference Book* [9] provides a thorough tabulation of the corrosion resistance of metals to chemical attack, and aluminium of *at least* 99.0% purity is quoted as being completely resistant to attack from sulphur dioxide. In fact, even moist sulphur dioxide, which forms highly corrosive sulphurous acid, is unable to tarnish aluminium of this purity. Aluminium has the additional advantage in that it can be polished to yield a highly reflective surface, which is an essential requirement of a Rayleigh horn. The Huletts Aluminium Company kindly donated us 10 kg of the purest aluminium pellets which they manufacture, the aluminium content exceeding 99.7%, and attempts were made to cast a new horn out of this metal. The casting of pure aluminium is troublesome, since shrinkage which occurs on cooling results in porosity. Indeed, when the first casting was pressure tested using water and a hydraulic pump it failed at 2 MPa, and a cross-sectional cut through the region of failure revealed a substantially porous interior. A second horn was cast using a much larger gate feeding off a big reservoir of molten aluminium, and a great deal of the hot metal in the reservoir was sucked away to replenish the casting as it shrunk on cooling. This horn was successfully pressure tested to 6 MPa, and was polished into an efficient light trap which is inert to sulphur dioxide as well as a host of other gases and vapours which might be investigated in the future. The horn was bolted to the cell with eight Allen screws, a teflon O-ring providing a leak-tight seal.

The measurement of the depolarization of light scattered at right angles out of an incident beam of pure linearly polarized light by gas molecules obviously requires that the entrance window and 90° exit window of the cell do not introduce significant spurious depolarization of the incident and scattered beams. Windows of Pockels glass were chosen because of their inherent low strain, and their low stress coefficient which is essential for high pressure work where shear stresses can be induced in the windows resulting in additional strains to those already present as a result of the clamping of the windows to the cell. The windows, which were 5.2 mm thick and 25.0 mm in diameter, were sandwiched between teflon discs with holes of 5.0 mm diameter to allow the unhindered passage of light, these in turn being sandwiched between two stainless steel discs with recessed holes. The discs were bolted together with eight Allen screws which had to be tightened systematically to ensure that the windows were exactly perpendicular to the incident light beams. Care was taken not to overtighten the screws, since this could result in unwanted strains in the windows. These steel discs were then fastened onto the cell flanges with Allen screws and using teflon O-rings for leak-tight seals, hence providing entrance and exit windows for the incident beam and an exit window for the 90° scattered beam.

Once again, hot sulphur dioxide vapour exhibited destructive behaviour, this time in its interaction with the windows. Wherever it came into contact with the Pockels glass, it left behind opaque white stains which penetrated beneath the surface, affecting both the transmission and the state of polarization of incident light. These stains could not be removed with organic solvents, and the windows were salvaged by a technician from the CSIR Optics Division who polished the deposits off. We investigated possibilities to overcome this problem, and decided to coat the windows with a protective film of quartz. We consulted the CSIR Optics Division, and established that they have thin-film coating facilities. They informed us that the ideal technique is to heat the Pockels glass to a high temperature so that adhesion of the coating can be guaranteed. However, since this could affect the low stress coefficient of the glass, which is achieved by cooling gradually over a

period of many months, we opted for the process to be carried out at room temperature. The windows were subsequently coated with a 0.5 μm layer of quartz, and the film appeared to adhere very well despite having been deposited at room temperature. We were concerned that the quartz might have been deposited in crystalline form, hence having the potential to affect the state of polarization of a transmitted beam. However, upon investigation, the protective layer was found not to induce a discernible spurious depolarization of polarized light. The windows were now quite inert to hot sulphur dioxide vapour, and measurements were recommenced.

The teflon O-rings used to seal the flanges of the cell were found to slowly absorb moisture from the atmosphere, this eventually leading to corruption of the seals. Tightening of the Allen screws would often be sufficient to re-seal these weak points, but from time to time the teflon would become completely degraded, new washers having to be made and fitted. The procedure for determining the precise location of a leak was greatly simplified with the use of an Edwards Spectron model 300E leak detection system. Whenever the presence of a new leak became apparent; either as a result of a steady drop in gas pressure (as measured by the pressure transducer attached to the cell) if the gas was compressed above atmospheric pressure, or a steady increase in pressure once the cell had been evacuated by a vacuum pump; the cell was filled to a pressure of 4 MPa with an 80:20 helium-oxygen mixture, the leak detector's sniffer probe then being used to detect where helium was emanating from the cell. This detection system proved to be highly efficient, the most minute leaks being readily located within minutes.

The cell was held in an aluminium cradle which could be firmly secured to the optical rail, and which allowed fine adjustments to the height of the cell as well as to the tilt of both the main and 90° tubes to be made with ease, hence ensuring that they could be aligned to co-incide exactly with the incident and 90° scattered light beams respectively. This need for manoeuverability of the cell necessitated a link between the cell and the gas system that was both flexible and capable of withstanding a pressure of at least 6 MPa. The flexible stainless steel cable used in the hydraulic systems of aircraft satisfied both of these

requirements, and was used to good effect. After complete assembly of the cell, it was pressure tested by filling it with water, attaching a suitable liquid pressure gauge, and elevating its pressure with a hydraulic pump. No leaks appeared for a pressure of up to 6 MPa, allowing a safe maximum working pressure of 5 MPa which is in any case the upper limit of the pressure transducer's measuring range.

When working with sulphur dioxide vapour, attempts to raise the temperature of the cell by winding heating tape around the exterior proved unsatisfactory, the temperature varying by as much as 20 °C at different points on the cell when aiming for a mean temperature of 100 °C. Uniform heating was achieved by encasing the body of the cell in a perspex bath filled with dimethicone oil. A Hewlett-Packard 3421A Data Acquisition/Control Unit was used to control a commercial 350 W immersion heater operating off mains: a simple BASIC program was written to instruct the 3421A unit to monitor the mean temperature of the oil as measured by two calibrated thermocouples, turning the heater on and off via a relay switch so as to maintain the desired temperature to within ±0.2 °C. A mechanical stirrer with variable speed control ensured rapid distribution of heated oil within the bath. The maximum temperature obtainable was limited to 100 °C, this being the upper limit of the WIKA pressure transducer. The interior temperature of the cell was monitored using a calibrated thermocouple positioned within the cell, and as close to the scattering volume as possible. The interior temperature was extremely stable (to within 0.1 °C) and hence well defined.

With each new gas, the cell was completely dismantled and cleaned of all grease, dust and other contaminants using petroleum ether. The aluminium horn was polished with Brasso to give a highly reflective interior surface, and the teflon washers were cleaned in ethanol and thoroughly dried. The coated Pockels windows were cleaned of dust using only freshly distilled ethanol and lens tissue.

As has already been alluded to, an extremely low level of stray light is essential if the very small horizontally polarized component of the scattered light is to be accurately measured. This condition was achieved by using a series of light stops 2 mm and 3 mm in diameter, and

positioning them at various locations along the axis of the main tube by screwing them along its thread. After passing the incident beam along the main axis of the cell, the light emanating from the 90° window was observed with the naked eye until the background radiation was seen to be at a bare minimum. It was found that if the incident beam so much as grazed a light stop, this acted as a powerful source of stray light. The optimum arrangement was found to be when a 3 mm stop was right against both the entrance and exit windows of the main tube, with a 2 mm stop very close to the entrance window. Stops were also placed in the 90° tube of the cell, not only to reduce the level of stray light, but also to limit the detector's field of view. This is necessary because the measurement of ρ for light scattered in exactly the 90° direction is not possible in practice, both the detector and the scattering volume being of finite size. Bridge and Buckingham [6] have investigated the effect of the divergence of the scattered light, showing that if the maximum divergence accepted by the detector is an angle C, in radians, then

$$\rho_{observed} = \rho_{true}(1 + \tfrac{1}{4} C^2) + \tfrac{1}{2\,4} C^4 + \ldots \quad . \qquad (3.2)$$

This error is very small: even if C is as large as 6°, the $\frac{1}{4} C^2 \rho_{true}$ term gives an error of only 0.25% while $\frac{1}{2\,4} C^4$ produces an error of 0.04% assuming ρ is of the order 10^{-2}. Three stops were used in the 90° tube, a 3 mm one being positioned very close to the centre of the cell while a 2 mm one was placed half way between the centre and the exit window of the tube, another 2 mm one being placed right against the exit window. The narrow cone of scattered light reaching the detector had a divergence of less than 3°, hence rendering the geometrical error in ρ completely negligible.

It was found that even a slight misalignment in the cell resulted in measured values of ρ which were sometimes as much as double the true value! Hence, the cell was painstakingly aligned, the photomultiplier and photon counting system (described in sections *3.1.6* and *3.1.8* respectively) being used in preference to visual methods to obtain the minimum background count rate when the incident beam was passed through the *evacuated* cell. It came as no surprise that when this requirement had been rigorously satisfied, the incident beam's reflection off the

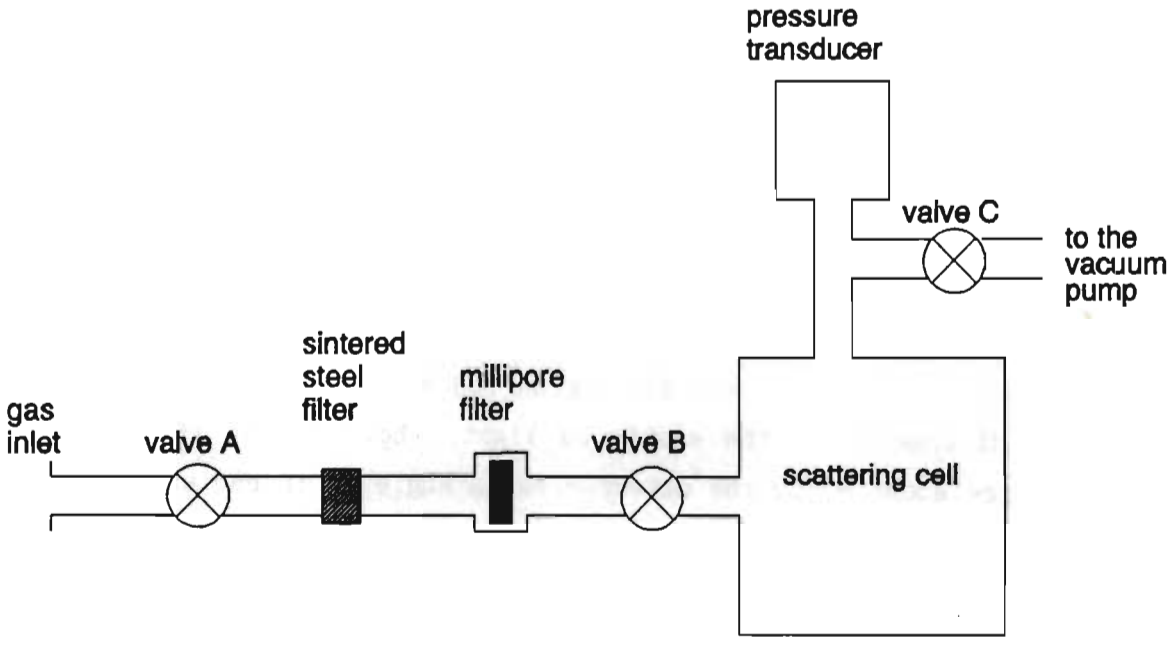

Figure 3.3 A schematic representation of the gas line.

entrance window was found to travel directly back into the output aperture of the laser.

3.1.4 The gas line

The gas line, shown in the adjacent figure 3.3, was designed to allow dust-free gas samples to be introduced into the scattering cell. Being constructed from standard Hoke high-pressure stainless steel tubing and valves, the system was capable of withstanding pressures in excess of 15 MPa.

The requirement that the gas sample be completely free of dust and other large particles arises because the light scattered from a single dust particle passing through the incident beam is far more intense than the light scattered by the gas sample itself, the light detector then producing a large and strongly fluctuating signal. A dust-free sample results in a steady signal being produced, hence providing a means of determining when this condition has been completely satisfied.

It was found that passing gas samples through a 2 μm sintered stainless steel filter before introducing them into the cell was inadequate. A steady detector signal was achieved only after placing a Millipore cellulose membrane with an average pore size of 0.2 μm in series with the steel filter. Sulphur dioxide was found to dissolve the cellulose, and so the more resilient Durapore polyvinylidene fluoride membranes were obtained, and used to good effect. A useful visual means of ensuring that the gas sample was dust-free was to increase the output power of the incident beam to its full 0.8 W and to then observe the 90° scattered beam with a travelling microscope, any dust particles being readily detected as bright specks of light drifting about randomly.

The cell itself was dedusted by flushing it with a constant stream of dry air which had been sucked through a 0.2 μm membrane filter by the rotary oil pump. After a few minutes of flushing, no dust particles could be detected with the microscope; the flushing being continued for

about an hour for good measure. The cell was then evacuated by closing the Hoke Micromite fine-metred valve while leaving the vacuum pump running. The entire gas line was then tested for leaks with the Edwards leak detection system, both when under vacuum and when filled with the helium-oxygen mixture to a pressure of about 4 MPa.

Gas samples were introduced by connecting the required gas cylinder to the inlet, opening all valves, and evacuating the entire line with the vacuum pump. After isolating the pump by closing valve C, a little of the gas was introduced into the system by closing the fine-metred valve A, opening the gas cylinder and then slowly opening A. This gas was then evacuated by opening valve C, the process being repeated once more to remove any remaining traces of air or gases from previous samples. Finally, the gas sample was admitted to the required pressure as measured by the Wika model 4501 pressure transducer connected directly to the scattering cell. This transducer had been calibrated against a CSIR calibrated Budenburg Master Test Gauge, ensuring a pressure reading correct to within 1% for pressures of the order 100 kPa, and correct to within 0.1% for pressures in excess of 1 MPa, with a maximum measurable pressure range of 0 kPa to 5.2 MPa.

Sulphur dioxide, which is a vapour at room temperature, was initially transferred into a 300 ml stainless steel cylinder which was connected in between the Durapore filter and valve B. An additional valve D was fitted between the filter and the cylinder. The procedure used to fill the cylinder with sulphur dioxide was as follows. All valves were opened, the entire gas line being evacuated. Valves A and B were then closed, after which the commercial gas cylinder was opened and the fine-metred valve A adjusted to allow a gentle flow-rate. The steel cylinder was placed in an empty dewar which was slowly filled with liquid nitrogen, hence freezing de-dusted vapour into the cylinder. After closing valves A and D, the dewar was removed, the cylinder and the tubing linking it to the scattering cell being wrapped in heating tape connected to a 48 V isolating transformer. The transformer was relay controlled by the same 3421A Control Unit used to maintain the temperature of the silicone oil bath, the temperature being measured by a thermocouple attached to the cylinder. Heated vapour was then admitted

to the cell by opening valve B as required.

Once samples had been introduced into the cell, it was isolated from the rest of the system by closing valve B, and was allowed to equilibrate before measurements of ρ were commenced. The flexible stainless steel hose connecting the gas line to the cell, and the rubber hose connecting tap C to the vacuum pump, ensured manoeuverability of the cell for accurate alignment purposes. Ethene, which is a highly flammable gas, could not be exhausted to the atmosphere after measurements had been taken, since our extractor fan is not spark proof. After consultation with the Chemistry Department's safety officer, it was decided that the spent gas should be burnt off in a controlled environment. Hence, the ethene was exhausted from the cell via valve C into a lecture bottle, being frozen out using liquid nitrogen. The bottle was then transferred to a fume hood where the nozzle was directed above a Bunsen burner flame. The bottle was allowed to warm up very gradually as the emerging gas burnt off. Sulphur dioxide was also exhausted into a frozen cylinder, was transferred to the fume hood and bubbled through a strong sodium hydroxide solution. In the light-scattering laboratory itself, we employed a gas alarm which could detect concentrations of ethene as small as 50 ppm, although no gas leaks occurred during our experiments.

3.1.5 The analyzer

Bearing in mind that the depolarization ratio ρ of the 90° scattered light is the ratio of the scattered intensities polarized parallel and perpendicular to the direction of the electric vector of the incident light beam respectively, the precise selection of these two components is seen to be crucial for the accurate measurement of ρ, which is commonly of the order 10^{-2}. A high quality prism polarizer is essential; and in this work, use was made of a Melles-Griot Glan-Thompson prism of square cross section and of dimensions 11 mm by 11 mm by 31 mm. The transmission axis was parallel to the end faces of the prism, which was bought already embedded in a cylindrical metal mount, the axis of rotation of which was perpendicular to the end faces of the prism. This

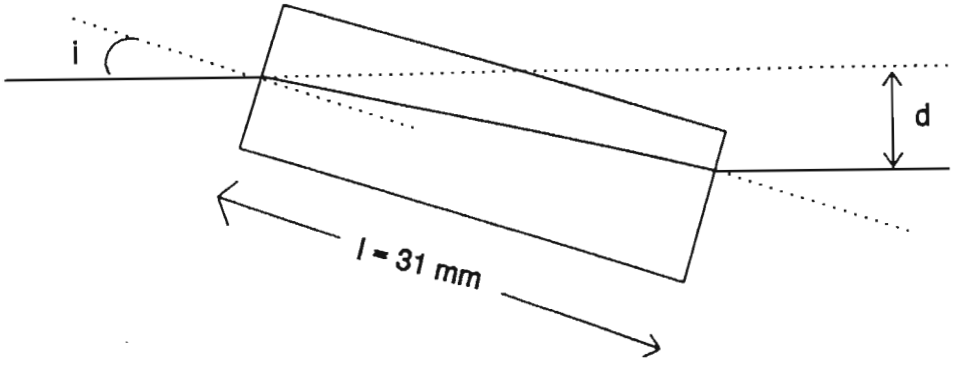

Figure 3.4 (a) Shift in the field of view caused by tilting the analyzer prism.

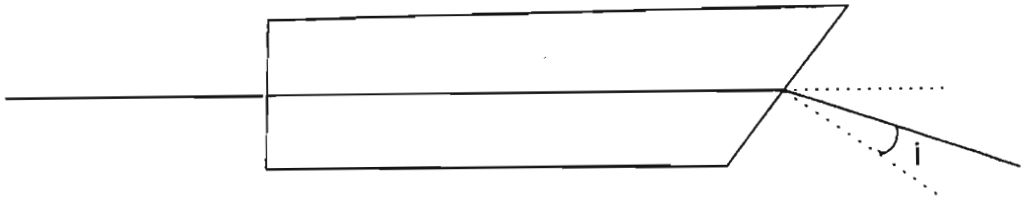

Figure 3.4 (b) Distance-dependent shift in the field of view due to non-parallel prism end faces.

cylinder enabled the prism to be mounted in a divided circle, with the transmission axis perpendicular to the axis of rotation. The vernier scale permitted angular settings with a precision of 2′ of arc.

The field of view of the scattered light detector should remain constant as the analyzer is rotated. Bridge [5] has shown that the shift in the field of view because of tilt in the prism, as shown in the adjacent figure 3.4 (a), is

$$d \approx l \frac{i(n-1)}{n} , \qquad (3.3)$$

where n is the extraordinary refractive index of calcite, l is the length of the prism, and i is the angle of incidence of the laser beam at the prism surface. Since there was no visually discernible wobble in the Melles-Griot prism as the divided circle was rotated, it was assumed that $i < 1^{\circ}$. Hence, putting $i = 1^{\circ}$ with $n = 1.488$ (for $\lambda = 514.5$ nm) and $l = 31$ mm, a d of 0.18 mm is obtained, which is negligible.

Of course, the transmitted beam with shift d is only parallel to the incident beam if the two end faces are exactly parallel to each other. In order to investigate this, the prism was mounted in a precision lathe, the axis of rotation of the cylindrical mount then co-inciding precisely with that of the lathe. A linearly polarized laser beam was passed through the prism, and was found to be deflected in opposite directions for the transmission axis being set parallel to the incident beam's plane of polarization, and then being rotated through 180°. The prism was removed from the lathe, the beam then falling exactly in between the two deflected points. A net deflection of 4 mm over a distance of 1.5 m from the prism was observed, the deflection as the beam left the prism being too small to be measured. The divergence of the transmitted beam away from the direction of the incident beam as found here indicates that the prism faces are in fact not parallel, as depicted in the exaggerated figure 3.4 (b). Fortunately, a divergence of 2 mm over 1.5 m means a negligible divergence of only 0.1 mm over a distance of about 10 cm, which is the distance of the detector from the analyzer.

The orientation of the transmission axis of the prism was determined using a second prism as described in *3.1.2*, with a helium-neon laser beam arranged to travel exactly parallel to the 90° optical rail and directly into the centre of the scattered light exit window. The laser was linearly polarized approximately vertically to the 90° optical rail. Once the transmission axis was exactly vertical, the angle was noted from the divided circle's scale to the nearest 2′ of arc, the other vertical position being 180° larger; and the two horizontal positions being 90° greater and 90° smaller than this vertical position. A good check to verify the alignment of the apparatus is that the intensity of the scattered light reaching the detector should be a minimum when the transmission axis of the analyzer is exactly horizontal.

Finally, the analyzer prism was linked to the 90° exit window of the scattering cell via a light-tight tube to prevent stray light from interfering with the scattered light signal. This tube was water-cooled during high-temperature work to prevent the analyzer from being heated up.

3.1.6 The photomultiplier

The intensity of the 90° scattered light is very small, and in particular that of the horizontal component which for a typical ρ of the order 10^{-2} is a hundred times smaller than the vertical component. The need for an extremely sensitive light detector can readily be appreciated.

A photomultiplier tube provides the necessary detection capabilities, and can in fact be used to count individual photons if the incident intensity is not too high. When light reaches the photomultiplier's photocathode, electrons are emitted as a result of the photoelectric effect. Electrostatic acceleration and focusing of these photoelectrons onto a dynode results in the emission of a number of secondary electrons, which in turn are accelerated and focused onto yet another in

a chain of dynodes. Finally, the electrons emitted from the last dynode are collected at the anode. If the ratio of this signal output current to the photoelectric signal current from the photocathode - this ratio being called the gain - is very high (i.e. above about 10^6), the amplified signal from a single photoelectron can be detected as a discrete pulse of current: hence the photomultiplier's ability to count discrete photons.

The advantage of photon counting over analogue measurement of the anode current lies in the ability of the counting technique to distinguish between true photon events and the spurious pulses originating from the spontaneous release of electrons from the dynodes. Electrons released spontaneously result in current pulses of different amplitudes to those arising from photon events, and these pulses can be discriminated against and disregarded by an electronic circuit in the photon counting technique, but not in the analogue measurements where all charge contributions to the anode are integrated regardless of their origin. Hence, photon counting leads to much greater accuracy and a far better signal-to-noise ratio than the analogue method. Furthermore, the photon counting output is of a digital nature, facilitating direct interfacing to a computer for automatic collection and analysis of data.

An EMI 9128B photomultiplier, recently developed explicitly for photon counting, was used throughout this work. It has a diameter of 29 mm, and has eleven linearly focused dynodes. These dynodes replace the older venetian blind systems, resulting in a higher gain, excellent single-electron response and good pulse height resolution, all of which are essential to the photon counting technique. The photocathode is sensitive to light in the blue-green region of the spectrum, which is an obvious requirement when working with an Ar^+ laser. The tube was placed in an EMI model QL30/RFI light-tight housing which also provided screening from stray electric and magnetic fields.

The photomultiplier housing was firmly mounted onto the 90° optical rail such that the incoming cone of 90° scattered light travelled perpendicular to the window of the photomultiplier tube, and fell symmetrically about its centre. The 9128B tube's window is plano-

concave, photons falling near the edges of the window being focused onto the photocathode as readily as those falling near the centre. A consequence of this is that the detector, positioned some 35 cm from the centre of the scattering cell, and with a window diameter of 29 mm, has a maximum angle of acceptance of 4.5°. This should not lead to significant geometrical errors as seen by equation 3.2; nevertheless, light stops reduced the angle of divergence of the cone of scattered light reaching the detector to less than 3°. This ensured that the background to the field of view was restricted to the Rayleigh horn, helping to keep the level of stray light to a minimum. The photomultiplier housing was connected to the analyzing prism by a light-tight tube with a slot allowing the insertion of a neutral density filter between the photomultiplier and the prism.

The optimum operating voltage of the photomultiplier tube which is used in conjunction with a pulse amplifier, pulse height discriminator and pulse counter has to be carefully ascertained. The 9128B photomultiplier used in this work was powered by a stabilized Fluke model 415B high voltage power supply, and the anode output pulses were fed into a Thorn EMI model C604-A amplifier/discriminator using a 10 cm length of 50 Ω BNC screened cable to minimize pulse distortion and spurious pick-up from stray fields. For each input pulse with amplitude within the acceptable limits, the amplifier/discriminator produces a single output pulse of well defined width and amplitude which is then fed into the photon counter. Following the output of a pulse, the output of further pulses from the C604-A is disabled for a well defined dead time, hence necessitating statistical correction of the count rates. A useful feature of the computer program which controls the C660 photon counting board used in this work (see section *3.1.8*) is the inclusion of a subroutine to calculate the statistical corrections for dead-time automatically.

To determine the optimum voltage, a scattering medium of approximately 100 kPa of CO_2 was introduced into the cell. The Ar^+ laser was tuned to deliver an incident beam of λ = 514.5 nm, the incident intensity being kept constant throughout the measurements. The vertical component of the 90° scattered light was selected by the analyzer, providing the

Figure 3.5. A plot to find the optimum operating voltage of PMT 9128B

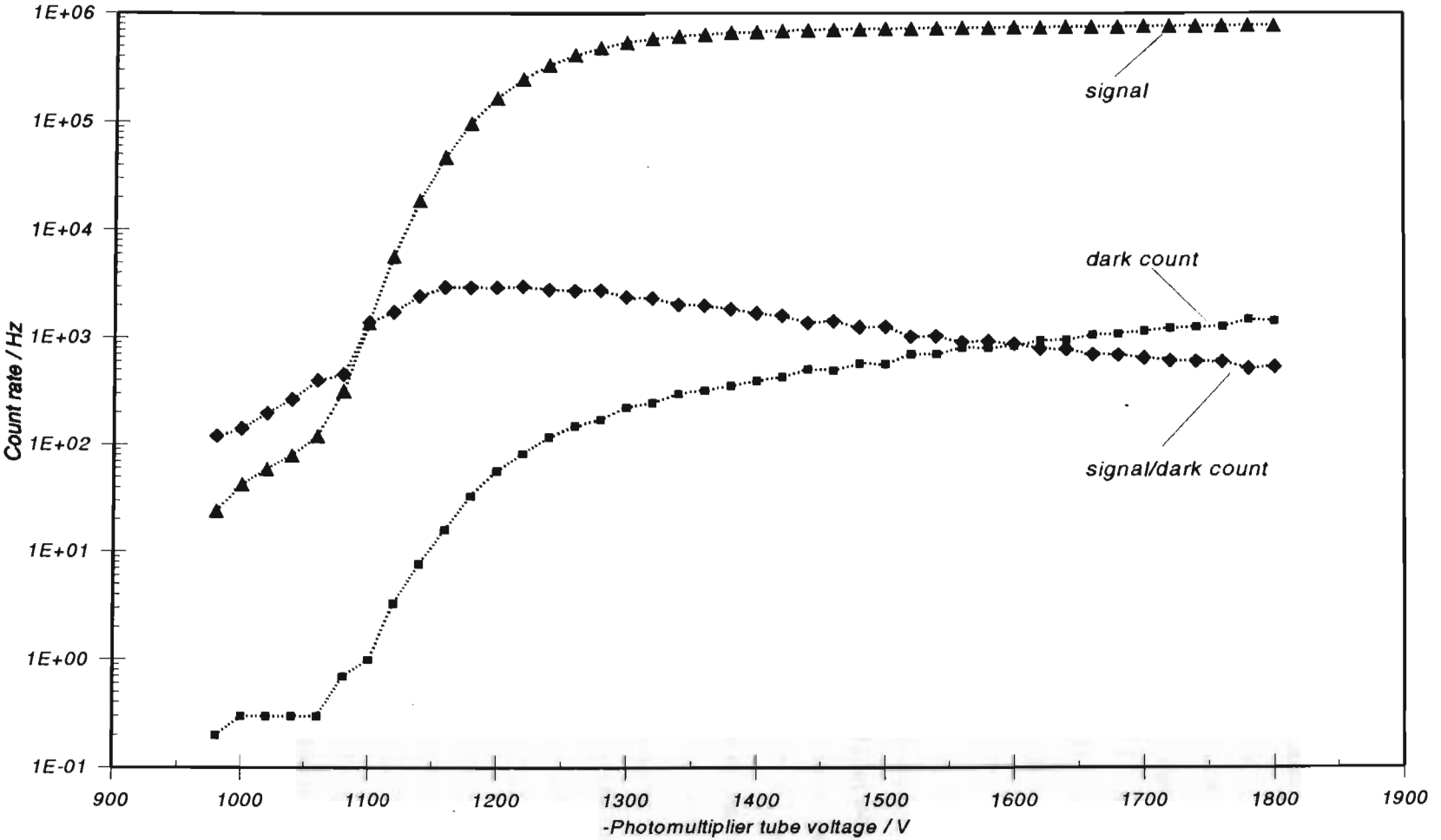

photomultiplier with a light source of constant intensity. Care had to be taken when selecting the intensity of the input beam such that the count rate of the photomultiplier did not exceed about 10^6 pulses per second, since the count rate can then become non-linear with respect to the input light signal due to "pulse pile-up" arising from the dead time of the electronic circuitry. The number of pulses arising per second from the C604-A output were counted for a series of tube operating voltages ranging from -900 V to -1800 V in steps of 20 V. The resulting curve is shown in figure 3.5 (labelled "signal"), and has a well-defined plateau. The dark count, obtained when the photomultiplier is in complete darkness and arising mainly from thermionic emission of electrons from the photocathode and dynodes, was then measured over the same voltage range, the resulting curve also being shown in figure 3.5 (labelled "dark count"). The curve showing the ratio of the signal count rate to the dark count rate is given in figure 3.5 (labelled "signal/dark"). The optimum operating voltage maximizes this signal/dark ratio while minimizing the dark count rate. This is because the dark count rate limits the lower level of light detection, with a high dark count rate obscuring a relatively tiny signal. The operating voltage should preferably also lie on the plateau region of the signal curve so that the count rate is independent of small fluctuations in the applied voltage or photomultiplier gain. Since the company-recommended operating voltage of -1270 V for the 9128B tube used here was found to satisfy the above considerations, this voltage was used throughout our experiments.

3.1.7 The neutral density filter

The 9128B photomultiplier's response was found to be slightly non-linear for count rates above about 100 kHz. Since the dark count rate of the photomultiplier when operated at -1270 V is about 200 Hz, it becomes necessary to adjust the incident laser beam intensity so that the small horizontal component of the scattered light has a count rate at least twenty times as large so as not to be degraded by the dark count 'noise'. Now, typical values of ρ are of the order 10^{-2}, so that the vertical component of the scattered light would thus have a typical

count rate of about 400 kHz which is well into the non-linear region. The solution to this problem is to attenuate the vertically polarized scattered light signal by a precisely known factor of about ten. This was achieved by placing a high quality neutral density filter *behind* the analyzer so as not to introduce spurious depolarization into the scattered light signal. It was slotted into a light-tight holder in order to prevent light from the room reaching the photomultiplier. The attenuation factor of the filter was measured using two different methods:

Firstly the method described by Bridge [5] was used, a scattered light signal of constant intensity being measured by the photomultiplier itself. The analyzer was set to transmit the vertically polarized component of the light scattered out of a medium of 150 kPa carbon monoxide. The incident beam intensity was chosen such that a photon count rate of approximately 25 kHz was obtained, which is well before non-linearity in the photomultiplier response occurs. One hundred count rates were obtained of the signal without the filter in place, followed by a hundred with the filter inserted in between the analyzer and detector, the mean count rates and standard deviations being calculated in each case. This was repeated with the cell evacuated, the means of these background readings being subtracted out so that the filter's attenuation factor was calculated only for light scattered from the gas sample itself. A filter attenuation factor of 10.1 ± 0.2 was obtained.

In the second method, a laser beam was diverged and allowed to fall on the photodiode of the Photamp model A-1805 light transducer, the output being measured using a digital voltmeter. The suppliers of the light transducer specified excellent linearity over a wide range of light intensities, even with the relative gain of the transducer being changed from 1× to 10×, 100×, or even 1000×. This was verified by measuring the intensity of a laser beam transmitted by crossed polarizers, a plot of $\cos^2$(crossed angle) versus measured intensity being linear to within 0.2% over a relative intensity range of 100. The neutral density filter was then inserted into the diverged laser beam such that its faces were perpendicular to the direction of propagation of the beam, the attenuated signal being measured. The Photamp output voltages were

extremely stable, allowing precise measurements to be taken. The filter was removed and re-inserted several times for several different laser beam intensities, and the mean filter attenuation factor was calculated to be 10.27 ± 0.05, which lies within the uncertainty of the factor obtained above using Bridge's method. The uncertainty here is much smaller, providing a more reliable value for the attenuation factor, and this value has been used throughout the measurements of ρ undertaken in this work.

3.1.8 The data acquisition system

The Thorn EMI model C660 counter/timer board was installed in an IBM compatible personal computer by insertion into one of the computer's 8 bit expansion slots. This effectively converted the computer into a low cost but high performance pulse counting instrument for recording the output from the 9128B photomultiplier when operating in the photon counting mode. The enormous advantage of this photon-counting system over the conventional counters is that computer programs can be used to greatly simplify the collection, storage, and analysis of data. Some specifications of the C660 counter/timer are summarized below.

The board has a 20 MHz 32 bit counter for ECL pulses, and is connected to the C604-A module via a 9-way 'D' plug allowing current to be transferred from the computer to power the amplifier/discriminator while enabling the pulses emanating from the C604-A to be transferred to the board for counting. A wide range of counting periods can be selected, from a very fast 52 μs to 20 s; and the counting period is accurate to within ±1 μs. The C660 board is controlled entirely by a set of computer programs written in Microsoft QuickBasic supplied by Thorn EMI. These programs are menu-driven, readily allowing selection of a range of features. For example, measured count rates can be collectively viewed on the computer screen, and can be printed out or stored in a data file which can later be accessed by other computer programs written for specific requirements. For example, the computer program "depol2.bas", written in BASIC as part of this project, accesses data files of

measured count rates for the 90° scattered light, and directly calculates the depolarization ratio ρ and its statistical uncertainty. Other features are the inclusion of a subroutine to statistically correct measured count rates for the dead-time in the photon-counting system's electronic circuitry, and the easy selection of the length of time desired for each period of counting (in the allowable range of 52 μs to 20 s), the counts accumulated during each period then being averaged to allow the number of counts per second to be displayed.

For the measurements taken in this work, use was made of the facility allowing the counter to cycle through a set of counts several times. A considerable reduction in the effects of noise can be achieved by accumulating large numbers of counts and taking an average. The count period was set to 1 second, and sets of 20 counts were measured and stored as elements in an array. Each count in every additional set was added to its corresponding array element, and this was continued until the desired number of cycles had been completed. A total of 10 cycles, for example, would require that each of the 20 elements in the final set of *accumulated* counts be divided by 10 to yield a set of 20 count rates representing the intensity of the observed light signal. These 20 values could then be averaged to yield a mean value $\bar{x}$, and a measure of the uncertainty is the standard deviation s_x given by

$$s_x = \sqrt{\frac{\sum_{i=1}^{N} (x_i - \bar{x})^2}{N - 1}} \quad , \tag{3.4}$$

where N is the total number of values (N = 20 here), with x_i being the i^{th} value.

The count rates were stored in data files which were later accessed and analyzed using the BASIC program written specifically to calculate the depolarization ratio ρ and its estimated uncertainty.

3.2 Experimental measurements and results

The density dependence of the depolarization ratio ρ of a gas has been described by means of the virial expansion in section *2.1.2* where, from equation (2.21),

$$\rho = \rho_o + \frac{B_\rho}{V_m} + \frac{C_\rho}{V_m^2} + \ldots \quad , \tag{3.5}$$

in which ρ_o is the extrapolated depolarization ratio at zero density. Here, the second light-scattering virial coefficient B_ρ describes contributions to ρ from the molecular interactions between pairs of molecules, with the third virial coefficient C_ρ describing contributions to ρ from triplet interactions etc. If B_ρ is to be obtained from a plot of experimentally observed values of ρ taken over a range of gas densities, care has to be taken that the gas is not compressed to such an extent that triplet or higher order interactions become significant. A plot of ρ versus V_m^{-1} will be linear for intermediate pressures where pair interactions predominate, deviations from linearity occurring at higher pressures where the higher order interactions begin to make relatively large contributions. The B_ρ value of a gas at a given temperature can thus be obtained as the slope of the linear region of a ρ versus V_m^{-1} plot for the gas, the intercept yielding a value for ρ_o. Since Graham [10] has emphasized the significant temperature dependence of B_ρ, it becomes obvious why such care has to be taken in the measurement and control of temperature during the determinations of ρ.

The experimental procedure undertaken in this work for the determination of ρ at a given pressure and temperature required the measurement of four distinct quantities, namely, (i) the intensity I_v of the 90° scattered light reaching the photomultiplier when the incident light beam was passed through the cell and the scattering medium contained therein, the transmission axis of the analyzer being set vertical (i.e. parallel to the electric vector of the incident beam); (ii) the scattered light intensity I_h with the analyzer rotated through 90° to set its transmission axis horizontal; (iii) the background intensity

$I_v(b)$ after the cell had been evacuated and the analyzer transmission axis had again been set vertical; and finally (iv) the background intensity $I_h(b)$ with the transmission axis set horizontal.

Of course, I_v was measured after attenuation of the full intensity by a neutral density filter to avoid errors due to non-linearity in the photomultiplier's response at higher intensities, and the observed reading then multiplied by the filter's attenuation factor to yield the true I_v.

The depolarization ratio ρ was then given by

$$\rho = \frac{I_h - I_h(b)}{I_v - I_v(b)} . \qquad (3.6)$$

A BASIC program was used to calculate ρ and its standard deviation from data files containing the count rates of the various I_v, I_h, $I_v(b)$, and $I_h(b)$ signals as measured by the C660 counter/timer for a particular gas sample.

Another important consideration in taking measurements of ρ was the stabilization of both the laser output intensity and the photomultiplier's dark count rate. The laser generally stabilized after one hour's operation, while the photomultiplier dark count generally stabilized fifteen to twenty minutes after applying the high voltage, provided it had been stored in its light-tight housing since it was last used. If the photocathode was exposed to light, and in particular to fluorescent light, when the tube was not in use then an extremely high dark count was observed after initial application of the high voltage, and stability was realized only after about an hour of operation.

For the molecules investigated here, ρ_o is sufficiently large to mask the contribution to the polarized light arising from vibrational Raman scattering, and no isolating filter was necessary.

3.2.1 Results for ethene

As seen in table 2.6, the theory indicates a ratio magnitude $(\mathcal{G}_\rho/2B)$ for ethene of about 0.33 at room temperature, which is not very favourable. However, the second pressure virial coefficient B(T) of this molecule is precisely known, table 2.4 containing a comparison of selected experimental values which are seen to be in agreement at least to within 0.5% over the temperature range 238.15 K to 448.15 K. Because of this, the value of $\mathcal{G}_\rho$ extracted from a measured B_ρ using the relationship

$$B_\rho = \rho_o\left(1 - \tfrac{4}{3}\rho_o\right)\left(2B + \mathcal{G}_\rho\right) \qquad (3.7)$$

is *not* rendered overly imprecise despite the dominant presence of 2B.

Our measurement of the pressure dependence of the depolarization ratio ρ of ethene was carried out at room temperature with no direct temperature control on the cell. It took a month to gather a complete set of measurements, and bearing in mind the significant temperature dependence of B_ρ, the work was performed in a laboratory with no windows to ensure a well insulated environment. Variations in the ambient temperature were less than 2 °C over the entire month, the mean being (294.9 ± 1.8) K.

C. P. grade ethene of 99.5% purity, supplied by Air Products, was admitted to the scattering cell without further purification, being passed through a 0.2 μm Millipore membrane to remove dust. ρ was measured over the pressure range 100 kPa to 3200 kPa in steps of about 100 kPa. The molar volume V_m for each gas pressure P and temperature T was determined first by finding $V_m^{ideal} = RT/P$ as an initial approximation, and then by substituting this value into the virial equation of state

$$V_m = \frac{R\,T}{P}\left[\,1 + \frac{B(T)}{V_m} + \frac{C(T)}{V_m^2}\,\right]. \qquad (3.8)$$

The 'corrected' value for V_m thus obtained was further refined by substituting it for V_m in the right hand side of equation (3.8) keeping all other variables the same, and the procedure reiterated until

Figure 3.6. Experimental depolarization ratio as a function of gas density for ethene

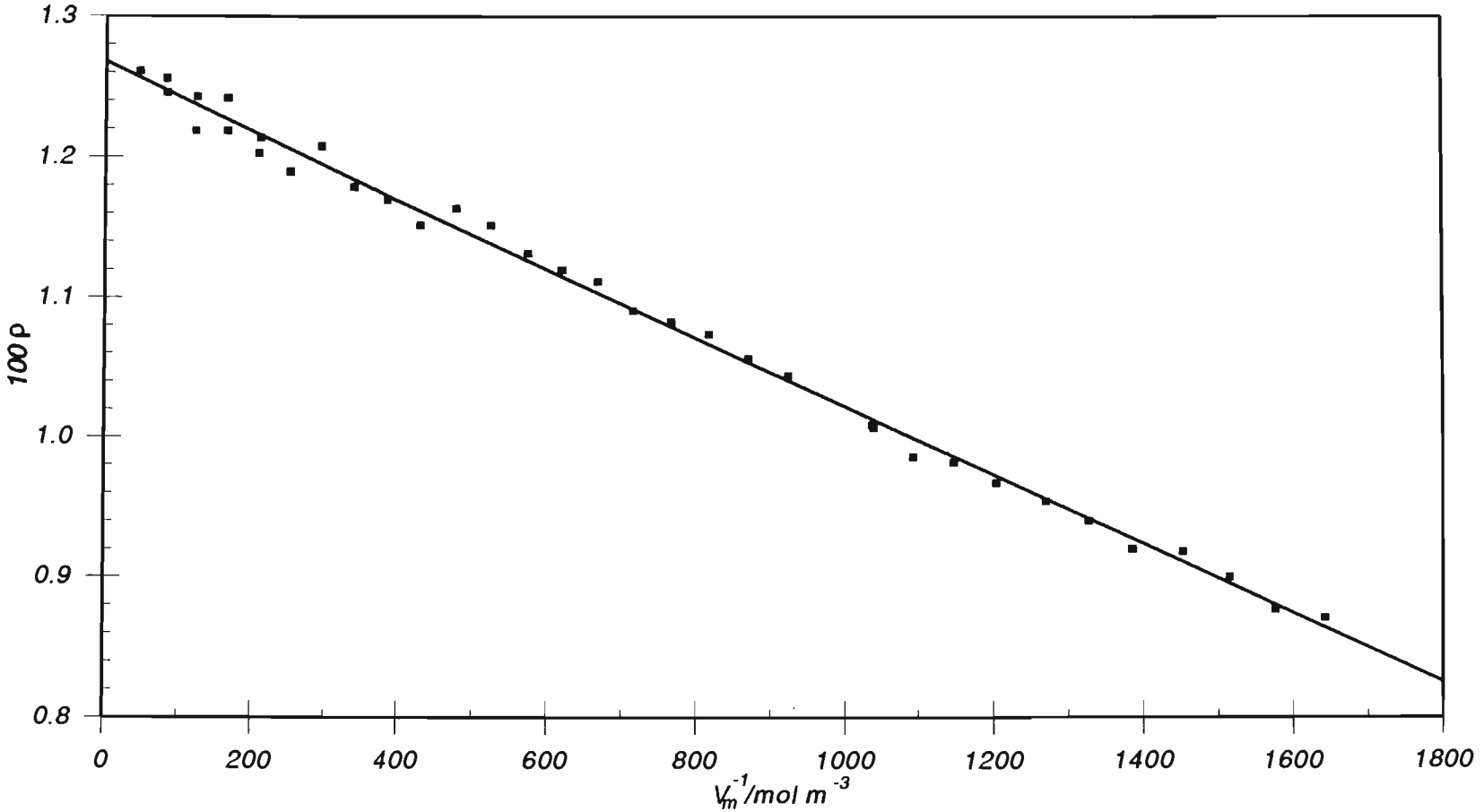

consecutive values differed by an amount less than one part in a million. The second and third pressure virial coefficients B(T) and C(T) in equation (3.7) were estimated by fitting fifth-order polynomials to the B(T) and C(T) values of Douslin and Harrison [11,12] in the temperature range 283.15 K to 303.15 K and interpolating to the experimental temperatures. The results follow:

Table 3.1. Measurement of the pressure-dependence of the depolarization ratio ρ of ethene at λ = 514.5 nm

reading	P/kPa	T/°C	V_m^{-1}/mol m^{-3}	100 × $(\rho \pm s_x)$
1	113	22.0	46.4	1.244 ± 0.016
2	202	20.5	83.7	1.229 ± 0.013
3	301	20.5	125.5	1.226 ± 0.013
4	399	19.8	167.9	1.203 ± 0.014
5	504	20.0	213.3	1.198 ± 0.014
6	202	22.7	83.1	1.239 ± 0.013
7	301	23.0	124.4	1.202 ± 0.016
8	403	22.4	168.0	1.225 ± 0.014
9	503	22.6	210.8	1.187 ± 0.012
10	603	22.9	254.0	1.174 ± 0.015
11	703	23.0	297.9	1.191 ± 0.016
12	798	21.3	342.5	1.163 ± 0.012
13	901	21.5	389.0	1.155 ± 0.014
14	1000	21.7	434.3	1.137 ± 0.012
15	1101	21.0	482.9	1.148 ± 0.014
16	1200	21.3	529.3	1.137 ± 0.016
17	1306	21.5	579.9	1.117 ± 0.013
18	1406	22.4	626.2	1.105 ± 0.014
19	1502	22.0	674.9	1.097 ± 0.014
20	1598	22.1	722.8	1.077 ± 0.017
21	1700	22.3	774.1	1.068 ± 0.018
22	1801	22.5	825.6	1.060 ± 0.020
23	1905	22.7	879.4	1.042 ± 0.016
24	1999	22.0	933.0	1.029 ± 0.012

(continued ...)

Table 3.2. Our measured B_ρ value for ethene, together with that of Berrue *et al.* Comparison is made with the theoretical values calculated in Chapter 2. Also, $\mathcal{G}_\rho$ values deduced from the measured B_ρ values are compared with the calculated $\mathcal{G}_\rho$ values.

Reference	T/K	$100 \times \rho_o$	$\frac{10^6 B_\rho^{exp}}{m^3 mol^{-1}}$	$\frac{10^6 B_\rho^{calc}}{m^3 mol^{-1}}$	$\frac{B_\rho^{exp}}{B_\rho^{calc}}$	$\frac{10^6 \mathcal{G}_\rho^{exp}}{m^3 mol^{-1}}$	$\frac{10^6 \mathcal{G}_\rho^{calc}}{m^3 mol^{-1}}$	$\frac{\mathcal{G}_\rho^{exp}}{\mathcal{G}_\rho^{calc}}$
this work	294.92	1.250 ± 0.002	-2.384 ± 0.027	-2.357	1.011	92.2 ± 4.8	94.36	0.977
[13]	328.0	1.357 ± 0.012	-1.78 ± 0.07	-1.671	1.065	85.0 ± 8.0[a]	91.87	0.925

[a] Deduced from the B_ρ of Berrue *et al.* using *our* value for ρ_o. Their value for ρ_o is some 8.6% higher than ours, and yields an $\mathcal{G}_\rho$ of 98.3×10^{-6} $m^3 mol^{-1}$ which is 7% higher than the theoretical value. The experimental uncertainty in their $\mathcal{G}_\rho$ value is from a least squares analysis of the data, and is almost certainly a conservative estimate.

Table 3.1. (Continued)

reading	P/kPa	T/°C	V_m^{-1}/mol m^{-3}	$100 \times (\rho \pm s_x)$
25	2203	21.2	1050	1.007 ± 0.012
26	2201	21.4	1048	1.009 ± 0.013
27	2304	21.7	1105	0.986 ± 0.013
28	2403	22.0	1160	0.982 ± 0.013
29	2500	22.0	1217	0.967 ± 0.012
30	2605	21.3	1286	0.954 ± 0.010
31	2702	21.5	1344	0.940 ± 0.011
32	2798	21.7	1403	0.920 ± 0.010
33	2902	21.5	1472	0.918 ± 0.011
34	3002	21.7	1536	0.900 ± 0.011
35	3100	22.0	1599	0.877 ± 0.010
36	3199	22.0	1667	0.871 ± 0.008

A plot of ρ versus V_m^{-1} is given in figure 3.6. From equation (3.5) it can be seen that B_ρ is obtained as the slope of the linear region of the plot, while the intercept yields a value for ρ_o. There is no apparent deviation from linearity in the plot, indicating that pair interactions are predominant over this range of densities. The statistical analysis of the data was performed using the Statgraphics package written by the Statistical Graphics Corporation. This package calculated the slope and intercept of the graph, and their estimated uncertainties, using a least squares analysis of the data. Deduced values of ρ_o and B_ρ are summarized in table 3.2, which also includes a comparison with the calculated theoretical value for B_ρ obtained in Chapter 2. Substitution of the ρ_o and B_ρ values into equation (3.7), together with a second pressure virial coefficient at 294.92 K of $(-143.1 \pm 1.0) \times 10^{-6}$ m^3mol^{-1}, yields the $\mathcal{G}_\rho$ value given in table 3.2. This value is also compared with the one calculated in Chapter 2. Note how our value for $100 \times \rho_o$ of 1.250 ± 0.002 agrees very favourably with that of $1.247_5 \pm 0.005$ measured at λ = 514.5 nm by Bogaard *et al.* [4].

Figure 3.7. Experimental depolarization ratio as a function of gas density for ethene using the data of Berrue et al. [13]

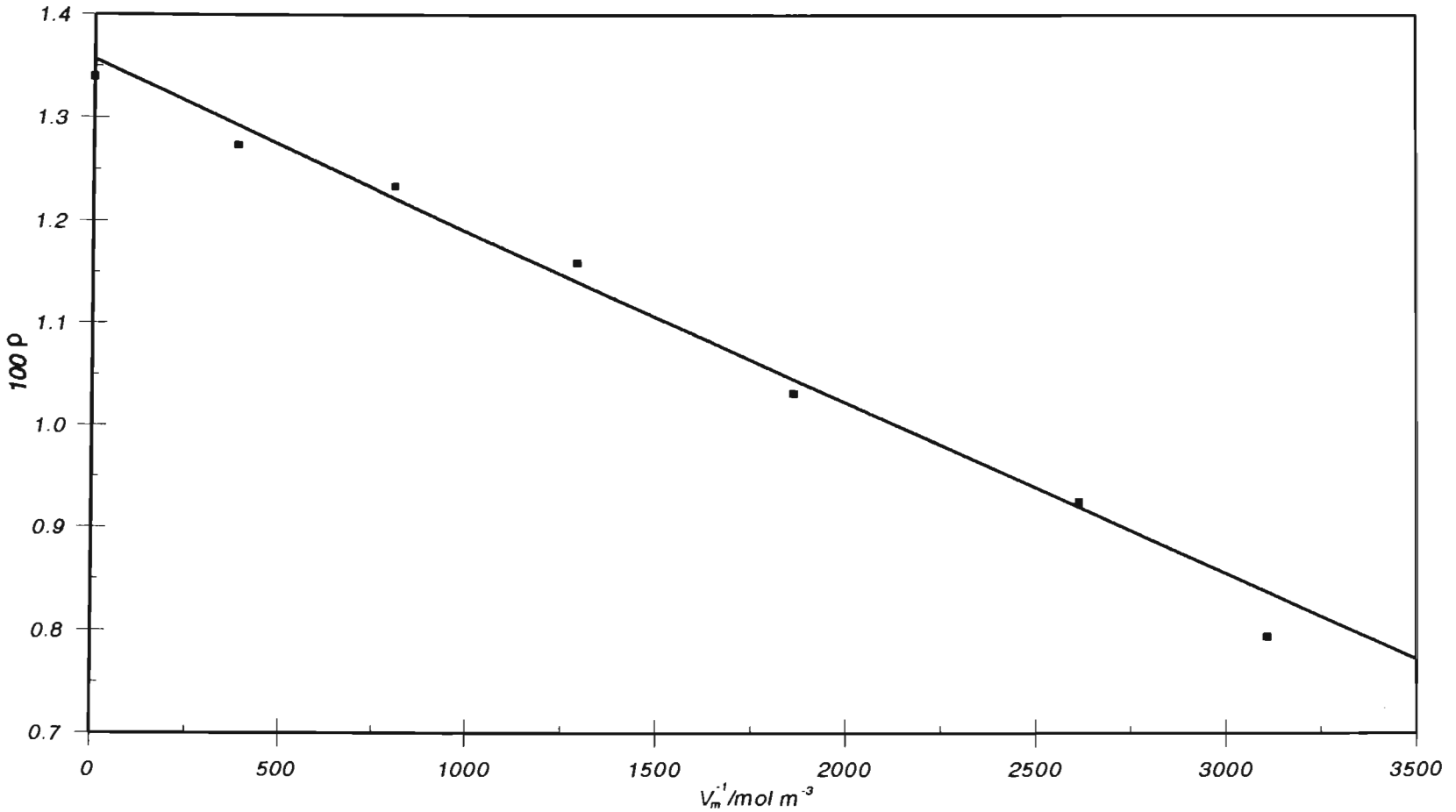

In 1977, Berrue *et al.* [13] made measurements of light-scattering density effects of ethene at 328 K, presenting their data in the form of a small graph of depolarization ratio versus pressure. The wavelength of the incident light was not stated, but was probably 514.5 nm as used in subsequent work on other gases [14]. For comparison with our B_ρ value calculated for ethene when treated as a quasi-linear molecule [10,15], the slope of this graph was estimated and multiplied by RT. This neglects the non-ideal behaviour of the gas as expressed by equation (3.8), and we have now improved our estimate of this B_ρ value. The graph was enlarged to allow extraction of the depolarization ratios and pressures of the seven points lying on the linear region up to about 60 bar pressure, and the molar volumes were calculated from equation (3.8). Figure 3.7 contains a plot of the ρ versus V_m^{-1} values, and the deduced values of ρ_o, B_ρ and $\mathcal{P}_\rho$ are summarized alongside ours in table 3.2. It must be emphasized that this estimation of B_ρ is extremely crude, and is included merely for completeness.

When ethene is approximated to have axial symmetry, it has a calculated $\mathcal{P}_\rho$ value of 66.04×10^{-6} m^3mol^{-1} at 298 K and a wavelength of 514.5 nm [16], which is some 40% lower than the experimentally deduced value of $(92.2 \pm 4.8) \times 10^{-6}$ m^3mol^{-1}. Indeed, we are poised to draw a striking conclusion: it is only after *full* account is taken of the molecule's low symmetry, both in the optical properties and the physical molecular shape, that we find acceptable agreement between the theoretical and measured values of $\mathcal{P}_\rho$.

3.2.2 Results for sulphur dioxide

The relatively imprecise measured B(T) values of sulphur dioxide as presented in table 2.10, coupled with the low $[\mathcal{P}_\rho/2B]$ ratio magnitude of ~ 0.4 at temperatures around 100 °C, are a cause for concern. In the case of ethene, the $\mathcal{P}_\rho$ value extracted from equation (3.7) had a rather high precision of 5% *despite* the low $[\mathcal{P}_\rho/2B]$ ratio magnitude of 0.33, the redeeming factor being the accurately known B(T) value. It is inevitable that the overriding presence of an *imprecise* B(T) in equation

(3.7) for sulphur dioxide will degrade the extracted $\mathcal{S}_\rho$ value no matter how precise the measured B_ρ for this molecule. However, should more accurate determinations of B(T) be forthcoming in the future, the B_ρ measured here can lead immediately to a more precise value for $\mathcal{S}_\rho$.

Commercial grade sulphur dioxide of 99.9% purity was supplied by the AECI in a 112 kg industrial cylinder, and samples were initially passed through a 0.2 μm Durapore polyvinylidene fluoride membrane before being frozen into a 300 ml stainless steel cylinder immersed in liquid nitrogen. The saturation vapour pressure at room temperature is of the order of 350 kPa, which is totally unsatisfactory for pressure-dependence studies of ρ. Hence, The cylinder temperature was elevated to about 70 °C using heating tape, raising the saturation vapour pressure to around 1.5 MPa. The scattering cell's oil bath was heated to give the cell an internal equilibrium vapour temperature of (65.2 ± 0.1) °C as measured by the calibrated thermocouple situated within the cell as close as possible to the scattering volume. The saturation vapour pressure at 65.2 °C is 1.298 MPa [17], allowing measurements of ρ to be taken from 100 kPa to 1000 kPa, higher pressures probably coming too close to the point of liquefaction where triplet and higher-order interactions come into play. Higher temperatures were avoided in the fear that the Pockels windows might be weakened and shatter at the elevated pressures used. The highly corrosive nature of suplhur dioxide, and possible damage to expensive equipment, was always uppermost in our minds.

The molar volume V_m for each vapour pressure P at T = 65.2 °C could not be determined by solving equation (3.8) because no C(T) values have been measured for sulphur dioxide. Instead, we made use of the compressibility factors Z measured by Kang *et al.* [17] for the isotherms 10 °C, 20 °C, 30 °C, 40 °C, 50 °C, 75 °C, 100 °C and 125 °C, interpolating the data to obtain Z for the isotherm 65.2 °C as presented in table 3.3. A polynomial was fitted to this isotherm, and was interpolated to find Z for each experimental pressure P, which through $Z = PV_m/RT$ yielded the molar volumes. The measured data for the pressure dependence of ρ is presented in table 3.4, where readings are presented in the order in which they were taken.

Figure 3.8. Experimental depolarization ratio as a function of gas density for sulphur dioxide

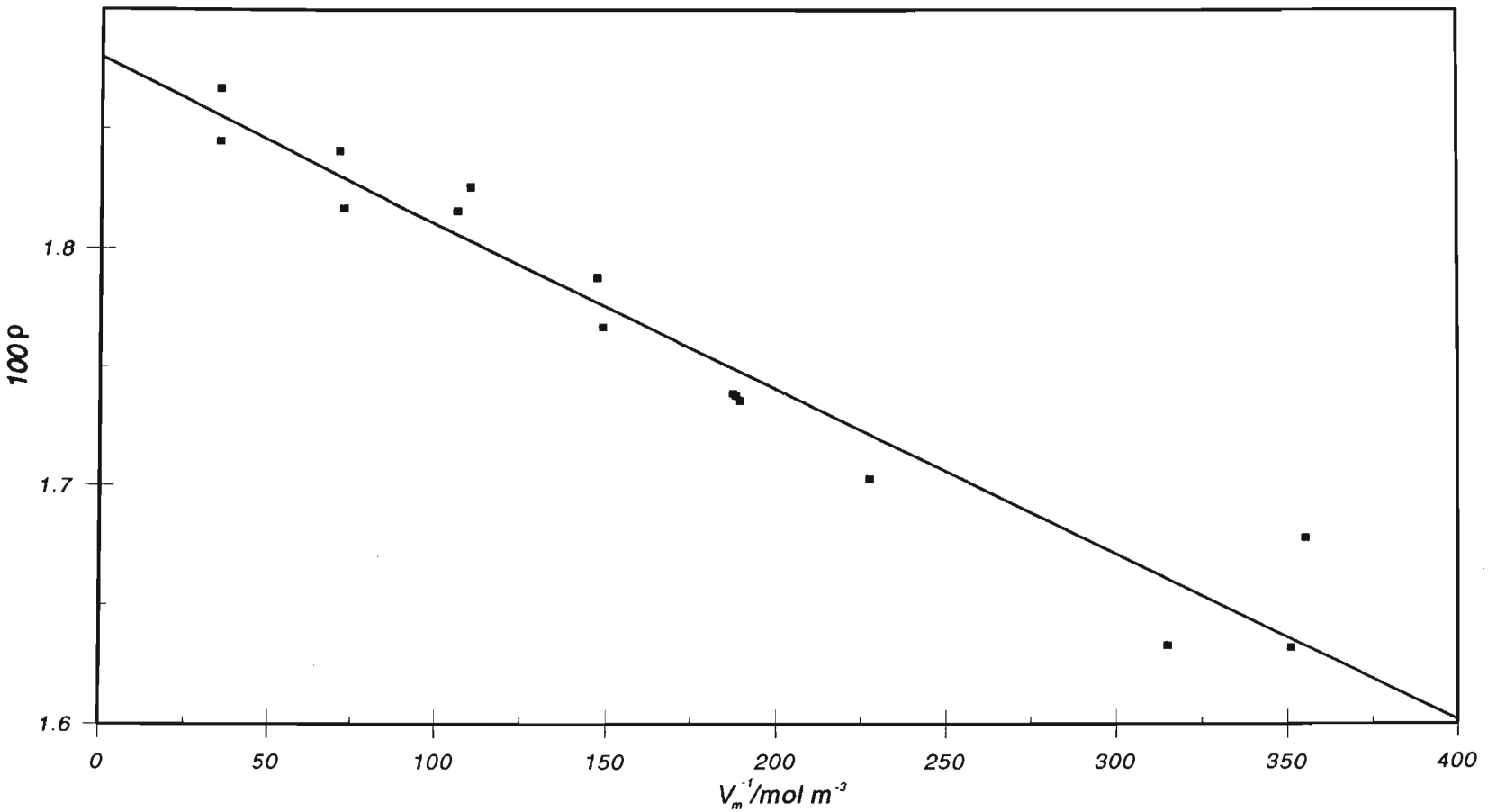

Table 3.3. The compressibility factor Z of sulphur dioxide for the isotherm T = 65.2 °C

P/kPa	Z
101.3	0.9891
202.7	0.9782
304.0	0.9673
405.3	0.9562
506.6	0.9452
608.0	0.9341
709.3	0.9215
810.6	0.9091
1298.3*	0.8348

*This is the saturation vapour pressure.

Table 3.4. Measurement of the pressure-dependence of the depolarization ratio ρ of sulphur dioxide at λ = 514.5 nm and T = 338.35 K

reading	P/kPa	V_m^{-1}/mol m^{-3}	$100 \times (\rho \pm s_x)$
1	98	35.2	1.867 ± 0.015
2	200	72.7	1.817 ± 0.011
3	300	110.2	1.826 ± 0.012
4	499	187.5	1.739 ± 0.014
5	98	35.2	1.845 ± 0.010
6	397	147.5	1.788 ± 0.011
7	501	188.3	1.738 ± 0.010
8	198	71.1	1.841 ± 0.015
9	401	149.0	1.767 ± 0.012
10	504	189.5	1.736 ± 0.018
11	599	227.7	1.703 ± 0.016
12	806	315.0	1.633 ± 0.016
13	908	355.3	1.678 ± 0.016
14	896	351.1	1.632 ± 0.013
15	290	106.4	1.816 ± 0.013

Table 3.5. Our measured B_ρ value for sulphur dioxide, together with the deduced φ_ρ value. Comparison is made with the theoretical values calculated in Chapter 2.

T/K	$100 \times \rho_o$	$\frac{10^6 B_\rho^{exp}}{m^3 mol^{-1}}$	$\frac{10^6 B_\rho^{calc}}{m^3 mol^{-1}}$	$\frac{B_\rho^{exp}}{B_\rho^{calc}}$	$\frac{10^6 \varphi_\rho^{exp}}{m^3 mol^{-1}}$	$\frac{10^6 \varphi_\rho^{calc}}{m^3 mol^{-1}}$	$\frac{\varphi_\rho^{exp}}{\varphi_\rho^{calc}}$
338.35	$1.880 \pm 0.009_7$	-6.96 ± 0.49	-6.328	1.100	215 ± 53	249.39	0.862

A plot of ρ versus V_m^{-1} is given in figure 3.8. There is no discernible deviation from linearity, indicating a predominance of pair interactions over this range of densities. Deduced values of ρ_o, B_ρ and $\mathcal{P}_\rho$ together with their estimated uncertainties are presented in table 3.5, which also contains the theoretical B_ρ and $\mathcal{P}_\rho$ values calculated in Chapter 2. Notice how well our $100 \times \rho_o$ of 1.88 ± 0.01 agrees with that of 1.85 ± 0.01 measured at $\lambda = 514.5$ nm by Bogaard *et al.* [4]. As was anticipated, the experimentally deduced $\mathcal{P}_\rho$ has quite a large uncertainty of some 25%. What is encouraging, though, is how the calculated $\mathcal{P}_\rho$ lies comfortably within the uncertainty limits of the measured value. We have discussed at length in Chapter 2 how the a_2A_1 term can make a significant negative contribution to $\mathcal{P}_\rho$, and hence B_ρ, in the case of polar molecules; and it is worth noting that *if* this term is in fact significant for sulphur dioxide, its effect will be to bring the calculated $\mathcal{P}_\rho$ closer to the measured value. This matter can only be resolved when estimates of A-tensor components become available.

For comparative purposes, we have calculated $\mathcal{P}_\rho$ for sulphur dioxide after approximating its molecular shape and optical properties to be of axial symmetry. The Lennard-Jones force-constants obtained for this molecule in section *2.6.1*, namely $R_o = 0.3850$ nm and $\varepsilon/k = 220.0$ K, were used in equation (1.87) to calculate the second pressure virial coefficient B(T). Choosing the shape factor D such that agreement between the calculated B(T) and the experimental data [17] was to within 5% over the temperature range 283.15 to 473.15 K yielded $D = 0.472$. This shape factor is *not* physically reasonable, being very close to the limit of $+\frac{1}{2}$ for infinitely thin rod-like linear molecules, as discussed in section *1.4.2*. The molecular properties of sulphur dioxide required in calculations of $\mathcal{P}_\rho$ have been given is section *2.6.1*, and it is obvious that the quadrupole moment and polarizability tensor of this molecule cannot reasonably be approximated to axial symmetry. For example, molecules with axial symmetry have $\theta_{11} = \theta_{22}$, while for sulphur dioxide we have $\theta_{11} = -16.4 \times 10^{-40}$ Cm^2 and $\theta_{22} = +12.9 \times 10^{-40}$ Cm^2. Furthermore, linear molecules have $\alpha_{11} = \alpha_{22}$, while sulphur dioxide has $\alpha_{11} = 5.93 \times 10^{-40}$ C^{2}m^{2}J^{-1} and $\alpha_{22} = 3.34 \times 10^{-40}$ C^{2}m^{2}J^{-1} at $\lambda = 514.5$ nm: a substantial difference of 78%. Using the dipole moment $\mu_3 = -5.4262 \times 10^{-30}$ Cm, the mean static polarizability tensor

$\alpha_s = 4.2072 \times 10^{-40}\ C^2m^2J^{-1}$, the dynamic polarizability components at $\lambda = 514.5$ nm for an 'axially-symmetric' sulphur dioxide molecule of $\alpha_{\parallel} = 2.816 \times 10^{-40}\ C^2m^2J^{-1}$ and $\alpha_{\perp} = 5.176 \times 10^{-40}\ C^2m^2J^{-1}$, and the approximate quadrupole moment $\theta = \theta_{33} = 3.5 \times 10^{-40}\ Cm^2$, we obtain a calculated $\mathcal{Y}_\rho$ for sulphur dioxide at $T = 338.35$ K of $\mathcal{Y}_\rho = 974.18 \times 10^{-6}m^3mol^{-1}$. This value is 3.91 times larger than the $\mathcal{Y}_\rho = 249.39 \times 10^{-6}m^3mol^{-1}$ obtained after considering the full symmetry of the molecule. When the two values are compared with the experimental estimate of $\mathcal{Y}_\rho = (215 \pm 53) \times 10^{-6}\ m^3mol^{-1}$, there can be no doubt as to the gross inadequacy of approximating non-linear molecules to be of axial symmetry in the theory of B_ρ. It is desirable to establish whether the second virial coefficients of the various other molecular-optic phenomena will confirm this finding, and we turn to the Kerr effect for guidance.

Calculations of the second Kerr-effect virial coefficients B_K of sulphur dioxide performed by Gentle *et al.* [18], using the statistical-mechanical theory of B_K presented by Buckingham *et al.* [19] for *axially-symmetric* molecules, yielded results which were more than double the experimental values. In the following chapter, we present a theory of B_K for non-linear molecules, and apply it to various molecules, including sulphur dioxide, with pleasing success.

3.3 References

[1] Cabannes, J, 1915, *Comptes Rendus*, **160**, 62.

[2] Strutt, J. W., (Third Baron Rayleigh), 1899, Scientific Papers IV, 397.

[3] Bridge, N. J., and Buckingham, A. D., 1964, *J. chem. Phys.*, **40**, 2733.

[4] Bogaard, M. P., Buckingham, A. D., Pierens, R. K., and White, A. H., 1978, *J. chem. Soc. Faraday Trans.* I, **74**, 3008.

[5] Bridge, N. J., 1966, M. Sc. Thesis, University of Oxford.

[6] Bridge, N. J., and Buckingham, A. D., 1966, *Proc. Roy. Soc. Lond.* A, **295**, 334.

[7] Strutt, R. J., (Fourth Baron Rayleigh), 1920, *Proc. Roy. Soc. Lond.* A, **97,** 435.

[8] Couling, V. W., and Graham, C., 1994, *Molec. Phys.*, **82,** 235.

[9] Smithells, C. J., 1967, *Metals Reference Book* (London: Butterworths).

[10] Graham, C., 1992, *Molec. Phys.*, **77,** 291.

[11] Douslin, D. R., and Harrison, R. H., 1976, *J. chem. Thermodyn.*, **8,** 301.

[12] Dymond, J. H., and Smith, E. B., 1980, *The Virial Coefficients of Pure Gases and Mixtures* (Oxford: Clarendon).

[13] Berrue, J., Chave, A., Dumon, B., and Thibeau, M., 1977, *Rev. Phys. Appl.*, **12,** 1743.

[14] Berrue, J., Chave, A., Dumon, B., and Thibeau, M., 1981, *Can. J. Phys.*, **59,** 1510.

[15] Couling, V. W., and Graham, C., 1993, *Molec. Phys.*, **79,** 859.

[16] Couling, V. W., 1993, M. Sc. Thesis, University of Natal.

[17] Kang, T. L., Hirth, L. J., Kobe, K. A., and McKetta, J. J., 1961, *J. chem. Engng. Data*, **6,** 220.

[18] Gentle, I. R., Laver, D. R., and Ritchie, G. L. D., 1990, *J. phys. Chem.*, **94,** 3434.

[19] Buckingham, A. D., Galwas, P. A., and Liu Fan-Chen, 1983, *J. Mol. Struct.*, **100,** 3.

CHAPTER 4

CALCULATION OF THE SECOND KERR-EFFECT VIRIAL COEFFICIENTS OF MOLECULES WITH LINEAR AND LOWER SYMMETRY

4.1 Introduction

The second light-scattering virial coefficient B_ρ has now been the subject of comprehensive experimental and theoretical investigation for molecular symmetries ranging from spherical to non-linear. It has been established that the dipole-induced-dipole (DID) model of Silberstein [1] reliably accounts for the contribution made by interacting pairs of molecules to the depolarization ratio ρ of Rayleigh-scattered light for the full range of molecular symmetries, although reasons for the discrepancies between experiment and theory for the *larger* quasi-spherical molecules [2] still need to be sought and explained. A significant aspect of the theoretical investigation has been the realization that attempts to treat non-linear molecules by approximating them to be of axial symmetry lead to grossly inaccurate calculated estimates of B_ρ. Certainly, such approximations *are* tempting; especially in view of the arduous task of developing a complete molecular tensor theory of B_ρ even for molecules with linear symmetry. However, it has been successfully demonstrated how, after invoking the aid of the powerful algebraic manipulation packages now available for personal computers, the development of a complete molecular tensor theory of B_ρ for non-linear molecules is feasible. This theory has yielded calculated estimates of B_ρ for ethene (of D_{2h} symmetry) and sulphur dioxide (of C_{2v} symmetry) which are in good accord with our measured values. Approximating ethene to be of axial symmetry sees the calculated $\mathcal{S}_\rho$ value significantly underestimating experiment by 40%, while a similar approximation for sulphur dioxide yields a calculated $\mathcal{S}_\rho$ which is four times larger than the measured value. It has been concluded that after taking full account of the symmetry of a particular molecule, both in its molecular property tensors and physical shape, the DID model

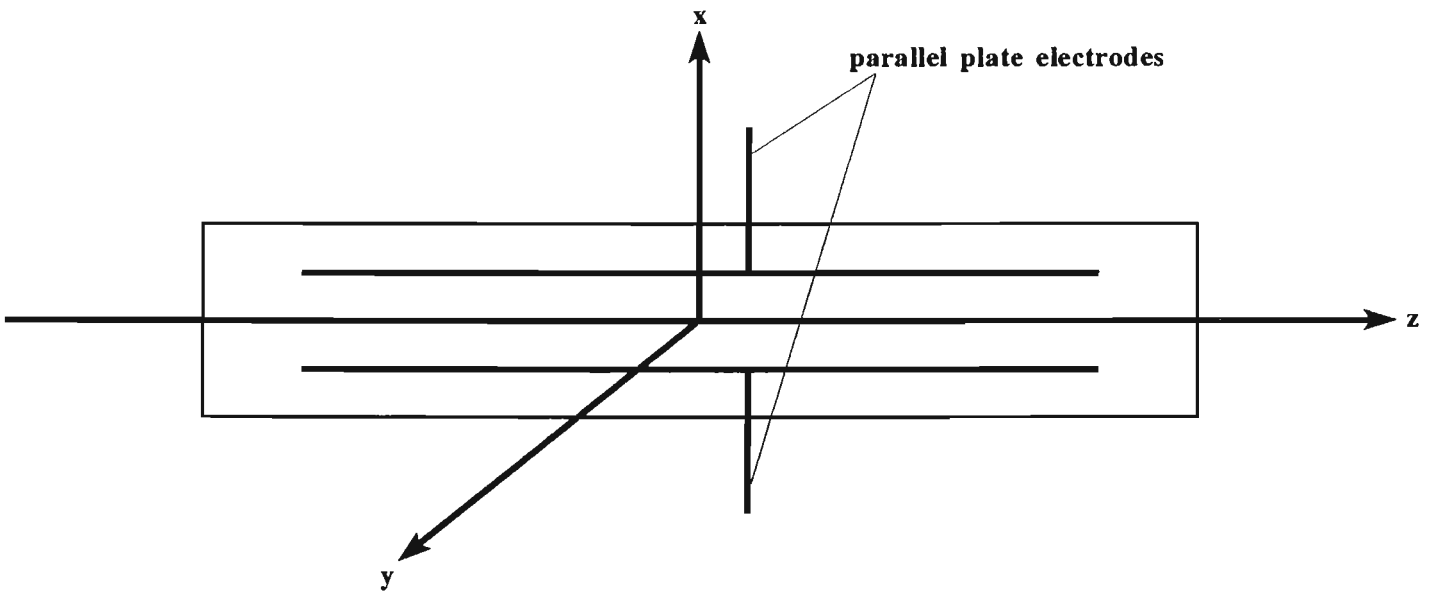

Figure 4.1. The Kerr cell, with space-fixed axes (x,y,z) where z is in the direction of propagation of the light beam, x is in the direction of the applied electric field, and y is perpendicular to the field.

accurately describes the effects of pair interactions on ρ.

It is now desirable to turn to other molecular-optic phenomena for a general confirmation of this conclusion. Of particular interest will be the development of DID theories describing the effects of pair interactions on these phenomena, followed by calculations where *the same* Lennard-Jones force constants and shape factors obtained in work on B(T) and B_ρ are utilized. Will good agreement between experiment and theory be maintained? Since substantial experimental investigation into the pressure-dependence of the Kerr effect has been carried out by various independent research groups for molecules with spherical [3-5], linear [6-10] and non-linear [11-13] symmetry; it seems natural to turn our attention to this particular effect in seeking an answer to our question.

4.2 A general theory of electro-optical birefringence in dense fluids

Kerr, in 1875, was the first to observe that an isotropic medium placed in a strong uniform electric field generally becomes birefringent [14]. The scope of our investigation will be limited to fluids, where the application of a static field leads to anisotropy in the molecular distribution either as a result of intrinsic anisotropy in the individual molecules, or because anisotropy is induced in the molecules by the applied field itself.

Consider the arrangement in figure 4.1 where the space-fixed system of axes O(x,y,z) is fixed in the Kerr cell such that z is in the direction of propagation of the light beam, x is in the direction of the applied electric field, and y is perpendicular to the field. When the cell is filled with a fluid and a uniform electric field is applied (by means of a pair of parallel-plate electrodes), a light beam propagating in the z-direction and vibrating in the xz plane will experience a refractive index n_x, which differs from the refractive index n_y experienced by a beam propagating in the z-direction and vibrating in the yz plane. The task in developing a theory of the Kerr effect lies in relating the macroscopic observable $(n_x - n_y)$ to the molecular property tensors of the individual molecules in the fluid, and this has been achieved for gases at low pressures by Buckingham and Pople [15].

4.2.1 Non-interacting molecules

For a dilute gas where molecular interactions are negligible in number, the oscillating dipole moment $\mu_i^{(p)}$ of molecule p arises solely due to the polarizing action of the oscillating electric field $\mathcal{E}_o$ associated with the light wave, there being no neighbouring molecules q which are close enough for their oscillating moments to set up significant fields and field gradients at molecule p. However, it is important to realize that the optical-frequency polarizability tensor α_{ij} of molecule p may be modified by the presence of the strong applied *static* electric field E_i, to a new effective polarizability tensor π_{ij}, written

$$\pi_{ij} = \frac{\partial \mu_i}{\partial \mathcal{E}_{oj}} = \alpha_{ij} + \beta_{ijk} E_k + \frac{1}{2}\gamma_{ijkl} E_k E_l + \ldots , \qquad (4.1)$$

where all tensors refer to the molecule-fixed axes O(1,2,3) of molecule p. Here, the polarizability tensor α_{ij}, and the first and second hyperpolarizability tensors β_{ijk} and γ_{ijkl} respectively, are dependent on the optical frequency of the incident light wave. Any orientational bias arising from intrinsic molecular anisotropy will be accounted for later on when we average over the biased orientational motion of the molecule.

To compare the refractive indices parallel and perpendicular to the applied static electric field E_i, we require the direction cosines a_i^x between the x space-fixed and i molecule-fixed axes, and a_i^y between the the y space-fixed and i molecule-fixed axes. Then, if the molecule is held in a *fixed* configuration σ, the difference between the differential polarizabilities *for this specific orientation* is

$$\pi(\sigma, E) = \pi_{ij}\left(a_i^x a_j^x - a_i^y a_j^y\right) . \qquad (4.2)$$

Since the molecule is in fact tumbling in space, this quantity has to be averaged over *all* configurations *in the presence of the biasing influence* E_i. Assuming the period of oscillation of the light waves to be much smaller than the time of rotation of the molecule, and assuming that the rotational energy levels are sufficiently close for the orientation to be effectively continuous, it is possible to average over configurations with a Boltzmann-type weighting factor. We write

$$\bar{\pi} = \frac{\int \pi(\sigma,E)\ \exp\left[-U(\sigma,E)/kT\right]d\tau}{\int \exp\left[-U(\sigma,E)/kT\right]d\tau} , \qquad (4.3)$$

where $U(\sigma,E)$ is the energy of the molecule in a particular configuration σ while in the presence of the applied field E_i. In molecule-fixed axes, this energy is given by

$$U(\sigma,E) = U^{(0)} - \mu_i^{(0)}E_i - \tfrac{1}{2}a_{ij}E_iE_j - \tfrac{1}{6}b_{ijk}E_iE_jE_k - \ldots , \qquad (4.4)$$

where $U^{(0)}$ is the energy of the molecule in the absence of the applied field, $\mu_i^{(0)}$ is the permanent dipole moment of the molecule, a_{ij} is the *static* polarizability, b_{ijk} is the *static* first-order hyperpolarizability, etc. The difference between the refractive indices may now be written as

$$n_x - n_y = \frac{2\pi N_A}{\left(4\pi\varepsilon_o\right)V_m}\,\bar{\pi} . \qquad (4.5)$$

We can write out the full expression for $\pi(\sigma,E)$ in equation (4.2) by writing Ea_i^x for E_i and by making use of equation (4.1):

$$\pi(\sigma,E) = \left(\alpha_{ij} + \beta_{ijk}Ea_k^x + \tfrac{1}{2}\gamma_{ijkl}E^2a_k^xa_l^x + \ldots\right)\left(a_i^xa_j^x - a_i^ya_j^y\right) . \qquad (4.6)$$

We already know how to average over unbiased rotational motion (see the *isotropic* averages in Chapter 2), and so the procedure adopted is to convert the biased average in equation (4.3) into isotropic averages by Taylor expanding $\bar{\pi}$ in powers of E while bearing in mind that it depends on E both through $\pi(\sigma,E)$ *and* through the energy $U(\sigma,E)$. It is fair to assume that the series converges rapidly since the distortion and orientational effects of E_i on gas molecules is extremely small. We have

$$\bar{\pi} = A + B\,E + C\,E^2 + \ldots \qquad (4.7)$$

where

$$A = \left(\bar{\pi}\right)_{E=0} , \qquad (4.8)$$

$$B = \left[\frac{\partial \bar{\pi}}{\partial E}\right]_{E=0} , \tag{4.9}$$

and

$$C = \frac{1}{2}\left[\frac{\partial^2 \bar{\pi}}{\partial E^2}\right]_{E=0} . \tag{4.10}$$

We will denote an isotropic average of a quantity $X(\sigma,E)$ with $E = 0$ as $\langle X \rangle$, that is

$$\langle X \rangle = \frac{\int X(\sigma,0)\, \exp\left[-U^{(0)}/kT\right] d\tau}{\int \exp\left[-U^{(0)}/kT\right] d\tau} . \tag{4.11}$$

Explicit expressions for the various coefficients A, B, C ... are then obtained by putting $E = 0$ after differentiating equation (4.3). We have

$$B = \left[\frac{\partial \bar{\pi}}{\partial E}\right]_{E=0} = \left\langle \frac{\partial \pi}{\partial E} \right\rangle - (kT)^{-1} \left\langle \pi \frac{\partial U}{\partial E} \right\rangle . \tag{4.12}$$

The quantities in angular brackets are easily obtained from equations (4.4) and (4.6), which yield

$$\left[\frac{\partial U}{\partial E}\right]_{E=0} = -\mu_i^{(0)} a_i^x \tag{4.13}$$

and

$$\left[\frac{\partial \pi}{\partial E}\right]_{E=0} = \beta_{ijk} a_k^x \left(a_i^x a_j^x - a_i^y a_j^y\right) . \tag{4.14}$$

It is clear that both terms in equation (4.12) average to zero over all directions of a_i^x, and so the leading non-vanishing term in the expansion of $\bar{\pi}$ is in E^2:

$$C = \frac{1}{2}\left[\frac{\partial^2 \bar{\pi}}{\partial E^2}\right]_{E=0} = \frac{1}{2}\left\langle \frac{\partial^2 \pi}{\partial E^2} \right\rangle - \frac{1}{2kT}\left\langle 2\frac{\partial \pi}{\partial E}\frac{\partial U}{\partial E} + \pi \frac{\partial^2 U}{\partial E^2} \right\rangle + \frac{1}{2k^2T^2}\left\langle \pi \left[\frac{\partial U}{\partial E}\right]^2 \right\rangle . \tag{4.15}$$

The second derivatives of equations (4.4) and (4.6) are

$$\left[\frac{\partial^2 U}{\partial E^2}\right]_{E=0} = -a_{ij}a_i^x a_j^x \tag{4.16}$$

and

$$\left[\frac{\partial^2 \pi}{\partial E^2}\right]_{E=0} = \gamma_{ijkl}\left(a_i^x a_j^x - a_i^y a_j^y\right)a_k^x a_l^x \ . \tag{4.17}$$

Considering each term in equation (4.15), and making use of the standard results for isotropic averages in equations (2.14) and (2.16) of Chapter 2, we obtain:

$$\begin{aligned}\frac{1}{2}\left\langle\frac{\partial^2\pi}{\partial E^2}\right\rangle &= \frac{1}{2}\gamma_{ijkl}\left\langle a_i^x a_j^x a_k^x a_l^x - a_i^y a_j^y a_k^x a_l^x\right\rangle \\ &= \frac{2}{30}\gamma_{iijj} \ ,\end{aligned} \tag{4.18}$$

$$\begin{aligned}-\frac{1}{2kT}\left\langle 2\frac{\partial\pi}{\partial E}\frac{\partial U}{\partial E} + \pi\frac{\partial^2 U}{\partial E^2}\right\rangle &= (kT)^{-1}\beta_{ijk}\mu_l^{(0)}\left\langle a_i^x a_j^x a_k^x a_l^x - a_i^y a_j^y a_k^x a_l^x\right\rangle \\ &\quad + \frac{1}{2kT}\alpha_{ij}a_{kl}\left\langle a_i^x a_j^x a_k^x a_l^x - a_i^y a_j^y a_k^x a_l^x\right\rangle \\ &= \frac{2}{15kT}\beta_{iij}\mu_j^{(0)} + \frac{1}{15kT}\left(\alpha_{ij}a_{ij} - 3\alpha a\right) \ ,\end{aligned} \tag{4.19}$$

$$\begin{aligned}\frac{1}{2k^2T^2}\left\langle\pi\left[\frac{\partial U}{\partial E}\right]^2\right\rangle &= \frac{1}{2k^2T^2}\alpha_{ij}\mu_k^{(0)}\mu_l^{(0)}\left\langle a_i^x a_j^x a_k^x a_l^x - a_i^y a_j^y a_k^x a_l^x\right\rangle \\ &= \frac{3}{15k^2T^2}\left[\alpha_{ij}\mu_i^{(0)}\mu_j^{(0)} - \alpha\left(\mu^{(0)}\right)^2\right] \ ,\end{aligned} \tag{4.20}$$

where α and a are the traces of α_{ij} and a_{ij} respectively. Hence, equation (4.7) becomes

$$\begin{aligned}\bar{\pi} = \Bigg\{&\frac{2}{30}\gamma_{iijj} + \frac{2}{15kT}\beta_{iij}\mu_j^{(0)} + \frac{1}{15kT}\left(\alpha_{ij}a_{ij} - 3\alpha a\right) \\ &+ \frac{3}{15k^2T^2}\left[\alpha_{ij}\mu_i^{(0)}\mu_j^{(0)} - \alpha\left(\mu^{(0)}\right)^2\right]\Bigg\} E^2 \ .\end{aligned} \tag{4.21}$$

Using the definition of the molecular Kerr constant K_m proposed by Otterbein [16] which, in the limit of low densities, reduces to

$$K_m = \lim_{V_m \to \infty} \left\{ \frac{2(n_x - n_y)V_m}{27(4\pi\varepsilon_o)E^2} \right\}_{E\to 0} = \frac{2\pi N_A}{27(4\pi\varepsilon_o)} \left[\frac{\partial^2 \bar{\pi}}{\partial E^2} \right]_{E=0} , \qquad (4.22)$$

we obtain

$$K_m = \frac{2\pi N_A}{405(4\pi\varepsilon_o)} \left\{ 2\gamma_{iijj} + (kT)^{-1} \left[4\beta_{iij}\mu_j^{(0)} + 3(\alpha_{ij}a_{ij} - 3\alpha a) \right] + \frac{3}{k^2T^2} \left[\alpha_{ij}\mu_i^{(0)}\mu_j^{(0)} - \alpha(\mu^{(0)})^2 \right] \right\} . \qquad (4.23)$$

This equation, first derived by Buckingham and Pople [15], is a generalization of the well-known Langevin-Born equation to include the effects of high field strengths on the polarizability.

For a gas of non-interacting spherical molecules, equation (4.23) reduces to

$$K_m = \frac{4\pi N_A}{81(4\pi\varepsilon_o)} \gamma \qquad (4.24)$$

where $\gamma = \frac{1}{5}\gamma_{ijij}$: measurement of the Kerr constant at low pressures can directly yield a value for the hyperpolarizability constant γ of the gas. This value, although peculiar to the frequency of the light beam used in the measurement of the refractive index, is unlikely to be substantially different from the static value provided the optical frequency is well below the electronic absorption band of the gas molecules.

4.2.2 Interacting spherical molecules

The above Langevin-Born and Buckingham-Pople theory of electro-optical birefringence pertains specifically to assemblies of non-interacting molecules. However, since the difference between refractive indices

parallel and perpendicular to the applied field is often very small at low gas pressures (especially for typical field strengths readily obtainable in the laboratory), experiments often have to be carried out on compressed gases. In such cases the molecular Kerr constant K_m differs from that obtained in the limit of infinite dilution. This density-dependence of K_m is conveniently described by means of the virial expansion [17]

$$K_m = A_K + \frac{B_K}{V_m} + \frac{C_K}{V_m^2} + \ldots , \tag{4.25}$$

where the coefficients A_K, B_K, C_K, ..., are the first, second, third, ..., Kerr-effect virial coefficients. A_K, equal to

$$\lim_{V_m \to \infty} \left(K_m\right) ,$$

is given by equation (4.24) of section *4.2.1*. B_K, which describes deviations from A_K due to pair interactions, is

$$B_K = \lim_{V_m \to \infty} \left(K_m - A_K\right)V_m . \tag{4.26}$$

In 1968, Buckingham and Dunmur [3] measured the pressure-dependence of the Kerr effect for the atomic species argon, krypton and xenon, and for the quasi-spherical molecule sulphur hexafluoride. The relationship between the induced birefringence and gas density was observed to be non-linear, indicating a significant presence of pair interactions. Invoking dipole-induced-dipole theory, B_K was written [3]

$$B_K = \frac{32\pi^2 N_A^2 \alpha^2 a^2}{45\left(4\pi\varepsilon_o\right)^3 kT} \int_0^\infty R^{-4} \exp\left[-U_{12}(R)/kT\right] dR \tag{4.27}$$

where N_A is Avogadro's number, α and a are the dynamic and static polarizabilities respectively, and $U_{12}(R)$ is the intermolecular potential between interacting molecules 1 and 2 which are separated by a distance R. It is worth noting that for atoms and spherical molecules, the second Kerr-effect and light-scattering virial coefficients are closely related [18]:

$$B_\rho = \frac{27\varepsilon_o kT}{N_A a^2} B_K \,. \qquad (4.28)$$

Buckingham and Pople [19] have provided a means of evaluating the integral in equation (4.27):

$$\int_0^\infty R^{-k} \exp\left[-U_{12}^L(R)/kT\right] R^2 \, dR = \frac{1}{1\,2} R_o^{3-k} \, y^{-4} \, H_k(y) \qquad (4.29)$$

where $U_{12}^L(R)$ is the Lennard-Jones 6:12 potential [20]. Values of $H_k(y)$ have been tabulated for k ranging from 6 to 17 in integral steps [19].

Table 4.1 presents the ratio of all measured values of B_K for atoms and spherical molecules with the values calculated according to equation (4.27). Also included are the ratio of measured second light-scattering virial coefficients B_ρ with the values calculated according to equations (4.27) and (4.28). The ratio B_K^{exp}/B_K^{calc} displays the same trend observed earlier by Watson and Rowell [2] for the ratio $B_\rho^{exp}/B_\rho^{calc}$, namely that the ratio is less than one for the rare gases, and increases more and more above unity as the molecular size increases. This appears to confirm the assertion made by Watson and Rowell [2] that the point-dipole approximation of the DID model for molecular interactions is inadequate for the larger quasi-spherical molecules. And yet, the DID theory of B_ρ for the linear molecules nitrogen, ethane, methyl chloride and carbon monoxide [24,25], and for the non-linear molecules ethene and sulphur dioxide (Chapter 2), is in good agreement with experiment (see [26-28] and Chapter 3). Discrepancies between experiment and theory for the large quasi-spherical molecules remain unresolved, and the problem warrants further attention.

Table 4.1. Comparison of measured and calculated second Kerr-effect and light-scattering virial coefficients for atoms and spherical molecules as reported by Dunmur *et al.* [5].

Atom/ molecule	$\frac{B_K^{exp}}{B_K^{calc}}$	$\frac{B_\rho^{exp}}{B_\rho^{calc}}$
argon	0.73 ± 0.11 [3]	0.62 ± 0.96 [21]
	0.65 ± 0.11 [5]	0.81 ± 0.12 [22]
		0.67 ± 0.03 [4]
krypton	0.62 ± 0.54 [3]	0.85 ± 0.11 [2]
	0.63 ± 0.09 [5]	
xenon	0.46 ± 0.16 [3]	
	0.67 ± 0.12 [5]	
methane	0.92 ± 0.09 [4]	0.75 ± 0.03 [4]
	1.40 ± 0.2 [5]	0.86 [23]
		1.20 ± 0.17 [2]
		1.03 ± 0.15 [22]
sulphur hexafluoride	1.77 ± 0.24 [3]	2.51 ± 0.08 [2]
	2.5 ± 0.4 [5]	
tetrafluoromethane	1.10 ± 0.1 [5]	
neopentane	3.9 ± 0.3 [5]	6.8 ± 0.9 [2]

4.2.3 Interacting linear molecules

The second Kerr-effect virial coefficient B_K has been deduced from pressure-dependence measurements of electric field induced birefringence for the linear molecules fluoromethane [6], trifluoromethane [6], carbon dioxide [7,10], nitrogen [7], ethane [7] and cyclopropane [7]; and for the non-linear molecules ethene [7], difluoromethane [6], dimethyl ether [11], hydrogen sulphide [12] and sulphur dioxide [13]. B_K has also been measured for cyclohexane and the n-alkanes from propane through to decane [9]. Some important features of these measurements are now

discussed.

B_K values for polar molecules are generally a hundred times larger than those for non-polar species. Values of B_K deduced from Kerr-effect measurements on polar gases often have poor precisions of around ±50%, with additional systematic errors arising from uncertainties in the pressure virial coefficients B(T) and C(T) used to obtain the molar volumes V_m of gas samples. In the case of non-polar gases, the experimental difficulties are further compounded by the much smaller density-dependence of the molar Kerr constant K_m. This is evidenced by the almost random fluctuation in the B_K values measured over a range of temperature for both nitrogen [7] and carbon dioxide [7,10].

In 1955, Buckingham [17] developed a statistical-mechanical theory of B_K for axially-symmetric molecules. Buckingham and Orr [6] extended this theory in 1969, including additional effects of polarizability and angle-dependent repulsive forces. They proceeded to calculate B_K for the fluoromethanes, and although approximate agreement with their experimental values [6] for fluoromethane was obtained, the calculated values for trifluoromethane were found to be much too small. This disagreement was attributed to effects of *short-range* interactions on the polarizability and potential energy, and it was argued that measurements of B_K for polar gases would probably not yield useful information about the nature of intermolecular forces.

It was only much later, in 1983, that Buckingham *et al.* [29] published a paper in which the order-of-magnitude discrepancy between experiment and theory for the fluoromethanes was resolved. The earlier theory of the Kerr effect [17] was extended to include collision-induced polarizability, which was found to be the dominant contributor to B_K. Use was made of a simple Stockmayer-type potential [30], in which the dipole-dipole interaction is added to a 6:12 Lennard-Jones potential; but the U_{shape} contribution to the intermolecular potential, which has been used before [19] to account for the angular dependence of short-range overlap repulsive forces for non-spherical molecules, was not included. Although no attempt was made to optimize the Lennard-Jones force constants R_o and ε/k, the new theory of B_K was found to provide what was said to be a reasonable fit to the observed values for the fluoromethanes [6] over a range of temperature. However, as will be shown later, this must be viewed in relation to a large uncertainty of

about 50% in the observed values.

It is noteworthy that although B_K has been measured for several non-polar molecules of linear symmetry, *no* calculated values of this quantity have appeared in the literature.

Recently, Gentle *et al.* [13] undertook measurements of the Kerr effect of sulphur dioxide over the temperature range 298.7 to 490.3 K, deducing rather precise B_K values over this temperature span. In view of the relative success of Buckingham, Galwas and Fan-Chen's extended theory of B_K for axially-symmetric molecules [29] when applied to the fluoromethanes, Gentle *et al.* thought it profitable to attempt an application of the theory to sulphur dioxide after approximating the molecule to be quasi-linear. The Lennard-Jones force constants R_o and ε/k *were* optimized, and when used in a simple Stockmayer potential to compute the second pressure virial coefficient B(T) of this gas, the calculated values were found to agree with experiment [31,32] to within ±6% over the full range of temperature. However, the calculated B_K values were generally more than double the experimental values, the model proving unsatisfactory. Perhaps this is not surprising, since for an axially symmetric molecule with the 3-axis as the principal axis, the polarizability components perpendicular to the 3-axis, α_{11} and α_{22}, are equal; while for sulphur dioxide we have $\alpha_{11} = 5.80 \times 10^{-40}$ $C^2m^2J^{-1}$ and $\alpha_{22} = 3.30 \times 10^{-40}$ $C^2m^2J^{-1}$ at $\lambda = 632.8$ nm [13]: a substantial difference of 76%. To definitively assess the extent to which the assumption of axial symmetry is responsible for the discrepancy between theory and experiment for sulphur dioxide, it is essential to develop a complete molecular tensor theory of B_K for molecules with non-linear symmetry. This theory is now presented, followed by application to both polar *and* non-polar molecules with linear and lower symmetry.

4.2.4 Interacting non-linear molecules

Recall that in the limit of infinite dilution, the refractive index difference $(n_x - n_y)$ of a gas in a strong static electric field E_x is

$$n_x - n_y = \frac{2\pi N_A}{(4\pi\varepsilon_o)V_m}\,\bar{\pi} \qquad (4.30)$$

where $\bar{\pi}$ is the average over all configurations σ of the quantity $\pi_{ij}\left(a_i^x a_j^x - a_i^y a_j^y\right)$ of a representative *isolated* molecule in the presence of the biasing influence E_x. The biased average $\bar{\pi}$ was converted into isotropic averages by Taylor expanding in powers of E, the leading contribution

$$\bar{\pi} = \frac{1}{2}\left(\frac{\partial^2 \bar{\pi}}{\partial E^2}\right)_{E=0} E^2$$

being expressed in terms of isotropic averages in equation (4.15).

For higher gas densities, we follow the philosophy established by Buckingham and Pople [33], and argue that the contribution of a representative molecule 1 to $\left(n_x - n_y\right)$ is now not always $\frac{2\pi N_A}{\left(4\pi\varepsilon_o\right)V_m}\bar{\pi}$, there being times when molecule 1 must be treated as half of an interacting pair. If molecule 1 has a neighbouring molecule 2, the relative configuration of which is given by the collective symbol τ, then the contribution of molecule 1 to $\left(n_x - n_y\right)$ *at that instant* is given by $\frac{1}{2}\left\{\frac{2\pi N_A}{\left(4\pi\varepsilon_o\right)V_m}\pi^{(12)}(\tau,E)\right\}$. Here,

$$\pi^{(12)}(\tau,E) = \pi_{ij}^{(12)}\left(a_i^x a_j^x - a_i^y a_j^y\right) \qquad (4.31)$$

where $\pi_{ij}^{(12)}$ is the differential polarizability of the interacting pair, and an explicit expression for this quantity will be derived in due course.

If the pair of molecules are held in a fixed relative configuration τ and are allowed to rotate *as a rigid whole* in the presence of the biasing influence E_i, the resulting biased orientational average $\overline{\pi^{(12)}(\tau,E)}$ can then be converted into isotropic averages by Taylor expanding in powers of E. Analogous to the case of an isolated molecule, the leading term is

$$\overline{\pi^{(12)}(\tau,E)} = \frac{1}{2}\left(\frac{\partial^2 \overline{\pi^{(12)}(\tau,E)}}{\partial E^2}\right)_{E=0} E^2 \qquad (4.32)$$

where

$$\frac{1}{2}\left[\frac{\partial^2\overline{\pi^{(12)}(\tau,E)}}{\partial E^2}\right]_{E=0} = \frac{1}{2}\left\langle\frac{\partial^2\pi^{(12)}}{\partial E^2}\right\rangle - \frac{1}{2kT}\left\langle 2\frac{\partial\pi^{(12)}}{\partial E}\frac{\partial U^{(12)}}{\partial E} + \pi^{(12)}\frac{\partial^2 U^{(12)}}{\partial E^2}\right\rangle + \frac{1}{2k^2T^2}\left\langle\pi^{(12)}\left[\frac{\partial U^{(12)}}{\partial E}\right]^2\right\rangle . \qquad (4.33)$$

Here, $U^{(12)}(\tau,E)$ is the potential energy of the interacting pair of molecules in the presence of E_i. If the quantities within angular brackets are all initially referred to the molecule-fixed axes (1,2,3) of molecule 1, then for a given relative interaction configuration τ, the tensor product in (1,2,3) is fixed. When the pair rotates as a rigid whole in space-fixed axes (x,y,z), the average projection of pair properties (referred to (1,2,3)) is averaged into (x,y,z) over all orientations. Averaging over the pair interaction parameters τ can subsequently be performed.

Recall from equation (4.22) that the definition of the molecular Kerr constant proposed by Otterbein [16], in the limit of low densities, is

$$A_K = \lim_{V_m \to \infty}\left\{\frac{2(n_x - n_y)V_m}{27(4\pi\varepsilon_o)E^2}\right\}_{E\to 0} = \frac{2\pi N_A}{27(4\pi\varepsilon_o)}\left[\frac{\partial^2\overline{\pi}}{\partial E^2}\right]_{E=0} .$$

We are now in a position to extrapolate this expression to higher densities, obtaining

$$K_m = A_K + \int_\tau \frac{2\pi N_A}{27(4\pi\varepsilon_o)}\left\{\frac{1}{2}\left[\frac{\partial^2\overline{\pi^{(12)}(\tau,E)}}{\partial E^2}\right]_{E=0} - \left[\frac{\partial^2\overline{\pi}}{\partial E^2}\right]_{E=0}\right\} P(\tau)d\tau \qquad (4.34)$$

where $P(\tau)d\tau$ is the probability of molecule 1 having a neighbour in the range $(\tau, \tau + d\tau)$. Buckingham and Pople [33] have related this probability to the intermolecular potential $U_{12}(\tau)$:

$$P(\tau) = \frac{N_A}{\Omega V_m}\exp\left[-U_{12}(\tau)/kT\right] . \qquad (4.35)$$

Comparing equation (4.34) to equation (4.25), we obtain for B_K

$$B_K = \frac{2\pi N_A^2}{27\Omega(4\pi\varepsilon_o)} \int_\tau \left\{ \frac{1}{2}\left[\frac{\partial^2 \overline{\pi^{(12)}(\tau,E)}}{\partial E^2}\right]_{E=0} - \left[\frac{\partial^2 \bar{\pi}}{\partial E^2}\right]_{E=0} \right\} \exp\left[-U_{12}(\tau)/kT\right] \qquad (4.36)$$

which for two *non-linear* molecules with interaction co-ordinates as described in section 2.2 of Chapter 2 becomes

$$B_K = \frac{N_A^2}{216\pi^2(4\pi\varepsilon_o)} \int_{R=0}^{\infty} \int_{\alpha_1=0}^{2\pi} \int_{\beta_1=0}^{\pi} \int_{\gamma_1=0}^{2\pi} \int_{\alpha_2=0}^{2\pi} \int_{\beta_2=0}^{\pi} \int_{\gamma_2=0}^{2\pi}$$

$$\times \left\{ \frac{1}{2}\left[\frac{\partial^2 \overline{\pi^{(12)}(\tau,E)}}{\partial E^2}\right]_{E=0} - \left[\frac{\partial^2 \bar{\pi}}{\partial E^2}\right]_{E=0} \right\} \exp\left[-U_{12}(\tau)/kT\right]$$

$$\times R^2 \sin\beta_1 \sin\beta_2 \, dR \, d\alpha_1 d\beta_1 d\gamma_1 d\alpha_2 d\beta_2 d\gamma_2 \, . \qquad (4.37)$$

$\left[\frac{\partial^2 \bar{\pi}}{\partial E^2}\right]_{E=0}$ has already been evaluated in section *4.1.1*, yielding

$$\left[\frac{\partial^2 \bar{\pi}}{\partial E^2}\right]_{E=0} = \left\{ \frac{4}{30}\gamma_{iijj} + \frac{4}{15kT}\beta_{iij}\mu_j^{(0)} + \frac{2}{15kT}\left(\alpha_{ij}a_{ij} - 3\alpha a\right) \right.$$

$$\left. + \frac{6}{15k^2T^2}\left[\alpha_{ij}\mu_i^{(0)}\mu_j^{(0)} - \alpha\left(\mu^{(0)}\right)^2\right] \right\} , \qquad (4.38)$$

and we must now turn our attention to evaluating $\frac{1}{2}\left[\frac{\partial^2 \overline{\pi^{(12)}(\tau,E)}}{\partial E^2}\right]_{E=0}$.

As for a dilute gas, the refractive index of a dense gas is determined by the total oscillating dipole moment induced in a molecule. The difference now is that the dipole moment of a representative molecule 1 is induced not only by the oscillating electric field $\mathcal{E}$ associated with the light wave, but also in part by the field $\mathcal{F}_i^{(1)}$ arising at molecule 1 due to the oscillating moments of a neighbouring molecule 2. If we neglect the small quadrupole and field gradient effects, we have

$$\mu_i^{(1)}(\mathcal{E}_o) = \left[\alpha_{ij}^{(1)} + \beta_{ijk}^{(1)}E_k + \frac{1}{2}\gamma_{ijkl}^{(1)}E_kE_l + \ldots\right]\left[\mathcal{E}_{oj} + \mathcal{F}_j^{(1)}\right] \qquad (4.39)$$

where E_j is the strong applied static field.

Invoking the T-tensors (see equations (2.28) to (2.30)), we see that $\mathcal{F}_j^{(1)}$ has the form

$$\mathcal{F}_j^{(1)} = T_{jk}^{(1)} \mu_k^{(2)} \quad . \tag{4.40}$$

It must be emphasized that $\mu_k^{(2)}$ itself is the oscillating dipole induced in molecule 2 by the field arising at 2 due not only to the direct influence of $\mathcal{E}_o$, but also to the oscillating dipole moment of molecule 1:

$$\mu_k^{(2)}\left(\mathcal{E}_o\right) = \left[\alpha_{kl}^{(2)} + \beta_{klm}^{(2)} E_m + \tfrac{1}{2}\gamma_{klmn}^{(2)} E_m E_n + \ldots\right]\left[\mathcal{E}_{ol} + \mathcal{F}_l^{(2)}\right] , \tag{4.41}$$

where $\mathcal{F}_l^{(2)}$ has the form given by equation (4.40):

$$\mathcal{F}_l^{(2)} = T_{lm}^{(2)} \mu_m^{(1)} \quad . \tag{4.42}$$

Substitution of equations (4.41) and (4.42) into equation (4.40), followed by successive substitutions of $\mathcal{F}_i^{(1)}$ and $\mathcal{F}_i^{(2)}$, leads to a lengthy series of terms contributing to the net field $\mathcal{F}_j^{(1)}$ in equation (4.40); and substitution of this series into equation (4.39) yields a final expression for the total oscillating dipole induced on molecule 1 by the light wave field in the presence of molecule 2:

$$\mu_i^{(1)}(\mathcal{E}_o) = \alpha^{(1)}_{iw}\mathcal{E}_{ow} + \alpha^{(1)}_{ij}T_{jk}\alpha^{(2)}_{kw}\mathcal{E}_{ow} + \alpha^{(1)}_{ij}T_{jk}\alpha^{(2)}_{kl}T_{lm}\alpha^{(1)}_{mw}\mathcal{E}_{ow}$$

$$+ \alpha^{(1)}_{ij}T_{jk}\alpha^{(2)}_{kl}T_{lm}\alpha^{(1)}_{mn}T_{np}\alpha^{(2)}_{pw}\mathcal{E}_{ow} + \ldots$$

$$+ \beta^{(1)}_{iwk}E_k\mathcal{E}_{ow} + \beta^{(1)}_{ijk}E_kT_{jl}\alpha^{(2)}_{lw}\mathcal{E}_{ow} + \beta^{(1)}_{ijk}E_kT_{jl}\alpha^{(2)}_{lm}T_{mn}\alpha^{(1)}_{nw}\mathcal{E}_{ow}$$

$$+ \beta^{(1)}_{ijk}E_kT_{jl}\alpha^{(2)}_{lm}T_{mn}\alpha^{(1)}_{np}T_{pq}\alpha^{(2)}_{qw}\mathcal{E}_{ow} + \alpha^{(1)}_{ij}T_{jk}\beta^{(2)}_{kwl}E_l\mathcal{E}_{ow}$$

$$+ \alpha^{(1)}_{ij}T_{jk}\beta^{(2)}_{klm}E_mT_{ln}\alpha^{(1)}_{nw}\mathcal{E}_{ow} + \alpha^{(1)}_{ij}T_{jk}\alpha^{(2)}_{kl}T_{lm}\beta^{(1)}_{mwn}E_n\mathcal{E}_{ow}$$

$$+ \alpha^{(1)}_{ij}T_{jk}\alpha^{(2)}_{kl}T_{lm}\alpha^{(1)}_{mn}T_{np}\beta^{(2)}_{pwq}E_q\mathcal{E}_{ow}$$

$$+ \alpha^{(1)}_{ij}T_{jk}\alpha^{(2)}_{kl}T_{lm}\beta^{(1)}_{mnp}E_pT_{nq}\alpha^{(2)}_{qw}\mathcal{E}_{ow}$$

$$+ \alpha^{(1)}_{ij}T_{jk}\beta^{(2)}_{klm}E_mT_{ln}\alpha^{(1)}_{np}T_{pq}\alpha^{(2)}_{qw}\mathcal{E}_{ow} + \ldots$$

$$+ \tfrac{1}{2}\gamma^{(1)}_{iwkl}E_kE_l\mathcal{E}_{ow} + \tfrac{1}{2}\gamma^{(1)}_{ijkl}E_kE_lT_{jm}\alpha^{(2)}_{mw}\mathcal{E}_{ow}$$

$$+ \tfrac{1}{2}\gamma^{(1)}_{ijkl}E_kE_lT_{jm}\alpha^{(2)}_{mn}T_{np}\alpha^{(1)}_{pw}\mathcal{E}_{ow}$$

$$+ \tfrac{1}{2}\gamma^{(1)}_{ijkl}E_kE_lT_{jm}\alpha^{(2)}_{mn}T_{np}\alpha^{(1)}_{pq}T_{qr}\alpha^{(2)}_{rw}\mathcal{E}_{ow}$$

$$+ \tfrac{1}{2}\alpha^{(1)}_{ij}T_{jk}\gamma^{(2)}_{kwmn}E_mE_n\mathcal{E}_{ow} + \tfrac{1}{2}\alpha^{(1)}_{ij}T_{jk}\gamma^{(2)}_{klmn}E_mE_nT_{lp}\alpha^{(1)}_{pw}\mathcal{E}_{ow}$$

$$+ \tfrac{1}{2}\alpha^{(1)}_{ij}T_{jk}\alpha^{(2)}_{kl}T_{lm}\gamma^{(1)}_{mwnp}E_nE_p\mathcal{E}_{ow}$$

$$+ \tfrac{1}{2}\alpha^{(1)}_{ij}T_{jk}\alpha^{(2)}_{kl}T_{lm}\alpha^{(1)}_{mn}T_{np}\gamma^{(2)}_{pwqr}E_qE_r\mathcal{E}_{ow}$$

$$+ \tfrac{1}{2}\alpha^{(1)}_{ij}T_{jk}\alpha^{(2)}_{kl}T_{lm}\gamma^{(1)}_{mnpq}E_pE_qT_{nr}\alpha^{(2)}_{rw}\mathcal{E}_{ow}$$

$$+ \tfrac{1}{2}\alpha^{(1)}_{ij}T_{jk}\gamma^{(2)}_{klmn}E_mE_nT_{lp}\alpha^{(1)}_{pq}T_{qr}\alpha^{(2)}_{rw}\mathcal{E}_{ow} + \ldots . \qquad (4.43)$$

When the operation $\frac{\partial}{\partial \mathcal{E}_{ow}}$ is performed on this expression for $\mu_i^{(1)}$, we find the resulting expression for the differential polarizability of a molecule p in the presence of both the applied static field E_i and a neighbouring molecule q in a specific relative configuration τ is

$$\pi_{iw}^{(p)} = \alpha_{iw}^{(p)} + \alpha_{ij}^{(p)}T_{jk}\alpha_{kw}^{(q)} + \alpha_{ij}^{(p)}T_{jk}\alpha_{kl}^{(q)}T_{lm}\alpha_{mw}^{(p)}$$

$$+ \alpha_{ij}^{(p)}T_{jk}\alpha_{kl}^{(q)}T_{lm}\alpha_{mn}^{(p)}T_{np}\alpha_{pw}^{(q)} + \ldots$$

$$+ \beta_{iwk}^{(p)}E_k + \beta_{ijk}^{(p)}E_kT_{jl}\alpha_{lw}^{(q)} + \alpha_{ij}^{(p)}T_{jk}\beta_{kwl}^{(q)}E_l$$

$$+ \beta_{ijk}^{(p)}E_kT_{jl}\alpha_{lm}^{(q)}T_{mn}\alpha_{nw}^{(p)} + \alpha_{ij}^{(p)}T_{jk}\beta_{klm}^{(q)}E_mT_{ln}\alpha_{nw}^{(p)}$$

$$+ \alpha_{ij}^{(p)}T_{jk}\alpha_{kl}^{(q)}T_{lm}\beta_{mwn}^{(p)}E_n + \beta_{ijk}^{(p)}E_kT_{jl}\alpha_{lm}^{(q)}T_{mn}\alpha_{np}^{(p)}T_{pq}\alpha_{qw}^{(q)}$$

$$+ \alpha_{ij}^{(p)}T_{jk}\alpha_{kl}^{(q)}T_{lm}\alpha_{mn}^{(p)}T_{np}\beta_{pwq}^{(q)}E_q + \alpha_{ij}^{(p)}T_{jk}\alpha_{kl}^{(q)}T_{lm}\beta_{mnp}^{(p)}E_pT_{nq}\alpha_{qw}^{(q)}$$

$$+ \alpha_{ij}^{(p)}T_{jk}\beta_{klm}^{(q)}E_mT_{ln}\alpha_{np}^{(p)}T_{pq}\alpha_{qw}^{(q)} + \ldots$$

$$+ \tfrac{1}{2}\gamma_{iwkl}^{(p)}E_kE_l + \tfrac{1}{2}\gamma_{ijkl}^{(p)}E_kE_lT_{jm}\alpha_{mw}^{(q)} + \tfrac{1}{2}\alpha_{ij}^{(p)}T_{jk}\gamma_{kwmn}^{(q)}E_mE_n$$

$$+ \tfrac{1}{2}\gamma_{ijkl}^{(p)}E_kE_lT_{jm}\alpha_{mn}^{(q)}T_{np}\alpha_{pw}^{(p)} + \tfrac{1}{2}\alpha_{ij}^{(p)}T_{jk}\gamma_{klmn}^{(q)}E_mE_nT_{lp}\alpha_{pw}^{(p)}$$

$$+ \tfrac{1}{2}\alpha_{ij}^{(p)}T_{jk}\alpha_{kl}^{(q)}T_{lm}\gamma_{mwnp}^{(p)}E_nE_p + \tfrac{1}{2}\gamma_{ijkl}^{(p)}E_kE_lT_{jm}\alpha_{mn}^{(q)}T_{np}\alpha_{pq}^{(p)}T_{qr}\alpha_{rw}^{(q)}$$

$$+ \tfrac{1}{2}\alpha_{ij}^{(p)}T_{jk}\alpha_{kl}^{(q)}T_{lm}\alpha_{mn}^{(p)}T_{np}\gamma_{pwqr}^{(q)}E_qE_r$$

$$+ \tfrac{1}{2}\alpha_{ij}^{(p)}T_{jk}\alpha_{kl}^{(q)}T_{lm}\gamma_{mnpq}^{(p)}E_pE_qT_{nr}\alpha_{rw}^{(q)}$$

$$+ \tfrac{1}{2}\alpha_{ij}^{(p)}T_{jk}\gamma_{klmn}^{(q)}E_mE_nT_{lp}\alpha_{pq}^{(p)}T_{qr}\alpha_{rw}^{(q)} + \ldots \,. \qquad (4.44)$$

Then, the difference between the differential polarizabilities $\pi_{iw}^{(p)}a_i^xa_w^x$ and $\pi_{iw}^{(p)}a_i^ya_w^y$ for a *specific relative interaction configuration* τ of molecules p and q in the presence of the applied field is

$$\pi^{(p)}(\tau,E) = \pi_{iw}^{(p)}\left(a_i^xa_w^x - a_i^ya_w^y\right) . \qquad (4.45)$$

Now, the differential polarizability of the interacting pair is

$$\pi_{iw}^{(12)} = \frac{\partial\mu_i^{(12)}}{\partial\mathcal{E}_{ow}} \qquad (4.46)$$

where $\mu_i^{(12)}\left(\mathcal{E}_{ow}\right)$ is the total oscillating dipole induced on the *interacting pair* by the light wave field. To proceed, we have to make

the assumption that the two interacting molecules *each retain their separate identities.* Certainly, in the long-range limit this assumption is perfectly valid. It is at very short range, when the charge distributions of the interacting molecules begin to overlap, that difficulties arise. The molecules can no longer be unambiguously defined, and for a definitive description of this arrangement, one has no alternative other than resorting to *ab initio* quantum-mechanical calculations. These are notoriously difficult, and have to be repeated for each system under consideration. Instead (and in keeping with the philosophy of this thesis) we follow the lead of past workers in the field [29,34-36] by treating the interacting molecules as if they retain their separate identities even in the overlap region.

With this assumption, equation (4.46) becomes

$$\pi_{iw}^{(12)} = \frac{\partial \mu_i^{(12)}}{\partial \mathcal{E}_{ow}} = \frac{\partial \left(\mu_i^{(1)} + \mu_i^{(2)}\right)}{\partial \mathcal{E}_{ow}} . \tag{4.47}$$

Then, the difference between the differential polarizabilities $\pi_{iw}^{(12)} a_i^x a_w^x$ and $\pi_{iw}^{(12)} a_i^y a_w^y$ of an interacting pair in a *specific relative interaction configuration* τ in the presence of the applied field may be written

$$\begin{aligned} \pi^{(12)}(\tau,E) &= \pi_{iw}^{(12)} \left(a_i^x a_w^x - a_i^y a_w^y\right) \\ &= \left[\pi_{iw}^{(1)} + \pi_{iw}^{(2)}\right] \left(a_i^x a_w^x - a_i^y a_w^y\right) \\ &= \pi^{(1)}(\tau,E) + \pi^{(2)}(\tau,E) \end{aligned} \tag{4.48}$$

where $\pi_{iw}^{(p)}$ is given by equation (4.44).

We follow Buckingham *et al.* [29] by writing the potential energy of the interacting pair in the presence of the static field E_i as

$$U^{(12)}(\tau,E) = U^{(12)}(\tau,0) - \int_0^E \mu_i^{(12)}(\tau,E) a_i^x \, dE \tag{4.49}$$

where E_i has been written as Ea_i^x, and where $\mu_i^{(12)}$ is the total dipole moment of the pair in the presence of E_i. As before, we write

$$\mu_i^{(12)} = \mu_i^{(1)} + \mu_i^{(2)} , \tag{4.50}$$

where $\mu_i^{(p)}$ is the total dipole moment of molecule p in the presence of E_i and molecule 2. We have

$$\mu_i^{(p)} = \mu_{oi}^{(p)} + a_{ij}^{(p)}\left(E_j + F_j^{(p)}\right) \tag{4.51}$$

where $\mu_{oi}^{(p)}$ is the permanent dipole moment of molecule p, and $F_j^{(p)}$ is the static field arising at molecule p due to the permanent *and* induced multipole moments of the neighbouring molecule q. Considering only the total dipole moment of molecule q, we can write

$$F_j^{(p)} = T_{jk}\mu_k^{(q)} \ . \tag{4.52}$$

Of course,

$$\mu_i^{(q)} = \mu_{oi}^{(q)} + a_{ij}^{(q)}\left(E_j + F_j^{(q)}\right) \tag{4.53}$$

where, in turn,

$$F_j^{(q)} = T_{jk}\mu_k^{(p)} \ . \tag{4.54}$$

Successive substitutions of $F_j^{(p)}$ and $F_j^{(q)}$ into equation (4.50) yield the series of terms contributing to the total static dipole moment on molecule p:

$$\begin{aligned}\mu_i^{(p)} = \mu_{oi}^{(p)} &+ a_{ij}^{(p)}T_{jv}\mu_{ov}^{(q)} + a_{ij}^{(p)}T_{jk}a_{kl}^{(q)}T_{lv}\mu_{ov}^{(p)} \\ &+ a_{ij}^{(p)}T_{jk}a_{kl}^{(q)}T_{lm}a_{mn}^{(p)}T_{nv}\mu_{ov}^{(q)} + \ldots \\ &+ a_{iv}^{(p)}E_v + a_{ij}^{(p)}T_{jk}a_{kv}^{(q)}E_v + a_{ij}^{(p)}T_{jk}a_{kl}^{(q)}T_{lm}a_{mv}^{(p)}E_v \\ &+ a_{ij}^{(p)}T_{jk}a_{kl}^{(q)}T_{lm}a_{mn}^{(p)}T_{np}a_{pv}^{(q)}E_v + \ldots + O\left(E^2\right) + \ldots \ .\end{aligned} \tag{4.55}$$

Hence, equation (4.49) becomes

$$U^{(12)}(\tau,E) = U^{(12)}(\tau,0) + U^{(1)}(\tau,E) + U^{(2)}(\tau,E) \tag{4.56}$$

where

$$U^{(p)}(\tau,E) = -\left(\mu_{oi}^{(p)} + a_{ij}^{(p)}T_{jv}\mu_{ov}^{(q)} + a_{ij}^{(p)}T_{jk}a_{kl}^{(q)}T_{lv}\mu_{ov}^{(p)}\right.$$

$$\left. + a_{ij}^{(p)}T_{jk}a_{kl}^{(q)}T_{lm}a_{mn}^{(p)}T_{nv}\mu_{ov}^{(q)} + \ldots\right)Ea_i^x$$

$$- \frac{1}{2}\left(a_{iv}^{(p)} + a_{ij}^{(p)}T_{jk}a_{kv}^{(q)} + a_{ij}^{(p)}T_{jk}a_{kl}^{(q)}T_{lm}a_{mv}^{(p)}\right.$$

$$\left. + a_{ij}^{(p)}T_{jk}a_{kl}^{(q)}T_{lm}a_{mn}^{(p)}T_{np}a_{pv}^{(q)} + \ldots\right)E^2a_i^xa_v^x$$

$$- O\left(E^3\right) - \ldots \quad . \tag{4.57}$$

We are now in a position to evaluate the term $\frac{1}{2}\left[\overline{\frac{\partial^2\pi^{(12)}(\tau,E)}{\partial E^2}}\right]_{E=0}$ in the expression for B_K given by equation (4.37). Recall from equation (4.33) that

$$\frac{1}{2}\left[\overline{\frac{\partial^2\pi^{(12)}(\tau,E)}{\partial E^2}}\right]_{E=0} = \frac{1}{2}\left\langle\frac{\partial^2\pi^{(12)}}{\partial E^2}\right\rangle - \frac{1}{2kT}\left\langle 2\frac{\partial\pi^{(12)}}{\partial E}\frac{\partial U^{(12)}}{\partial E} + \pi^{(12)}\frac{\partial^2U^{(12)}}{\partial E^2}\right\rangle$$

$$+ \frac{1}{2k^2T^2}\left\langle\pi^{(12)}\left[\frac{\partial U^{(12)}}{\partial E}\right]^2\right\rangle . \tag{4.58}$$

These isotropic averages are now systematically evaluated.

Invoking equation (4.48), the average $\frac{1}{2}\left\langle\frac{\partial^2\pi^{(12)}}{\partial E^2}\right\rangle$ may be written as $\frac{1}{2}\left\langle\frac{\partial^2\pi^{(1)}}{\partial E^2}\right\rangle + \frac{1}{2}\left\langle\frac{\partial^2\pi^{(2)}}{\partial E^2}\right\rangle$, and since molecules 1 and 2 are identical, *the isotropic averages of their polarizabilities must be the same.* Hence,

$$\frac{1}{2}\left\langle\frac{\partial^2\pi^{(12)}}{\partial E^2}\right\rangle = \left\langle\frac{\partial^2\pi^{(1)}}{\partial E^2}\right\rangle . \tag{4.59}$$

Using similar arguments, together with equation (4.56), we have

$$-(kT)^{-1}\left\langle\frac{\partial\pi^{(12)}}{\partial E}\frac{\partial U^{(12)}}{\partial E}\right\rangle = -2(kT)^{-1}\left\{\left\langle 2\frac{\partial\pi^{(1)}}{\partial E}\frac{\partial U^{(1)}}{\partial E}\right\rangle + \left\langle 2\frac{\partial\pi^{(1)}}{\partial E}\frac{\partial U^{(2)}}{\partial E}\right\rangle\right\} , \tag{4.60}$$

$$-\frac{1}{2kT}\left\langle\pi^{(12)}\frac{\partial^2U^{(12)}}{\partial E^2}\right\rangle = -(kT)^{-1}\left\{\left\langle\pi^{(1)}\frac{\partial^2U^{(1)}}{\partial E^2}\right\rangle + \left\langle\pi^{(1)}\frac{\partial^2U^{(2)}}{\partial E^2}\right\rangle\right\} \tag{4.61}$$

and

$$\frac{1}{2k^2T^2}\left\langle \pi^{(12)}\left[\frac{\partial U^{(12)}}{\partial E}\right]^2\right\rangle = (kT)^{-2}\left\{\left\langle \pi^{(1)}\left[\frac{\partial U^{(1)}}{\partial E}\right]^2\right\rangle + \left\langle \pi^{(1)}\left[\frac{\partial U^{(2)}}{\partial E}\right]^2\right\rangle + \left\langle \pi^{(1)}\frac{\partial U^{(1)}}{\partial E}\frac{\partial U^{(2)}}{\partial E}\right\rangle\right\} . \qquad (4.62)$$

Collecting these expressions, we obtain

$$\begin{aligned}\frac{1}{2}\left[\frac{\partial^2\overline{\pi^{(12)}(\tau,E)}}{\partial E^2}\right]_{E=0} &= \left\langle\frac{\partial^2\pi^{(1)}}{\partial E^2}\right\rangle \\ &\quad - 2(kT)^{-1}\left\{\left\langle 2\frac{\partial\pi^{(1)}}{\partial E}\frac{\partial U^{(1)}}{\partial E}\right\rangle + \left\langle 2\frac{\partial\pi^{(1)}}{\partial E}\frac{\partial U^{(2)}}{\partial E}\right\rangle\right\} \\ &\quad - (kT)^{-1}\left\{\left\langle \pi^{(1)}\frac{\partial^2U^{(1)}}{\partial E^2}\right\rangle + \left\langle \pi^{(1)}\frac{\partial^2U^{(2)}}{\partial E^2}\right\rangle\right\} \\ &\quad + (kT)^{-2}\left\{\left\langle \pi^{(1)}\left[\frac{\partial U^{(1)}}{\partial E}\right]^2\right\rangle + \left\langle \pi^{(1)}\frac{\partial U^{(1)}}{\partial E}\frac{\partial U^{(2)}}{\partial E}\right\rangle \right. \\ &\quad \left. + \left\langle \pi^{(1)}\left[\frac{\partial U^{(2)}}{\partial E}\right]^2\right\rangle\right\} . \qquad (4.63)\end{aligned}$$

Substituting in the explicit expressions for $\pi^{(p)}(\tau,E)$ and $U^{(p)}(\tau,E)$ (given in equations (4.45) and (4.57) respectively) with E = 0, as well as their first and second derivatives with respect to the applied field where appropriate, we obtain the contributions to $\frac{1}{2}\left[\frac{\partial^2\overline{\pi^{(12)}(\tau,E)}}{\partial E^2}\right]_{E=0}$, and hence, through equation (4.37), to B_K. We have

$$\begin{aligned}\left\{\frac{1}{2}\left[\frac{\partial^2\overline{\pi^{(12)}(\tau,E)}}{\partial E^2}\right]_{E=0} - \left[\frac{\partial^2\overline{\pi}}{\partial E^2}\right]_{E=0}\right\} &= \alpha_2 + \alpha_3 + \alpha_4 + \alpha_5 + \ldots \\ &\quad + \gamma_1\alpha_1 + \gamma_1\alpha_2 + \ldots \\ &\quad + \mu_2\alpha_1 + \mu_2\alpha_2 + \mu_2\alpha_3 + \ldots \\ &\quad + \mu_1\beta_1 + \mu_1\beta_1\alpha_1 + \ldots , \qquad (4.64)\end{aligned}$$

where

$$\alpha_2 = (kT)^{-1}\left\{\alpha^{(1)}_{ab}a^{(2)}_{pq}\right\}\left\langle a^x_a a^x_b a^x_p a^x_q - a^y_a a^y_b a^x_p a^x_q\right\rangle , \qquad (4.65)$$

$$\alpha_3 = (kT)^{-1}\Big\{\alpha^{(1)}_{ad}a^{(1)}_{pq}T_{qr}a^{(2)}_{rs} + \alpha^{(1)}_{ad}a^{(2)}_{pq}T_{qr}a^{(1)}_{rs} + \alpha^{(1)}_{ab}T_{bc}\alpha^{(2)}_{cd}a^{(1)}_{ps} + \alpha^{(1)}_{ab}T_{bc}\alpha^{(2)}_{cd}a^{(2)}_{ps}\Big\} \times \left\langle a^x_{ad}a^x_{ps}a^x_{ps} - a^y_{ad}a^y_{ps}a^x_{ps}\right\rangle , \tag{4.66}$$

$$\alpha_4 = (kT)^{-1}\Big\{\alpha^{(1)}_{af}a^{(1)}_{pq}T_{qr}a^{(2)}_{rs}T_{st}a^{(1)}_{tu} + \alpha^{(1)}_{af}a^{(2)}_{pq}T_{qr}a^{(1)}_{rs}T_{st}a^{(2)}_{tu} + \alpha^{(1)}_{ab}T_{bc}\alpha^{(2)}_{cf}a^{(1)}_{pq}T_{qr}a^{(2)}_{ru} + \alpha^{(1)}_{ab}T_{bc}\alpha^{(2)}_{cf}a^{(2)}_{pq}T_{qr}a^{(1)}_{ru} + \alpha^{(1)}_{ab}T_{bc}\alpha^{(2)}_{cd}T_{de}\alpha^{(1)}_{ef}a^{(1)}_{pu} + \alpha^{(1)}_{ab}T_{bc}\alpha^{(2)}_{cd}T_{de}\alpha^{(1)}_{ef}a^{(2)}_{pu}\Big\} \times \left\langle a^x_{af}a^x_{pu}a^x_{pu} - a^y_{af}a^y_{pu}a^x_{pu}\right\rangle , \tag{4.67}$$

$$\begin{aligned}\alpha_5 = (kT)^{-1}\Big\{&\alpha^{(1)}_{ah}a^{(1)}_{pq}T_{qr}a^{(2)}_{rs}T_{st}a^{(1)}_{tu}T_{uv}a^{(2)}_{vw} + \alpha^{(1)}_{ah}a^{(2)}_{pq}T_{qr}a^{(1)}_{rs}T_{st}a^{(2)}_{tu}T_{uv}a^{(1)}_{vw} + \alpha^{(1)}_{ab}T_{bc}\alpha^{(2)}_{ch}a^{(1)}_{pq}T_{qr}a^{(2)}_{rs}T_{st}a^{(1)}_{tw} + \alpha^{(1)}_{ab}T_{bc}\alpha^{(2)}_{ch}a^{(2)}_{pq}T_{qr}a^{(1)}_{rs}T_{st}a^{(2)}_{tw} \\ &+ \alpha^{(1)}_{ab}T_{bc}\alpha^{(2)}_{cd}T_{de}\alpha^{(1)}_{eh}a^{(1)}_{pq}T_{qr}a^{(2)}_{rw} + \alpha^{(1)}_{ab}T_{bc}\alpha^{(2)}_{cd}T_{de}\alpha^{(1)}_{eh}a^{(2)}_{pq}T_{qr}a^{(1)}_{rw} + \alpha^{(1)}_{ab}T_{bc}\alpha^{(2)}_{cd}T_{de}\alpha^{(1)}_{ef}T_{fg}\alpha^{(2)}_{gh}a^{(1)}_{pw} \\ &+ \alpha^{(1)}_{ab}T_{bc}\alpha^{(2)}_{cd}T_{de}\alpha^{(1)}_{ef}T_{fg}\alpha^{(2)}_{gh}a^{(2)}_{pw}\Big\} \times \left\langle a^x_{ah}a^x_{pw}a^x_{pw} - a^y_{ah}a^y_{pw}a^x_{pw}\right\rangle ,\end{aligned} \tag{4.68}$$

$$\gamma_1\alpha_1 = \left\{\gamma^{(1)}_{abcd}T_{be}\alpha^{(2)}_{ef} + \alpha^{(1)}_{ab}T_{be}\gamma^{(2)}_{efcd}\right\}\left\langle a^x_{af}a^x_{cd}a^x_{cd} - a^y_{af}a^y_{cd}a^x_{cd}\right\rangle , \tag{4.69}$$

$$\mu_2\alpha_1 = (kT)^{-2}\left\{\alpha^{(1)}_{ab}\mu^{(2)}_{oi}\mu^{(2)}_{op} + 2\alpha^{(1)}_{ab}\mu^{(1)}_{oi}\mu^{(2)}_{op}\right\} \times \left\langle a^x_a a^x_b a^x_i a^x_p - a^y_a a^y_b a^x_i a^x_p \right\rangle , \tag{4.70}$$

$$\begin{aligned}\mu_2\alpha_2 = (kT)^{-2}\Big\{&2\alpha^{(1)}_{ad}\mu^{(1)}_{oi}a^{(1)}_{pq}T_{qr}\mu^{(2)}_{or} + 2\alpha^{(1)}_{ad}\mu^{(2)}_{oi}a^{(2)}_{pq}T_{qr}\mu^{(1)}_{or} \\ &+ 2\alpha^{(1)}_{ad}\mu^{(1)}_{oi}a^{(2)}_{pq}T_{qr}\mu^{(1)}_{or} + 2\alpha^{(1)}_{ad}\mu^{(2)}_{oi}a^{(1)}_{pq}T_{qr}\mu^{(2)}_{or} \\ &+ \alpha^{(1)}_{ab}T_{bc}\alpha^{(2)}_{cd}\mu^{(1)}_{oi}\mu^{(1)}_{op} + \alpha^{(1)}_{ab}T_{bc}\alpha^{(2)}_{cd}\mu^{(2)}_{oi}\mu^{(2)}_{op} \\ &+ 2\alpha^{(1)}_{ab}T_{bc}\alpha^{(2)}_{cd}\mu^{(1)}_{oi}\mu^{(2)}_{op}\Big\}\left\langle a^x_a a^x_d a^x_i a^x_p - a^y_a a^y_d a^x_i a^x_p \right\rangle ,\end{aligned} \tag{4.71}$$

$$\begin{aligned}\mu_2\alpha_3 = (kT)^{-2}\Big\{&\alpha^{(1)}_{af}a^{(1)}_{ij}T_{jk}\mu^{(2)}_{ok}a^{(1)}_{pq}T_{qr}\mu^{(2)}_{or} + \alpha^{(1)}_{af}a^{(2)}_{ij}T_{jk}\mu^{(1)}_{ok}a^{(2)}_{pq}T_{qr}\mu^{(1)}_{or} \\ &+ \alpha^{(1)}_{af}a^{(1)}_{ij}T_{jk}\mu^{(2)}_{ok}a^{(2)}_{pq}T_{qr}\mu^{(1)}_{or} + 2\alpha^{(1)}_{ab}T_{bc}\alpha^{(2)}_{cf}\mu^{(1)}_{oi}a^{(1)}_{pq}T_{qr}\mu^{(2)}_{or} \\ &+ 2\alpha^{(1)}_{ab}T_{bc}\alpha^{(2)}_{cf}\mu^{(2)}_{oi}a^{(2)}_{pq}T_{qr}\mu^{(1)}_{or} + 2\alpha^{(1)}_{ab}T_{bc}\alpha^{(2)}_{cf}\mu^{(1)}_{oi}a^{(2)}_{pq}T_{qr}\mu^{(1)}_{or} \\ &+ 2\alpha^{(1)}_{ab}T_{bc}\alpha^{(2)}_{cf}\mu^{(2)}_{oi}a^{(1)}_{pq}T_{qr}\mu^{(2)}_{or} + 2\alpha^{(1)}_{af}\mu^{(1)}_{oi}a^{(1)}_{pq}T_{qr}a^{(2)}_{rs}T_{st}\mu^{(1)}_{ot} \\ &+ 2\alpha^{(1)}_{af}\mu^{(2)}_{oi}a^{(2)}_{pq}T_{qr}a^{(1)}_{rs}T_{st}\mu^{(2)}_{ot} + 2\alpha^{(1)}_{af}\mu^{(1)}_{oi}a^{(2)}_{pq}T_{qr}a^{(1)}_{rs}T_{st}\mu^{(2)}_{ot} \\ &+ 2\alpha^{(1)}_{af}\mu^{(2)}_{oi}a^{(1)}_{pq}T_{qr}a^{(2)}_{rs}T_{st}\mu^{(1)}_{ot} + \alpha^{(1)}_{ab}T_{bc}\alpha^{(2)}_{cd}T_{de}\alpha^{(1)}_{ef}\mu^{(1)}_{oi}\mu^{(1)}_{op} \\ &+ \alpha^{(1)}_{ab}T_{bc}\alpha^{(2)}_{cd}T_{de}\alpha^{(1)}_{ef}\mu^{(2)}_{oi}\mu^{(2)}_{op} + 2\alpha^{(1)}_{ab}T_{bc}\alpha^{(2)}_{cd}T_{de}\alpha^{(1)}_{ef}\mu^{(1)}_{oi}\mu^{(2)}_{op}\Big\} \\ &\times \left\langle a^x_a a^x_d a^x_i a^x_p - a^y_a a^y_d a^x_i a^x_p \right\rangle ,\end{aligned} \tag{4.72}$$

$$\mu_1\beta_1 = 2(kT)^{-1}\left\{\beta^{(1)}_{abi}\mu^{(2)}_{op}\right\}\left\langle a^x_a a^x_b a^x_i a^x_p - a^y_a a^y_b a^x_i a^x_p \right\rangle . \tag{4.73}$$

The isotropic averages in equations (4.65) to (4.73) are carried out using the standard results in equations (2.14) and (2.16) of Chapter 2. We illustrate the procedure by considering the term for α_2 in equation

(4.65):

$$\alpha_2 = (kT)^{-1}\left\{\alpha^{(1)}_{ab}a^{(2)}_{pq}\right\}\left\langle a^x_a a^x_b a^x_p a^x_q - a^y_a a^y_b a^x_p a^x_q\right\rangle$$

$$= (kT)^{-1}\left\{\alpha^{(1)}_{ab}a^{(2)}_{pq}\right\}\frac{1}{3\ 0}\left[-2\delta_{ab}\delta_{pq} + 3\delta_{ap}\delta_{bq} + 3\delta_{aq}\delta_{bp}\right]$$

$$= \frac{6}{30kT}\left\{\alpha^{(1)}_{ap}a^{(2)}_{ap} - 3\alpha a\right\}. \qquad (4.74)$$

Here, $\alpha^{(1)}_{ap}$ is the dynamic polarizability tensor of molecule 1 expressed in the molecule-fixed axes of molecule 1, (1,2,3), while α is the mean dynamic polarizability. Similarly, $a^{(2)}_{ap}$ is the static polarizability tensor of molecule 2 expressed in (1,2,3), while a is the mean static polarizability.

It is useful to check that the above terms reduce to expressions previously derived for linear molecules when the molecular tensors are reduced to their simplified forms. For such molecules, $\alpha^{(1)}_{ij}$ is diagonal with $\alpha_{11} = \alpha_{22} = \alpha_\perp$ and $\alpha_{33} = \alpha_\parallel$; while $a^{(2)}_{ij} = a_\perp\delta_{ij} + \left(a_\parallel - a_\perp\right)\ell^{(2)}_i\ell^{(2)}_j$ [37], $\underset{\sim}{\ell}^{(2)}$ being a unit vector along the dipole axis of molecule 2. α and a are the traces of $\alpha^{(1)}_{ij}$ and $a^{(1)}_{ij}$ respectively. Using these tensors in equation (4.74) yields

$$\alpha_2 = \frac{6}{30kT}\Delta\alpha\ \Delta a\ \left(\cos^2\theta_{12} - \frac{1}{3}\right) \qquad (4.75)$$

where θ_{12} is the angle between the symmetry axes of molecules 1 and 2. This is exactly the polarizability contribution to B_K originally derived by Buckingham [17]. Similarly, the permanent dipole contribution to B_K in Buckingham's original theory [17] is exactly reproduced by the term $\mu_2\alpha_1$ in equation (4.70) when applied to axially-symmetric polar molecules. The higher-order terms of Buckingham *et al.* [29], which describe the collision-induced polarizability contributions to B_K, are approximate, the polarizability tensors having been rewritten as *isotropic* polarizabilities; and so a direct comparison with our higher-order terms is not possible.

The exact forms of $\alpha^{(1)}_{ap}$ and α for molecules with D_{2h} and C_{2v} symmetries have already been quoted in Chapter 2, but are repeated here for convenience:

$$\alpha_{ij}^{(1)} = \alpha_{i'j'}^{(2)} = \begin{bmatrix} \alpha_{11} & 0 & 0 \\ 0 & \alpha_{22} & 0 \\ 0 & 0 & \alpha_{33} \end{bmatrix} , \tag{4.76}$$

and

$$\alpha = \frac{1}{3} \alpha_{ii} = \frac{1}{3} \left(\alpha_{11} + \alpha_{22} + \alpha_{33} \right) . \tag{4.77}$$

The form of the static polarizability tensor is exactly analogous to equation (4.76),

$$a_{ij}^{(1)} = a_{i'j'}^{(2)} = \begin{bmatrix} a_{11} & 0 & 0 \\ 0 & a_{22} & 0 \\ 0 & 0 & a_{33} \end{bmatrix} , \tag{4.78}$$

while the mean static polarizability is

$$a = \frac{1}{3} a_{ii} = \frac{1}{3} \left(a_{11} + a_{22} + a_{33} \right) . \tag{4.79}$$

$a_{ap}^{(2)}$ in equation (4.74) is the static polarizability tensor of molecule 2 when expressed in the molecule-fixed axes of molecule 1, and our procedure for expressing $a_{i'j'}^{(2)}$, in (1,2,3) is identical to that given in equations (2.58) and (2.59), yielding

$$a_{ap}^{(2)} = \begin{bmatrix} W_{11} & W_{12} & W_{13} \\ W_{12} & W_{22} & W_{23} \\ W_{13} & W_{23} & W_{33} \end{bmatrix} . \tag{4.80}$$

Here, the coefficients W_{11}, W_{12}, ..., W_{33} are exactly analogous to the Z_{ij} coefficients for $\alpha_{ij}^{(2)}$ given in equation (2.76), the dynamic components α_{11}, α_{22} and α_{33} being replaced by the static components a_{11}, a_{22} and a_{33} respectively.

We are now poised to obtain an explicit expression for α_2 in equation (4.74), and although the summation over indices is trivial for this example, Macsyma's tensor manipulation facilities are indispensable for the higher-order terms:

$$\alpha_2 = \frac{6}{30kT} \left(\alpha_{11} W_{11} + \alpha_{22} W_{22} + \alpha_{33} W_{33} - 3\alpha a \right) . \tag{4.81}$$

Substitution of this term into equation (4.37) followed by numerical integration over the pair interaction co-ordinates R, α_1, β_1, γ_1, α_2, β_2 and γ_2, yields the α_2 contribution to the second Kerr-effect virial coefficient B_K.

The procedure for evaluating the higher-order terms is much the same, and is illustrated by considering a specific example, namely the $(kT)^{-1}\left\{\alpha^{(1)}_{ad}a^{(1)}_{pq}T_{qr}a^{(2)}_{rs}\right\}\left\langle a^x_a a^x_d a^x_p a^x_s - a^y_a a^y_d a^x_p a^x_s\right\rangle$ term in equation (4.66). For a *fixed* interaction configuration, $\left\{\alpha^{(1)}_{ad}a^{(1)}_{pq}T_{qr}a^{(2)}_{rs}\right\}$ is a constant, and if the pair of molecules is allowed to rotate isotropically as a rigid whole, then use of equations (2.14) and (2.16) leads to the average projection

$$(kT)^{-1}\left\{\alpha^{(1)}_{ad}a^{(1)}_{pq}T_{qr}a^{(2)}_{rs}\right\}\left\langle a^x_a a^x_d a^x_p a^x_s - a^y_a a^y_d a^x_p a^x_s\right\rangle$$

$$= \frac{1}{5kT}\left\{\alpha^{(1)}_{ad}a^{(1)}_{dq}T_{qr}a^{(2)}_{ra} - \alpha \times a^{(1)}_{pq}T_{qr}a^{(2)}_{rp}\right\}. \qquad (4.82)$$

The form of the dynamic and static polarizability tensors is already known, and the form of the second-rank T-tensor is

$$T_{ij} = \left(4\pi\varepsilon_o\right)^{-1} R^{-3}\begin{bmatrix} T_{11} & T_{12} & T_{13} \\ T_{12} & T_{22} & T_{23} \\ T_{13} & T_{23} & T_{33} \end{bmatrix} \qquad (4.83)$$

where T_{11}, T_{12}, ..., T_{33} have already been expressed in terms of direction cosines in equation (2.74). The tensor manipulation facilities of Macsyma can now be invoked to evaluate an expression for equation (4.82) which, when averaged over pair interaction co-ordinates by equation (4.37), yields the term's contribution to B_K. Repeating the process for the other three terms in equation (4.66) yields the net α_3 contribution to B_K.

The final Macsyma-generated expressions for the α_3, α_4, ..., terms in equation (4.64) will not be quoted, since even after compression they are often immense, and too unwieldy to reproduce. It is felt that our comprehensive outline of the procedure used to obtain the final expressions, coupled with the ubiquitous availability of symbolic

manipulation packages such as Macsyma, would allow interested readers to reproduce the expressions if required. Attempts by future workers to manually produce faithful Fortran-code translations of these immense expressions from the text would almost certainly fail; and this is a further reason for interested readers to re-work the expressions in Macsyma, which has the ability to translate them directly into Fortran code without the introduction of errors.

The evaluation of B_K by integrating (i.e. averaging) terms over the pair interaction co-ordinates according to equation (4.37) requires the classical intermolecular potential $U_{12}(\tau)$, which has already been extended to molecules with non-linear symmetry in section *2.4.1* of Chapter 2 (see equation (2.109)). The integrals were calculated, as for B_ρ, by numerical integration using Gaussian quadrature. The ranges of α_1, β_1, γ_1, α_2, β_2 and γ_2 were again divided into sixteen intervals each, while R was given the range of 0.1 to 3.0 nm divided into sixty four intervals. Examples of the Fortran programs, which were run in double precision, are given in Appendix 2.

We proceed by applying our theory of B_K to polar molecules, since their molar Kerr constants K_m generally have a much greater pressure dependence than those of non-polar molecules, and so are more amenable to precise experimental determination. In the first instance, we calculate B_K for the quasi-linear fluoromethanes, comparing our values to both experimental data and the calculations of Buckingham *et al.* [29]. Two molecules with C_{2v} symmetry, namely sulphur dioxide and dimethyl ether, are then investigated. Finally, we turn our attention to non-polar molecules, and in particular the axially-symmetric species of nitrogen, carbon dioxide and ethane, and the non-linear candidate ethene.

4.3 Calculations of B_K for fluoromethane

4.3.1 Molecular properties of fluoromethane

Optimized values for the Lennard-Jones force constants R_o and ε/k, and the shape parameter D, of fluoromethane (obtained by fitting the second pressure virial coefficient B(T) calculated according to equation (1.87) to experimental data over a range of temperature [31]) have been presented in table 1.2. For convenience, we list the values again, together with the dipole and quadrupole moment tensor components and mean static polarizability required in the expressions for $U_{12}(\tau)$:

Table 4.1. A summary of the Lennard-Jones force constants, shape parameter, and wavelength-independent molecular properties required in the intermolecular potential $U_{12}(\tau)$ of fluoromethane.

$R_o = 0.380$ nm	$D = D_1 = 0.2540$
$\varepsilon/k = 190.0$ K	$D_2 = 0.0000$

$$\mu_3 = 6.170 \times 10^{-30} \text{ Cm [38]}$$

$$\left.\begin{aligned} \theta_{11} &= -3.85 \times 10^{-40} \text{ Cm}^2 \\ \theta_{22} &= -3.85 \times 10^{-40} \text{ Cm}^2 \\ \theta_{33} &= \ \ 7.70 \times 10^{-40} \text{ Cm}^2 \end{aligned}\right\} \text{ [38]}$$

$$a = 3.305 \times 10^{-40} \text{ C}^2\text{m}^2\text{J}^{-1} \text{ [39]}$$

Buckingham *et al.* [6] have measured $B_K(T)$ for the fluoromethanes at $\lambda = 632.8$ nm, and the dynamic polarizability tensor components $\alpha_{\parallel} = \alpha_{33}$ and $\alpha_{\perp} = \alpha_{11} = \alpha_{22}$ required for our calculations are obtained from measured values of the mean polarizability α [35,36] and the polarizability anisotropy $\Delta\alpha$ [40] at this wavelength, as listed in table 4.2. The mean static polarizability a [39] is combined with the static anisotropy Δa (obtained by *ab initio* calculation at the MP2 level of theory [41,42]) to obtain the components $a_{\parallel} = a_{33}$ and $a_{\perp} = a_{11} = a_{22}$, also listed in table 4.2. We note that in 1981, Miller *et al.* [43] refer to experimental measurements of $\Delta\alpha$ undertaken by Bogaard *et al.* [44] at $\lambda = 632.8$ nm where the vibrational Raman contributions to the depolarization ratio ρ are excluded, leading to much smaller

anisotropies $\Delta\alpha$ for the fluoromethanes. We have not considered these values in our calculations, the *ab initio* values [41,42] tending to support the earlier measurements of $\Delta\alpha$ [40]. However, this uncertainty in the preferred $\Delta\alpha$ should be borne in mind, since it does lead to ambiguity in the calculated B_K values for the fluoromethanes. Further experimental measurements of $\Delta\alpha$ for these gases seem to be warranted.

Table 4.2. The components of the optical-frequency and static polarizability tensors α_{ij} and a_{ij} of fluoromethane.

λ/nm	$\frac{10^{40}\alpha}{C^2m^2J^{-1}}$	$\frac{10^{40}\Delta\alpha}{C^2m^2J^{-1}}$	$\frac{10^{40}\alpha_{\parallel}}{C^2m^2J^{-1}}$	$\frac{10^{40}\alpha_{\perp}}{C^2m^2J^{-1}}$
632.8	2.916 [35,36]	0.345 [40]	3.147	2.800
$\lambda \rightarrow \infty$	3.305 [39]	0.29 [41,42]	3.498	3.208

There are no available values for the components of the dynamic hyperpolarizability tensor β_{ijk}, and so the $\mu_1\beta_1$ term's contribution to B_K cannot be calculated. This contribution is, however, found to be negligible for sulphur dioxide (see section **4.5**), and since the property

$$\beta = \frac{3}{10}\left(3\beta_{131} - \beta_{113}\right) \tag{4.84}$$

for sulphur dioxide has the value $\beta = -(0.05 \pm 0.15) \times 10^{-50}\ C^3m^3J^{-2}$ [13], which is comparable in magnitude to that of $\beta = -(0.19 \pm 0.15) \times 10^{-50}\ C^3m^3J^{-2}$ [6] for fluoromethane, we proceed by omitting the hyperpolarizability contribution with with some reassurance.

4.3.2 Results of calculations for fluoromethane

Table 4.3 gives the relative magnitudes of the various contributions to B_K calculated at the particular temperature T = 250.8 K. Here, the dominant contribution to B_K is seen to arise from the $\mu_2\alpha_2$ term. This predominance of a collision-induced contribution to B_K for polar molecules is in keeping with the findings of Buckingham *et al.* [29]. Despite the $\mu_2\alpha_2$ term's dominant contribution to B_K of 105.67%, we

Figure 4.2. Temperature dependence of the calculated and measured second Kerr-effect virial coefficients of fluoromethane.

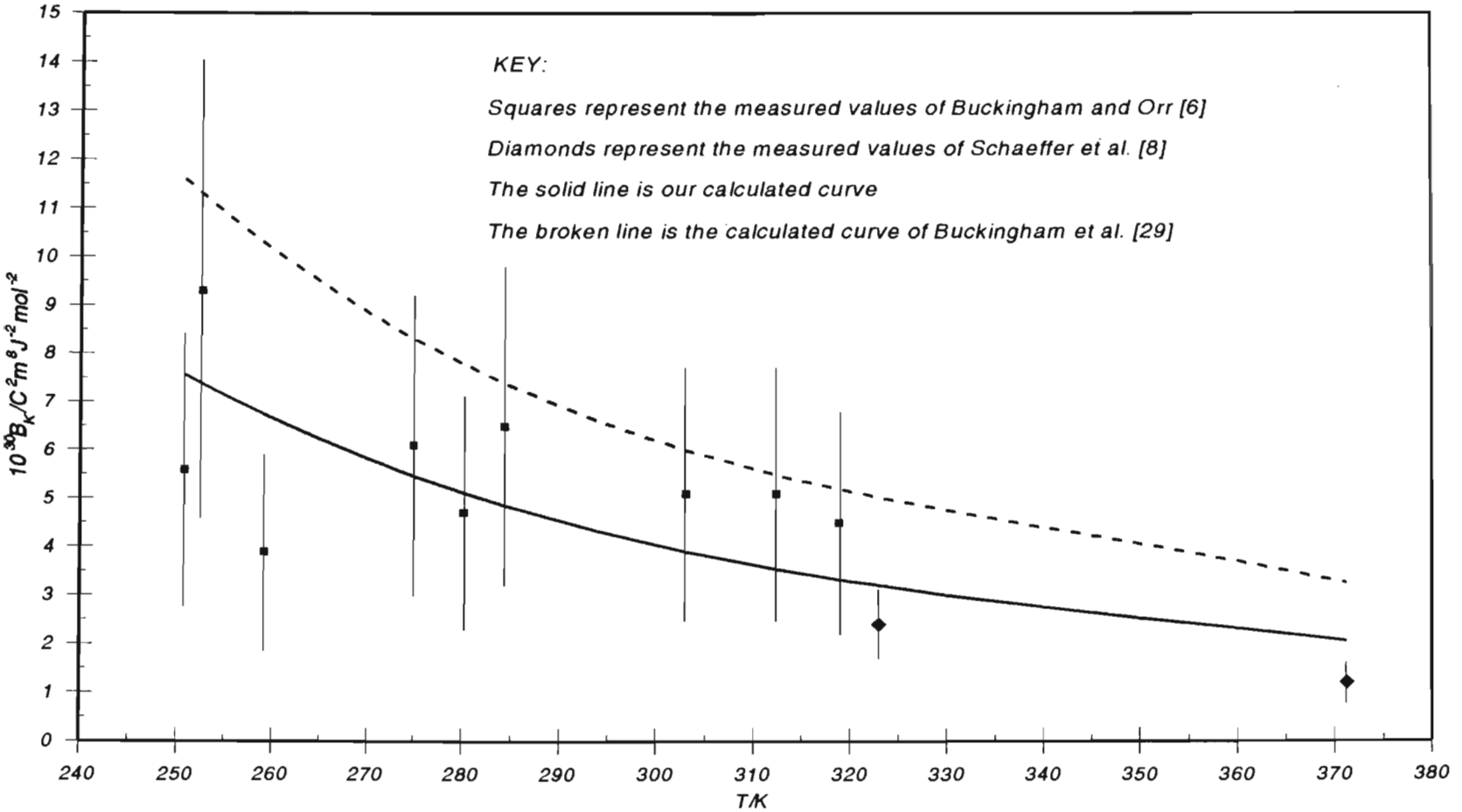

cannot definitively claim convergence of the series of terms in $\mu\alpha$, the $\mu_2\alpha_3$ term contributing as much as 31.44%. Although derivation of the $\mu_2\alpha_4$ term is not beyond our reach, especially in view of the substantial capabilities of the Macsyma algebraic manipulation package, it would nevertheless be an enormous undertaking requiring a few months of human input. Time constraints have prevented derivation of the $\mu_2\alpha_4$ term for the purposes of this thesis, but it is possible to argue from past experience that it is usually one or two interaction terms that make the dominant contribution to the second virial coefficients of the various molecular-optic phenomena [24,25,29,34-36], with higher order contributions dropping off rapidly as the series of terms converges. It seems reasonable to expect the $\mu_2\alpha_4$ contribution to be a few percent at most.

Table 4.3. The relative magnitudes of the various contributions to B_K for fluoromethane calculated at T = 250.8 K.

Contributing Term	$\frac{10^{30} \times \text{Value}}{C^2m^8J^{-2}mol^{-2}}$	% Contribution to B_K
$\mu_2\alpha_1$	-2.905	-38.41
$\mu_2\alpha_2$	7.992	105.67
$\mu_2\alpha_3$	2.378	31.44
α_2	0.002	0.03
α_3	-0.009	-0.12
α_4	0.098	1.30
α_5	0.007	0.09

$$B_K = 7.563 \times 10^{-30}\ C^2m^8J^{-2}mol^{-2}$$

The temperature dependence of our calculated B_K values are compared graphically with the experimental data [6,8] as well as the calculated values of Buckingham *et al.* [29], in figure 4.2. The experimental values of Buckingham and Orr [6] have quite a high imprecision of ±50%, while those of Schaeffer *et al.* [8] are much more precise, perhaps providing a better standard against which to judge the theory. Our calculated values agree with the values of Schaeffer *et al.* to within 25%.

4.4 Calculations of B_K for trifluoromethane

4.4.1 Molecular properties of trifluoromethane

Table 4.4 contains the optimized Lennard-Jones force constants, shape factor and wavelength-independent molecular properties required for the calculations of B_K.

Table 4.4. A summary of the Lennard-Jones force constants, shape parameter, and wavelength-independent molecular properties required in the intermolecular potential $U_{12}(\tau)$ of trifluoromethane.

$R_o = 0.440$ nm	$D = D_1 = -0.050$
$\varepsilon/k = 178.5$ K	$D_2 = 0.0000$

$$\mu_3 = 5.50 \times 10^{-30} \text{ Cm [38]}$$

$$\left.\begin{aligned} \theta_{11} &= -7.5 \times 10^{-40} \text{ Cm}^2 \\ \theta_{22} &= -7.5 \times 10^{-40} \text{ Cm}^2 \\ \theta_{33} &= 15.0 \times 10^{-40} \text{ Cm}^2 \end{aligned}\right\} \text{ [38]}$$

$$a = 3.970 \times 10^{-40} \text{ C}^2\text{m}^2\text{J}^{-1} \text{ [39]}$$

The dynamic and static polarizability tensor components at $\lambda = 632.8$ nm are listed in table 4.5. The static $\Delta\alpha$ was obtained by extrapolating the measured dynamic values [40] to zero frequency. Once again, we have not considered the revised values of $\Delta\alpha$ reported in [43,44], noting that subsequent measurements of the depolarization ratio ρ_o by Monan *et al.* [45], in which the vibrational Raman contribution was also explicitly excluded, *reconfirmed* the earlier measurements of Bogaard *et al.* [40].

Table 4.5. The components of the optical-frequency and static polarizability tensors α_{ij} and a_{ij} of trifluoromethane.

λ/nm	$\frac{10^{40}\alpha}{C^2m^2J^{-1}}$	$\frac{10^{40}\Delta\alpha}{C^2m^2J^{-1}}$	$\frac{10^{40}\alpha_{\parallel}}{C^2m^2J^{-1}}$	$\frac{10^{40}\alpha_{\perp}}{C^2m^2J^{-1}}$
632.8	3.097 [35,36]	-0.27 [40]	2.917	3.187
$\lambda \rightarrow \infty$	3.970 [39]	-0.19†	3.843	4.033

† obtained by extrapolating measured dynamic polarizability anisotropies [40] to zero frequency.

Once again, there are no available values for the components of the dynamic hyperpolarizability tensor β_{ijk}, and so the $\mu_1\beta_1$ term cannot be considered.

4.4.2 Results of calculations for trifluoromethane

Table 4.6 summarizes the relative magnitudes of the various contributions to B_K as calculated at T = 245.5 K. Once again, the dominant contribution to B_K arises from the $\mu_2\alpha_2$ term, with the $\mu_2\alpha_3$ term making a not insignificant contribution of 23.16%.

Figure 4.3. Temperature dependence of the calculated and measured second Kerr-effect virial coefficients of trifluoromethane.

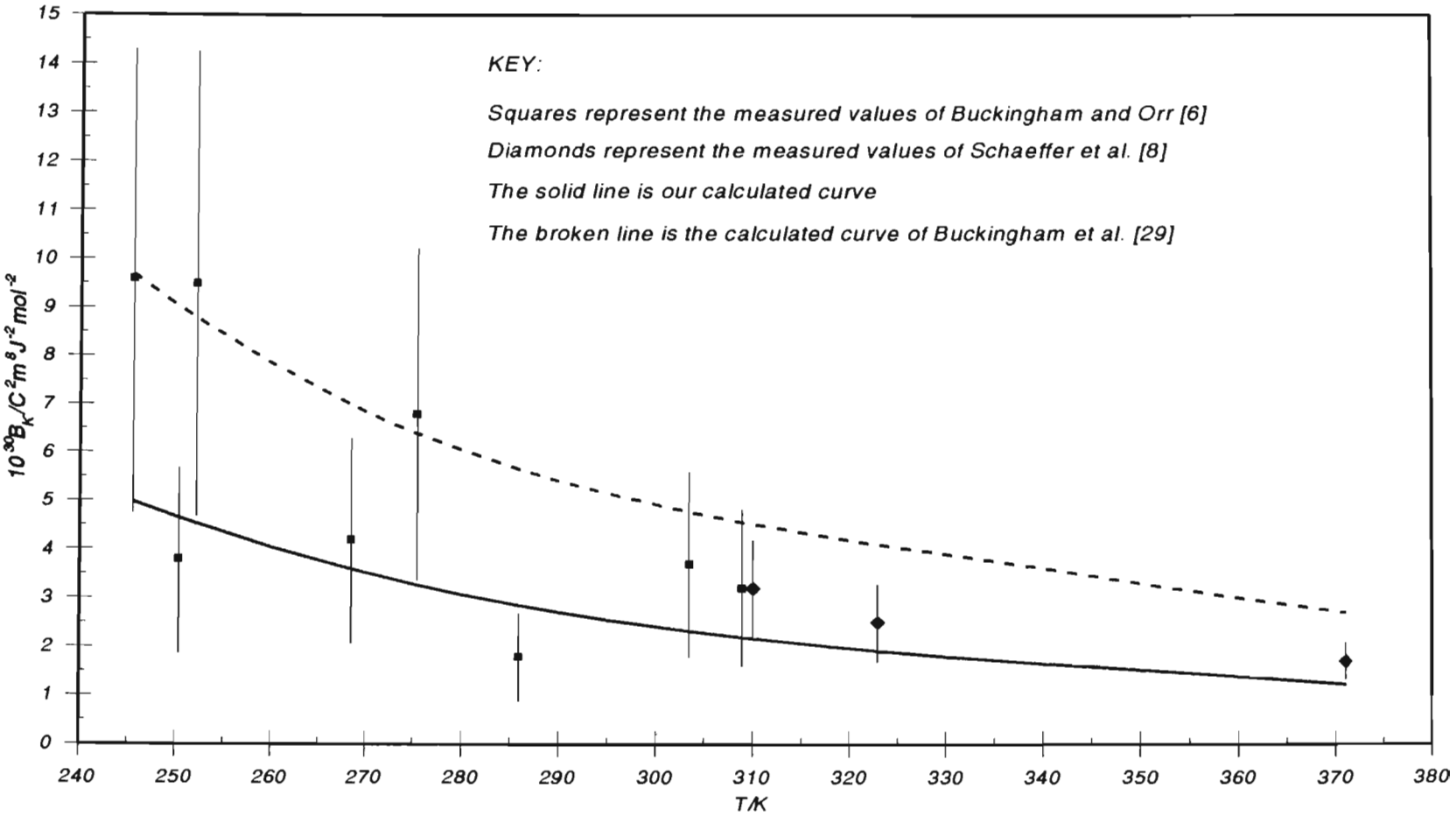

Table 4.6. The relative magnitudes of the various contributions to B_K for trifluoromethane calculated at T = 245.5 K.

Contributing Term	$\frac{10^{30} \times \text{Value}}{C^2 m^8 J^{-2} mol^{-2}}$	% Contribution to B_K
$\mu_2\alpha_1$	0.202	4.05
$\mu_2\alpha_2$	3.561	71.39
$\mu_2\alpha_3$	1.155	23.16
α_2	0.000_2	0.00_4
α_3	-0.006	-0.12
α_4	0.072	1.44
α_5	0.004	0.08

$$B_K = 4.988 \times 10^{-30}\ C^2 m^8 J^{-2} mol^{-2}$$

Figure 4.3 contains a comparison of the temperature-dependence of our calculated B_K values with both the experimental data [6,8] and the calculated values of Buckingham *et al.* [29]. Again, the experimental values of Buckingham and Orr have a rather substantial imprecision of ±50%. The more precise values of Schaeffer *et al.* [8] lie within 30% of our calculated curve. We now turn our attention to non-linear polar molecules.

4.5 Calculations of B_K for sulphur dioxide

4.5.1 Molecular properties of sulphur dioxide

Sulphur dioxide is a non-linear molecule belonging to the C_{2v} symmetry point group. Optimized values for the Lennard-Jones force constants and shape factors of sulphur dioxide, obtained by fitting the second pressure virial coefficients calculated according to equation (2.111) to the experimental data over a range of temperature, have been presented in section **2.6** of Chapter 2. These values, together with the dipole and quadrupole moment tensor components and mean static polarizability required in the expressions for $U_{12}(\tau)$, are presented in table 4.7

below.

Table 4.7. A summary of the Lennard-Jones force constants, shape parameters, and wavelength-independent molecular properties required in the intermolecular potential $U_{12}(\tau)$ of sulphur dioxide.

$R_o = 0.3850$ nm	$D_1 = 0.0873$
$\varepsilon/k = 220.0$ K	$D_2 = 0.1008$

$$\mu_3 = -5.4262 \times 10^{-30} \text{ Cm} \quad [46]$$

$$\left.\begin{aligned} \theta_{11} &= -16.4 \times 10^{-40} \text{ Cm}^2 \\ \theta_{22} &= 12.9 \times 10^{-40} \text{ Cm}^2 \\ \theta_{33} &= 3.5 \times 10^{-40} \text{ Cm}^2 \end{aligned}\right\} \quad [47]$$

$$a = 4.2072 \times 10^{-40} \text{ C}^2\text{m}^2\text{J}^{-1} \ \dagger$$

† Obtained by extrapolating measured dynamic polarizabilities [40] to zero frequency

All measured and calculated values for the dynamic polarizability tensor components of sulphur dioxide at $\lambda = 514.5$ nm and $\lambda = 632.8$ nm have already been summarized in table 2.9. Gentle *et al.* [13] deduced values for $B_K(T)$ from Kerr-effect experiments at $\lambda = 632.8$ nm, and so our calculations for $B_K(T)$ were performed using the most precise values at this wavelength as listed in table 4.8.

Table 4.8. The components of the optical-frequency polarizability tensor of sulphr dioxide deduced from Kerr-effect measurements at $\lambda = 632.8$ nm by Gentle *et al.* [13].

$\frac{10^{40}\alpha_{11}}{C^2m^2J^{-1}}$	$\frac{10^{40}\alpha_{22}}{C^2m^2J^{-1}}$	$\frac{10^{40}\alpha_{33}}{C^2m^2J^{-1}}$
5.80 ± 0.06	3.30 ± 0.04	3.88 ± 0.06

Since there are no experimental estimates of the individual static polarizability tensor components, we use *ab initio* calculated values as

Table 4.9. The wavelength dependence of ρ_o, α and $\Delta\alpha$ for sulphur dioxide, together with values extrapolated to infinite wavelength. All data is taken from reference [40].

λ/nm	$\frac{10^{40}\alpha}{C^2m^2J^{-1}}$	$100 \times \rho_o$	$\frac{10^{40}(\Delta\alpha)}{C^2m^2J^{-1}}$
488.0	4.411	1.86 ± 0.01	2.359
514.5	4.389	1.85 ± 0.01	2.341
632.8	4.326	1.79 ± 0.01	2.269
$\lambda \rightarrow \infty$	4.207 ± 0.001		2.136 ± 0.010

a basis. These values can be refined by comparing their trace with the mean static polarizability extrapolated from reported optical-frequency values [40], and scaling accordingly. For this purpose, we list in table 4.9 the wavelength dependences of ρ_o and α together with their corresponding $\Delta\alpha$ values deduced via equation (2.18); and include values extrapolated to zero frequency. Table 4.10 contains the *ab initio* principal static polarizabilities calculated using CPF(ED) theory [48], together with the scaled values. The 'quality' of the scaled values can be cross-checked by comparing the scaled Δa with the value in table 4.9 extrapolated from experimental data: the values agree to within 4.5%, allowing confident use of the scaled a_{11}, a_{22} and a_{33} values in our calculations of B_K.

Table 4.10. *Ab initio* calculated static polarizability tensor components of sulphur dioxide together with the mean polarizability a and anisotropy Δa. Included are the values scaled according to the extrapolated a given in table 4.9.

Polarizability property	$\frac{10^{40} \times \text{CPF(ED) Calculations}^{[48]}}{C^2m^2J^{-1}}$	$\frac{10^{40} \times \text{Scaled values}}{C^2m^2J^{-1}}$
a_{11}	5.347	5.661
a_{22}	3.027	3.205
a_{33}	3.548	3.756
a	3.974	4.207
Δa	2.108	2.232

Sulphur dioxide is a polar molecule, with contributions to B_K arising from the μ_i and β_{ijk} tensors through equations (4.70) to (4.73). μ_i is quoted in table 4.7, while table 4.11 contains a summary of the *ab initio* SCF calculations of the three independent components of the static first-order hyperpolarizability tensor b_{ijk} as performed by Maroulis [49]. Our means for verifying that the difference between the optical-frequency components and those in the static limit is sufficiently small is as follows:

The property

$$\beta = \frac{3}{10}\left(3\beta_{131} - \beta_{113}\right) \qquad (4.85)$$

for sulphur dioxide has been deduced by Gentle *et al.* [13] from their Kerr-effect measurements at $\lambda = 632.8$ nm to have the value $\beta = -(0.05 \pm 0.15) \times 10^{-50}\ C^3m^3J^{-2}$, while the static analogue obtained from Maroulis' calculated b_{ijk} components, namely $b = 0.024 \times 10^{-50}\ C^3m^3J^{-2}$ [49], is well within the experimental uncertainty limits. Hence, Maroulis' values should yield at worst an order of magnitude estimate of the $\mu_1\beta_1$ contribution to B_K.

Table 4.11. *Ab initio* SCF calculations of the static first-order hyperpolarizability tensor components of sulphur dioxide [49].

$b_{113} = 7.05 \times 10^{-52}\ C^3m^3J^{-2}$
$b_{223} = 2.05 \times 10^{-52}\ C^3m^3J^{-2}$
$b_{333} = 8.50 \times 10^{-52}\ C^3m^3J^{-2}$

Maroulis has also calculated values for the static second-order hyperpolarizability tensor g_{ijkl} [49], but since the first-order hyperpolarizability will make a much more significant contribution to B_K, the $\gamma_1\alpha_1$ term is not considered here.

4.5.2 Results of calculations for sulphur dioxide

Table 4.12 gives the relative magnitudes of the various contributions to B_K calculated at the particular temperature 298.7 K. Here, as for the quasi-linear fluoromethanes, the dominant contributor to B_K is the $\mu_2\alpha_2$ term. Again, however, it is not possible to definitively claim convergence of the series of terms in $\mu\alpha$ since the $\mu_2\alpha_3$ term contributes as much as 37.33% to B_K. Notice how the $\mu_1\beta_1$ term makes a completely negligible contribution to B_K of 0.33%, hence lending justification to our omission of the $\gamma_1\alpha_1$ term.

Figure 4.4. Temperature dependence of the calculated and measured second Kerr-effect virial coefficients of sulphur dioxide as listed in table 4.13.

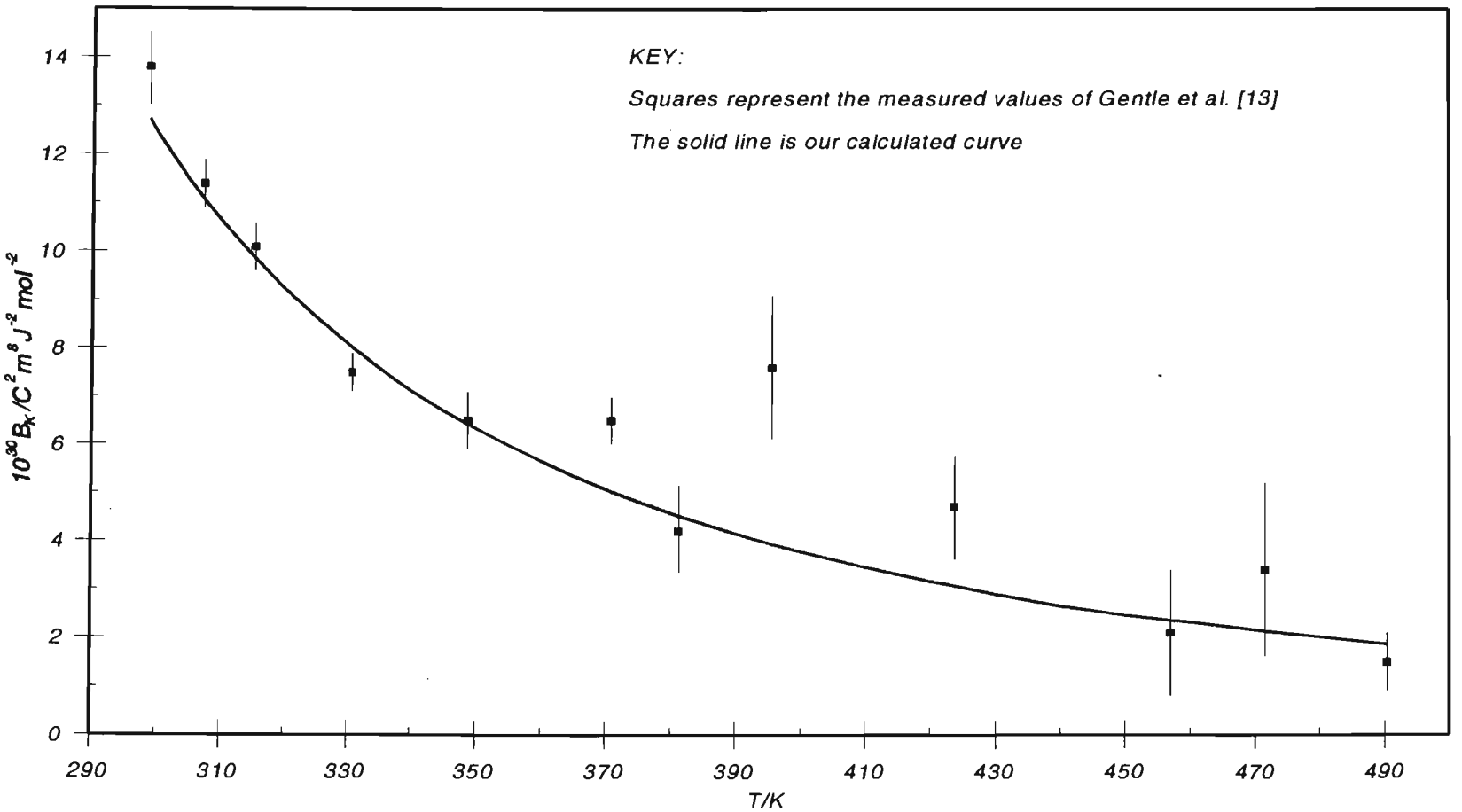

Table 4.12. The relative magnitudes of the various contributions to B_K for sulphur dioxide calculated at T = 298.7 K.

Contributing Term	$\frac{10^{30} \times \text{Value}}{C^2 m^8 J^{-2} mol^{-2}}$	% Contribution to B_K
$\mu_2\alpha_1$	1.542	12.11
$\mu_2\alpha_2$	5.730	45.02
$\mu_2\alpha_3$	4.752	37.33
α_2	-0.063	-0.49
α_3	0.166	1.30
α_4	0.503	3.95
α_5	0.057	0.45
$\mu_1\beta_1$	0.042	0.33

$$B_K = 12.729 \times 10^{-30}\ C^2 m^8 J^{-2} mol^{-2}$$

Table 4.13 presents the temperature dependence of the calculated B_K values, and includes a comparison with the rather precise experimental values recently measured by Gentle *et al.* [13]. A graphical comparison of the calculated and measured data is given in figure 4.4.

Table 4.13. Temperature dependence of the calculated B_K values of sulphur dioxide, together with the measured values at λ = 632.8 nm [13].

$\frac{T}{K}$	$\frac{10^{30}B_K^{exp}}{C^2m^8J^{-2}mol^{-2}}$	$\frac{10^{30}B_K^{calc}}{C^2m^8J^{-2}mol^{-2}}$	$\frac{B_K^{exp}}{B_K^{calc}}$
298.7	13.8 ± 0.8	12.73	1.084
307.3	11.4 ± 0.5	11.08	1.029
315.4	10.1 ± 0.5	9.86	1.024
330.7	7.5 ± 0.4	8.02	0.935
348.8	6.5 ± 0.6	6.42	1.012
370.9	6.5 ± 0.5	5.03	1.292
381.2	4.2 ± 0.9	4.52	0.929
395.7	7.6 ± 1.5	3.93	1.934
423.7	4.7 ± 1.1	3.07	1.531
457.0	2.1 ± 1.3	2.36	0.890
471.5	3.4 ± 1.8	2.13	1.596
490.3	1.5 ± 0.6	1.87	0.802

It is immediately apparent that the theory and experiment are in excellent agreement. But could this level of agreement have been obtained by approximating the molecular property tensors and physical shape of the sulphur dioxide molecule to be of axial symmetry? Gentle *et al.* [13] attempted such an analysis using the statistical-mechanical theory of B_K for axially-symmetric molecules developed by Buckingham *et al.* [29], and generally found the calculated B_K values to be more than twice as large as the experimental values. This finding substantiates our earlier claim (see Chapter 2) that the effects which interacting *non-linear* molecules have on molecular-optic phenomena can only be calculated after full consideration of molecular symmetry.

4.6 Calculations of B_K for dimethyl ether

4.6.1 Molecular properties of dimethyl ether

Like sulphur dioxide, dimethyl ether belongs to the C_{2v} point group. Table 4.14 lists the optimized values for the Lennard-Jones force constants and shape factors of dimethyl ether obtained in section **2.7** of Chapter 2, together with the dipole and quadrupole moment tensor components and mean static polarizability required in the expressions for $U_{12}(\tau)$.

Table 4.14. A summary of the Lennard-Jones force constants, shape parameters, and wavelength-independent molecular properties required in the intermolecular potential $U_{12}(\tau)$ of dimethyl ether.

$R_o = 0.390$ nm	$D_1 = 0.1923$
$\varepsilon/k = 370.0$ K	$D_2 = 0.2137$

$$\mu_3 = -4.37 \times 10^{-30} \text{ Cm [50]}$$

$$\left.\begin{aligned} \theta_{11} &= 11.0 \times 10^{-40} \text{ Cm}^2 \\ \theta_{22} &= -4.3 \times 10^{-40} \text{ Cm}^2 \\ \theta_{33} &= -6.7 \times 10^{-40} \text{ Cm}^2 \end{aligned}\right\} \text{ [51]}$$

$$a = 5.726 \times 10^{-40} \text{ C}^2\text{m}^2\text{J}^{-1} \dagger$$

† Obtained by extrapolating measured dynamic polarizabilities [40] to zero frequency

Since values of $B_K(T)$ for dimethyl ether have been deduced from Kerr-effect measurements at $\lambda = 632.8$ nm [11], the dynamic polarizability tensor components at this wavelength are required for our calculations. Table 4.15 lists the relevant data, the more precise set of measured values obtained by Bogaard *et al.* [11] being used in our work.

Table 4.15. The components of the optical-frequency polarizability tensor of dimethyl ether at λ = 632.8 nm.

Method	$\frac{10^{40}\alpha_{11}}{C^2m^2J^{-1}}$	$\frac{10^{40}\alpha_{22}}{C^2m^2J^{-1}}$	$\frac{10^{40}\alpha_{33}}{C^2m^2J^{-1}}$
Experimental derivation from the Kerr effect [11]	6.69 ± 0.17	5.46 ± 0.14	5.28 ± 0.13
Experimental derivation from the Cotton-Mouton effect [52]	6.60 ± 0.22	5.64 ± 0.60	5.19 ± 0.40
Ab initio calculation from MP2 theory (scaled) [52]	6.68	4.47	5.28

Once again, scaled *ab initio* values of the static polarizability tensor components are used in our calculations. Table 4.16 lists the MP2 values obtained by Spackman *et al.* [53], together with the values scaled according to the mean static polarizability extrapolated from the measured dynamic polarizabilities [40]. The scaled Δa of 1.299×10^{-40} $C^2m^2J^{-1}$ agrees with the value of $(1.242 \pm 0.005) \times 10^{-40}$ $C^2m^2J^{-1}$ extrapolated from experimental data [40] to within 4.6%.

Table 4.16. *Ab initio* calculated static polarizability tensor components of dimethyl ether together with the mean polarizability a and anisotropy Δa. Included are the values scaled according to the extrapolated a given in table 4.14.

Polarizability property	$\frac{10^{40} \times \text{MP2 Calculated value}^{[53]}}{C^2m^2J^{-1}}$	$\frac{10^{40} \times \text{Scaled values}}{C^2m^2J^{-1}}$
a_{11}	6.232	6.584
a_{22}	4.917	5.195
a_{33}	5.110	5.399
a	5.420	5.726
Δa	1.230	1.299

There are no experimental or calculated estimates of the components of the first-order hyperpolarizability tensor β_{ijk} for dimethyl ether, and we ignore this contribution to B_K bearing in mind that it was found to be completely negligible in the case of sulphur dioxide.

4.6.2 Results of calculations for dimethyl ether

Table 4.17 summarizes the relative magnitudes of the various contributions to B_K at T = 259.0 K. As was found for sulphur dioxide, the dominant contributors to B_K are the interaction-induced terms in $\mu\alpha$. Here, unlike in the fluoromethanes and sulphur dioxide, the term $\mu_2\alpha_3$ contributes a higher percentage (44.73%) to B_K than the *lower-order* term $\mu_2\alpha_2$, and it is more difficult to be assured of convergence of this series of terms. The $\mu_2\alpha_4$ term of this molecule definitely warrants investigation in the near future.

Table 4.17. The relative magnitudes of the various contributions to B_K for dimethyl ether calculated at T = 259.0 K.

Contributing Term	$\frac{10^{30} \times \text{Value}}{C^2m^8J^{-2}mol^{-2}}$	% Contribution to B_K
$\mu_2\alpha_1$	5.587	22.87
$\mu_2\alpha_2$	4.302	17.61
$\mu_2\alpha_3$	10.925	44.73
α_2	0.056	0.23
α_3	0.482	1.97
α_4	2.677	10.96
α_5	0.397	1.63

$$B_K = 24.426 \times 10^{-30}\ C^2m^8J^{-2}mol^{-2}$$

Figure 4.5. Temperature dependence of the calculated and measured second Kerr-effect virial coefficients of dimethyl ether listed in table 4.18.

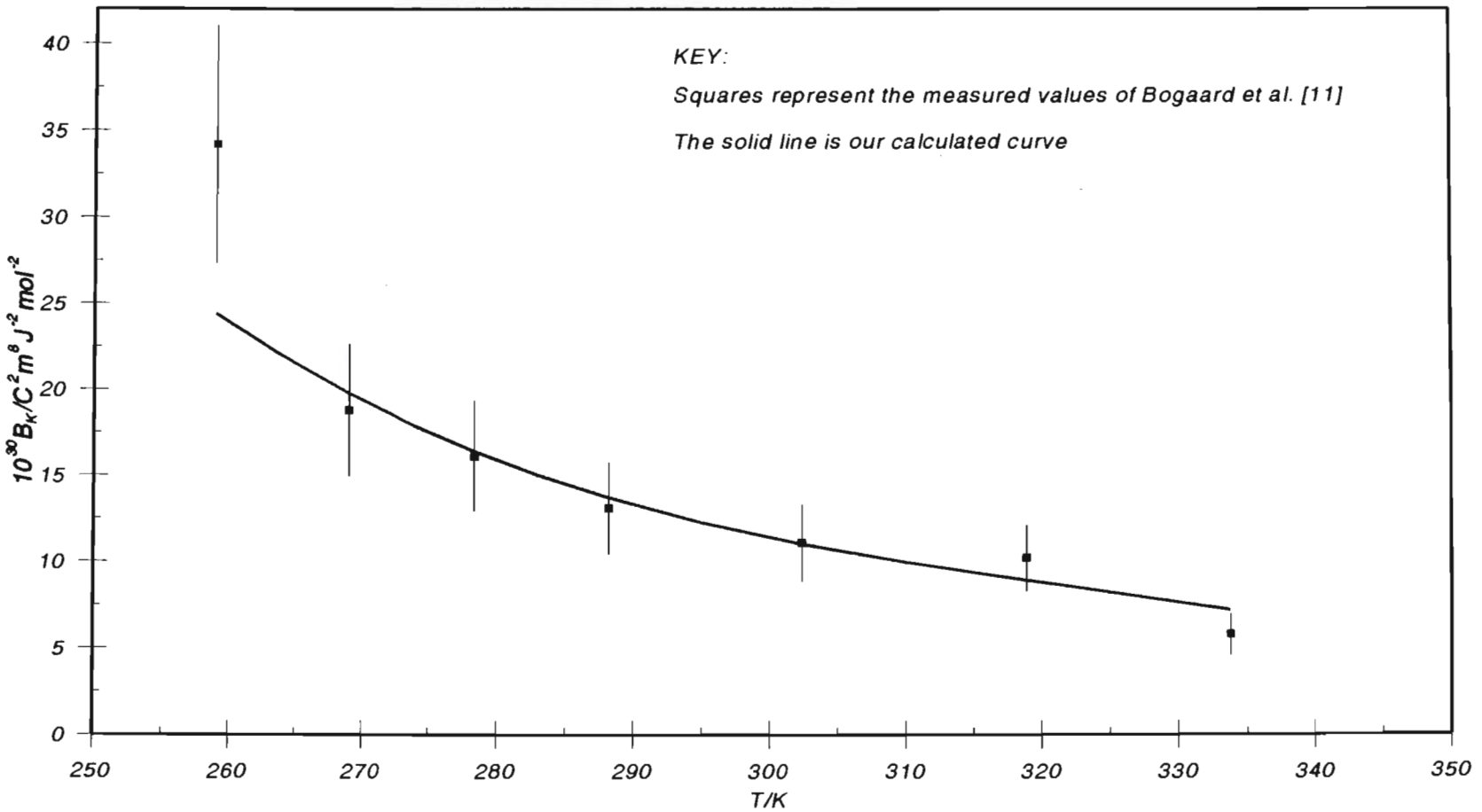

Table 4.18 presents the temperature dependence of the calculated B_K values, and includes a comparison with the experimental values of Bogaard *et al.* [11]. The experimental uncertainties in B_K were quoted to be in the range ±10% to ±20%. A graphical comparison of the calculated and measured data is given in figure 4.5.

Table 4.18. Temperature dependence of the calculated B_K values of dimethyl ether, together with the measured values at λ = 632.8 nm [11].

$\frac{T}{K}$	$\frac{10^{30}B_K^{exp}}{C^2m^8J^{-2}mol^{-2}}$	$\frac{10^{30}B_K^{calc}}{C^2m^8J^{-2}mol^{-2}}$	$\frac{B_K^{exp}}{B_K^{calc}}$
259.0	34.2 ± 6.8	24.4	1.40
269.0	18.8 ± 3.8	19.8	0.95
278.4	16.1 ± 3.2	16.4	0.98
288.2	13.1 ± 2.6	13.7	0.96
302.4	11.1 ± 2.2	11.0	1.01
318.9	10.2 ± 2.0	8.9	1.15
333.8	5.8 ± 1.2	7.2	0.81

By following the lead of Buckingham *et al.* [29] and including the collision-induced polarizability contribution into our theory of B_K for non-linear polar molecules, we have obtained good fits to the observed values for the quasi-linear fluoromethanes as well as for the low-symmetry sulphur dioxide and dimethyl ether molecules. Measurements of B_K for hydrogen sulphide [12] and difluoromethane [6], both of which are of C_{2v} symmetry, have been undertaken; but since the quadrupole moments of these molecules have not yet been measured, calculations of B_K cannot be performed.

The very small pressure dependence of the molar Kerr constant K_m for non-polar gases, with resultant high uncertainties in deduced B_K values, has already been discussed. Nevertheless, we think it profitable to obtain calculated values of B_K for those gases in which the

Table 4.19. Wavelength-independent molecular parameters used in calculations of B_K for linear non-polar molecules.

Molecule	$\frac{10^{40}a^{\dagger}}{C^2m^2J^{-1}}$	$\frac{10^{40}\Delta a^{\ddagger}}{C^2m^2J^{-1}}$	$\frac{10^{40}a_{\parallel}}{C^2m^2J^{-1}}$	$\frac{10^{40}a_{\perp}}{C^2m^2J^{-1}}$	$\frac{10^{40}\theta_{33}}{Cm^2}$	$\frac{R_o}{nm}$	$\frac{\varepsilon/k}{K}$	D^*
N_2	1.936 [54]	0.734‡ [57]	2.425	1.691	-4.72 [59]	0.368 [62]	91.50 [62]	0.112
CO_2	2.885† [55]	2.252‡ [57]	4.387	2.134	-15.0 [60]	0.400 [63]	190.0 [63]	0.250
CH_3CH_3	4.870† [56]	0.638‡ [58]	5.295	4.657	-3.34 [61]	0.4418 [62]	230 [62]	0.200

† Obtained by extrapolating recent high-precision measurements of dynamic polarizabilities [55,56] to zero frequency.

‡ Obtained by extarpolating the measured dynamic $\Delta\alpha$ values in references [57] and [58] to zero frequency.

* Obtained by fitting to the pressure virial coefficients quoted in [31].

pressure-dependence of the Kerr effect has been measured, since this will help to establish whether any correlation between theory and experiment can be obtained. The linear molecules nitrogen, carbon dioxide and ethane, and the non-linear molecule ethene, will be investigated.

4.7 Calculations of B_K for the linear non-polar molecules nitrogen, carbon dioxide and ethane

4.7.1 Molecular properties of nitrogen, carbon dioxide and ethane

Wavelength-independent parameters required in the calculations of B_K for the linear non-polar molecules nitrogen, carbon dioxide and ethane are listed in table 4.19. The static anisotropies Δa are the values obtained by extrapolating measured optical-frequency anisotropies $\Delta\alpha$ to zero frequency. Table 4.20 contains the principal polarizability components of the three molecules at the wavelength 632.8 nm. The leading hyperpolarizability tensor for non-polar molecules is the second-order γ_{ijkl}, and values for the individual components are generally not available. Contributions arising from this tensor are, however, expected to be negligibly small.

4.7.2 Results of calculations for nitrogen, carbon dioxide and ethane

Table 4.21 summarizes the relative magnitudes of the contributions to B_K for nitrogen, carbon dioxide and ethane; each at a particular temperature chosen from the respective experimental measurements reported in [7]. For all three molecules, the α_4 term is the dominant contributor at over 100%, while the α_5 term generally contributes of the order of 5% to B_K. Higher-order collision-induced polarizability contributions are expected to be negligibly small, the series having converged rapidly.

Table 4.20. The components of the optical-frequency polarizability tensors of nitrogen, carbon dioxide and ethane at a wavelength of 632.8 nm, as obtained from measured values for ρ_o and α.

Molecule	$100\rho_o$	$\frac{10^{40}\alpha}{C^2m^2J^{-1}}$	$\frac{10^{40}\Delta\alpha}{C^2m^2J^{-1}}$	$\frac{10^{40}\alpha_{\parallel}}{C^2m^2J^{-1}}$	$\frac{10^{40}\alpha_{\perp}}{C^2m^2J^{-1}}$
N_2	1.042 ± 0.006 [40]	1.967 [40]	0.783	2.498	1.715
CO_2	4.05 ± 0.02 [40]	2.9314 [55]	2.349	4.497	2.149
CH_3CH_3	0.149 ± 0.006 [58]	4.9680 [56]	0.743	5.464	4.720

Table 4.21. Relative magnitudes of the various contributions to B_K at λ = 632.8 nm for the non-polar axially-symmetric molecules nitrogen, carbon dioxide and ethane.

	nitrogen (T = 248 K)		carbon dioxide (T = 252 K)		ethane (T = 255 K)	
Term	$\frac{10^{32} \times \text{Value}}{C^2m^8J^{-2}mol^{-2}}$	% Contribution to B_K	$\frac{10^{32} \times \text{Value}}{C^2m^8J^{-2}mol^{-2}}$	% Contribution to B_K	$\frac{10^{32} \times \text{Value}}{C^2m^8J^{-2}mol^{-2}}$	% Contribution to B_K
α_2	0.009	1.03	1.531	44.04	0.143	0.70
α_3	-0.149	-17.01	-3.353	-96.46	-4.079	-19.90
α_4	0.984	112.33	5.124	147.41	23.049	112.47
α_5	0.032	3.65	0.174	5.01	1.380	6.73
	$B_K = 0.876 \times 10^{32}\ C^2m^8J^{-2}mol^{-2}$		$B_K = 3.476 \times 10^{32}\ C^2m^8J^{-2}mol^{-2}$		$B_K = 20.493 \times 10^{32}\ C^2m^8J^{-2}mol^{-2}$	

The temperature dependence of the calculated B_K values for nitrogen, carbon dioxide and ethane are presented in tables 4.22 to 4.24 respectively, each table including a comparison with the available experimental values. Notice how the experimental values of B_K for nitrogen and carbon dioxide are particularly poorly defined. This is not at all surprising in view of the extremely small calculated values, which indicate that measurement of the tiny pressure-dependence of the molar Kerr constant K_m for these two gases is a considerable experimental challenge. Ethane has B_K values which are an order of magnitude larger than the corresponding calculated data for nitrogen and carbon dioxide, and it is not surprising that the measured values are more clearly defined. Here, agreement with the calculated values is to within 15%.

Table 4.22. Temperature dependence of the calculated B_K values of nitrogen, together with the measured values at λ = 632.8 nm [7].

$\frac{T}{K}$	$\frac{10^{32}B_K^{exp}}{C^2m^8J^{-2}mol^{-2}}$	$\frac{10^{32}B_K^{calc}}{C^2m^8J^{-2}mol^{-2}}$
248	-0.08 ± 0.28	0.875
260	0.07 ± 0.39	0.834
277	-0.21 ± 0.33	0.782
286	-0.23 ± 0.45	0.757
299	-0.30 ± 0.59	0.725
315	0.04 ± 0.30	0.689
334	-0.41 ± 0.18	0.650

Table 4.23. Temperature dependence of the calculated B_K values of carbon dioxide, together with the measured values at λ = 632.8 nm [7,10].

$\frac{T}{K}$	$\frac{10^{32} B_K^{exp}}{C^2 m^8 J^{-2} mol^{-2}}$		$\frac{10^{32} B_K^{calc}}{C^2 m^8 J^{-2} mol^{-2}}$
252	23 ± 19	[7]↓	3.47
259	5 ± 27		3.29
267	-6 ± 11		3.11
279	-1 ± 13		2.86
287	-3 ± 9		2.71
301	-3 ± 7		2.48
302	0 ± 10		2.47
318	-11 ± 8		2.25
337	-9 ± 9		2.06
299.2	6 ± 1	[10]↓	2.51
314.9	0 ± 1		2.29
330.9	4 ± 2		2.11
348.8	2 ± 1		1.96
370.9	-6 ± 2		1.82
394.5	2 ± 2		1.71
422.8	-3 ± 2		1.60
455.8	-3 ± 4		1.47
489.5	-5 ± 3		1.27

Table 4.24. Temperature dependence of the calculated B_K values of ethane, together with the measured values at λ = 632.8 nm [7].

$\frac{T}{K}$	$\frac{10^{32}B_K^{exp}}{C^2m^8J^{-2}mol^{-2}}$	$\frac{10^{32}B_K^{calc}}{C^2m^8J^{-2}mol^{-2}}$
255	18.2 ± 3.7	20.49
259	17.7 ± 3.6	20.04
269	16.7 ± 3.3	19.00
278	18.0 ± 3.6	18.15
278	15.7 ± 3.1	18.15
287	16.8 ± 3.3	17.37
299	17.7 ± 3.6	16.43
304	14.9 ± 3.0	16.07
309	14.2 ± 2.9	15.73
318	15.0 ± 3.0	15.15

We now turn our attention to the only non-polar non-linear molecule for which B_K data has been measured, namely ethene.

4.8 Calculations of B_K for ethene

4.8.1 Molecular properties of ethene

Optimized values for the Lennard-Jones force constants R_o and ε/k, and shape parameters D_1 and D_2, of ethene (obtained by fitting the second pressure virial coefficient calculated according to equation (2.111) to experimental data over a range of temperature) have been presented in section **2.5** of Chapter 2. For convenience, we list the values again, together with the quadrupole moment tensor components and mean static polarizability required in the expressions for $U_{12}(\tau)$:

Table 4.26. The components of the optical-frequency polarizability tensor of ethene at a wavelength of 632.8 nm obtained from the measured values for ρ_o, α and R_{20}.

$100\rho_o$	$\frac{10^{40}\alpha}{C^2m^2J^{-1}}$	$\frac{10^{40}(\Delta\alpha)}{C^2m^2J^{-1}}$	R_{20}	$\frac{10^{40}\alpha_{11}}{C^2m^2J^{-1}}$	$\frac{10^{40}\alpha_{22}}{C^2m^2J^{-1}}$	$\frac{10^{40}\alpha_{33}}{C^2m^2J^{-1}}$
1.207 ± 0.002 [40]	4.7124 [56]	2.021_5	0.21 ± 0.03 [65]	4.30_5	3.80_4	6.02_9

Table 4.27. The wavelength dependence of ρ_o, α and $\Delta\alpha$; together with values extrapolated to infinite wavelength.

λ/nm	$\frac{10^{40}\alpha}{C^2m^2J^{-1}}$ [56]	$100 \times \rho_o$ [40	$\frac{10^{40}(\Delta\alpha)}{C^2m^2J^{-1}}$
632.8	4.7124 ± 0.0005	1.207 ± 0.002	2.0215
514.5	4.7871 ± 0.0005	1.247 ± 0.005	2.0882
488.0	4.7978 ± 0.0005	1.266 ± 0.005	2.1087
$\lambda \rightarrow \infty$	4.5717 ± 0.0008		1.893 ± 0.0024

Table 4.25. A summary of the Lennard-Jones force constants, shape parameters, and wavelength-independent molecular properties required in the intermolecular potential $U_{12}(\tau)$ of ethene.

$R_o = 0.4232$ nm	$D_1 = 0.22965$
$\varepsilon/k = 190.0$ K	$D_2 = 0.21383$

$$\left.\begin{aligned} \theta_{11} &= 5.370 \times 10^{-40}\ \mathrm{Cm}^2 \\ \theta_{22} &= -10.92 \times 10^{-40}\ \mathrm{Cm}^2 \\ \theta_{33} &= 5.549 \times 10^{-40}\ \mathrm{Cm}^2 \end{aligned}\right\} \quad [64]$$

$$a = 4.5717 \times 10^{-40}\ \mathrm{C^2 m^2 J^{-1}}\ \dagger$$

† Obtained by extrapolating measured dynamic polarizabilities [56] to zero frequency

Whereas our measurement of B_ρ for ethene was performed using an incident light beam with $\lambda = 514.5$ nm, the measurements of $B_K(T)$ undertaken by Buckingham *et al.* [7] were performed at $\lambda = 632.8$ nm. The dynamic polarizability tensor components must be evaluated at the new wavelength, and table 4.26 contains the values of ρ_o, α and R_{20} which allow equations (2.12), (2.13) and (2.110) to be solved simultaneously, hence yielding α_{11}, α_{22} and α_{33} at 632.8 nm.

There are no experimental estimates of the individual static polarizability tensor components, and so the *ab initio* calculated values of Spackman [41] at the MP2 level of theory are used as a basis. As before, these values are refined by scaling according to the mean static polarizability extrapolated from measured dynamic values [56]. Listed in table 4.27 are the wavelength dependences of ρ_o, α and $\Delta\alpha$, together with the values extrapolated to zero frequency. Table 4.28 quotes Spackman's calculated a_{ij} components, mean static polarizability a and polarizability anisotropy Δa; together with the scaled values. The usual cross-check is performed, the scaled Δa and the one extrapolated from the experimental data in table 4.27 agreeing to within 1.1%. The scaled a_{11}, a_{22} and a_{33} values can be used with reasonable confidence in our calculations of B_K.

Table 4.28. *Ab initio* calculated static polarizability tensor components of ethene together with the mean polarizability a and anisotropy Δa. Also included are the values scaled according to the extrapolated a given in table 4.27.

Polarizability property	10^{40} × MP2 Calculated values[41] / $C^2m^2J^{-1}$	10^{40} × Scaled values / $C^2m^2J^{-1}$
a_{11}	4.092	4.245
a_{22}	3.534	3.666
a_{33}	5.594	5.803
a	4.407	4.571
Δa	1.845	1.914

Both the dipole moment μ_i and the first-order hyperpolarizability tensor β_{ijk} vanish for molecules with D_{2h} symmetry, and the only remaining terms are those in the second-order hyperpolarizability tensor γ_{ijkl}. *Ab initio* SCF calculations of the six independent components of the static hyperpolarizability tensor g_{ijkl} of ethene have been undertaken by Maroulis [66], and these values , which are summarized in table 4.29, are unlikely to differ substantially from the corresponding optical-frequency ones. This assumption has been confirmed by Maroulis [66] who compared the experimental value for the property

$$\gamma = \frac{1}{10}\left(3\gamma_{ijij} - \gamma_{iijj}\right) \qquad (4.86)$$

of ethene; which has been deduced by Ward and Elliott [67] from measurements of dc electric-field induced optical second harmonic generation (SHG) at $\lambda = 694$ nm, yielding $\gamma = (0.563 \pm 0.013) \times 10^{-60}$ $C^4m^4J^{-3}$; with his value of $g = (0.421 \pm 0.015) \times 10^{-60}$ $C^4m^4J^{-3}$ obtained from the components in table 4.29. Since the two values are consistent, it can concluded that the use of these components allows at least order of magnitude estimates of the $\gamma_1\alpha_1$ term's contribution to B_K to be made.

Table 4.29. The SCF *ab initio* calculated estimates of the static hyperpolarizability tensor components of ethene [66]

$$g_{1111} = (0.2429 \pm 0.0049) \times 10^{-60}\ C^4m^4J^{-3}$$

$$g_{2222} = (0.6367 \pm 0.0263) \times 10^{-60}\ C^4m^4J^{-3}$$

$$g_{3333} = (0.1445 \pm 0.0054) \times 10^{-60}\ C^4m^4J^{-3}$$

$$g_{1122} = (0.1407 \pm 0.0063) \times 10^{-60}\ C^4m^4J^{-3}$$

$$g_{1133} = (0.1185 \pm 0.0039) \times 10^{-60}\ C^4m^4J^{-3}$$

$$g_{2233} = (0.1706 \pm 0.0083) \times 10^{-60}\ C^4m^4J^{-3}$$

4.8.2 Results of calculations for ethene

Table 4.30 gives the relative magnitudes of the various contributions to B_K calculated at T = 333 K. Notice how the α_4 term is the dominant contributor to B_K, while the α_5 term makes a substantially smaller, yet still significant, contribution of 7.45%. The series is now rapidly converging so that the α_6 and higher-order terms in the collision-induced polarizability should contribute negligibly to B_K. As would be expected, the leading hyperpolarizability term $\gamma_1\alpha_1$ makes a completely negligible contribution to B_K (0.04%).

Table 4.30. The relative magnitudes of the various contributions to B_K for ethene calculated at T = 333 K.

Contributing Term	$\frac{10^{32} \times \text{Value}}{C^2 m^8 J^{-2} mol^{-2}}$	% Contribution to B_K
α_2	2.268	18.00
α_3	-7.127	-56.58
α_4	16.513	131.09
α_5	0.938	7.45
$\gamma_1 \alpha_1$	0.005	0.04

$$B_K = 12.597 \times 10^{-32}\ C^2 m^8 J^{-2} mol^{-2}$$

Table 4.31 presents the temperature dependence of the calculated B_K values, and includes a comparison with the experimentally measured values of Buckingham *et al.* [7]. We note that the quoted uncertainties in the measured values were obtained from a least squares analysis of the experimental data [7], and hence do not take into consideration any systematic errors arising from uncertainties in the pressure virial coefficients used to obtain the molar volume V_m. There are substantial discrepancies between the experiment and theory, generally of about 20% to 50%; and the reasons for this are speculative. Certainly, the B_K values are very small, and hence difficult to meausure accurately. An independent set of measurements of B_K for ethene seems desirable, since this will allow a definitive assessment of whether or not the DID model is failing.

Table 4.31. Temperature dependence of the calculated B_K values of ethene, together with the measured values at λ = 632.8 nm [7].

$\frac{T}{K}$	$\frac{10^{32}B_K^{exp}}{C^2m^8J^{-2}mol^{-2}}$	$\frac{10^{32}B_K^{calc}}{C^2m^8J^{-2}mol^{-2}}$	$\frac{B_K^{exp}}{B_K^{calc}}$
262	34 ± 7	17.06	2.034
268	26 ± 6	16.54	1.572
273	23 ± 5	16.13	1.426
280	18 ± 3	15.60	1.154
286	22 ± 5	15.18	1.449
294	24 ± 5	14.66	1.637
298	18 ± 3	14.42	1.248
302	18 ± 3	14.19	1.269
313	16 ± 3	13.59	1.177
314	18 ± 3	13.53	1.330
333	17 ± 3	12.60	1.350
334	17 ± 3	12.54	1.356

PS. While this thesis was being printed, we received our copy of the October edition of the journal Molecular Physics. Therein is a paper by Tammer and Hüttner [68] describing their investigation into the Kerr effect of gaseous ethene. First and second Kerr-effect virial coefficients are given over the temperature range 202.4 to 363.7 K. The A_K are generally 15% lower than those of Buckingham *et al.* [7], while the B_K are within 7% to 45% of [7]. The authors have calculated B_K using the theories of Buckingham and Dunmur [17,3], and obtain values which are 15% lower than ours quoted in table 4.31.

4.9 References

[1] Silberstein, L., 1917, *Phil. Mag.*, **33,** 92, 521.

[2] Watson, R. C. and Rowell, R. L., 1974, *J. chem. Phys.*, **52,** 132.

[3] Buckingham, A. D., and Dunmur, D. A., 1968, *Trans. Faraday Soc.*, **64,** 1776.

[4] Thibeau, M., Tabisz, G. C., Oksengorn, B., and Vodar, B., 1970, *J. quant. Spectrosc. rad. Transfer*, **10,** 839.

[5] Dunmur, D. A., Hunt, D. C., and Jessup, N. E., 1979, *Molec. Phys.*, **37,** 713.

[6] Buckingham, A. D., and Orr, B. J., 1969, *Trans. Faraday Soc.*, **65,** 673.

[7] Buckingham, A. D., Bogaard, M. P., Dunmur, D. A., Hobbs, C. P., and Orr, B. J., 1970, *Trans. Faraday Soc.*, **66,** 1548.

[8] Schaeffer, D. W., Sears, R. E. J., and Waugh, J. S., 1970, *J. chem. Phys.*, **53,** 1970.

[9] Buckingham, A. D., and Sutter, H., 1976, *J. chem. Phys.*, **64,** 364.

[10] Gentle, I. R., Laver, D. R., and Ritchie, G. L. D., 1989, *J. phys. Chem.*, **93,** 3035.

[11] Bogaard, M. P., Buckingham, A. D., and Ritchie, G. L. D., 1981, *J. chem. Soc. Faraday Trans.* II, **77,** 1547.

[12] Bogaard, M. P., Buckingham, A. D., and Ritchie, G. L. D., 1982, *Chem. Phys. Lett.*, **90,** 183.

[13] Gentle, I. R., Laver, D. R., and Ritchie, G. L. D., 1990, *J. phys. Chem.*, **94,** 3434.

[14] Kerr, J., 1875, *Phil. Mag.*, **50,** 337, 446.

[15] Buckingham, A. D., and Pople, J. A., 1955, *Proc. Phys. Soc.* A, **68,** 905.

[16] Otterbein, G., 1934, *Phys. Z.*, **35,** 249.

[17] Buckingham, A. D., 1955, *Proc. Phys. Soc.* A, **68,** 910.

[18] Gray, C. G., and Ralph, H. I., 1970, *Phys. Lett.* A, **33,** 165.

[19] Buckingham, A. D., and Pople, J. A., 1955, *Trans. Faraday Soc.*, **51,** 1173.

[20] Lennard-Jones, J. E., 1924, *Proc. Roy. Soc. Lond.* A, **106,** 441.

[21] McTague, J. P., Ellenson, W. D., and Hall, L. H., 1972, *J. Phys. Paris*, **33,** C1-241.

[22] Lallemand, P., 1971, *J. Phys. Paris*, **32,** 119.

[23] Barocchi, F., and McTague, J. P., 1975, *Phys. Lett.* A, **53,** 488.

[24] Graham, C., 1992, *Molec. Phys.*, **77,** 291.

[25] Couling, V. W., and Graham, C., 1993, *Molec. Phys.*, **79,** 859.

[26] Burrue, J., Chave, A., Dumon, B., and Thibeau, M., 1977, *Rev. Phys. appl.*, **12,** 1743.

[27] Dayan., E., Dunmur, D. A., and Manterfield, M. R., 1980, *J. chem. Soc. Faraday Trans.* II, **76,** 309.

[28] Couling, V. W., and Graham, C., 1994, *Molec. Phys.*, **82,** 235.

[29] Buckingham, A. D., Galwas, P. A., and Liu Fan-Chen, 1983, *J. Mol. Struct.*, **100,** 3.

[30] Stockmayer, W. H., 1941, *J. chem. Phys.*, **9,** 398.

[31] Dymond, J. H., and Smith, E. B., 1980, *The Virial Coefficients of Pure Gases and Mixtures* (Oxford: Clarendon).

[32] Kang, T. L., Hirth, L. J., Kobe, K. A., and McKetta, J. J., 1961, *J. chem. Engng. Data*, **6,** 220.

[33] Buckingham, A. D., and Pople, J. A., 1956, *Far. Soc. Disc.*, **22,** 17.

[34] Graham, C., 1971, Ph. D. Thesis, University of Cambridge.

[35] Burns, R. C., 1978, Ph. D. Thesis, University of Natal.

[36] Burns, R. C., Graham, C., and Weller, A. R. M., 1986, *Molec. Phys.*, **59,** 41.

[37] Buckingham, A. D., 1967, *Adv. chem. Phys.*, **12,** 107.

[38] Copeland, T. G., and Cole, R. H., 1976, *J. chem. Phys.*, **64,** 1741.

[39] Sutter, H., and Cole, R. H., 1970, *J. chem. Phys.*, **52,** 132.

[40] Bogaard, M. P., Buckingham, A. D., Pierens, R. K., and White, A. H., 1978, *J. chem. Soc. Faraday Trans.* I, **78,** 3008.

[41] Spackman, M. A., 1989, *J. phys. Chem.*, **93,** 7594.

[42] Dougherty, J., and Spackman, M. A., 1994, *Molec. Phys.*, **82,** 193.

[43] Miller, C. K., Orr, B. J., and Ward, J. F., 1981, *J. chem. Phys.*, **74,** 4858.

[44] Bogaard, M. P., Orr, B. J., Murphy, W. F., Srinivasan, K., and Buckingham, A. D., (to be published).

[45] Monan, M., Bribes, J-L, and Gaufrès, R., 1982, *J. Raman Spectrosc.*, **12,** 190.

[46] Patel, D., Margolese, D., and Dyke, T. R., 1979, *J. chem. Phys.*, **70,** 2740.

[47] Ellenbroek, A. W., and Dymanus, A., 1976, *Chem. Phys. Lett.*, **42,** 303.

[48] Bacskay, G. B., Rendell, A. P. L., and Hush, N. S., 1988, *J. chem. Phys.*, **89,** 5721.

[49] Maroulis, G., 1992, *Chem. Phys. Lett.*, **189,** 112.

[50] Blukis, U., Kasai, P. H., and Myers, R. J., 1963, *J. chem. Phys.*, **38,** 2753.

[51] Benson, R. C., and Flygare, W. H., 1970, *J. chem. Phys.*, **52,** 5291.

[52] Coonan, M. H., Craven, I. E., Hesling, M. R., Ritchie, G. L. D., and Spackman, M. A., 1992, *J. phys. Chem.*, **96**, 7301.

[53] Spackman, M. A., and Ritchie, G. L. D., *Private Communication.*

[54] Orcutt, R. H., and Cole, R. H., 1967, *J. chem. Phys.*, **46**, 697.

[55] Hohm, U., 1994, *Chem. Phys.*, **179**, 533.

[56] Hohm, U., 1993, *Molec. Phys.*, **78**, 929.

[57] Alms, G. R., Burnham, A. K., and Flygare, W. H., 1975, *J. chem. Phys.*, **63**, 3321.

[58] Baas, F., and van den Hout, K. D., 1979, *Physica A*, **95**, 597.

[59] Graham, C., Pierrus, J. and Raab, R. E., 1989, *Molec. Phys.*, **67**, 939.

[60] Battaglia, M. R., Buckingham, A. D., Neumark, D., Pierens, R. K., and Williams, J. H., 1981, *Molec. Phys.*, **43**, 1015.

[61] Buckingham, A. D., Graham, C., and Williams, J. H., 1983, *Molec. Phys.*, **49**, 703.

[62] Hirschfelder, J. O., Curtiss, C. F., and Bird, R. B., 1954, *Molecular Theory of Gases and Liquids* (Chichester: Wiley).

[63] Mason, E. A., and Spurling, T. H., 1969, *The Virial Equation of State* (Oxford: Pergamon).

[64] Maroulis, G., 1993, *J. Phys. B: At. Mol. Opt. Phys.*, **2**, 775.

[65] Barbès, H., 1987, *J. Raman Spectrosc.*, **18**, 507.

[66] Maroulis, G., 1992, *J. chem. Phys.*, **97**, 4188.

[67] Ward, J. F., and Elliott, D. S., 1978, *J. chem. Phys.*, **69**, 5438.

[68] Tammer, R., and Hüttner, W., 1994, *Molec. Phys.*, **83**, 579.

APPENDIX 1

A1.1 Electric multipole moments

A static distribution of electric charges q_i at positions $\underset{\sim}{r}_i$ relative to an arbitrarily chosen origin O, positioned within the arrangement of charges, gives rise to an electric potential ϕ at all points in space. For any given point P, with a vector displacement $\underset{\sim}{R}$ from O with $R >> r_i$, the electric potential is given by the multipole expansion (Buckingham [1])

$$\phi = \frac{1}{4\pi\varepsilon}\left[\frac{1}{R}\sum_i q_i + \frac{R_\alpha}{R^3}\sum_i q_i r_{i\alpha} + \frac{\left(3R_\alpha R_\beta - R^2\delta_{\alpha\beta}\right)}{2R^5}\sum_i q_i r_{i\alpha} r_{i\beta} + \ldots\right]. \tag{A1.1}$$

Here, Greek subscripts denote Cartesian tensor components x, y, or z; with a repeated subscript implying summation over these components. The second-rank tensor $\delta_{\alpha\beta}$ is the Kronecker delta.

The summations in equation (A1.1) are the electric multipole moments of the charge distribution:

$$q = \sum_i q_i \tag{A1.2}$$

is the electric monopole, or the total charge of the distribution;

$$\mu_\alpha = \sum_i q_i r_{i\alpha} \tag{A1.3}$$

is the electric dipole moment; and

$$\theta_{\alpha\beta} = \sum_i q_i r_{i\alpha} r_{i\beta} \tag{A1.4}$$

is the *primitive* electric quadrupole moment, etc.

Different definitions have been adopted for electric multipole moments of higher order than the dipole. For instance, an alternative form of the electric quadrupole moment is the *traceless* moment

$$\theta_{\alpha\beta} = \frac{1}{2} \sum_i q_i \left[3r_{i\alpha} r_{i\beta} - r_i^2 \delta_{\alpha\beta}\right] . \qquad \text{(A1.5)}$$

This form of the quadrupole moment is often used by molecular physicists because it vanishes for a spherically-symmetric electric charge distribution, and so is intuitively appealing. Raab [2] has, however, cautioned against the indiscriminate use of the *traceless* multipole moments, pointing out the existence of electrodynamic situations where it is necessary to retain the *primitive* definitions of multipole moments.

References

[1] Buckingham, A. D., 1959, *J. Q. Chem. Rev. Soc.*, **13,** 183.

[2] Raab, R. E., 1975, *Molec. Phys.*, **29,** 1323.

APPENDIX 2

A2.1 An example of a Fortran program to calculate contributions to B_ρ

```
      PROGRAM SO2_A3
C
C 14 AUGUST 1994
C PROGRAM TO CALCULATE TERM A3 FOR SO2 USING GAUSSIAN INTEGRATION WITH
C 64 INTERVALS FOR THE RANGE, AND 16 INTERVALS FOR ALL ANGULAR VARIABLES
C (I.E. ALPHA1, BETA1, GAMMA1, ALPHA2, BETA2 AND GAMMA2).
C DOUBLE PRECISION IS USED THROUGHOUT.
C

C ----------------------
C SYSTEM INITIALIZATION:
C ----------------------

      IMPLICIT DOUBLE PRECISION (A-H,O-Z)
      COMMON COEF1,DCTC
      DIMENSION COEF2(64,2),COEF1(16,2),SEP(64),AL1(16),BE1(16),GA1(16)
     + ,AL2(16),BE2(16),GA2(16),DCTC(9,16,16,16),FI(16,16,16,16,16),D1(6
     + 4),E1(16,16,16,16,16),F1(16,16,16,16,16),SE3(64),SE4(64),SE5(64),
     + SE6(64),SE8(64),SE12(64),G1(16,16,16),DDP(16,16,16,16,16),DQP(16,
     + 16,16,16,16),DIDP(16,16,16,16,16)
      INTEGER X1,X2,X3,X4,X5,X6,X7
      CHARACTER*30 FDATE@

C MOLECULAR DATA FOR SO2:

      SS1=0.0
      SS2=0.0
      SS3=0.0
      SS4=0.0
      SS5=0.0
      SS6=0.0
      SS7=0.0
      DIP=-5.42620
      ALSTAT=3.9740
      A11=5.941
      A22=3.328
      A33=3.898
      Q1=-16.38
      Q2=12.90
      AMIN1=0.1
      AMAX1=3.0
      ALPHA=(A11+A22+A33)/3
      DELTA2=(A11**2+A22**2+A33**2-A11*A22-A11*A33-A22*A33)

C
C READ THE GAUSSIAN COEFFICIENTS FROM THE DATAFILE GAUSS64.DAT:
C
      OPEN(UNIT=10,FILE='GAUSS64.DAT')
  DO 10 ICTR1=1,64
    DO 20 ICTR2=1,2
      READ(10,1010,END=11)COEF2(ICTR1,ICTR2)
1010          FORMAT(F18.15)
```

```
20          CONTINUE
10        CONTINUE
11      CLOSE(UNIT=10)

C
C CALCULATE THE INTEGRATION POINTS FOR THE RANGE:
C
        SEP1=(AMAX1-AMIN1)/2
        SEP2=(AMAX1+AMIN1)/2
        DO 30 INDX=1,64
  SEP(INDX)=SEP1*COEF2(INDX,1)+SEP2
30      CONTINUE

C
C READ THE GAUSSIAN COEFFICIENTS FROM THE DATAFILE GAUSS16.DAT:
C
        OPEN(UNIT=11,FILE='GAUSS16.DAT')
   DO 100 ICTR1=1,16
     DO 110 ICTR2=1,2
       READ(11,6000,END=12)COEF1(ICTR1,ICTR2)
6000          FORMAT(F18.15)
110       CONTINUE
100     CONTINUE
12      CLOSE(UNIT=11)

C
C CALCULATE THE INTEGRATION POINTS FOR ALPHA1:
C
        AMIN=0.0
        AMAX=2.*3.14159265358979323846

        AL11=(AMAX-AMIN)/2.
        AL12=(AMAX+AMIN)/2.
        DO 120 INDX=1,16
  AL1(INDX)=AL11*COEF1(INDX,1)+AL12
120     CONTINUE

C
C CALCULATE THE INTEGRATION POINTS FOR BETA1:
C
        AMIN=0.0
        AMAX=3.14159265358979323846

        BE11=(AMAX-AMIN)/2.
        BE12=(AMAX+AMIN)/2.
        DO 121 INDX=1,16
  BE1(INDX)=BE11*COEF1(INDX,1)+BE12
121     CONTINUE

C
C CALCULATE THE INTEGRATION POINTS FOR GAMMA1:
C
        AMIN=0.0
        AMAX=2.*3.14159265358979323846

        GA11=(AMAX-AMIN)/2.
        GA12=(AMAX+AMIN)/2.
        DO 122 INDX=1,16
  GA1(INDX)=GA11*COEF1(INDX,1)+GA12
122     CONTINUE
```

```
C
C CALCULATE THE INTEGRATION POINTS FOR ALPHA2:
C
       AMIN=0.0
       AMAX=2.*3.14159265358979323846

       AL21=(AMAX-AMIN)/2.
       AL22=(AMAX+AMIN)/2.
       DO 123 INDX=1,16
  AL2(INDX)=AL21*COEF1(INDX,1)+AL22
123    CONTINUE

C
C CALCULATE THE INTEGRATION POINTS FOR BETA2:
C
       AMIN=0.0
       AMAX=3.14159265358979323846

       BE21=(AMAX-AMIN)/2.
       BE22=(AMAX+AMIN)/2.
       DO 124 INDX=1,16
  BE2(INDX)=BE21*COEF1(INDX,1)+BE22
124    CONTINUE

C
C CALCULATE THE INTEGRATION POINTS FOR GAMMA2:
C
       AMIN=0.0
       AMAX=2.*3.14159265358979323846

       GA21=(AMAX-AMIN)/2.
       GA22=(AMAX+AMIN)/2.
       DO 125 INDX=1,16
  GA2(INDX)=GA21*COEF1(INDX,1)+GA22
125    CONTINUE

C -------------
C MAIN PROGRAM:
C -------------

       OPEN(UNIT=4,FILE='LPT1')
       CALL BEEP@

C
C INPUT MOLECULAR PARAMETERS FROM THE KEYBOARD:
C

c WRITE(6,470)
c470 FORMAT(1X,'INPUT THE TEMPERATURE (IN KELVIN)')
c READ(5,471)TEMP
c471 FORMAT(F10.5)
       TEMP=348.15
       TEMPK=TEMP*1.380622E-23
c
c WRITE(6,472)
c472 FORMAT(1X,'INPUT R(0) (IN nm)')
c READ(5,473)R
c473 FORMAT(F10.5)
       r=0.3800
```

```
c WRITE(6,474)
c474 FORMAT(1X,'INPUT E/K (IN K)')
c READ(5,475)PARAM2
c475 FORMAT(F10.5)
       param2=217.0
c WRITE(6,476)
c476 FORMAT(1X,'INPUT SHAPE1 ')
c READ(5,477)SHAPE1
c477 FORMAT(F10.5)
       shape1=0.0280
c WRITE(6,478)
c478 FORMAT(1X,'INPUT SHAPE2 ')
c READ(5,479)SHAPE2
c479 FORMAT(F10.5)
       shape2=0.0560
       CALL SECONDS_SINCE_1980@(START)

C
C CALCULATION OF THE LENNARD-JONES 6:12 POTENTIAL & STORAGE OF THE
C VALUES IN AN ARRAY:
C

       DO 61 X1=1,64

       D1(X1)=4.*PARAM2*1.380622E-23*((R/SEP(X1))**12-(R/SEP(X1))**6)
       SE12(X1)=SEP(X1)**12
       SE5(X1)=SEP(X1)**5
       SE8(X1)=SEP(X1)**8
       SE3(X1)=SEP(X1)**3
       SE4(X1)=SEP(X1)**4
       SE6(X1)=SEP(X1)**6

61     CONTINUE


C
C THE DIRECTION COSINE TENSOR COMPONENTS ARE STORED IN AN ARRAY:
C

       DO 66 X4=1,16
  DO 77 X3=1,16
    DO 88 X2=1,16

C
C DIRECTION COSINE TENSOR COMPONENTS:
C

       A1=COS(AL1(X2))*COS(BE1(X3))*COS(GA1(X4))-1.*SIN(AL1(X2))*SIN(GA1
     + (X4))
       A2=SIN(AL1(X2))*COS(BE1(X3))*COS(GA1(X4))+COS(AL1(X2))*SIN(GA1(X4
     + ))
       A3=-1.*SIN(BE1(X3))*COS(GA1(X4))
       A4=-1.*COS(AL1(X2))*COS(BE1(X3))*SIN(GA1(X4))-1.*SIN(AL1(X2))*COS
     + (GA1(X4))
       A5=-1.*SIN(AL1(X2))*COS(BE1(X3))*SIN(GA1(X4))+COS(AL1(X2))*COS(GA
     + 1(X4))
       A6=SIN(BE1(X3))*SIN(GA1(X4))
       A7=COS(AL1(X2))*SIN(BE1(X3))
       A8=SIN(AL1(X2))*SIN(BE1(X3))
       A9=COS(BE1(X3))
```

```
        DCTC(1,X2,X3,X4)=A1
        DCTC(2,X2,X3,X4)=A2
        DCTC(3,X2,X3,X4)=A3
        DCTC(4,X2,X3,X4)=A4
        DCTC(5,X2,X3,X4)=A5
        DCTC(6,X2,X3,X4)=A6
        DCTC(7,X2,X3,X4)=A7
        DCTC(8,X2,X3,X4)=A8
        DCTC(9,X2,X3,X4)=A9

88          CONTINUE
77        CONTINUE
66      CONTINUE


C
C THE MULTIPOLE INTERACTION ENERGIES ARE CALCULATED AND STORED
C IN ARRAYS:
C

        DO 939 X7=1,16
        WRITE(6,1000)X7
1000    FORMAT (1X, 'INDEX (IN RANGE 1 TO 16) IS CURRENTLY ',I2 )
  DO 40 X6=1,16
C        WRITE(6,1111)X6
C1111 FORMAT (1X, 'sub-index (in range 1 to 16) is currently ',I2 )
    DO 50 X5=1,16

C
C MOLECULE 2'S DIRECTION COSINE TENSOR COMPONENTS:
C

        B1=DCTC(1,X5,X6,X7)
        B2=DCTC(2,X5,X6,X7)
        B3=DCTC(3,X5,X6,X7)
        B4=DCTC(4,X5,X6,X7)
        B5=DCTC(5,X5,X6,X7)
        B6=DCTC(6,X5,X6,X7)
        B7=DCTC(7,X5,X6,X7)
        B8=DCTC(8,X5,X6,X7)
        B9=DCTC(9,X5,X6,X7)


      DO 60 X4=1,16
   DO 70 X3=1,16
   DO 80 X2=1,16

C
C MOLECULE 1'S DIRECTION COSINE TENSOR COMPONENTS:
C

        A1=DCTC(1,X2,X3,X4)
        A2=DCTC(2,X2,X3,X4)
        A3=DCTC(3,X2,X3,X4)
        A4=DCTC(4,X2,X3,X4)
        A5=DCTC(5,X2,X3,X4)
        A6=DCTC(6,X2,X3,X4)
        A7=DCTC(7,X2,X3,X4)
        A8=DCTC(8,X2,X3,X4)
```

```
      A9=DCTC(9,X2,X3,X4)

C
C CALCULATION OF THE DIPOLE-DIPOLE POTENTIAL:
C
      DDP(X2,X3,X4,X5,X6)=8.98758E-24*DIP**2*(-2*A9*B9+A6*B6+A3*B3)

C
C CALCULATION OF THE DIPOLE-QUADRUPOLE POTENTIAL:
C
      DQP(X2,X3,X4,X5,X6)=8.98758E-25*DIP*(Q2*(-2*A9*B9**2+(2*A6*B6+2*A
     + 3*B3+2*A9**2-2*A8**2-A6**2+A5**2-A3**2+A2**2)*B9+2*A9*B8**2+(-2*A
     + 6*B5-2*A3*B2)*B8+A9*B6**2+(2*A5*A8-2*A6*A9)*B6-A9*B5**2+A9*B3**2+
     + (2*A2*A8-2*A3*A9)*B3-A9*B2**2)+Q1*(-2*A9*B9**2+(2*A6*B6+2*A3*B3+2
     + *A9**2-2*A7**2-A6**2+A4**2-A3**2+A1**2)*B9+2*A9*B7**2+(-2*A6*B4-2
     + *A3*B1)*B7+A9*B6**2+(2*A4*A7-2*A6*A9)*B6-A9*B4**2+A9*B3**2+(2*A1*
     + A7-2*A3*A9)*B3-A9*B1**2))

C
C CALCULATION OF THE DIPOLE-INDUCED DIPOLE POTENTIAL:
C
      DIDP(X2,X3,X4,X5,X6)=-0.50*ALSTAT*8.07765E-27*DIP**2*(3*B9**2
     + +3*A9**2-2)

C
C CALCULATION OF THE QUADRUPOLE-QUADRUPOLE POTENTIAL:
C
      quad1=-16.*(a6*a9-a5*a8)*(b6*b9-b5*b8)-16.*(a3*a9-a2*a8)*(b3*b9-b
     + 2*b8)+4.*(2.*a9**2-2.*a8**2-a6**2+a5**2-a3**2+a2**2)*(b9-b8)*(b9+
     + b8)+(-4.*a9**2+4.*a8**2+3.*a6**2-3.*a5**2+a3**2-a2**2)*(b6**2-b5*
     + *2)+4.*(a3*a6-a2*a5)*(b3*b6-b2*b5)+(-4.*a9**2+4.*a8**2+a6**2-a5**
     + 2+3.*a3**2-3.*a2**2)*(b3**2-b2**2)

      quad2=-16.*(a6*a9-a4*a7)*(b6*b9-b4*b7)-16.*(a3*a9-a1*a7)*(b3*b9-b
     + 1*b7)+4.*(2.*a9**2-2.*a7**2-a6**2+a4**2-a3**2+a1**2)*(b9-b7)*(b9+
     + b7)+(-4.*a9**2+4.*a7**2+3.*a6**2-3.*a4**2+a3**2-a1**2)*(b6**2-b4*
     + *2)+4.*(a3*a6-a1*a4)*(b3*b6-b1*b4)+(-4.*a9**2+4.*a7**2+a6**2-a4**
     + 2+3.*a3**2-3.*a1**2)*(b3**2-b1**2)

      quad3=4.*(4.*A9**2-2.*(A8**2+A7**2+A6**2+A3**2)+A5**2+A4**2+A2**2
     + +A1**2)*B9**2-16.*(2.*A6*A9-A5*A8-A4*A7)*B6*B9-16*(2.*A3*A9-A2*A8
     + -A1*A7)*B3*B9-4.*(2.*A9**2-2.*A7**2-A6**2+A4**2-A3**2+A1**2)*B8**
     + 2+16.*(A6*A9-A4*A7)*B5*B8+16.*(A3*A9-A1*A7)*B2*B8-4.*(2.*A9**2-2.
     + *A8**2-A6**2+A5**2-A3**2+A2**2)*B7**2+16.*(A6*A9-A5*A8)*B4*B7+16.
     + *(A3*A9-A2*A8)*B1*B7+(-8.*A9**2+4.*(A8**2+A7**2)+6.*A6**2-3.*(A5*
     + *2+A4**2)+2*A3**2-A2**2-A1**2)*B6**2+4.*(2.*A3*A6-A2*A5-A1*A4)*B3
     + *B6+(4.*A9**2-4.*A7**2-3.*A6**2+3.*A4**2-A3**2+A1**2)*B5**2-4.*(A
     + 3*A6-A1*A4)*B2*B5+(4.*A9**2-4.*A8**2-3.*A6**2+3.*A5**2-A3**2+A2**
     + 2)*B4**2-4.*(A3*A6-A2*A5)*B1*B4+(-8.*A9**2+4.*(A8**2+A7**2)+2.*A6
     + **2-A5**2-A4**2+6.*A3**2-3.*(A2**2+A1**2))*B3**2+(4.*A9**2-4.*A7*
     + *2-A6**2+A4**2-3.*A3**2+3.*A1**2)*B2**2+(4.*A9**2-4.*A8**2-A6**2+
     + A5**2-3.*A3**2+3.*A2**2)*B1**2

      E1(X2,X3,X4,X5,X6)=8.98758E-26*(1./3.)*(Q2**2*QUAD1+Q1**2*QUAD
     + 2+Q1*Q2*QUAD3)


C
C CALCULATION OF THE QUADRUPOLE-INDUCED DIPOLE POTENTIAL:
C
```

```
      QID1=Q2**2*(4.*A9**4+(-8.*A8**2+4.*A5**2+4.*A2**2)*A9**2+(-8.*A5*
     + A6-8.*A2*A3)*A8*A9+4.*A8**4+(4.*A6**2+4.*A3**2)*A8**2+A6**4+(-2.*
     + A5**2+2.*A3**2-2.*A2**2)*A6**2+A5**4+(2.*A2**2-2.*A3**2)*A5**2+A3
     + **4-2.*A2**2*A3**2+A2**4)+Q1**2*(4.*A9**4+(-8.*A7**2+4.*A4**2+4.*
     + A1**2)*A9**2+(-8.*A4*A6-8.*A1*A3)*A7*A9+4.*A7**4+(4.*A6**2+4.*A3*
     + *2)*A7**2+A6**4+(-2.*A4**2+2.*A3**2-2.*A1**2)*A6**2+A4**4+(2.*A1*
     + *2-2.*A3**2)*A4**2+A3**4-2.*A1**2*A3**2+A1**4)+Q1*Q2*(8.*A9**4+(-
     + 8.*A8**2-8.*A7**2+4.*A5**2+4.*A4**2+4.*A2**2+4.*A1**2)*A9**2+((-8
     + .*A5*A6-8.*A2*A3)*A8+(-8.*A4*A6-8.*A1*A3)*A7)*A9+(8.*A7**2+4.*A6*
     + *2-4.*A4**2+4.*A3**2-4.*A1**2)*A8**2+(8.*A4*A5+8.*A1*A2)*A7*A8+(4
     + .*A6**2-4.*A5**2+4.*A3**2-4.*A2**2)*A7**2+2.*A6**4+(-2.*A5**2-2.*
     + A4**2+4.*A3**2-2.*A2**2-2.*A1**2)*A6**2+(2.*A4**2-2.*A3**2+2.*A1*
     + *2)*A5**2+(2.*A2**2-2.*A3**2)*A4**2+2.*A3**4+(-2.*A2**2-2.*A1**2)
     + *A3**2+2.*A1**2*A2**2)

      QID2=Q2**2*(4.*B9**4+(-8.*B8**2+4.*B5**2+4.*B2**2)*B9**2+(-8.*B5*
     + B6-8.*B2*B3)*B8*B9+4.*B8**4+(4.*B6**2+4.*B3**2)*B8**2+B6**4+(-2.*
     + B5**2+2.*B3**2-2.*B2**2)*B6**2+B5**4+(2.*B2**2-2.*B3**2)*B5**2+B3
     + **4-2.*B2**2*B3**2+B2**4)+Q1**2*(4.*B9**4+(-8.*B7**2+4.*B4**2+4.*
     + B1**2)*B9**2+(-8.*B4*B6-8.*B1*B3)*B7*B9+4.*B7**4+(4.*B6**2+4.*B3*
     + *2)*B7**2+B6**4+(-2.*B4**2+2.*B3**2-2.*B1**2)*B6**2+B4**4+(2.*B1*
     + *2-2.*B3**2)*B4**2+B3**4-2.*B1**2*B3**2+B1**4)+Q1*Q2*(8.*B9**4+(-
     + 8.*B8**2-8.*B7**2+4.*B5**2+4.*B4**2+4.*B2**2+4.*B1**2)*B9**2+((-8
     + .*B5*B6-8.*B2*B3)*B8+(-8.*B4*B6-8.*B1*B3)*B7)*B9+(8.*B7**2+4.*B6*
     + *2-4.*B4**2+4.*B3**2-4.*B1**2)*B8**2+(8.*B4*B5+8.*B1*B2)*B7*B8+(4
     + .*B6**2-4.*B5**2+4.*B3**2-4.*B2**2)*B7**2+2.*B6**4+(-2.*B5**2-2.*
     + B4**2+4.*B3**2-2.*B2**2-2.*B1**2)*B6**2+(2.*B4**2-2.*B3**2+2.*B1*
     + *2)*B5**2+(2.*B2**2-2.*B3**2)*B4**2+2.*B3**4+(-2.*B2**2-2.*B1**2)
     + *B3**2+2.*B1**2*B2**2)

      F1(X2,X3,X4,X5,X6)=-0.5*8.07765E-29*ALSTAT*(QID1+QID2)

C
C CALCULATION OF THE INTEGRATION ARGUMENT:
C

      T11=2.*A7**2-A4**2-A1**2
      T22=2.*A8**2-A5**2-A2**2
      T33=2.*A9**2-A6**2-A3**2
      T12=2.*A7*A8-A4*A5-A1*A2
      T13=2.*A7*A9-A4*A6-A1*A3
      T23=2.*A8*A9-A5*A6-A2*A3

      Z11 = A33*(A7**2*B9**2+(2*A4*A7*B6+2*A1*A7*B3)*B9+A4**2*B6**2+2*A
     +   1*A4*B3*B6+A1**2*B3**2)+A22*(A7**2*B8**2+(2*A4*A7*B5+2*A1*A7*B2
     +   )*B8+A4**2*B5**2+2*A1*A4*B2*B5+A1**2*B2**2)+A11*(A7**2*B7**2+(2
     +   *A4*A7*B4+2*A1*A7*B1)*B7+A4**2*B4**2+2*A1*A4*B1*B4+A1**2*B1**2)

      Z22 = A33*(A8**2*B9**2+(2*A5*A8*B6+2*A2*A8*B3)*B9+A5**2*B6**2+2*A
     +   2*A5*B3*B6+A2**2*B3**2)+A22*(A8**2*B8**2+(2*A5*A8*B5+2*A2*A8*B2
     +   )*B8+A5**2*B5**2+2*A2*A5*B2*B5+A2**2*B2**2)+A11*(A8**2*B7**2+(2
     +   *A5*A8*B4+2*A2*A8*B1)*B7+A5**2*B4**2+2*A2*A5*B1*B4+A2**2*B1**2)

      Z33 = A33*(A9**2*B9**2+(2*A6*A9*B6+2*A3*A9*B3)*B9+A6**2*B6**2+2*A
     +   3*A6*B3*B6+A3**2*B3**2)+A22*(A9**2*B8**2+(2*A6*A9*B5+2*A3*A9*B2
     +   )*B8+A6**2*B5**2+2*A3*A6*B2*B5+A3**2*B2**2)+A11*(A9**2*B7**2+(2
     +   *A6*A9*B4+2*A3*A9*B1)*B7+A6**2*B4**2+2*A3*A6*B1*B4+A3**2*B1**2)

      Z12 = A33*(A7*A8*B9**2+((A4*A8+A5*A7)*B6+(A1*A8+A2*A7)*B3)*B9+A4*
```

```
     +    A5*B6**2+(A1*A5+A2*A4)*B3*B6+A1*A2*B3**2)+A22*(A7*A8*B8**2+((A4
     +    *A8+A5*A7)*B5+(A1*A8+A2*A7)*B2)*B8+A4*A5*B5**2+(A1*A5+A2*A4)*B2
     +    *B5+A1*A2*B2**2)+A11*(A7*A8*B7**2+((A4*A8+A5*A7)*B4+(A1*A8+A2*A
     +    7)*B1)*B7+A4*A5*B4**2+(A1*A5+A2*A4)*B1*B4+A1*A2*B1**2)

       Z13 = A33*(A7*A9*B9**2+((A4*A9+A6*A7)*B6+(A1*A9+A3*A7)*B3)*B9+A4*
     +    A6*B6**2+(A1*A6+A3*A4)*B3*B6+A1*A3*B3**2)+A22*(A7*A9*B8**2+((A4
     +    *A9+A6*A7)*B5+(A1*A9+A3*A7)*B2)*B8+A4*A6*B5**2+(A1*A6+A3*A4)*B2
     +    *B5+A1*A3*B2**2)+A11*(A7*A9*B7**2+((A4*A9+A6*A7)*B4+(A1*A9+A3*A
     +    7)*B1)*B7+A4*A6*B4**2+(A1*A6+A3*A4)*B1*B4+A1*A3*B1**2)

       Z23 = A33*(A8*A9*B9**2+((A5*A9+A6*A8)*B6+(A2*A9+A3*A8)*B3)*B9+A5*
     +    A6*B6**2+(A2*A6+A3*A5)*B3*B6+A2*A3*B3**2)+A22*(A8*A9*B8**2+((A5
     +    *A9+A6*A8)*B5+(A2*A9+A3*A8)*B2)*B8+A5*A6*B5**2+(A2*A6+A3*A5)*B2
     +    *B5+A2*A3*B2**2)+A11*(A8*A9*B7**2+((A5*A9+A6*A8)*B4+(A2*A9+A3*A
     +    8)*B1)*B7+A5*A6*B4**2+(A2*A6+A3*A5)*B1*B4+A2*A3*B1**2)


      TERM4=-4.*ALPHA*(A33*(Z33*T33+Z23*T23+Z13*T13)+A22*(Z23*T23+Z22*T2
     + 2+Z12*T12)+A11*(Z13*T13+Z12*T12+Z11*T11))+3.*(A33**2*(Z33*T33+Z23
     + *T23+Z13*T13)+A22**2*(Z23*T23+Z22*T22+Z12*T12)+A11**2*(Z13*T13+Z1
     + 2*T12+Z11*T11))+A33*((Z33**2+Z23**2+Z13**2)*T33+(Z23*Z33+Z22*Z23+
     + Z12*Z13)*T23+(Z13*Z33+Z12*Z23+Z11*Z13)*T13)+A22*((Z23*Z33+Z22*Z23
     + +Z12*Z13)*T23+(Z23**2+Z22**2+Z12**2)*T22+(Z13*Z23+Z12*Z22+Z11*Z12
     + )*T12)+A11*((Z13*Z33+Z12*Z23+Z11*Z13)*T13+(Z13*Z23+Z12*Z22+Z11*Z1
     + 2)*T12+(Z13**2+Z12**2+Z11**2)*T11)

       FI(X2,X3,X4,X5,X6)=(1/(16.*3.14159265358979323846**3))*(SI
     + N(BE1(X3))*SIN(BE2(X6)))*TERM4

C
C CALCULATION OF THE SHAPE POTENTIAL:
C

       G1(X3,X4,X6)=4.*PARAM2*1.380622E-23*R**12*(SHAPE1*(3.*COS(BE1(X3)
     + )**2+3.*COS(BE2(X6))**2-2.)+SHAPE2*(3.*COS(GA1(X4))**2*SIN(BE1(X3
     + ))**2+3.*COS(GA2(X7))**2*SIN(BE2(X6))**2-2.))


80              CONTINUE
70            CONTINUE
60          CONTINUE
50        CONTINUE
40      CONTINUE

C
C THE INTEGRAL IS CALCULATED:
C

  SS6=0.00
  DO 940 X6=1,16
C       WRITE(6,1911)X6
C1911 FORMAT (1X, 'sub-index (in range 1 to 16) is currently ',I2 )
    SS5=0.00
    DO 950 X5=1,16
      SS4=0.00
      DO 960 X4=1,16
        SS3=0.00
   DO 970 X3=1,16
   SS2=0.00
```

```
   DO 980 X2=1,16
     SS1=0.00
     DO 990 X1=1,64


C
C SUMMATION OF THE ENERGY TERMS WITH SUBSEQUENT DIVISION BY (-kT):
C

       G3=-1.*(D1(X1)+E1(X2,X3,X4,X5,X6)/SE5(X1)+F1(X2,X3,X4,X5,X6)/SE8(
     + X1)+G1(X3,X4,X6)/SE12(X1)+DDP(X2,X3,X4,X5,X6)/SE3(X1)+DIDP(X2,X3,
     + X4,X5,X6)/SE6(X1)+DQP(X2,X3,X4,X5,X6)/SE4(X1))/TEMPK

       IF(G3.LT.-85) GO TO 5000
       G4=2.71828**G3
       GO TO 5010
5000   G4=0
5010   SS1=SS1+(FI(X2,X3,X4,X5,X6)/SEP(X1))*G4*COEF2(X1,2)
990                 CONTINUE
       SS2=SS2+SS1*COEF1(X2,2)
C
C
980              CONTINUE
       SS3=SS3+SS2*COEF1(X3,2)
C
C
970            CONTINUE
       SS4=SS4+SS3*COEF1(X4,2)
C
C
960          CONTINUE
       SS5=SS5+SS4*COEF1(X5,2)
C
C
950        CONTINUE
       SS6=SS6+SS5*COEF1(X6,2)
C
C
940      CONTINUE
       SS7=SS7+SS6*COEF1(X7,2)

C
C
939    CONTINUE
       ANS=SS7*SEP1*AL11*BE11*GA11*AL21*BE21*GA21*1.E-9*6.022169*8.9875
     + 8*30.*(1./(2.*DELTA2)+2./(45.*alpha**2))
       CALL BEEP@

C
C THE INTEGRAL IS PRINTED TOGETHER WITH MOLECULAR DATA USED
C

       WRITE(4,2266)
2266   FORMAT(1X,'THE A3 TERM CONTRIBUTION TO B(Rho) FOR SO2:')
       WRITE(4,2267)
2267   FORMAT(1X,'    ')
       CALL SECONDS_SINCE_1980@(FINISH)
       WRITE(4,2250)(FINISH-START)
2250   FORMAT(1X,'CPU time used = ',F12.3)
       WRITE(4,2260)FDATE@()
```

```
2260   FORMAT(1X,'Program run on  ',A30)
       WRITE(4,2269)
2269   FORMAT(1X,'    ')
       WRITE(4,1140)ANS
1140   FORMAT(1X,'THE INTEGRAL IS',E15.7)
       WRITE(4,2150)
2150   FORMAT(1X,'INPUT DATA:')
       WRITE(4,2155)TEMP
2155   FORMAT(1X,'TEMPERATURE:              ',F10.5)
       WRITE(4,9259)DIP
9259   FORMAT(1X,'DIPOLE MOMENT:            ',F10.5)
       WRITE(4,9260)ALPHA
9260   FORMAT(1X,'MEAN DYNAMIC ALPHA:       ',F10.5)
       WRITE(4,9261)A11
9261   FORMAT(1X,'DYNAMIC ALPHA11:          ',F10.5)
       WRITE(4,9262)A22
9262   FORMAT(1X,'DYNAMIC ALPHA22:          ',F10.5)
       WRITE(4,9263)A33
9263   FORMAT(1X,'DYNAMIC ALPHA33:          ',F10.5)
       WRITE(4,9265)DELTA2
9265   FORMAT(1X,'(DELTA DYNAMIC ALPHA)**2:',F10.5)
       WRITE(4,9264)ALSTAT
9264   FORMAT(1X,'MEAN STATIC ALPHA:        ',F10.5)
       WRITE(4,2190)Q1
2190   FORMAT(1X,'THETA11:                  ',F10.5)
       WRITE(4,2241)Q2
2241   FORMAT(1X,'THETA22:                  ',F10.5)
       WRITE(4,2210)R
2210   FORMAT(1X,'R(0):                        ',F6.5)
       WRITE(4,2220)SHAPE1
2220   FORMAT(1X,'SHAPE FACTOR 1:           ',F10.5)
       WRITE(4,2221)SHAPE2
2221   FORMAT(1X,'SHAPE FACTOR 2:           ',F10.5)
       WRITE(4,2230)PARAM2
2230   FORMAT(1X,'E/K:                       ',F9.5)
       WRITE(4,2235)AMIN1,AMAX1
2235   FORMAT(1X,'MIN AND MAX POINTS OF RANGE (64 INTERVALS):',2(F10.5,3
     + X))
       WRITE(4,2240)
2240   FORMAT(1X,'END B(Rho)')
       WRITE(4,2261)
2261   FORMAT(1X,'    ')
       WRITE(4,2262)
2262   FORMAT(1X,'    ')
       WRITE(4,2263)
2263   FORMAT(1X,'    ')
       WRITE(4,2264)
2264   FORMAT(1X,'    ')
       WRITE(4,2265)
2265   FORMAT(1X,'    ')

       END
```

A2.2 An example of a Fortran program to calculate contributions to B_K

```
      PROGRAM KSO2D2A3
C
C 29 JULY 1994.
C PROGRAM TO CALCULATE THE D2A3 TERM'S CONTRIBUTION TO B(Kerr) FOR SO2
C USING GAUSSIAN INTEGRATION WITH 64 INTERVALS FOR THE RANGE, AND
C 16 INTERVALS FOR ALL ANGULAR VARIABLES
C (I.E. ALPHA1, BETA1, GAMMA1, ALPHA2, BETA2 AND GAMMA2).
C DOUBLE PRECISION IS USED THROUGHOUT.
C

C ----------------------
C SYSTEM INITIALIZATION:
C ----------------------

      IMPLICIT DOUBLE PRECISION (A-H,O-Z)
      COMMON COEF1,DCTC
      DIMENSION COEF2(64,2),COEF1(16,2),SEP(64),AL1(16),BE1(16),GA1(16)
     + ,AL2(16),BE2(16),GA2(16),DCTC(9,16,16,16),FI(16,16,16,16,16),D1(6
     + 4),E1(16,16,16,16,16),F1(16,16,16,16,16),SE3(64),SE4(64),SE5(64),
     + SE6(64),SE8(64),SE12(64),G1(16,16,16),DDP(16,16,16,16,16),DQP(16,
     + 16,16,16,16),DIDP(16,16,16,16,16)
      INTEGER X1,X2,X3,X4,X5,X6,X7
      CHARACTER*30 FDATE@

C MOLECULAR DATA FOR SO2 (632.8 NM):

      SS1=0.000000
      SS2=0.000000
      SS3=0.000000
      SS4=0.000000
      SS5=0.000000
      SS6=0.000000
      SS7=0.000000
      DIP=-5.426200
      A11=5.80
      A22=3.30
      A33=3.88
      ALDYN=(A11+A22+A33)/3
      V11=5.347
      V22=3.027
      V33=3.548
      ALSTAT=(V11+V22+V33)/3
      Q1=-16.38000
      Q2=12.900000
      AMIN1=0.1000
      AMAX1=3.0000


C
C READ THE GAUSSIAN COEFFICIENTS FROM THE DATAFILE GAUSS64.DAT:
C
      OPEN(UNIT=10,FILE='GAUSS64.DAT')
        DO 10 ICTR1=1,64
          DO 20 ICTR2=1,2
            READ(10,1010,END=11)COEF2(ICTR1,ICTR2)
```

```
1010          FORMAT(F18.15)
20          CONTINUE
10        CONTINUE
11      CLOSE(UNIT=10)

C
C CALCULATE THE INTEGRATION POINTS FOR THE RANGE:
C
        SEP1=(AMAX1-AMIN1)/2
        SEP2=(AMAX1+AMIN1)/2
        DO 30 INDX=1,64
          SEP(INDX)=SEP1*COEF2(INDX,1)+SEP2
30      CONTINUE

C
C READ THE GAUSSIAN COEFFICIENTS FROM THE DATAFILE GAUSS16.DAT:
C
        OPEN(UNIT=11,FILE='GAUSS16.DAT')
  DO 100 ICTR1=1,16
            DO 110 ICTR2=1,2
              READ(11,6000,END=12)COEF1(ICTR1,ICTR2)
6000          FORMAT(F18.15)
110       CONTINUE
100     CONTINUE
12      CLOSE(UNIT=11)

C
C CALCULATE THE INTEGRATION POINTS FOR ALPHA1:
C
        AMIN=0.0
        AMAX=2.*3.14159265358979323846

        AL11=(AMAX-AMIN)/2.
        AL12=(AMAX+AMIN)/2.
        DO 120 INDX=1,16
          AL1(INDX)=AL11*COEF1(INDX,1)+AL12
120     CONTINUE

C
C CALCULATE THE INTEGRATION POINTS FOR BETA1:
C
        AMIN=0.0
        AMAX=3.14159265358979323846

        BE11=(AMAX-AMIN)/2.
        BE12=(AMAX+AMIN)/2.
        DO 121 INDX=1,16
          BE1(INDX)=BE11*COEF1(INDX,1)+BE12
121     CONTINUE

C
C CALCULATE THE INTEGRATION POINTS FOR GAMMA1:
C
        AMIN=0.0
        AMAX=2.*3.14159265358979323846

        GA11=(AMAX-AMIN)/2.
        GA12=(AMAX+AMIN)/2.
        DO 122 INDX=1,16
          GA1(INDX)=GA11*COEF1(INDX,1)+GA12
```

```
122     CONTINUE

C
C CALCULATE THE INTEGRATION POINTS FOR ALPHA2:
C
        AMIN=0.0
        AMAX=2.*3.14159265358979323846

        AL21=(AMAX-AMIN)/2.
        AL22=(AMAX+AMIN)/2.
        DO 123 INDX=1,16
          AL2(INDX)=AL21*COEF1(INDX,1)+AL22
123     CONTINUE

C
C CALCULATE THE INTEGRATION POINTS FOR BETA2:
C
        AMIN=0.0
        AMAX=3.14159265358979323846

        BE21=(AMAX-AMIN)/2.
        BE22=(AMAX+AMIN)/2.
        DO 124 INDX=1,16
          BE2(INDX)=BE21*COEF1(INDX,1)+BE22
124     CONTINUE

C
C CALCULATE THE INTEGRATION POINTS FOR GAMMA2:
C
        AMIN=0.0
        AMAX=2.*3.14159265358979323846

        GA21=(AMAX-AMIN)/2.
        GA22=(AMAX+AMIN)/2.
        DO 125 INDX=1,16
          GA2(INDX)=GA21*COEF1(INDX,1)+GA22
125     CONTINUE

C -------------
C MAIN PROGRAM:
C -------------

        OPEN(UNIT=4,FILE='LPT1')
        CALL BEEP@

C
C INPUT MOLECULAR PARAMETERS FROM THE KEYBOARD:
C

C        WRITE(6,470)
C470     FORMAT(1X,'INPUT THE TEMPERATURE (IN KELVIN)')
C        READ(5,471)TEMP
C471     FORMAT(F10.5)
        TEMP=457.0
        TEMPK=TEMP*1.380622E-23

C        WRITE(6,472)
C472     FORMAT(1X,'INPUT R(0) (IN nm)')
C        READ(5,473)R
C473     FORMAT(F10.5)
```

```
      R=0.3800
C      WRITE(6,474)
C474   FORMAT(1X,'E/K (IN K)')
C      READ(5,475)PARAM2
C475   FORMAT(F10.5)
      PARAM2=221.0
C      WRITE(6,476)
C476   FORMAT(1X,'SHAPE1 ')
C      READ(5,477)SHAPE1
C477   FORMAT(F10.5)
      SHAPE1=0.0000
C      WRITE(6,478)
C478   FORMAT(1X,'SHAPE2 ')
C      READ(5,479)SHAPE2
C479   FORMAT(F10.5)
      SHAPE2=0.0000
      CALL SECONDS_SINCE_1980@(START)

C
C CALCULATION OF THE LENNARD-JONES 6:12 POTENTIAL & STORAGE OF THE
C VALUES IN AN ARRAY:
C

      DO 61 X1=1,64

      D1(X1)=4.*PARAM2*1.380622E-23*((R/SEP(X1))**12-(R/SEP(X1))**6)
      SE3(X1)=SEP(X1)**3
      SE4(X1)=SEP(X1)**4
      SE5(X1)=SEP(X1)**5
      SE6(X1)=SEP(X1)**6
      SE8(X1)=SEP(X1)**8
      SE12(X1)=SEP(X1)**12

61    CONTINUE


C
C THE DIRECTION COSINE TENSOR COMPONENTS ARE STORED IN AN ARRAY:
C

      DO 66 X4=1,16
  DO 77 X3=1,16
    DO 88 X2=1,16

C
C DIRECTION COSINE TENSOR COMPONENTS:
C

      A1=COS(AL1(X2))*COS(BE1(X3))*COS(GA1(X4))-1.*SIN(AL1(X2))*SIN(GA1
     + (X4))
      A2=SIN(AL1(X2))*COS(BE1(X3))*COS(GA1(X4))+COS(AL1(X2))*SIN(GA1(X4
     + ))
      A3=-1.*SIN(BE1(X3))*COS(GA1(X4))
      A4=-1.*COS(AL1(X2))*COS(BE1(X3))*SIN(GA1(X4))-1.*SIN(AL1(X2))*COS
     + (GA1(X4))
      A5=-1.*SIN(AL1(X2))*COS(BE1(X3))*SIN(GA1(X4))+COS(AL1(X2))*COS(GA
     + 1(X4))
      A6=SIN(BE1(X3))*SIN(GA1(X4))
      A7=COS(AL1(X2))*SIN(BE1(X3))
      A8=SIN(AL1(X2))*SIN(BE1(X3))
```

```
        A9=COS(BE1(X3))

        DCTC(1,X2,X3,X4)=A1
        DCTC(2,X2,X3,X4)=A2
        DCTC(3,X2,X3,X4)=A3
        DCTC(4,X2,X3,X4)=A4
        DCTC(5,X2,X3,X4)=A5
        DCTC(6,X2,X3,X4)=A6
        DCTC(7,X2,X3,X4)=A7
        DCTC(8,X2,X3,X4)=A8
        DCTC(9,X2,X3,X4)=A9

88          CONTINUE
77        CONTINUE
66      CONTINUE


C
C THE MULTIPOLE INTERACTION ENERGIES ARE CALCULATED AND STORED
C IN ARRAYS:
C

        DO 939 X7=1,16
        WRITE(6,1000)X7
1000    FORMAT (1X, 'INDEX (IN RANGE 1 TO 16) IS CURRENTLY ',I2 )
  DO 40 X6=1,16
        WRITE(6,1111)X6
1111    FORMAT (1X, 'sub-index (in range 1 to 16) is currently ',I2 )
     DO 50 X5=1,16

C
C MOLECULE 2'S DIRECTION COSINE TENSOR COMPONENTS:
C

        B1=DCTC(1,X5,X6,X7)
        B2=DCTC(2,X5,X6,X7)
        B3=DCTC(3,X5,X6,X7)
        B4=DCTC(4,X5,X6,X7)
        B5=DCTC(5,X5,X6,X7)
        B6=DCTC(6,X5,X6,X7)
        B7=DCTC(7,X5,X6,X7)
        B8=DCTC(8,X5,X6,X7)
        B9=DCTC(9,X5,X6,X7)


      DO 60 X4=1,16
        DO 70 X3=1,16
   DO 80 X2=1,16

C
C MOLECULE 1'S DIRECTION COSINE TENSOR COMPONENTS:
C

        A1=DCTC(1,X2,X3,X4)
        A2=DCTC(2,X2,X3,X4)
        A3=DCTC(3,X2,X3,X4)
        A4=DCTC(4,X2,X3,X4)
        A5=DCTC(5,X2,X3,X4)
        A6=DCTC(6,X2,X3,X4)
        A7=DCTC(7,X2,X3,X4)
```

```
      A8=DCTC(8,X2,X3,X4)
      A9=DCTC(9,X2,X3,X4)

C
C CALCULATION OF THE DIPOLE-DIPOLE POTENTIAL:
C
      DDP(X2,X3,X4,X5,X6)=8.98758E-24*DIP**2*(-2*A9*B9+A6*B6+A3*B3)

C
C CALCULATION OF THE DIPOLE-QUADRUPOLE POTENTIAL:
C
      DQP(X2,X3,X4,X5,X6)=8.98758E-25*DIP*(Q2*(-2*A9*B9**2+(2*A6*B6+2*A
     + 3*B3+2*A9**2-2*A8**2-A6**2+A5**2-A3**2+A2**2)*B9+2*A9*B8**2+(-2*A
     + 6*B5-2*A3*B2)*B8+A9*B6**2+(2*A5*A8-2*A6*A9)*B6-A9*B5**2+A9*B3**2+
     + (2*A2*A8-2*A3*A9)*B3-A9*B2**2)+Q1*(-2*A9*B9**2+(2*A6*B6+2*A3*B3+2
     + *A9**2-2*A7**2-A6**2+A4**2-A3**2+A1**2)*B9+2*A9*B7**2+(-2*A6*B4-2
     + *A3*B1)*B7+A9*B6**2+(2*A4*A7-2*A6*A9)*B6-A9*B4**2+A9*B3**2+(2*A1*
     + A7-2*A3*A9)*B3-A9*B1**2))

C
C CALCULATION OF THE DIPOLE-INDUCED DIPOLE POTENTIAL:
C
      DIDP(X2,X3,X4,X5,X6)=-0.50*ALSTAT*8.07765E-27*DIP**2*(3*B9**2
     + +3*A9**2-2)

C
C CALCULATION OF THE QUADRUPOLE-QUADRUPOLE POTENTIAL:
C
      QUAD1=-16.*(A6*A9-A5*A8)*(B6*B9-B5*B8)-16.*(A3*A9-A2*A8)*(B3*B9-B
     + 2*B8)+4.*(2.*A9**2-2.*A8**2-A6**2+A5**2-A3**2+A2**2)*(B9-B8)*(B9+
     + B8)+(-4.*A9**2+4.*A8**2+3.*A6**2-3.*A5**2+A3**2-A2**2)*(B6**2-B5*
     + *2)+4.*(A3*A6-A2*A5)*(B3*B6-B2*B5)+(-4.*A9**2+4.*A8**2+A6**2-A5**
     + 2+3.*A3**2-3.*A2**2)*(B3**2-B2**2)

      QUAD2=-16.*(A6*A9-A4*A7)*(B6*B9-B4*B7)-16.*(A3*A9-A1*A7)*(B3*B9-B
     + 1*B7)+4.*(2.*A9**2-2.*A7**2-A6**2+A4**2-A3**2+A1**2)*(B9-B7)*(B9+
     + B7)+(-4.*A9**2+4.*A7**2+3.*A6**2-3.*A4**2+A3**2-A1**2)*(B6**2-B4*
     + *2)+4.*(A3*A6-A1*A4)*(B3*B6-B1*B4)+(-4.*A9**2+4.*A7**2+A6**2-A4**
     + 2+3.*A3**2-3.*A1**2)*(B3**2-B1**2)

      QUAD3=4.*(4.*A9**2-2.*(A8**2+A7**2+A6**2+A3**2)+A5**2+A4**2+A2**2
     + +A1**2)*B9**2-16.*(2.*A6*A9-A5*A8-A4*A7)*B6*B9-16*(2.*A3*A9-A2*A8
     + -A1*A7)*B3*B9-4.*(2.*A9**2-2.*A7**2-A6**2+A4**2-A3**2+A1**2)*B8**
     + 2+16.*(A6*A9-A4*A7)*B5*B8+16.*(A3*A9-A1*A7)*B2*B8-4.*(2.*A9**2-2.
     + *A8**2-A6**2+A5**2-A3**2+A2**2)*B7**2+16.*(A6*A9-A5*A8)*B4*B7+16.
     + *(A3*A9-A2*A8)*B1*B7+(-8.*A9**2+4.*(A8**2+A7**2)+6.*A6**2-3.*(A5*
     + *2+A4**2)+2*A3**2-A2**2-A1**2)*B6**2+4.*(2.*A3*A6-A2*A5-A1*A4)*B3
     + *B6+(4.*A9**2-4.*A7**2-3.*A6**2+3.*A4**2-A3**2+A1**2)*B5**2-4.*(A
     + 3*A6-A1*A4)*B2*B5+(4.*A9**2-4.*A8**2-3.*A6**2+3.*A5**2-A3**2+A2**
     + 2)*B4**2-4.*(A3*A6-A2*A5)*B1*B4+(-8.*A9**2+4.*(A8**2+A7**2)+2.*A6
     + **2-A5**2-A4**2+6.*A3**2-3.*(A2**2+A1**2))*B3**2+(4.*A9**2-4.*A7*
     + *2-A6**2+A4**2-3.*A3**2+3.*A1**2)*B2**2+(4.*A9**2-4.*A8**2-A6**2+
     + A5**2-3.*A3**2+3.*A2**2)*B1**2

      E1(X2,X3,X4,X5,X6)=8.98758E-26*(1./3.)*(Q2**2*QUAD1+Q1**2*QUAD
     + 2+Q1*Q2*QUAD3)


C
C CALCULATION OF THE QUADRUPOLE-INDUCED DIPOLE POTENTIAL:
```

```
C
      QID1=Q2**2*(4.*A9**4+(-8.*A8**2+4.*A5**2+4.*A2**2)*A9**2+(-8.*A5*
     + A6-8.*A2*A3)*A8*A9+4.*A8**4+(4.*A6**2+4.*A3**2)*A8**2+A6**4+(-2.*
     + A5**2+2.*A3**2-2.*A2**2)*A6**2+A5**4+(2.*A2**2-2.*A3**2)*A5**2+A3
     + **4-2.*A2**2*A3**2+A2**4)+Q1**2*(4.*A9**4+(-8.*A7**2+4.*A4**2+4.*
     + A1**2)*A9**2+(-8.*A4*A6-8.*A1*A3)*A7*A9+4.*A7**4+(4.*A6**2+4.*A3*
     + *2)*A7**2+A6**4+(-2.*A4**2+2.*A3**2-2.*A1**2)*A6**2+A4**4+(2.*A1*
     + *2-2.*A3**2)*A4**2+A3**4-2.*A1**2*A3**2+A1**4)+Q1*Q2*(8.*A9**4+(-
     + 8.*A8**2-8.*A7**2+4.*A5**2+4.*A4**2+4.*A2**2+4.*A1**2)*A9**2+((-8
     + .*A5*A6-8.*A2*A3)*A8+(-8.*A4*A6-8.*A1*A3)*A7)*A9+(8.*A7**2+4.*A6*
     + *2-4.*A4**2+4.*A3**2-4.*A1**2)*A8**2+(8.*A4*A5+8.*A1*A2)*A7*A8+(4
     + .*A6**2-4.*A5**2+4.*A3**2-4.*A2**2)*A7**2+2.*A6**4+(-2.*A5**2-2.*
     + A4**2+4.*A3**2-2.*A2**2-2.*A1**2)*A6**2+(2.*A4**2-2.*A3**2+2.*A1*
     + *2)*A5**2+(2.*A2**2-2.*A3**2)*A4**2+2.*A3**4+(-2.*A2**2-2.*A1**2)
     + *A3**2+2.*A1**2*A2**2)

      QID2=Q2**2*(4.*B9**4+(-8.*B8**2+4.*B5**2+4.*B2**2)*B9**2+(-8.*B5*
     + B6-8.*B2*B3)*B8*B9+4.*B8**4+(4.*B6**2+4.*B3**2)*B8**2+B6**4+(-2.*
     + B5**2+2.*B3**2-2.*B2**2)*B6**2+B5**4+(2.*B2**2-2.*B3**2)*B5**2+B3
     + **4-2.*B2**2*B3**2+B2**4)+Q1**2*(4.*B9**4+(-8.*B7**2+4.*B4**2+4.*
     + B1**2)*B9**2+(-8.*B4*B6-8.*B1*B3)*B7*B9+4.*B7**4+(4.*B6**2+4.*B3*
     + *2)*B7**2+B6**4+(-2.*B4**2+2.*B3**2-2.*B1**2)*B6**2+B4**4+(2.*B1*
     + *2-2.*B3**2)*B4**2+B3**4-2.*B1**2*B3**2+B1**4)+Q1*Q2*(8.*B9**4+(-
     + 8.*B8**2-8.*B7**2+4.*B5**2+4.*B4**2+4.*B2**2+4.*B1**2)*B9**2+((-8
     + .*B5*B6-8.*B2*B3)*B8+(-8.*B4*B6-8.*B1*B3)*B7)*B9+(8.*B7**2+4.*B6*
     + *2-4.*B4**2+4.*B3**2-4.*B1**2)*B8**2+(8.*B4*B5+8.*B1*B2)*B7*B8+(4
     + .*B6**2-4.*B5**2+4.*B3**2-4.*B2**2)*B7**2+2.*B6**4+(-2.*B5**2-2.*
     + B4**2+4.*B3**2-2.*B2**2-2.*B1**2)*B6**2+(2.*B4**2-2.*B3**2+2.*B1*
     + *2)*B5**2+(2.*B2**2-2.*B3**2)*B4**2+2.*B3**4+(-2.*B2**2-2.*B1**2)
     + *B3**2+2.*B1**2*B2**2)

      F1(X2,X3,X4,X5,X6)=-0.5*8.07765E-29*ALSTAT*(QID1+QID2)

C
C CALCULATION OF THE INTEGRATION ARGUMENT:
C

      T11=2.*A7**2-A4**2-A1**2
      T22=2.*A8**2-A5**2-A2**2
      T33=2.*A9**2-A6**2-A3**2
      T12=2.*A7*A8-A4*A5-A1*A2
      T13=2.*A7*A9-A4*A6-A1*A3
      T23=2.*A8*A9-A5*A6-A2*A3

      Z11 = A33*(A7**2*B9**2+(2*A4*A7*B6+2*A1*A7*B3)*B9+A4**2*B6**2+2*A
     +   1*A4*B3*B6+A1**2*B3**2)+A22*(A7**2*B8**2+(2*A4*A7*B5+2*A1*A7*B2
     +   )*B8+A4**2*B5**2+2*A1*A4*B2*B5+A1**2*B2**2)+A11*(A7**2*B7**2+(2
     +   *A4*A7*B4+2*A1*A7*B1)*B7+A4**2*B4**2+2*A1*A4*B1*B4+A1**2*B1**2)

      Z22 = A33*(A8**2*B9**2+(2*A5*A8*B6+2*A2*A8*B3)*B9+A5**2*B6**2+2*A
     +   2*A5*B3*B6+A2**2*B3**2)+A22*(A8**2*B8**2+(2*A5*A8*B5+2*A2*A8*B2
     +   )*B8+A5**2*B5**2+2*A2*A5*B2*B5+A2**2*B2**2)+A11*(A8**2*B7**2+(2
     +   *A5*A8*B4+2*A2*A8*B1)*B7+A5**2*B4**2+2*A2*A5*B1*B4+A2**2*B1**2)

      Z33 = A33*(A9**2*B9**2+(2*A6*A9*B6+2*A3*A9*B3)*B9+A6**2*B6**2+2*A
     +   3*A6*B3*B6+A3**2*B3**2)+A22*(A9**2*B8**2+(2*A6*A9*B5+2*A3*A9*B2
     +   )*B8+A6**2*B5**2+2*A3*A6*B2*B5+A3**2*B2**2)+A11*(A9**2*B7**2+(2
     +   *A6*A9*B4+2*A3*A9*B1)*B7+A6**2*B4**2+2*A3*A6*B1*B4+A3**2*B1**2)
```

```
      Z12 = A33*(A7*A8*B9**2+((A4*A8+A5*A7)*B6+(A1*A8+A2*A7)*B3)*B9+A4*
     +   A5*B6**2+(A1*A5+A2*A4)*B3*B6+A1*A2*B3**2)+A22*(A7*A8*B8**2+((A4
     +   *A8+A5*A7)*B5+(A1*A8+A2*A7)*B2)*B8+A4*A5*B5**2+(A1*A5+A2*A4)*B2
     +   *B5+A1*A2*B2**2)+A11*(A7*A8*B7**2+((A4*A8+A5*A7)*B4+(A1*A8+A2*A
     +   7)*B1)*B7+A4*A5*B4**2+(A1*A5+A2*A4)*B1*B4+A1*A2*B1**2)

      Z13 = A33*(A7*A9*B9**2+((A4*A9+A6*A7)*B6+(A1*A9+A3*A7)*B3)*B9+A4*
     +   A6*B6**2+(A1*A6+A3*A4)*B3*B6+A1*A3*B3**2)+A22*(A7*A9*B8**2+((A4
     +   *A9+A6*A7)*B5+(A1*A9+A3*A7)*B2)*B8+A4*A6*B5**2+(A1*A6+A3*A4)*B2
     +   *B5+A1*A3*B2**2)+A11*(A7*A9*B7**2+((A4*A9+A6*A7)*B4+(A1*A9+A3*A
     +   7)*B1)*B7+A4*A6*B4**2+(A1*A6+A3*A4)*B1*B4+A1*A3*B1**2)

      Z23 = A33*(A8*A9*B9**2+((A5*A9+A6*A8)*B6+(A2*A9+A3*A8)*B3)*B9+A5*
     +   A6*B6**2+(A2*A6+A3*A5)*B3*B6+A2*A3*B3**2)+A22*(A8*A9*B8**2+((A5
     +   *A9+A6*A8)*B5+(A2*A9+A3*A8)*B2)*B8+A5*A6*B5**2+(A2*A6+A3*A5)*B2
     +   *B5+A2*A3*B2**2)+A11*(A8*A9*B7**2+((A5*A9+A6*A8)*B4+(A2*A9+A3*A
     +   8)*B1)*B7+A5*A6*B4**2+(A2*A6+A3*A5)*B1*B4+A2*A3*B1**2)

      W11 = V33*(A7**2*B9**2+(2*A4*A7*B6+2*A1*A7*B3)*B9+A4**2*B6**2+2*A
     +   1*A4*B3*B6+A1**2*B3**2)+V22*(A7**2*B8**2+(2*A4*A7*B5+2*A1*A7*B2
     +   )*B8+A4**2*B5**2+2*A1*A4*B2*B5+A1**2*B2**2)+V11*(A7**2*B7**2+(2
     +   *A4*A7*B4+2*A1*A7*B1)*B7+A4**2*B4**2+2*A1*A4*B1*B4+A1**2*B1**2)

      W22 = V33*(A8**2*B9**2+(2*A5*A8*B6+2*A2*A8*B3)*B9+A5**2*B6**2+2*A
     +   2*A5*B3*B6+A2**2*B3**2)+V22*(A8**2*B8**2+(2*A5*A8*B5+2*A2*A8*B2
     +   )*B8+A5**2*B5**2+2*A2*A5*B2*B5+A2**2*B2**2)+V11*(A8**2*B7**2+(2
     +   *A5*A8*B4+2*A2*A8*B1)*B7+A5**2*B4**2+2*A2*A5*B1*B4+A2**2*B1**2)

      W33 = V33*(A9**2*B9**2+(2*A6*A9*B6+2*A3*A9*B3)*B9+A6**2*B6**2+2*A
     +   3*A6*B3*B6+A3**2*B3**2)+V22*(A9**2*B8**2+(2*A6*A9*B5+2*A3*A9*B2
     +   )*B8+A6**2*B5**2+2*A3*A6*B2*B5+A3**2*B2**2)+V11*(A9**2*B7**2+(2
     +   *A6*A9*B4+2*A3*A9*B1)*B7+A6**2*B4**2+2*A3*A6*B1*B4+A3**2*B1**2)

      W12 = V33*(A7*A8*B9**2+((A4*A8+A5*A7)*B6+(A1*A8+A2*A7)*B3)*B9+A4*
     +   A5*B6**2+(A1*A5+A2*A4)*B3*B6+A1*A2*B3**2)+V22*(A7*A8*B8**2+((A4
     +   *A8+A5*A7)*B5+(A1*A8+A2*A7)*B2)*B8+A4*A5*B5**2+(A1*A5+A2*A4)*B2
     +   *B5+A1*A2*B2**2)+V11*(A7*A8*B7**2+((A4*A8+A5*A7)*B4+(A1*A8+A2*A
     +   7)*B1)*B7+A4*A5*B4**2+(A1*A5+A2*A4)*B1*B4+A1*A2*B1**2)

      W13 = V33*(A7*A9*B9**2+((A4*A9+A6*A7)*B6+(A1*A9+A3*A7)*B3)*B9+A4*
     +   A6*B6**2+(A1*A6+A3*A4)*B3*B6+A1*A3*B3**2)+V22*(A7*A9*B8**2+((A4
     +   *A9+A6*A7)*B5+(A1*A9+A3*A7)*B2)*B8+A4*A6*B5**2+(A1*A6+A3*A4)*B2
     +   *B5+A1*A3*B2**2)+V11*(A7*A9*B7**2+((A4*A9+A6*A7)*B4+(A1*A9+A3*A
     +   7)*B1)*B7+A4*A6*B4**2+(A1*A6+A3*A4)*B1*B4+A1*A3*B1**2)

      W23 = V33*(A8*A9*B9**2+((A5*A9+A6*A8)*B6+(A2*A9+A3*A8)*B3)*B9+A5*
     +   A6*B6**2+(A2*A6+A3*A5)*B3*B6+A2*A3*B3**2)+V22*(A8*A9*B8**2+((A5
     +   *A9+A6*A8)*B5+(A2*A9+A3*A8)*B2)*B8+A5*A6*B5**2+(A2*A6+A3*A5)*B2
     +   *B5+A2*A3*B2**2)+V11*(A8*A9*B7**2+((A5*A9+A6*A8)*B4+(A2*A9+A3*A
     +   8)*B1)*B7+A5*A6*B4**2+(A2*A6+A3*A5)*B1*B4+A2*A3*B1**2)


      O1=A7*B9+A4*B6+A1*B3
      O2=A8*B9+A5*B6+A2*B3
      O3=A9*B9+A6*B6+A3*B3

C(c593) FORTRAN(6*D426);
       TERM1=-6*DIP**2*
     +   (((ALDYN-A33)*O3**2*T33**2+((2*ALDYN-2*A33)*O2*O3*T23+(2*
     1   ALDYN-2*A33)*O1*O3*T13)*T33+(ALDYN-A33)*O2**2*T23**2+(2*ALDYN-2
```

```
     2   *A33)*O1*O2*T13*T23+(ALDYN-A33)*O1**2*T13**2)*V33**2+((ALDYN-A2
     3   2)*O3**2*T23**2+((2*ALDYN-2*A22)*O2*O3*T22+(2*ALDYN-2*A22)*O1*O
     4   3*T12)*T23+(ALDYN-A22)*O2**2*T22**2+(2*ALDYN-2*A22)*O1*O2*T12*T
     5   22+(ALDYN-A22)*O1**2*T12**2)*V22**2+((ALDYN-A11)*O3**2*T13**2+(
     6   (2*ALDYN-2*A11)*O2*O3*T12+(2*ALDYN-2*A11)*O1*O3*T11)*T13+(ALDYN
     7   -A11)*O2**2*T12**2+(2*ALDYN-2*A11)*O1*O2*T11*T12+(ALDYN-A11)*O1
     8   **2*T11**2)*V11**2)

C(c594) FORTRAN(2*D454);
      TERM2=2*
     +(3*DIP**2*(A33*((O3*T33**2+(O2*T23+O1*T13)*T33)*V33*Z33+(O3*T23*T
     1   33+O2*T23**2+O1*T13*T23)*V33*Z23+(O3*T13*T33+O2*T13*T23+O1*T13*
     2   *2)*V33*Z13)+A22*((O3*T23**2+(O2*T22+O1*T12)*T23)*V22*Z33+(O3*T
     3   22*T23+O2*T22**2+O1*T12*T22)*V22*Z23+(O3*T12*T23+O2*T12*T22+O1*
     4   T12**2)*V22*Z13)+A11*((O3*T13**2+(O2*T12+O1*T11)*T13)*V11*Z33+(
     5   O3*T12*T13+O2*T12**2+O1*T11*T12)*V11*Z23+(O3*T11*T13+O2*T11*T12
     6  +O1*T11**2)*V11*Z13))-2*DIP**2*(O3*T33+O2*T23+O1*T13)*V33*(A33*(
     7   T33*Z33+T23*Z23+T13*Z13)+A22*(T23*Z23+T22*Z22+T12*Z12)+A11*(T13
     8  *Z13+T12*Z12+T11*Z11))+3*A33*DIP**2*((O3*T33**2+(O2*T23+O1*T13)*
     9   T33)*V33*Z33+((O3*T23*T33+O2*T23**2+O1*T13*T23)*V33+(O3*T23+O2*
     :   T22+O1*T12)*T33*V22)*Z23+(O3*T23**2+(O2*T22+O1*T12)*T23)*V22*Z2
     ;   2+((O3*T13*T33+O2*T13*T23+O1*T13**2)*V33+(O3*T13+O2*T12+O1*T11)
     <   *T33*V11)*Z13+((O3*T13*T23+O2*T13*T22+O1*T12*T13)*V22+(O3*T13+O
     =   2*T12+O1*T11)*T23*V11)*Z12+(O3*T13**2+(O2*T12+O1*T11)*T13)*V11*
     >   Z11))

C(c595) FORTRAN(6*D469);
      TERM3=-6*
     + (ALDYN-A33)*DIP**2*V33*(T33**2*W33+2*T23*T33*W23+T23**2*W22+2*T1
     1   3*T33*W13+2*T13*T23*W12+T13**2*W11)

C(c596) FORTRAN(2*D477);
      TERM4=-2*
     +DIP**2*(A33**2*(-2*T33**2*Z33-4*T23*T33*Z23-2*T23**2*Z22-4*T13*T
     1   33*Z13-4*T13*T23*Z12-2*T13**2*Z11)+A22**2*(T23**2*Z33+2*T22*T23
     2   *Z23+T22**2*Z22+2*T12*T23*Z13+2*T12*T22*Z12+T12**2*Z11)+A11**2*
     3   (T13**2*Z33+2*T12*T13*Z23+T12**2*Z22+2*T11*T13*Z13+2*T11*T12*Z1
     4   2+T11**2*Z11))

C(c597) FORTRAN(6*D485);

      TERM5=-6*
     +DIP**2*((ALDYN-A33)*T33**2*W33**2+((2*ALDYN-2*A33)*T23*T33*W23+(
     1   2*ALDYN-2*A33)*T13*T33*W13)*W33+((ALDYN-A22)*T33**2+(ALDYN-A33)
     2   *T23**2)*W23**2+((2*ALDYN-2*A22)*T23*T33*W22+(2*ALDYN-2*A33)*T1
     3   3*T23*W13+(2*ALDYN-2*A22)*T13*T33*W12)*W23+(ALDYN-A22)*T23**2*W
     4   22**2+(2*ALDYN-2*A22)*T13*T23*W12*W22+((ALDYN-A11)*T33**2+(ALDY
     5   N-A33)*T13**2)*W13**2+((2*ALDYN-2*A11)*T23*T33*W12+(2*ALDYN-2*A
     6   11)*T13*T33*W11)*W13+((ALDYN-A11)*T23**2+(ALDYN-A22)*T13**2)*W1
     7   2**2+(2*ALDYN-2*A11)*T13*T23*W11*W12+(ALDYN-A11)*T13**2*W11**2)

C(c598) FORTRAN(2*D504);
      TERM6A=-2*
     +(3*DIP**2*(A33*((O3*T33**2*W33+O3*T23*T33*W23+O3*T13*T33*W13)*Z33
     1   +((O2*T33**2+O3*T23*T33)*W33+(O2*T23*T33+O3*T23**2)*W23+(O2*T13
     2   *T33+O3*T13*T23)*W13)*Z23+(O2*T23*T33*W33+O2*T23**2*W23+O2*T13*
     3   T23*W13)*Z22+((O1*T33**2+O3*T13*T33)*W33+(O1*T23*T33+O3*T13*T23
     4   )*W23+(O1*T13*T33+O3*T13**2)*W13)*Z13+((O1*T23+O2*T13)*T33*W33+
     5   (O1*T23**2+O2*T13*T23)*W23+(O1*T13*T23+O2*T13**2)*W13)*Z12+(O1*
     6   T13*T33*W33+O1*T13*T23*W23+O1*T13**2*W13)*Z11)+A22*((O3*T23*T33
```

```
     7    *W23+O3*T23**2*W22+O3*T13*T23*W12)*Z33+((O2*T23+O3*T22)*T33*W23
     8    +(O2*T23**2+O3*T22*T23)*W22+(O2*T13*T23+O3*T13*T22)*W12)*Z23+(O
     9    2*T22*T33*W23+O2*T22*T23*W22+O2*T13*T22*W12)*Z22+((O1*T23+O3*T1
     :    2)*T33*W23+(O1*T23**2+O3*T12*T23)*W22+(O1*T13*T23+O3*T12*T13)*W
     ;    12)*Z13+((O1*T22+O2*T12)*T33*W23+(O1*T22+O2*T12)*T23*W22+(O1*T1
     <    3*T22+O2*T12*T13)*W12)*Z12+(O1*T12*T33*W23+O1*T12*T23*W22+O1*T1
     =    2*T13*W12)*Z11)+A11*((O3*T13*T33*W13+O3*T13*T23*W12+O3*T13**2*W
     >    11)*Z33+((O2*T13+O3*T12)*T33*W13+(O2*T13+O3*T12)*T23*W12+(O2*T1
     ?    3**2+O3*T12*T13)*W11)*Z23+(O2*T12*T33*W13+O2*T12*T23*W12+O2*T12
     @    *T13*W11)*Z22+((O1*T13+O3*T11)*T33*W13+(O1*T13+O3*T11)*T23*W12+
     1    (O1*T13**2+O3*T11*T13)*W11)*Z13+((O1*T12+O2*T11)*T33*W13+(O1*T1
     2    2+O2*T11)*T23*W12+(O1*T12+O2*T11)*T13*W11)*Z12+(O1*T11*T33*W13+
     3    O1*T11*T23*W12+O1*T11*T13*W11)*Z11)))
      TERM6B=-2*(3*DIP**2*(A33*((O3*T33**2*W
     4    33+O3*T23*T33*W23+O3*T13*T33*W13)*Z33+(O3*T23*T33*W33+(O3*T33**
     5    2+O3*T23**2)*W23+O3*T23*T33*W22+O3*T13*T23*W13+O3*T13*T33*W12)*
     6    Z23+(O3*T23*T33*W23+O3*T23**2*W22+O3*T13*T23*W12)*Z22+(O3*T13*T
     7    33*W33+O3*T13*T23*W23+(O3*T33**2+O3*T13**2)*W13+O3*T23*T33*W12+
     8    O3*T13*T33*W11)*Z13+(O3*T13*T33*W23+O3*T13*T23*W22+O3*T23*T33*W
     9    13+(O3*T23**2+O3*T13**2)*W12+O3*T13*T23*W11)*Z12+(O3*T13*T33*W1
     :    3+O3*T13*T23*W12+O3*T13**2*W11)*Z11)+A22*((O2*T23*T33*W33+O2*T2
     ;    3**2*W23+O2*T13*T23*W13)*Z33+(O2*T22*T33*W33+(O2*T23*T33+O2*T22
     <    *T23)*W23+O2*T23**2*W22+O2*T13*T22*W13+O2*T13*T23*W12)*Z23+(O2*
     =    T22*T33*W23+O2*T22*T23*W22+O2*T13*T22*W12)*Z22+(O2*T12*T33*W33+
     >    O2*T12*T23*W23+(O2*T23*T33+O2*T12*T13)*W13+O2*T23**2*W12+O2*T13
     ?    *T23*W11)*Z13+(O2*T12*T33*W23+O2*T12*T23*W22+O2*T22*T33*W13+(O2
     @    *T22*T23+O2*T12*T13)*W12+O2*T13*T22*W11)*Z12+(O2*T12*T33*W13+O2
     1    *T12*T23*W12+O2*T12*T13*W11)*Z11)+A11*((O1*T13*T33*W33+O1*T13*T
     2    23*W23+O1*T13**2*W13)*Z33+(O1*T12*T33*W33+(O1*T13*T33+O1*T12*T2
     3    3)*W23+O1*T13*T23*W22+O1*T12*T13*W13+O1*T13**2*W12)*Z23+(O1*T12
     4    *T33*W23+O1*T12*T23*W22+O1*T12*T13*W12)*Z22+(O1*T11*T33*W33+O1*
     5    T11*T23*W23+(O1*T13*T33+O1*T11*T13)*W13+O1*T13*T23*W12+O1*T13**
     6    2*W11)*Z13+(O1*T11*T33*W23+O1*T11*T23*W22+O1*T12*T33*W13+(O1*T1
     7    2*T23+O1*T11*T13)*W12+O1*T12*T13*W11)*Z12+(O1*T11*T33*W13+O1*T1
     8    1*T23*W12+O1*T11*T13*W11)*Z11)))
      TERM6C=-2*(-2*DIP**2*(O3*T33*W33+(O2*T33+O3*
     9    T23)*W23+O2*T23*W22+(O1*T33+O3*T13)*W13+(O1*T23+O2*T13)*W12+O1*
     :    T13*W11)*(A33*(T33*Z33+T23*Z23+T13*Z13)+A22*(T23*Z23+T22*Z22+T1
     ;    2*Z12)+A11*(T13*Z13+T12*Z12+T11*Z11)))

        TERM6=TERM6A+TERM6B+TERM6C

C(c599) FORTRAN(6*D519);
       TERM7A=-6*DIP**2*
     +((((ALDYN-A33)*O3**2*T33**2+((ALDYN-A33)*O2*O3*T23+(ALDYN
     1    -A33)*O1*O3*T13)*T33)*V33+((ALDYN-A33)*O3**2*T23**2+((ALDYN-A33
     2    )*O2*O3*T22+(ALDYN-A33)*O1*O3*T12)*T23)*V22+((ALDYN-A33)*O3**2*
     3    T13**2+((ALDYN-A33)*O2*O3*T12+(ALDYN-A33)*O1*O3*T11)*T13)*V11)*
     4    W33+(((ALDYN-A22)*O2*O3*T33**2+(((ALDYN-A33)*O3**2+(ALDYN-A22)*
     5    O2**2)*T23+(ALDYN-A22)*O1*O2*T13)*T33+(ALDYN-A33)*O2*O3*T23**2+
     6    (ALDYN-A33)*O1*O3*T13*T23)*V33+((ALDYN-A22)*O2*O3*T23**2+(((ALD
     7    YN-A33)*O3**2+(ALDYN-A22)*O2**2)*T22+(ALDYN-A22)*O1*O2*T12)*T23
     8    +(ALDYN-A33)*O2*O3*T22**2+(ALDYN-A33)*O1*O3*T12*T22)*V22+((ALDY
     9    N-A22)*O2*O3*T13**2+(((ALDYN-A33)*O3**2+(ALDYN-A22)*O2**2)*T12+
     :    (ALDYN-A22)*O1*O2*T11)*T13+(ALDYN-A33)*O2*O3*T12**2+(ALDYN-A33)
     ;    *O1*O3*T11*T12)*V11)*W23+(((ALDYN-A22)*O2*O3*T23*T33+(ALDYN-A22
     <    )*O2**2*T23**2+(ALDYN-A22)*O1*O2*T13*T23)*V33+((ALDYN-A22)*O2*O
     =    3*T22*T23+(ALDYN-A22)*O2**2*T22**2+(ALDYN-A22)*O1*O2*T12*T22)*V
     >    22+((ALDYN-A22)*O2*O3*T12*T13+(ALDYN-A22)*O2**2*T12**2+(ALDYN-A
     ?    22)*O1*O2*T11*T12)*V11)*W22+(((ALDYN-A11)*O1*O3*T33**2+((ALDYN-
```

```
     @    A11)*O1*O2*T23+((ALDYN-A33)*O3**2+(ALDYN-A11)*O1**2)*T13)*T33+(
     1    ALDYN-A33)*O2*O3*T13*T23+(ALDYN-A33)*O1*O3*T13**2)*V33+((ALDYN-
     2    A11)*O1*O3*T23**2+((ALDYN-A11)*O1*O2*T22+((ALDYN-A33)*O3**2+(AL
     3    DYN-A11)*O1**2)*T12)*T23+(ALDYN-A33)*O2*O3*T12*T22+(ALDYN-A33)*
     4    O1*O3*T12**2)*V22+((ALDYN-A11)*O1*O3*T13**2+((ALDYN-A11)*O1*O2*
     5    T12+((ALDYN-A33)*O3**2+(ALDYN-A11)*O1**2)*T11)*T13+(ALDYN-A33)*
     6    O2*O3*T11*T12+(ALDYN-A33)*O1*O3*T11**2)*V11)*W13)

      TERM7B=-6*DIP**2*(((((ALDYN-A11)
     7    *O1*O3*T23+(ALDYN-A22)*O2*O3*T13)*T33+(ALDYN-A11)*O1*O2*T23**2+
     8    ((ALDYN-A22)*O2**2+(ALDYN-A11)*O1**2)*T13*T23+(ALDYN-A22)*O1*O2
     9    *T13**2)*V33+(((ALDYN-A11)*O1*O3*T22+(ALDYN-A22)*O2*O3*T12)*T23
     :    +(ALDYN-A11)*O1*O2*T22**2+((ALDYN-A22)*O2**2+(ALDYN-A11)*O1**2)
     ;    *T12*T22+(ALDYN-A22)*O1*O2*T12**2)*V22+(((ALDYN-A11)*O1*O3*T12+
     <    (ALDYN-A22)*O2*O3*T11)*T13+(ALDYN-A11)*O1*O2*T12**2+((ALDYN-A22
     =    )*O2**2+(ALDYN-A11)*O1**2)*T11*T12+(ALDYN-A22)*O1*O2*T11**2)*V1
     >    1)*W12+(((ALDYN-A11)*O1*O3*T13*T33+(ALDYN-A11)*O1*O2*T13*T23+(A
     ?    LDYN-A11)*O1**2*T13**2)*V33+((ALDYN-A11)*O1*O3*T12*T23+(ALDYN-A
     @    11)*O1*O2*T12*T22+(ALDYN-A11)*O1**2*T12**2)*V22+((ALDYN-A11)*O1
     1    *O3*T11*T13+(ALDYN-A11)*O1*O2*T11*T12+(ALDYN-A11)*O1**2*T11**2)
     2    *V11)*W11)

         TERM7=TERM7A+TERM7B

C(c600) FORTRAN(2*D530);
      TERM8=-2*
     +DIP**2*(A11*(A33*(-6*O1*O3*T13*T33*Z33+(-6*O1*O3*T12*T33-6*O1*O3
     1    *T13*T23)*Z23-6*O1*O3*T12*T23*Z22+(-6*O1*O3*T11*T33-6*O1*O3*T13
     2    **2)*Z13+(-6*O1*O3*T11*T23-6*O1*O3*T12*T13)*Z12-6*O1*O3*T11*T13
     3    *Z11)+A22*(-6*O1*O2*T13*T23*Z33+(-6*O1*O2*T12*T23-6*O1*O2*T13*T
     4    22)*Z23-6*O1*O2*T12*T22*Z22+(-6*O1*O2*T11*T23-6*O1*O2*T12*T13)*
     5    Z13+(-6*O1*O2*T11*T22-6*O1*O2*T12**2)*Z12-6*O1*O2*T11*T12*Z11))
     6    +A33**2*((-2*O3**2+O2**2+O1**2)*T33**2*Z33+(-4*O3**2+2*O2**2+2*
     7    O1**2)*T23*T33*Z23+(-2*O3**2+O2**2+O1**2)*T23**2*Z22+(-4*O3**2+
     8    2*O2**2+2*O1**2)*T13*T33*Z13+(-4*O3**2+2*O2**2+2*O1**2)*T13*T23
     9    *Z12+(-2*O3**2+O2**2+O1**2)*T13**2*Z11)+A22*A33*(-6*O2*O3*T23*T
     :    33*Z33+(-6*O2*O3*T22*T33-6*O2*O3*T23**2)*Z23-6*O2*O3*T22*T23*Z2
     ;    2+(-6*O2*O3*T12*T33-6*O2*O3*T13*T23)*Z13+(-6*O2*O3*T12*T23-6*O2
     <    *O3*T13*T22)*Z12-6*O2*O3*T12*T13*Z11)+A22**2*((O3**2-2*O2**2+O1
     =    **2)*T23**2*Z33+(2*O3**2-4*O2**2+2*O1**2)*T22*T23*Z23+(O3**2-2*
     >    O2**2+O1**2)*T22**2*Z22+(2*O3**2-4*O2**2+2*O1**2)*T12*T23*Z13+(
     ?    2*O3**2-4*O2**2+2*O1**2)*T12*T22*Z12+(O3**2-2*O2**2+O1**2)*T12*
     @    *2*Z11)+A11**2*((O3**2+O2**2-2*O1**2)*T13**2*Z33+(2*O3**2+2*O2*
     1    *2-4*O1**2)*T12*T13*Z23+(O3**2+O2**2-2*O1**2)*T12**2*Z22+(2*O3*
     2    *2+2*O2**2-4*O1**2)*T11*T13*Z13+(2*O3**2+2*O2**2-4*O1**2)*T11*T
     3    12*Z12+(O3**2+O2**2-2*O1**2)*T11**2*Z11))

C(c601) FORTRAN(12*D538);
      TERM9=-12*
     +DIP**2*(((ALDYN-A33)*O3*T33**2+((ALDYN-A33)*O2*T23+(ALDYN-A33)*
     1    O1*T13)*T33)*V33*W33+(((ALDYN-A33)*O3*T23*T33+(ALDYN-A33)*O2*T2
     2    3**2+(ALDYN-A33)*O1*T13*T23)*V33+((ALDYN-A22)*O3*T23+(ALDYN-A22
     3    )*O2*T22+(ALDYN-A22)*O1*T12)*T33*V22)*W23+((ALDYN-A22)*O3*T23**
     4    2+((ALDYN-A22)*O2*T22+(ALDYN-A22)*O1*T12)*T23)*V22*W22+(((ALDYN
     5    -A33)*O3*T13*T33+(ALDYN-A33)*O2*T13*T23+(ALDYN-A33)*O1*T13**2)*
     6    V33+((ALDYN-A11)*O3*T13+(ALDYN-A11)*O2*T12+(ALDYN-A11)*O1*T11)*
     7    T33*V11)*W13+(((ALDYN-A22)*O3*T13*T23+(ALDYN-A22)*O2*T13*T22+(A
     8    LDYN-A22)*O1*T12*T13)*V22+((ALDYN-A11)*O3*T13+(ALDYN-A11)*O2*T1
     9    2+(ALDYN-A11)*O1*T11)*T23*V11)*W12+((ALDYN-A11)*O3*T13**2+((ALD
     :    YN-A11)*O2*T12+(ALDYN-A11)*O1*T11)*T13)*V11*W11)
```

```
C(c602) FORTRAN(12*D545);
      TERM10=-12*
     +(ALDYN-A33)*DIP**2*(((O3*T33**2+(O2*T23+O1*T13)*T33)*V33+(O3*T2
     1   3**2+(O2*T22+O1*T12)*T23)*V22+(O3*T13**2+(O2*T12+O1*T11)*T13)*V
     2   11)*W33+((O3*T23*T33+O2*T23**2+O1*T13*T23)*V33+(O3*T22*T23+O2*T
     3   22**2+O1*T12*T22)*V22+(O3*T12*T13+O2*T12**2+O1*T11*T12)*V11)*W2
     4   3+((O3*T13*T33+O2*T13*T23+O1*T13**2)*V33+(O3*T12*T23+O2*T12*T22
     5   +O1*T12**2)*V22+(O3*T11*T13+O2*T11*T12+O1*T11**2)*V11)*W13)

C(c603) FORTRAN(12*D552);
      TERM11=-12*
     +DIP**2*(((ALDYN-A33)*O3*T33**2*V33+(ALDYN-A22)*O2*T23*T33*V22+(
     1   ALDYN-A11)*O1*T13*T33*V11)*W33+((2*ALDYN-2*A33)*O3*T23*T33*V33+
     2   ((ALDYN-A22)*O2*T22*T33+(ALDYN-A22)*O2*T23**2)*V22+((ALDYN-A11)
     3   *O1*T12*T33+(ALDYN-A11)*O1*T13*T23)*V11)*W23+((ALDYN-A33)*O3*T2
     4   3**2*V33+(ALDYN-A22)*O2*T22*T23*V22+(ALDYN-A11)*O1*T12*T23*V11)
     5   *W22+((2*ALDYN-2*A33)*O3*T13*T33*V33+((ALDYN-A22)*O2*T12*T33+(A
     6   LDYN-A22)*O2*T13*T23)*V22+((ALDYN-A11)*O1*T11*T33+(ALDYN-A11)*O
     7   1*T13**2)*V11)*W13+((2*ALDYN-2*A33)*O3*T13*T23*V33+((ALDYN-A22)
     8   *O2*T12*T23+(ALDYN-A22)*O2*T13*T22)*V22+((ALDYN-A11)*O1*T11*T23
     9   +(ALDYN-A11)*O1*T12*T13)*V11)*W12+((ALDYN-A33)*O3*T13**2*V33+(A
     :   LDYN-A22)*O2*T12*T13*V22+(ALDYN-A11)*O1*T11*T13*V11)*W11)

C(c605) FORTRAN(2*D569);
      TERM12=2*
     +(3*DIP**2*(A33*((T33**2*W33+T23*T33*W23+T13*T33*W13)*Z33+(T23*T33
     1   *W33+T23**2*W23+T13*T23*W13)*Z23+(T13*T33*W33+T13*T23*W23+T13**
     2   2*W13)*Z13)+A22*((T23*T33*W23+T23**2*W22+T13*T23*W12)*Z33+(T22*
     3   T33*W23+T22*T23*W22+T13*T22*W12)*Z23+(T12*T33*W23+T12*T23*W22+T
     4   12*T13*W12)*Z13)+A11*((T13*T33*W13+T13*T23*W12+T13**2*W11)*Z33+
     5   (T12*T33*W13+T12*T23*W12+T12*T13*W11)*Z23+(T11*T33*W13+T11*T23*
     6  W12+T11*T13*W11)*Z13))-2*DIP**2*(T33*W33+T23*W23+T13*W13)*(A33*(
     7   T33*Z33+T23*Z23+T13*Z13)+A22*(T23*Z23+T22*Z22+T12*Z12)+A11*(T13
     8  *Z13+T12*Z12+T11*Z11))+3*A33*DIP**2*((T33**2*W33+T23*T33*W23+T13
     9   *T33*W13)*Z33+(T23*T33*W33+(T33**2+T23**2)*W23+T23*T33*W22+T13*
     :   T23*W13+T13*T33*W12)*Z23+(T23*T33*W23+T23**2*W22+T13*T23*W12)*Z
     ;   22+(T13*T33*W33+T13*T23*W23+(T33**2+T13**2)*W13+T23*T33*W12+T13
     <   *T33*W11)*Z13+(T13*T33*W23+T13*T23*W22+T23*T33*W13+(T23**2+T13*
     =   *2)*W12+T13*T23*W11)*Z12+(T13*T33*W13+T13*T23*W12+T13**2*W11)*Z
     >   11))

C(c606) FORTRAN(2*D582);
      TERM13A=2*
     +(3*DIP**2*(A33*((O3**2*T33**2+(O2*O3*T23+O1*O3*T13)*T33)*V33*Z33+
     1   ((O3**2*T23*T33+O2*O3*T23**2+O1*O3*T13*T23)*V33+(O3**2*T23+O2*O
     2   3*T22+O1*O3*T12)*T33*V22)*Z23+(O3**2*T23**2+(O2*O3*T22+O1*O3*T1
     3   2)*T23)*V22*Z22+((O3**2*T13*T33+O2*O3*T13*T23+O1*O3*T13**2)*V33
     4   +(O3**2*T13+O2*O3*T12+O1*O3*T11)*T33*V11)*Z13+((O3**2*T13*T23+O
     5   2*O3*T13*T22+O1*O3*T12*T13)*V22+(O3**2*T13+O2*O3*T12+O1*O3*T11)
     6   *T23*V11)*Z12+(O3**2*T13**2+(O2*O3*T12+O1*O3*T11)*T13)*V11*Z11)
     7   +A22*((O2*O3*T23*T33+O2**2*T23**2+O1*O2*T13*T23)*V33*Z33+((O2*O
     8   3*T22*T33+O2**2*T22*T23+O1*O2*T13*T22)*V33+(O2*O3*T23**2+(O2**2
     9   *T22+O1*O2*T12)*T23)*V22)*Z23+(O2*O3*T22*T23+O2**2*T22**2+O1*O2
     :   *T12*T22)*V22*Z22+((O2*O3*T12*T33+O2**2*T12*T23+O1*O2*T12*T13)*
     ;   V33+(O2*O3*T13+O2**2*T12+O1*O2*T11)*T23*V11)*Z13+((O2*O3*T12*T2
     <   3+O2**2*T12*T22+O1*O2*T12**2)*V22+(O2*O3*T13+O2**2*T12+O1*O2*T1
     =   1)*T22*V11)*Z12+(O2*O3*T12*T13+O2**2*T12**2+O1*O2*T11*T12)*V11*
     >   Z11)+A11*((O1*O3*T13*T33+O1*O2*T13*T23+O1**2*T13**2)*V33*Z33+((
     ?   O1*O3*T12*T33+O1*O2*T12*T23+O1**2*T12*T13)*V33+(O1*O3*T13*T23+O
```

```
     @    1*O2*T13*T22+O1**2*T12*T13)*V22)*Z23+(O1*O3*T12*T23+O1*O2*T12*T
     1    22+O1**2*T12**2)*V22*Z22+((O1*O3*T11*T33+O1*O2*T11*T23+O1**2*T1
     2    1*T13)*V33+(O1*O3*T13**2+(O1*O2*T12+O1**2*T11)*T13)*V11)*Z13+((
     3    O1*O3*T11*T23+O1*O2*T11*T22+O1**2*T11*T12)*V22+(O1*O3*T12*T13+O
     4    1*O2*T12**2+O1**2*T11*T12)*V11)*Z12+(O1*O3*T11*T13+O1*O2*T11*T1
     5    2+O1**2*T11**2)*V11*Z11)))

      TERM13B=2*(3*DIP**2*(A33*((O3**2*T33**2+(O2*O3*T2
     6    3+O1*O3*T13)*T33)*V33*Z33+(O2*O3*T33**2+((O3**2+O2**2)*T23+O1*O
     7    2*T13)*T33+O2*O3*T23**2+O1*O3*T13*T23)*V33*Z23+(O2*O3*T23*T33+O
     8    2**2*T23**2+O1*O2*T13*T23)*V33*Z22+(O1*O3*T33**2+(O1*O2*T23+(O3
     9    **2+O1**2)*T13)*T33+O2*O3*T13*T23+O1*O3*T13**2)*V33*Z13+((O1*O3
     :    *T23+O2*O3*T13)*T33+O1*O2*T23**2+(O2**2+O1**2)*T13*T23+O1*O2*T1
     ;    3**2)*V33*Z12+(O1*O3*T13*T33+O1*O2*T13*T23+O1**2*T13**2)*V33*Z1
     <    1)+A22*((O3**2*T23**2+(O2*O3*T22+O1*O3*T12)*T23)*V22*Z33+(O2*O3
     =    *T23**2+((O3**2+O2**2)*T22+O1*O2*T12)*T23+O2*O3*T22**2+O1*O3*T1
     >    2*T22)*V22*Z23+(O2*O3*T22*T23+O2**2*T22**2+O1*O2*T12*T22)*V22*Z
     ?    22+(O1*O3*T23**2+(O1*O2*T22+(O3**2+O1**2)*T12)*T23+O2*O3*T12*T2
     @    2+O1*O3*T12**2)*V22*Z13+((O1*O3*T22+O2*O3*T12)*T23+O1*O2*T22**2
     1    +(O2**2+O1**2)*T12*T22+O1*O2*T12**2)*V22*Z12+(O1*O3*T12*T23+O1*
     2    O2*T12*T22+O1**2*T12**2)*V22*Z11)+A11*((O3**2*T13**2+(O2*O3*T12
     3    +O1*O3*T11)*T13)*V11*Z33+(O2*O3*T13**2+((O3**2+O2**2)*T12+O1*O2
     4    *T11)*T13+O2*O3*T12**2+O1*O3*T11*T12)*V11*Z23+(O2*O3*T12*T13+O2
     5    **2*T12**2+O1*O2*T11*T12)*V11*Z22+(O1*O3*T13**2+(O1*O2*T12+(O3*
     6    *2+O1**2)*T11)*T13+O2*O3*T11*T12+O1*O3*T11**2)*V11*Z13+((O1*O3*
     7    T12+O2*O3*T11)*T13+O1*O2*T12**2+(O2**2+O1**2)*T11*T12+O1*O2*T11
     8    **2)*V11*Z12+(O1*O3*T11*T13+O1*O2*T11*T12+O1**2*T11**2)*V11*Z11
     9   ))-2*DIP**2*((O3**2*T33+O2*O3*T23+O1*O3*T13)*V33+(O2*O3*T23+O2**
     :    2*T22+O1*O2*T12)*V22+(O1*O3*T13+O1*O2*T12+O1**2*T11)*V11)*(A33*
     ;    (T33*Z33+T23*Z23+T13*Z13)+A22*(T23*Z23+T22*Z22+T12*Z12)+A11*(T1
     <    3*Z13+T12*Z12+T11*Z11)))

        TERM13=TERM13A+TERM13B
C(c607) FORTRAN(4*D590);
       TERM14=-4*
     +DIP**2*(A33**2*(-2*O3*T33**2*Z33-4*O3*T23*T33*Z23-2*O3*T23**2*Z2
     1    2-4*O3*T13*T33*Z13-4*O3*T13*T23*Z12-2*O3*T13**2*Z11)+A22*A33*(-
     2    3*O2*T23*T33*Z33+(-3*O2*T22*T33-3*O2*T23**2)*Z23-3*O2*T22*T23*Z
     3    22+(-3*O2*T12*T33-3*O2*T13*T23)*Z13+(-3*O2*T12*T23-3*O2*T13*T22
     4    )*Z12-3*O2*T12*T13*Z11)+A11*A33*(-3*O1*T13*T33*Z33+(-3*O1*T12*T
     5    33-3*O1*T13*T23)*Z23-3*O1*T12*T23*Z22+(-3*O1*T11*T33-3*O1*T13**
     6    2)*Z13+(-3*O1*T11*T23-3*O1*T12*T13)*Z12-3*O1*T11*T13*Z11)+A22**
     7    2*(O3*T23**2*Z33+2*O3*T22*T23*Z23+O3*T22**2*Z22+2*O3*T12*T23*Z1
     8    3+2*O3*T12*T22*Z12+O3*T12**2*Z11)+A11**2*(O3*T13**2*Z33+2*O3*T1
     9    2*T13*Z23+O3*T12**2*Z22+2*O3*T11*T13*Z13+2*O3*T11*T12*Z12+O3*T1
     :    1**2*Z11))

        TERM=TERM1+TERM2+TERM3+TERM4+TERM5+TERM6+TERM7+TERM8+TERM9+TERM10
     + +TERM11+TERM12+TERM13+TERM14

        FI(X2,X3,X4,X5,X6)=(1/(6480.*3.14159265358979323846**2))*(SI
     + N(BE1(X3))*SIN(BE2(X6)))*TERM


C
C CALCULATION OF THE SHAPE POTENTIAL:
C

C       G1(X3,X4,X6)=4.*PARAM2*1.380622E-23*R**12*(SHAPE1
C     + *(3.*COS(BE1(X3))**2+3.*COS(BE2(X6))**2-2.))
```

```
      G1(X3,X4,X6)=4.*PARAM2*1.380622E-23*R**12*(SHAPE1*(3.*COS(BE1(X3)
     + )**2+3.*COS(BE2(X6))**2-2.)+SHAPE2*(3.*COS(GA1(X4))**2*SIN(BE1(X3
     + ))**2+3.*COS(GA2(X7))**2*SIN(BE2(X6))**2-2.))



80              CONTINUE
70            CONTINUE
60          CONTINUE
50        CONTINUE
40      CONTINUE

C
C THE INTEGRAL IS CALCULATED:
C

        SS6=0.00
  DO 940 X6=1,16
      WRITE(6,1911)X6
1911   FORMAT (1X, 'sub-index (in range 1 to 16) is currently ',I2 )
          SS5=0.00
    DO 950 X5=1,16
            SS4=0.00
      DO 960 X4=1,16
              SS3=0.00
        DO 970 X3=1,16
                SS2=0.00
   DO 980 X2=1,16
                  SS1=0.00
                  DO 990 X1=1,64


C
C SUMMATION OF THE ENERGY TERMS WITH SUBSEQUENT DIVISION BY (-kT):
C

      G3=-1.*(D1(X1)+E1(X2,X3,X4,X5,X6)/SE5(X1)+F1(X2,X3,X4,X5,X6)/SE8(
     + X1)+G1(X3,X4,X6)/SE12(X1)+DDP(X2,X3,X4,X5,X6)/SE3(X1)+DIDP(X2,X3,
     + X4,X5,X6)/SE6(X1)+DQP(X2,X3,X4,X5,X6)/SE4(X1))/TEMPK

      IF(G3.LT.-85) GO TO 5000
      G4=2.71828**G3
      GO TO 5010
5000  G4=0
5010  SS1=SS1+(FI(X2,X3,X4,X5,X6)/(SEP(X1)**4))*G4*COEF2(X1,2)
990               CONTINUE
      SS2=SS2+SS1*COEF1(X2,2)
C
C
980             CONTINUE
      SS3=SS3+SS2*COEF1(X3,2)
C
C
970           CONTINUE
      SS4=SS4+SS3*COEF1(X4,2)
C
C
960         CONTINUE
      SS5=SS5+SS4*COEF1(X5,2)
```

```
C
C
950         CONTINUE
        SS6=SS6+SS5*COEF1(X6,2)
C
C
940       CONTINUE
        SS7=SS7+SS6*COEF1(X7,2)

C
C
939     CONTINUE
        ANS=SS7*SEP1*AL11*BE11*GA11*AL21*BE21*GA21*1.E-34*6.022169**2*
     + 8.9875**3/(TEMP*1.380622)**2

        CALL BEEP@

C
C THE INTEGRAL IS PRINTED TOGETHER WITH MOLECULAR DATA USED
C

        WRITE(4,2266)
2266    FORMAT(1X,'THE D2A3 TERM CONTRIBUTION TO B(Kerr) FOR SO2')
        WRITE(4,2268)
2268    FORMAT(1X,'AT THE WAVELENGTH 632.8 nm')
        WRITE(4,2267)
2267    FORMAT(1X,'    ')
        CALL SECONDS_SINCE_1980@(FINISH)
        WRITE(4,2250)(FINISH-START)
2250    FORMAT(1X,'CPU time used = ',F12.3)
        WRITE(4,2260)FDATE@()
2260    FORMAT(1X,'Program run on  ',A30)
        WRITE(4,2269)
2269    FORMAT(1X,'    ')
        WRITE(4,1140)ANS
1140    FORMAT(1X,'THE INTEGRAL IS',E15.7)
        WRITE(4,2150)
2150    FORMAT(1X,'INPUT DATA:     ')
        WRITE(4,2155)TEMP
2155    FORMAT(1X,'TEMPERATURE:           ',F10.5)
        WRITE(4,2156)DIP
2156    FORMAT(1X,'DIPOLE MOMENT:         ',F10.5)
        WRITE(4,2911)ALDYN
2911    FORMAT(1X,'MEAN DYNAMIC ALPHA:    ',F10.5)
        WRITE(4,2912)A11
2912    FORMAT(1X,'DYNAMIC ALPHA11:       ',F10.5)
        WRITE(4,2913)A22
2913    FORMAT(1X,'DYNAMIC ALPHA22:       ',F10.5)
        WRITE(4,2914)A33
2914    FORMAT(1X,'DYNAMIC ALPHA33:       ',F10.5)
        WRITE(4,2160)ALSTAT
2160    FORMAT(1X,'MEAN STATIC ALPHA:     ',F10.5)
        WRITE(4,2161)V11
2161    FORMAT(1X,'STATIC ALPHA11:        ',F10.5)
        WRITE(4,2162)V22
2162    FORMAT(1X,'STATIC ALPHA22:        ',F10.5)
        WRITE(4,2163)V33
2163    FORMAT(1X,'STATIC ALPHA33:        ',F10.5)
        WRITE(4,2190)Q1
2190    FORMAT(1X,'THETA11:               ',F10.5)
```

```
      WRITE(4,2241)Q2
2241  FORMAT(1X,'THETA22:                ',F10.5)
      WRITE(4,2210)R
2210  FORMAT(1X,'R(0):                      ',F6.5)
      WRITE(4,2220)SHAPE1
2220  FORMAT(1X,'SHAPE FACTOR 1:         ',F10.5)
      WRITE(4,2221)SHAPE2
2221  FORMAT(1X,'SHAPE FACTOR 2:         ',F10.5)
      WRITE(4,2230)PARAM2
2230  FORMAT(1X,'E/K:                     ',F9.5)
      WRITE(4,2235)AMIN1,AMAX1
2235  FORMAT(1X,'MIN AND MAX POINTS OF RANGE:',2(F10.5,3X))
      WRITE(4,2240)
2240  FORMAT(1X,'END Bk')
      WRITE(4,2261)
2261  FORMAT(1X,'    ')
      WRITE(4,2262)
2262  FORMAT(1X,'    ')
      WRITE(4,2263)
2263  FORMAT(1X,'    ')
      WRITE(4,2264)
2264  FORMAT(1X,'    ')
      WRITE(4,2265)
2265  FORMAT(1X,'    ')

      END
```